Universidad del País Vasco
Euskal Herriko Unibertsitatea

Mesenchymal stromal cells and mathematical modeling for the improvement of cell microencapsulation technologies

Tania Belén López Méndez
NanoBiocel Group, Laboratory of Pharmaceutics
University of the Basque Country (UPV/EHU)
Faculty of Pharmacy
Vitoria-Gasteiz 2020

NanoBioCel
Grupo de Micro y Nano Tecnologías, Biomateriales y Células

ACKNOWLEDGMENTS

Después de todos estos años he aprendido que, en investigación, los experimentos nuevos nunca salen a la primera, que a veces hay que descartar hipótesis sin llegar a entender el por qué, que la planificación hay que hacerla siempre a lápiz para poder reescribirla una y otra vez, que las células no entienden de fines de semana, que algunos experimentos se hacen mejor por la noche y que la frustración forma parte del día a día de cualquier laboratorio. Sin embargo, también he aprendido que el día que por fin los experimentos cuadran y todo cobra sentido, compensa todos los intentos en los que no tuviste éxito y que, si te rodeas de las personas adecuadas, recordarás con cariño hasta los peores momentos.

Mis primeros agradecimientos tienen que ser, sin duda, para Aurora y Ernesto, mis padres. Por quererme como soy y por apoyarme en todas mis decisiones. Por darme la mano en cada uno de los pasos que he dado en la vida, y hacer lo imposible por eliminar los obstáculos de mi camino. Gracias a vuestro ejemplo sé que es importante trabajar duro para lograr lo que me proponga, pero siempre con la perspectiva clara de saber cuáles son las cosas que de verdad importan. Si cuidas esas, todo lo demás irá saliendo. Una gran parte de cada uno de mis logros es siempre vuestro. A mi hermano, Héctor, posiblemente la persona más integra y honesta que conozco, por acompañarme y cuidarme siempre, aunque él sea el pequeño. No sé en qué momento nos hemos hecho tan mayores, pero estoy deseando seguir viéndote cumplir cada una de las metas que te propongas. A mis abuelos y yayos, Enedina, Manuel, Teresa y Joaquín, por ser los mayores admiradores de sus nietos y por inculcarnos que nuestra felicidad solo depende de nosotros mismos. Vuestras enseñanzas son las que me dan ánimo para seguir cuando solo quiero rendirme. A mis tíos y tías, Montse, Angelines, Luis, Manolo y Yoli, y a mi primo Pablo (que siempre seguirá siendo Pablito tenga la edad que tenga), que completan esta pequeña familia que siempre se mantiene unida. No todo el mundo tiene la suerte de tener alrededor tanta gente en la que confía sin reservas. Os quiero mucho a todos, familia.

Además, me gustaría agradecer a Puri, Ibai, Mikel y toda la familia de cumples molones habernos hecho sentir uno más desde el principio y haber estado presentes en tantos momentos importantes en nuestras vidas. No sé si este grupo dará

suerte de verdad, pero lo que está claro es que todas las cosas que celebramos son siempre más que merecidas.

Quiero dar las gracias también a mis amigos de siempre y a esos que han aparecido en mi vida hace menos para hacerse imprescindibles. También a los que vivís lejos y día a día me demostráis que la distancia no es impedimento para estar cerca. Los que habéis escuchado una y otra vez mis historias caóticas y aun así tenéis la paciencia para volver a prestarme atención una vez más. Que habéis compartido conmigo tantísimos momentos, pero conseguís que cada uno de ellos siga siendo especial. Una charla con vosotros es lo único que necesito para acabar riéndome de muchos de los que antes me parecían problemas. Y por supuesto, estáis presentes en muchos de los recuerdos más bonitos que tengo. Vosotros sabéis mejor que nadie todo lo que hay detrás de esta tesis y me habéis dado ánimos hasta el nivel de acompañarme a la biblioteca, ayudarme a diseñar unas fórmulas o darme soluciones salvavidas de último minuto. Soy muy consciente de lo afortunada que soy de teneros y espero que lo que viene sea por lo menos igual de bonito que lo que hemos vivido hasta ahora.

Y aunque todo lo que he escrito en el párrafo anterior también les aplique a ellos, me gustaría hacer una mención especial a todos los que empezaron siendo mis compañeros de tesis y desde entonces han vivido conmigo excursiones, vacaciones, fiestas, bodas, nacimientos y, por supuesto, experimentos interminables que se hacen más llevaderos a ritmo de reggaetón y con pizzas de madrugada. Para vosotros siempre habrá un huequito fundamental en mi vida.

To my labmates in London, thank you for welcoming me so kindly into your group. Especially to Álvaro Mata and Estelle Collin for accepting me in the lab and giving me the opportunity to learn so much. Thank you all for so many beautiful memories in such an amazing city.

Finalmente, me gustaría agradecer a mis directores, Rosa Hernández y Gorka Orive, el haberme dado la oportunidad de llevar a cabo esta tesis en NanoBioCel. Este trabajo no hubiera sido posible sin su ayuda. Y a José Luis Pedraz, investigador principal del grupo y mi jefe en esta última etapa, por confiar en mí desde el principio

y darme la oportunidad de crecer y aprender tanto.

Muchas gracias a todos los que habéis contribuido a que este proyecto sea una realidad.

ACKNOWLEDGMENT FOR THE FINANCIAL SUPPORT

This thesis has been partially supported by the Basque Government (Consolidated Groups, IT-407-07) and the Univeristy of the Basque Country (UPV/EHU) (UFI 11/32). The intellectual and technical assistance from the ICTS "NANBIOSIS", more specifically, by the Drug Formulation Unit (U10) of the CIBER in Bioengineering, Biomaterials & Nanomedicine (CIBER-BBN) at the University of Basque Country (UPV/EHU) is acknowledge. Tania Belén Lopez Méndez thanks the Basque Government (Department of Education, Universities andResearch) for the Ph.D. fellowship.

ACKNOWLEDGMENT TO THE EDITORIALS

Authors would like to thank the editorials for granting permission to reuse their previously published articles in this thesis:

Lopez-Mendez *et al.* International Journal of Pharmaceutics 2017; 533: 62-72

El conocimiento no es una vasija que se llena,
es un fuego que se enciende

Plutarco

The mind is not a vessel to be filled,
but a fire to be kindled

Plutarch

GLOSSARY

7AAD: 7-Aminoactinomycin D

AD: Alzheimer's disease

APA: Alginate-PLL-alginate (APA-PLL) or alginate-PLO-alginate (APA-PLO) microcapsules

BHK: Baby hamster kidney cells

BrdU: 5-bromo-2´-deoxyuridine

CB: Carboxybetaine

CCK-8: Cell counting kit

ChP: Choroidal plexus

CNS: Central nervous system

CNTF: Ciliary neurotrophic factor

CXCL12: C-X-C motif chemokine 12

CYP2B1: Cytochrome P450 2B1

DAMPs: Damage-associated molecular patterns

DM: Diabetes Mellitus

DMEM: Dubecco's modified Eagle' medium

ECM: Extracellular matrix

EPO: Erythropoietin

FBS: Fetal bovine serum

FGF: Fibroblast growth factor

GAD65: Glutamic acid decarboxylase 65

Gal: Galactosil

GDNF: Glial cell-derived neurotrophic factor

GLP-1: Glucagon-1-like peptide

HA: Hyaluronic acid

hESCs: Human embryonic stem cells

hPSCs: Human pluripotent stem cells

hUCMS: Human umbilical cord Wharton jelly-derived mesenchymal stem cells

IGF-1: Insulin-like growth factor

IgM: Immunoglobulin M

IL-13: Interleukin 13

IL-1R: Interleukin-1 receptor

IL-1β: Interleukin 1β

IL-4: Interleukin 4

IL-6: Interleukin 6

iPSCs: Induced pluripotent stem cells

LPS: Lipopolysaccharides

MHC I: Mayor histocompatibility complex I

MHC II: Mayor histocompatibility complex II

MRI: Magnetic resonance imaging

MSC: Mesenchymal stromal cells/mesenchymal stem cells

MWCO: Molecular weight cut-off

Neu5Gc: N-glycolyl neuraminic acid

NGF: Nerve growth factor

PAMPs: Pathogen-associated molecular patterns

PBS: Phosphate buffered saline

PD: Parkinson's disease

PEG: Polyethylene glycol

PLGA: Poly(lactic-co-glycolic acid)

PLL: Poly-L-lysine

PLO: Poly-L-ornithine

PMCG: Poly(methylene-co-guanidine)

PMM: Poly(methylvinylether-alt-maleic anhydride)

PRR: Pattern recognition receptors

PVA: Polyvinyl alcohol

RCP: Random close packing

RGD: Arginine-glycine-aspartic acid

SB: Sulfobetaine

SC-β: Human stem cell derived β cells

SPIO: Superparamagnetic iron oxide nanoparticles

T1D: Type 1 diabetes mellitus

T2D: Type 2 diabetes mellitus

TLR-4: Toll-like receptor 4

TLRs: Toll-like receptors

TNF-α: Tumor necrosis factor α

VEGF: Vascular endothelial growth factor

TABLE OF CONTENTS

INTRODUCTION

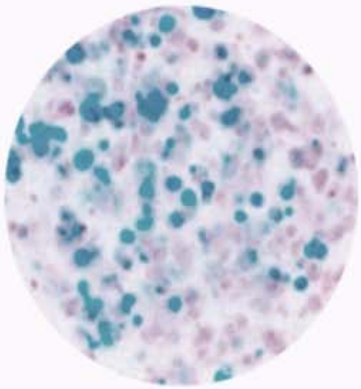

1

Introduction
Chapter 1

CELL MICROENCAPSULATION TECHNOLOGIES FOR SUSTAINED DRUG DELIVERY: LATEST ADVANCES IN EFFICACY AND BIOSAFETY

Tania B. Lopez-Mendez[1,2], Edorta Santos-Vizcaino[1,2], Jose Luis Pedraz[1,2], Gorka Orive[1,2,3,4*], Rosa Maria Hernandez[1,2*]

[1]NanoBioCel Group, School of Pharmacy, University of the Basque Country (UPV/EHU), Paseo de la Universidad, 7, 01006, Vitoria-Gasteiz, Spain.

[2]Biomedical Research Networking Center in Bioengineering, Biomaterials and Nanomedicine (CIBER-BBN), Instituto de Salud Carlos III, C/Monforte de Lemos 3-5, 28029 Madrid, Spain

[3]University Institute for Regenerative Medicine and Oral Implantology - UIRMI (UPV/EHU-Fundación Eduardo Anitua); BTI Biotechnology Institute, Vitoria-Gasteiz, (Spain).

[4]Singapore Eye Research Institute, The Academia, 20 College Road, Discovery Tower, Singapore.

*Corresponding authors: Hernandez RM (rosa.hernandez@ehu.eus)
Orive G (gorka.orive@ehu.eus)

ABSTRACT

The development of cell microencapsulation systems began several decades ago. However, today few systems have been tested in clinical trials. For this reason, in the last years, researchers have directed efforts towards trying to solve some of the key aspects that still limit efficacy and biosafety, the two major criteria that must be satisfied to reach the clinical practice. Regarding the efficacy, which is closely related to biocompatibility, substantial improvements have been made, such as the purification or chemical modification of the alginates that normally form the microspheres. Each of the components that make up the microcapsules has been carefully selected to avoid toxicities that can damage the encapsulated cells or generate an immune response leading to pericapsular fibrosis. As for the biosafety, researchers have developed biological circuits capable of actively responding to the needs of the patients to precisely and accurately release the demanded drug dose. Furthermore, the structure of the devices has been subject of study to adequately protect the encapsulated cells and prevent their spread in the body. The objective of this chapter is to describe the latest advances made by scientist to improve the efficacy and biosafety of cell microencapsulation systems for sustained drug delivery, also highlighting those points that still need to be optimized.

Keywords: Cell encapsulation, efficacy, biosafety, biocompatibility, biomaterial, alginate.

1. INTRODUCTION

For more than four decades, different materials, both of natural and synthetic origin, have been used to manufacture sustained drug delivery systems. Among them, we find those that allow the sustained release of encapsulated growth factors, proteins or drugs; but also others, of greater complexity, that are capable of immobilizing and protecting living cells, selectively isolating them from their environment while they secrete the therapeutic molecules of interest. Cell encapsulation systems have shown wide applicability in pathologies with very diverse characteristics, such as diabetes mellitus (DM), anemia, hemophilia B or pathologies of the central nervous system (CNS), among others [1]. They are especially convenient for pathologies in which maintaining a strict control over the release of the therapeutic molecule is essential.

Cell encapsulation can be classified based on the size of the system. On the one hand, we find cell macroencapsulation systems, in which the cells are immobilized in relatively large diffusion chambers, with semipermeable properties. They can have different shapes, such as discs, flat sheets or hollow fibers. The application of cell macroencapsulation devices have shown very good results *in vivo* demonstrating their undeniable therapeutic potential. However, macrocapsules are characterized by a relatively small surface/volume ratio, which is probably their worst disadvantage, since this implies the need for large amounts of nutrients and oxygen to achieve an adequate diffusion into the chamber and limits the amount of cells that can be encapsulated without creating necrotic nuclei in the innermost and inaccessible areas [2].

Cell microencapsulation represents a very interesting alternative, greatly improving the surface/volume ratio and increasing the diffusion of nutrients and oxygen inside the capsules. Cell microencapsulation strategy is based on the immobilization of cells that produce therapeutically relevant molecules in spherical particles between 100 and 1500 μm in diameter, approximately. The particles are elaborated with biocompatible materials and usually surrounded by a semi-permeable polymeric membrane that prevents the passage of high molecular weight molecules — antibodies and other components of the immune system —, protecting these cells from the host's immune response and from the mechanical stress that may occur

when the implant is placed in the selected tissue [3]. In addition, the microcapsule must exert a tight control over the bidirectional diffusion of molecules — entrance of nutrients and oxygen; and release of *de novo* synthesized therapeutic factors and metabolic subproducts —, and provide cells with a suitable environment to enhance and modulate their function. This technology also suppresses, or at least reduces, the chronic administration of immunosuppressive agents, thus avoiding some of the adverse events associated with organ and tissue transplantation. On the other hand, the constant improvements in imaging techniques and robotic surgery procedures allow the access to difficult to reach areas for implantation [4].

To date, the results obtained in the various clinical trials carried out, make clear the advantages and potential applications of this promising technology. However, there are still aspects that need to be improved so that cell microencapsulation systems can be applied routinely in clinical practice. For this reason, in the last years, researchers have directed efforts towards trying to solve some of the key aspects that still limit efficacy and biosafety, the two major criteria that must be satisfied to reach the clinical practice. Those two concepts are closely related to each other and must be carefully defined and regulated due to their implications regarding patient well-being. The objective of this chapter is, therefore, to group and describe the extensive work carried out with the aim to improve these criteria, emphasizing the points that still need to be optimized.

2. EFFICACY-BIOCOMPATIBILITY

When talking about efficacy of cell microencapsulation, biocompatibility is one of the most important aspects to be considered. It will determine implant's viability, functionality and durability, becoming in many cases a limiting factor to succeed. The biocompatibility of the implant must be given in 2 directions **(Figure 1)**. From outside to inside, the materials used must protect the immobilized cells, avoiding direct toxicity or the blockage of nutrients and oxygen diffusion. From inside to outside, none of the system components — cells, biomaterials, crosslinking agents, etc. — or procedures used must be toxic for the patient or elicit an immune response in the host. When this occurs, the foreign body reaction **(Box 1)** can

eventually isolate the implant within a fibrotic capsule, thereby preventing the access of essential molecules and leading to graft failure. In addition, the biocompatibility must last over time, since live cell therapies are normally used for long-term treatments. In this sense, several experts in the field of cell encapsulation have decided to define the term "biotolerability", considering it more appropriate than "biocompatibility" [5].

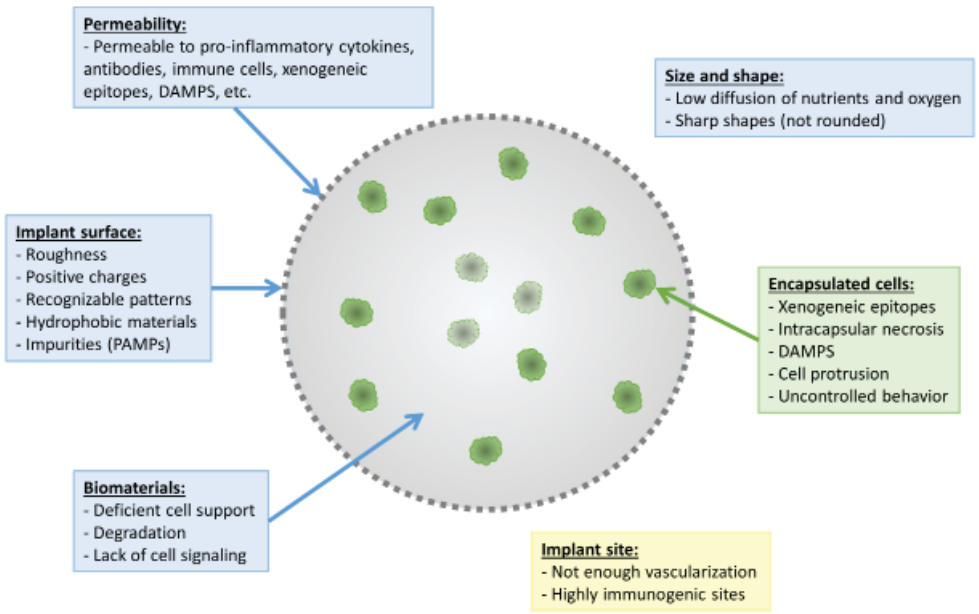

Figure 1. Factors that may compromise implant biocompatibility/biotolerability.

Despite the undeniable improvement occurred in recent decades, the biomaterials and cells that are used today continue to produce, to a greater or lesser extent, an inflammatory response by the host, so searching for suitable components remains a priority. The final performance of the device will depend not only on the biomaterials and cells used, but also on the site of implant, the local application of immunosuppressive drugs, or even the size and shape of the implant.

2.1. Biomaterials, crosslinkers and coatings

2.1.1. Biomaterials and crosslinkers

On the one hand, the elaborated devices must present a suitable structure, resistant to unwanted degradation that avoids contact between the encapsulated cells and the host immune system. Furthermore, the biomaterials must guide the processes

Box 1. Foreign body reaction against biomaterials

Although the materials and therapeutic applications differ, the process by which the body produces rejection against implants has many points in common. This is known as "foreign body reaction" and consists of the following phases:

Immediately after the implantation and depending on the characteristics of its surface —material, shape, roughness, electrostatic charge, etc. — and the injury caused during the surgical process, various host proteins — such as albumin, fibronectin or complement molecules — will start to adhere to the surface of the implant. This creates a chemoattractive gradient for the innate immune response [193]. Neutrophils are the first cell type present at the implant site and their function is to engulf the microorganism remains and dead cells. Neutrophils also secrete proteases, lysozymes, reactive species and other enzymes to eliminate any type of biodegradable material. At the same time, they secrete cytokines and other factors that cause the activation of macrophages (differentiated from the recruited monocytes), which will be the predominant cell type in the following phases of the foreign body response. This acute phase of the inflammatory reaction would end with a return to homeostasis if the material recognized as foreign disappeares completely.

On the contrary, if the host cannot destroy the implant, its continued presence can lead to a second phase of chronic inflammation. The "frustrated" macrophages start to fuse into multinucleated cells around the implant, giving rise to foreign-body giant cells [194]. At the molecular level, pro-inflammatory cytokines, such as IL-6, TNF-α, interleukin 4 (IL-4), and interleukin 13 (IL-13), have been reported to be overexpressed [195]. In this phase, there is a continuous presence of monocytes and lymphocytes and a constant activation of macrophages and neutrophils, which secrete enzymes and reactive species. At the same time, neovascularization phenomena are observed, with the appearance of functional capillaries.

In the final phase, fibroblasts, activated by macrophages, deposit collagen fibers to form a dense and fibrous acellular capsule that isolates the implant from the surrounding tissue [196]. This prevents the passage of nutrients and oxygen, and eventually leads to compromising the viability of the encapsulated cells.

In vivo the chronology varies depending on the organism, ranging from the appearance of fibrosis in just 7 days, in the case of mini-pigs, to 14 days in rats [197].

of proliferation and differentiation of encapsulated cells, enhancing their viability and functionality. On the other hand, the choice of all the materials must be made taking into account possible toxicities. The latter includes, in addition to the main materials, cross-linkers, physicochemical modifications and possible degradation produts.

Today, the materials used include ceramics, plastics and various polymers, among others. The latter can be classified as natural (polysaccharides, polypeptides and polynucleotides) or synthetic. Among natural polymers, polysaccharides are the most used because they allow relatively smooth encapsulation processes that are compatible with cell viability. Examples of natural polymers are alginate, agarose, collagen, or cellulose. On the other hand, polyethylene glycol (PEG) continues to be the most widely used option among synthetic polymers, along with poly(lactic-co-glycolic acid) (PLGA) and polyvinyl alcohol (PVA) [6,7].

Among all the available polymers, alginate is by far the most widely used biomaterial in cell microencapsulation systems, due to its excellent biocompatibility and easy handling [8]. Alginate is a natural anionic polysaccharide that creates three-dimensional structures, going from sol to gel, when it reacts with divalent ions. It is made up of different proportions of residues of β-D-manuronic acid (M) and α-L-guluronic acid (G) that create different structures according to the ratio of G to M. Determining and standardizing this proportion is essential since it has a great influence on some of alginate hydrogels properties, such as their biocompatibility, stability, mechanical resistance and permeability, among others [8]. In general, alginates with a higher proportion of G blocks are stiffer, compared to those with a higher proportion of M blocks that have better elastic properties, due to the greater affinity of guluronic acid for divalent ions, and these physical-mechanical differences affect the way the immune system reacts against the implant [9].

On the other hand, the purity degree of the alginate is directly related to its biocompatibility. Low purity alginates contain endotoxins, proteins and polyphenols that reduce the biocompatibility of the implants and can damage the encapsulated cells [10]. Several commercial alginates have been described to contain pathogen-associated molecular patterns (PAMPs). These are potent initiators of inflammatory responses [11] and produce the release of small proinflammatory cytokines — such as interleukin 1β (IL-1β), the tumor necrosis factor α (TNF-α) or interleukin 6 (IL-6) —, which can come into contact with the encapsulated cells and cause damage. The most common endotoxin that can be found in alginate are lipopolysaccharides (LPS), which can bind to toll-like receptors 4 (TLR-4) [12], producing an inflammatory

response mediated by a variety of cells of the immune system [13]. Therefore, in recent years, different purification methods have been developed in order to obtain ultra-pure alginates with less immunogenicity *in vivo* [14-17]. However, there is great variability between the procedures used in the different research groups and it is still necessary to improve the tools for the screening and elimination of these and other impurities, such as peptidoglycans and lipoteicoic acid [18-22].

In this sense, there are divided opinions on whether or not it will be possible to achieve an adequate and sufficient level of purification of the alginate — so that it becomes nearly inert to the immune system — or whether it will also be necessary to chemically modify its structure. Indeed, pericapsular fibrosis has been one of the major drawbacks in clinical studies carried out to date with alginate as the main material. However, the composition of the alginate and the variability between administration protocols, cell types or the concomitant use of different coating materials, among others, make the comparison complicated.

In recent years, alginate purification protocols have been refined [22], while some groups have begun to include chemical modifications in the alginates [23,24]. A few years ago, Paredes-Juarez *et al.* created a platform that allows the identification of pattern recognition receptor (PRR) activating polymers, in order to identify contaminants in the biomaterials [11]. On the other hand, in a study carried out by Vegas *et al.*, a combinatorial approach was used to generate a wide range of alginate variants with the aim of finding those that were able to decrease the foreign body response [23]. After a first selection, the most promising ones were evaluated *in vivo*, in rodents and non-human primates. Three triazole-containing analogues were identified, which significantly reduced the foreign body response, inhibiting macrophage recognition and fibrosis formation **(Figure 2)**.

In another interesting and more recent study, Qingsheng Liu *et al.* proposed a group of zwitterionic sulfobetaine (SB) and carboxybetaine (CB) modifications of alginate that reduced cell accumulation and fibrotic processes around the capsules in mice, dogs and pigs [25]. Finally, pancreatic islets immobilized in alginate microbeads modified with these molecules, were implanted, for 200 days, in a diabetic mouse model, improving the glycemic control **(Figure 3)**.

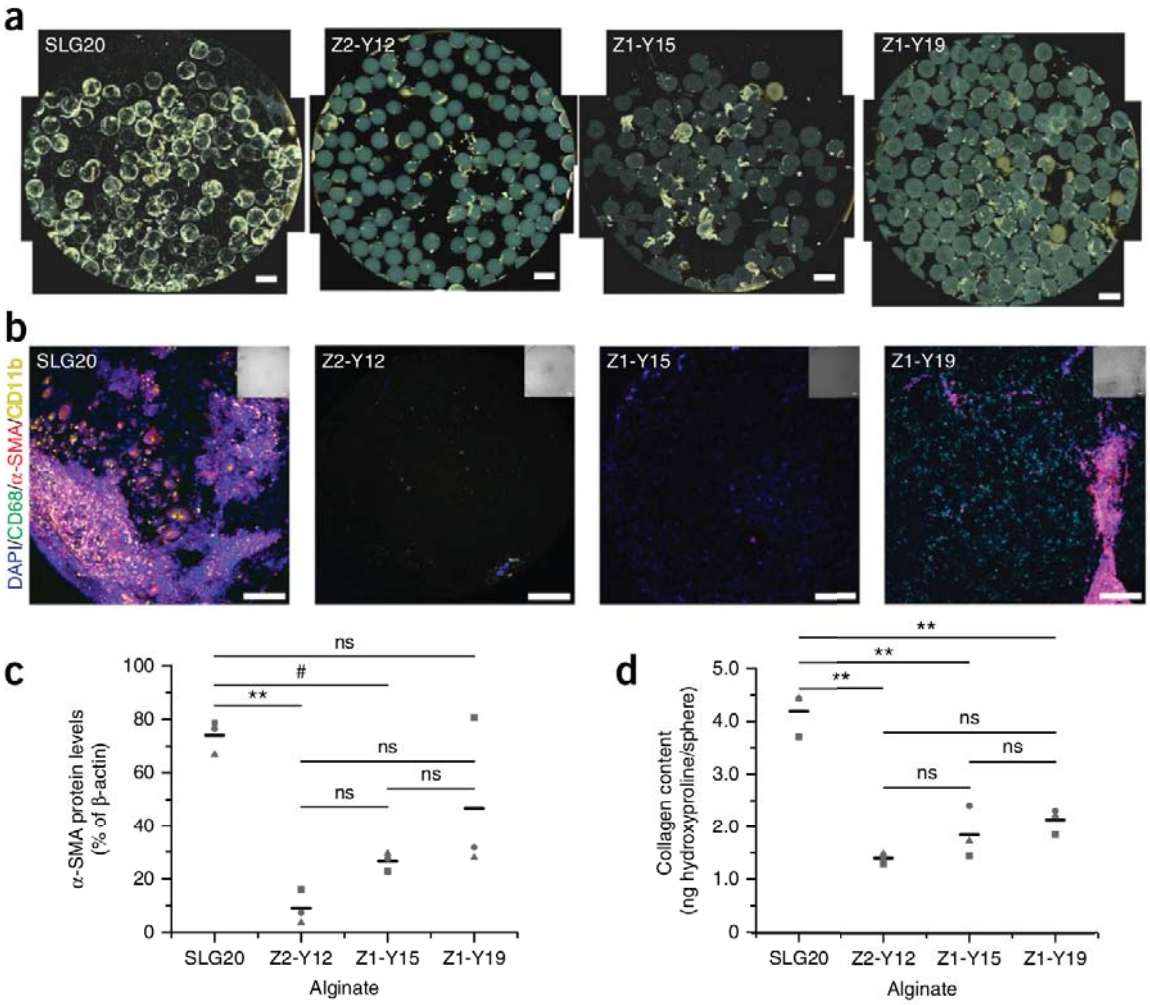

Figure 2. Modified hydrogels mitigate foreign body response in non-human primates. Z2-Y12, Z1-Y15 and Z1-Y19 alginate spheres significantly reduce fibrosis in cynomolgus macaques, while conventional SLG20 alginate spheres become fibrotic. **a** Phase contrast imaging of spheres retrieved after 4 weeks in the intraperitoneal space show less fibrosis on Z2-Y12, Z1-Y15 and Z1-Y19 spheres than on SLG20. Scale bars, 2,000 μm; n = 3. **b** Confocal imaging of retrieved spheres from a after 4 weeks in the intraperitoneal space show significantly less macrophage (CD68, CD11b), myofibroblast (SMA) and general cellular deposition (DAPI) on Z2-Y12 spheres. Sacle bars, 200 μm; n = 3. Brightfield images of the stained spheres are inset; scale bars, 100 μm. **c** Western-blot analysis of protein extracted from the top three alginate analog spheres and control spheres in **a**; n = 3. Blots were stained for SMA and loading was normalized to β-actin. Dots represent measurements from individual biological replicates, and lines show the average of the three replicates. One-way ANOVA with Bonferroni correction was used to allow for statistical comparison of multiple means. #P < 0.05; **P < 0.001; ns, not significant. **d** Collagen content using a hydroxyproline quantification assay of protein extracted from the top three alginate analog spheres and control spheres in **a**. n = 3. Dots represent measurements from individual biological replicates and lines show the average of the three replicates. One-way ANOVA with Bonferroni correction was used to allow for statistical comparison of multiple means. #P < 0.05; **P < 0.001; ns, not significant. Reprinted from ref. [23], with permission from Springer Nature.

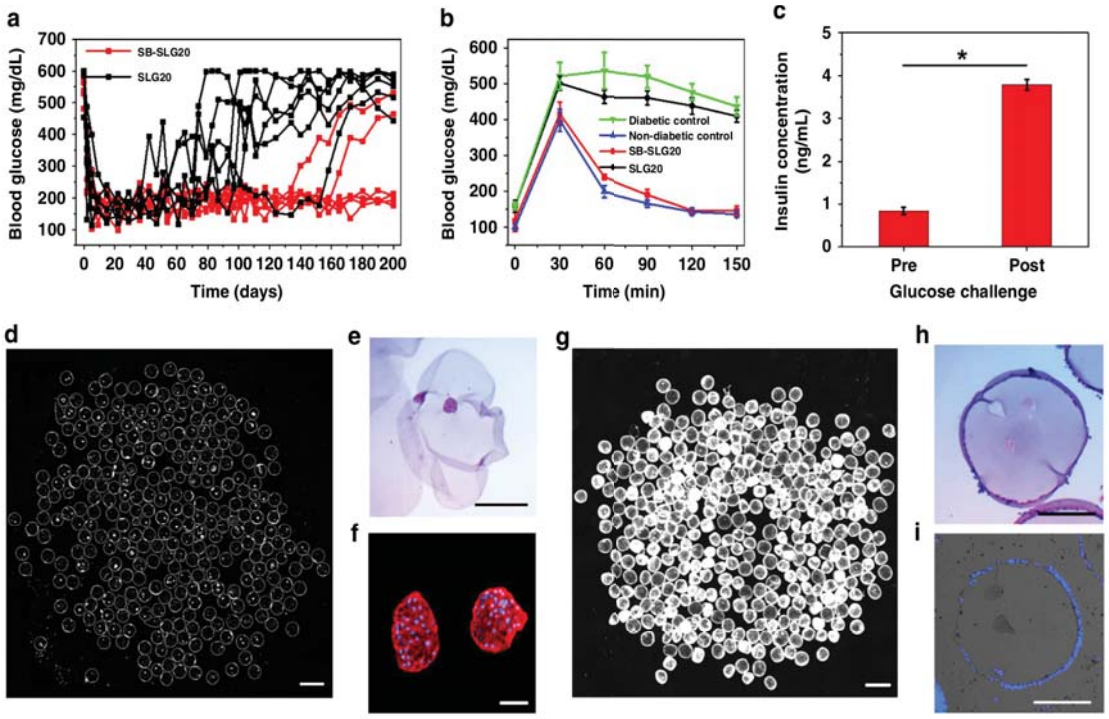

Figure 3. Sulfobetaine-alginate (SB-SLG20) microcapsules improve diabetes correction in mice in a 200-day study. a Blood glucose concentrations of mice (n = 6 mice per treatment group). **b** Intraperitoneal glucose tolerance test (IPGTT) before retrieval (n = 3). **c** *Ex vivo* glucose-stimulated insulin secretion test (GSIS) of the retrieved rat islets from SB-SLG20 microcapsules, n = 3, Mean ± SEM, *P < 0.05. **d** A dark-field phase contrast image of retrieved islet-containing SB-SLG20 microcapsules. (n = 6; scale bar, 2 mm). **e** An hematoxylin-eosin (H&E) stained cross-sectional image of retrieved islet-containing SB-SLG20 microcapsules. Scale bar, 500 µm. **f** Immunohistochemical staining of rat islets in retrieved SB-SLG20 microcapsules. Insulin is stained red and nuclei are stained blue (Scale bar: 50 µm). **g** A dark-field phase contrast image of retrieved islet-containing SLG20 microcapsules. (n = 6; scale bar, 2 mm). **h** An H&E stained cross-sectional image of retrieved islet-containing SLG20 microcapsules. Scale bar, 500 µm. **i** Immunohistochemical staining of rat islets in retrieved SLG20 microcapsules. Insulin staining is negative and nuclei are stained blue. Scale bar, 500 µm. Reprinted from ref. [25] http://creativecommons.org/licenses/by/4.0/

Microencapsulation systems based on the gelation of alginate mainly use barium and calcium as crosslinking agents and, in some cases, strontium [26]. Today there is no clear preference between calcium or barium and its use depends mainly on the protocol adopted in the different research groups. The arguments in favor of using calcium as a crosslinking ion revolve around the lower toxicity [27]. However, the resistance of the spheres cross-linked with calcium is lower than that achieved with barium, and that is why other groups opt for this option when developing their systems [23,24]. Some authors argue that, barium-cross-linked beads could be significantly less immunogenic as they do not need subsequent coatings to increase the immunoisolation, which are usually necessary when calcium is selected as the

crosslinker [28]. This last statement is still in doubt, since some studies seem to indicate that the level of immunoisolation would not be sufficient in the barium beads if they do not have posterior coatings. In addition, the *in vivo* implantation of alginate and barium beads have originated a fibrotic response to the implant in different administration routes [21]. On the other hand, the release of cross-linking ions must also be taken into account, especially when barium is selected, due to its toxicity [29].

However, despite the advantages of alginate, there are still aspects that need to be optimized. Among them its mechanical properties, since the systems made with alginate and different ions tend to undergo changes in size due to the osmotic processes that occur in the physiological environment, increasing the permeability of the capsule, weakening its structure and finally causing rupture of the system [26].

Ion concentration, the selected crosslinking agent or the alginate composition are determining factors in obtaining adequate and homogeneous gelation. Simply varying the gelling conditions, the spatial distribution of the alginate chains in the microsphere can vary from homogeneous to very heterogeneous, with up to 10 times more concentration on the surface than in the nucleus [26]. Some studies have suggested that a truly homogeneous distribution of alginate chains can only be achieved by internal and external gelation applied simultaneously [30].

Release of components from the microcapsules can also stimulate an inflammatory response. This includes degradation products that may arise from reactions occurring under physiological conditions, detachments of parts of the system or ion exchange, among others. Alginate is subjected to hydrolytic and enzymatic degradation. It has been described to have a very low rate of hydrolysis at physiological pH and the low molecular weight chains released are excreted via the urinary tract. These degradation processes have been extensively studied, *in vitro* and *in vivo* [31,32], in the subcutaneous space, the peritoneum and in some areas of the brain.

Some groups have devised strategies to improve the mechanical stability of alginate hydrogels, covalently crosslinking it with different polymers, via photocrosslinking solutions or enzymatic reactions, for example [33-35]. In a recent

study, sodium alginate was functionalized, with cross-reactive PEG derivatives presenting a terminal thiol and carbon electrophile functionalities, and the spheres formed by a combination of Ca-alginate interactions and sulfur-carbon covalent bonds. The resulting spheres showed greater mechanical resistance and better preserved shape, compared to the simple alginate and calcium beads. When these spheres were implanted in the intraperitoneal space of immunocompetent mice, tissue adherence was not observed and integrity was not compromised in the 30 days of the study [36]. In another interesting study, it was shown that modifying the alginate with 2-aminomethyl methacrylate hydrochloride can decrease immune reactions against the implant. The authors performed a first ionic crosslinking, followed by the application of UV light to form the covalent bonds. This showed greater mechanical stability when it was evaluated *in vivo* for 3 weeks [37].

Material selection is especially demanding in this type of system since the resulting particles must not only have a high durability after implantation, they must also be capable of responding to the biological needs of the immobilized cells for long periods of time. However, many materials, such as alginate, do not have cellular signaling motifs and must be biofunctionalized to improve their interaction with encapsulated cells. In this regard, in recent years, different proteins — such as collagen, laminin or fibronectin — or small short peptides — such as RGD (arginine-glycine-aspartic acid) — have been incorporated into microcapsules, trying to imitate the physical and biomechanical characteristics of the native environment of the encapsulated cells to improve and control cellular behavior [38-41]. In this regard, there are divided opinions on whether it is more appropriate to use complete extracellular matrix proteins, such as fibronectin or collagen, or small synthetic peptides, such as RGD [42,43]. Interestingly, the best strategy in every case seem to be strongly cell-dependent.

For example, Garate *et al.* evaluated the influence of RGD functionalization of alginate encapsulating C_2C_{12} myoblasts, baby hamster kidney (BHK) fibroblast or mesenchymal stromal cells (MSCs) and the results showed different optimal concentrations of RGD in every case [42,44,45]. In this sense, Gonzalez-Pujana *et al.* designed a sensitive analytical tool that permits the evaluation of different

cell adhesion kinetics, but also the integrin profiling and their contribution to cell attachment and adhesion strengthening via clustering, which allows the design of specific biofunctionalization strategies depending on the cell type [46].

Other components of the extracellular matrix (ECM), such as hyaluronic acid (HA) have also been added to the alginate matrix of microcapsules. Recently, pancreatic pseudo-islets derived from MSCs were immobilized in alginate-HA microcapsules and the results showed better cell viability, with lower levels of initial apoptosis[47]. Moreover, the inclusion of HA in the alginate matrix, enhanced the differentiation of the MSCs towards pancreatic progenitors and increased the insulin release [48,49].

2.1.2. Coating materials

In some cases, and depending on the application, the microbeads composed of different biomaterials and cells, are the final product to be administered. However, the obtained pore size in most cases is too large and does not present a real barrier against the threats that the implant will face once implanted. Therefore, many groups coat these beads with different polymers to elaborate microcapsules that control the molecules and cells that can come into contact with the immobilized cells. Currently, this filtering is carried out by defining a minimum molecular weight — molecular weight cut-off (MWCO) — of solute that is totally excluded by the semipermeable membrane [50]. This definition can be misleading since molecules of similar molecular weight can have very different sizes, as is the case with proteins and polysaccharides.

Today, there is still no consensus regarding what should be the most optimal criterion for the exclusion of molecules that can access the interior of the microcapsule, despite Chick *et al.* already named the concept of the immuno-barrier in 1977 [51]. Adequately defining this concept is essential to develop biocompatible and biotolerable systems and it should be a priority issue.

To create a biocompatible and biotolerable environment, the semipermeable membrane must first avoid contact of the encapsulated cells with the cellular components of the immune system and the antibodies. A MWCO of around 70 kDa

seem to be adequate for many drug delivery applications, but it has been found that this is not enough if bi-directional flow of antigenic, chemotactic and cytotoxic molecules — such as reactive oxygen species or pro-inflammatory cytokines — is allowed. With the classic approach of size-exclusion, low molecular weight molecules such as IL-1β (17.5 kDa) or TNF-α (51 kDa) will be able to easily access the interior of the capsule and cause damage to the encapsulated cells, as they are even smaller than some of the therapeutic molecules that are usually released from these systems. On the other hand, encapsulated cells secrete antigens — e.g. chemokines as low as 8-13 kDa in molecular weight — to the exterior of the microcapsules that are responsible for recruiting cells from the host immune system.

For the elaboration of the semi-permeable membrane, different polymers have been used, such as chitosan, oligo-chitosan or poly(methylene-co-guanidine) (PMCG), but both in preclinical studies and in human trials, the most used molecules are poly-L-lysine (PLL) and poly-L-ornithine (PLO) [52-54]. However, both molecules are known to be immunogenic, so many groups choose to add a last layer of alginate on the particles to mask the positive charges that would otherwise be exposed to the components of the immune system. Resulting microcapsules are known as APA (alginate-poly-L-lysine-alginate or alginate-poly-L-ornithine-alginate) [55,56]. This strategy has been intensely debated since there are studies showing that this second layer of alginate may not be sufficient to inactivate all the exposed positive charges [57-59]. In fact, the studies carried out to analyze the surface of the microcapsules coated with these polycations, showed that these molecules are exposed — and in great quantity — in the outermost 1-2 monolayers of the membrane, thus the outer alginate layer appears to overlap with the PLL layer, rather than form an additional outer membrane [60,61]. In addition, both polycations show limited physicochemical properties but most works chose PLO for apparently having greater mechanical stability, biocompatibility and permeability [58].

The increased immunogenicity of microcapsules coated with this type of polycations is mainly due to the physicochemical changes that affect protein adhesion on the surface of the microcapsules, such as zeta potential, hydrophobicity or roughness. On the one hand, the zeta potential of this type of implant must be

negative and similar to that of the membranes of adjacent cells. In a study carried out by De Vos *et al.* [62], it was found that the zeta potential of APA-PLL microcapsules showed a more negative value before they were implanted. Although all the values were less negative than those described in other studies for the uncoated alginate microbeads [63]. On the other hand, in a study carried out by Lekka *et al.* [64], a lower surface roughness, of less than 1 nm deep, was associated with the uncoated alginate microspheres and with the PLL-coated microcapsules, compared to much higher values, of up to 14.4 nm, of PMCG-sulfate coated microcapsules. Finally, the addition of coatings to the alginate microbeads increases the hydrophobicity of the system [58], although the type of alginate used in each case also influences the final result.

Taking into account the obvious need to improve the coatings of these particles, in recent years several groups have analyzed other molecules that may be appropriate, both to substitute the PLL/PLO molecules or in combination with them [65-67]. In a recent study, genipin was used in association with PLL [68]. Using force spectroscopy-based simultaneous topographical and mechanical characterization to study polymer to polymer interaction, the study concluded that genipin crosslinking avoided membrane detachment in alginate microspheres with double polycation coatings.

Attempts have also been made to improve the biocompatibility of the microcapsules by coating them with polymers capable of reducing protein adsorption and the fibrotic response to the implant. By coating the alginate microcapsules with hydrophilic polymers such as PEG [69-71], the biocompatibility of the implant can be improved, although the level of protein adsorption will depend on the density, length and conformation of its chains. In one study, alginate-PEG microcapsules containing allogenic islets were evaluated and their biocompatibility was improved when transplanted into the intraperitoneal space, but not into the epididymal fat pad [72]. The strategy of coating the alginate microcapsules with PEG and rapamycin, evaluated by another group, was also able to reduce macrophage proliferation and fibrotic response [73].

Modifying the surface of the microcapsules with a patented macromolecular heparin conjugate has also been shown to improve biocompatibility and significantly reduce the fibrotic response against the implant, in syngeneic and allogeneic transplant models [74]. With a similar strategy, but coating the alginate microcapsules with the C-X-C motif chemokine 12 (CXCL12) (also known as "stroma-derived factor 1", SDF-1), the biocompatibility was also improved but, in this case, a long-term improvement in xenogeneic pancreatic islet survival and functionality was also achieved, due to the recruitment of immunosuppressive regulatory T cells to the implant site [75]. Recently, in another study, coating the alginate spheres with chitosan also significantly reduced the fibrotic response against the implant, improving its biocompatibility, while maintaining glucose levels for one year, in a canine allogeneic transplant model and in a xenotransplant in rodents [76].

Another strategy that may be very interesting is to incorporate motifs that have anti-inflammatory properties into the microcapsule. Sulfated alginates [77] or the interleukin-1 receptor (IL-1R) [78] are good examples of this, as they decrease the production of some cytokines and improve the viability of encapsulated cells.

In some systems, such as those made by the alginate-PLL combination, it is not possible to independently adjust the mechanical stability and the permeability of the microcapsules, which is a notable limitation [79]. However, there are studies in which this permeability-stiffness relationship has been divided using various polymers [80]. The possibility of independently modifying critical parameters for cell encapsulation, such as capsule size, thickness, mechanical resistance and membrane permeability, offers great advantages in the design of this type of system.

Poor mechanical resistance can lead to protrusion of encapsulated cells, a phenomenon that needs to be fixed when designing these systems [81]. In this sense, Johnson *et al*. carried out an analysis quantifying cell protrusion in alginate microcapsules, coated with PLL and 50% hydrolyzed poly(methylvinylether-alt-maleic anhydride) (PMM). According to the results obtained, around 30% of the encapsulated INS-1E β cells were located in the last 20μm of the alginate-PLL-PMM50 layer, with 7% of the cells protruding [82]. Reinforcing the capsules with cross-linked shells may help preventing cell exposure and scape.

Lastly, in some cases, for example if the secreted molecule is especially large, it will be necessary to optimize the system so that it allows the passage of the therapeutic molecule out of the capsule, without compromising the protection of the encapsulated cells. In this sense, recently Montanucci *et al*. modified the permeability of alginate microcapsules to allow the continuous secretion of immunoglobulin M (IgM), with no signs of inflammation [83].

2.2. Cell source and target pathology

Both allogenic and xenogeneic cells have been incorporated into the microencapsulation systems. In case of human origin cells, their acquisition can be complicated and expensive. Besides, they can be subject to biological, ethical and legal limitations. Therefore, the use of xenogeneic cells has spread in the field of cell microencapsulation, thanks to the immunoisolation produced by the semipermeable membrane [84]. However, the systems used to date to encapsulate both cell types have been practically identical, without taking into account that the different immunological responses caused by allogenic or xenogenic cells require capsular configurations capable of protecting the cellular content against variable immunological environments.

In the case of allogeneic transplants, it is probably sufficient to avoid contact between the encapsulated cells and the cells of the host's immune system [85]. Therefore, the simplest microcapsules of cations and alginate, without great limitations in the diffusion of molecules, may be suitable. When a xenotransplantation is performed, the scenario is more complex and the simplest systems may not be effective in avoiding immune rejection **(Figure 4)**. These cells produce xenogenic epitopes, such as galactosyl (Gal) residues, that are secreted outside the capsule and are recognized by the immune system of higher mammals, including humans. In addition, in recent years the role of N-glycolyl neuraminic acid (Neu5Gc), another pig xenoantigen, is being studied as a possible obstacle in xenotransplantation [86].

The complexes formed by Gal residues and the antibodies linked to them, are powerful activators of the classical complement pathway. As these complexes begin to accumulate on the capsular surface, chemotaxis of different cell types, such

as neutrophils [87] occurs, which initiate powerful inflammatory reactions. During this first phase, many small cytokines are able to cross the semipermeable membrane of the microcapsules, causing damage to the encapsulated cells.

Following the first innate response, a second IgM-mediated [87] delayed hypersensitivity response to xenogeneic epitopes begins, promoting the recruitment of new cells of the immune system to the implant site and the secretion of more chemokines and cytokines. After these events, the microcapsules are usually surrounded by inflammatory cells and fibroblasts that hinder the passage of nutrients and oxygen, compromising the survival of the encapsulated cells. Finally, the appearance of fibrosis can lead to total isolation of the implant.

Due to these differences between allo and xenografts, the latter require systems that protect encapsulated cells against more potent threats. The membranes must be less permeable and, ideally, prevent the passage of molecules produced by the immune system, while preventing the exit of hyperinflammatory xenogeneic epitopes, such as Gal residues.

Another way of activating the immune response may occur when cell necrosis appears inside the microcapsules [88] **(Figure 4)**. Unfortunately, this is still quite common, when there are problems in the diffusion of nutrients and oxygen, due to insufficient permeability of the biomaterials, fibrotic processes associated with foreign body reaction or an excess of encapsulated cell mass [89]. Necrotic phenomena are directly related to damage-associated molecular patterns (DAMPs). These molecules are normally found inside the cells, but are released outside when cell damage occurs [90]. Some examples are heat shock proteins or DNA/RNA fragments. The mammalian immune system has specific receptors for this type of signals, the PRRs, such as Toll-like receptors (TLRs). The DAMPs released from the microcapsules are powerful activators of the immune system, activating inflammatory and angiogenesis processes, which mediate the release of large amounts of cytokines that jeopardize the survival of the encapsulated cells [91].

In this sense, there are different studies that tried to improve the viability of microencapsulated cells, incorporating chemical compounds capable of generating oxygen [92,93] or through strategies that promote the vascularization of the implant.

For the latter, several strategies have been tested. On the one hand, the ability of different angiogenesis-inducing growth factors, such as fibroblast growth factor (FGF) [94,95] or vascular endothelial growth factor (VEGF) [96,97] has been exploited to promote the neovascularization of the implant, thus improving the results of the therapy . On the other hand, the implantation of the microcapsules in pre-vascularized spaces is also considered as a beneficial option, either generated in the host's organism or in macrodevices [98,99].

Even if the risks associated with xenotransplantation are being reduced, the advances in the field of stem cell use have unlocked an unthinkable potential. The ability to differentiate human stem cells, from different sources, to obtain the desired cell type or the possibility of reprogramming adult cells to induced pluripotent stem cells (iPSCs) [100,101] have defined the path to a sufficient source of human cells. Furthermore, in the particular case of iPSCs, there are not ethical restrictions [102].

In this vein, the studies carried out to date have shown that it is possible to obtain fully functional beta cells or pancreatic progenitors, starting from human pluripotent stem cells (hPSCs) — either human embryonic stem cells (hESCs) [103-108] or iPSC [109]. In recent years, these cells, known as human stem cell derived β cells (SC-β), have been seen as an excellent source of unlimited pancreatic cells [25,106,110]. For example, Vegas *et al.* implanted human SC-β, immobilized on alginate beads, in the intraperitoneal space of immunocompetent C57BL/6J mice previously treated with streptozocin. C-peptide levels and blood glucose concentration showed therapeutically relevant results up to 174 days, without immunosuppressive treatment [111]. In another recent study, the maturation of SC-β was stimulated by forming aggregates, similar in size to pancreatic islets, which make them respond to glucose stimulation in just 3 days after transplantation [112].

Likewise, stem cells from other origins, such as amniotic fluid or adipose tissue, can also be transformed into insulin-producing cells, which can be encapsulated and transplanted in diabetic animal models to normalize blood glucose values [113,114]. For example, Montanucci *et al.* managed to remit hyperglycemia in diabetic mice, implanting human umbilical cord Wharton jelly-derived mesenchymal stem cells (hUCMS), immobilized in alginate and PLO microcapsules [115].

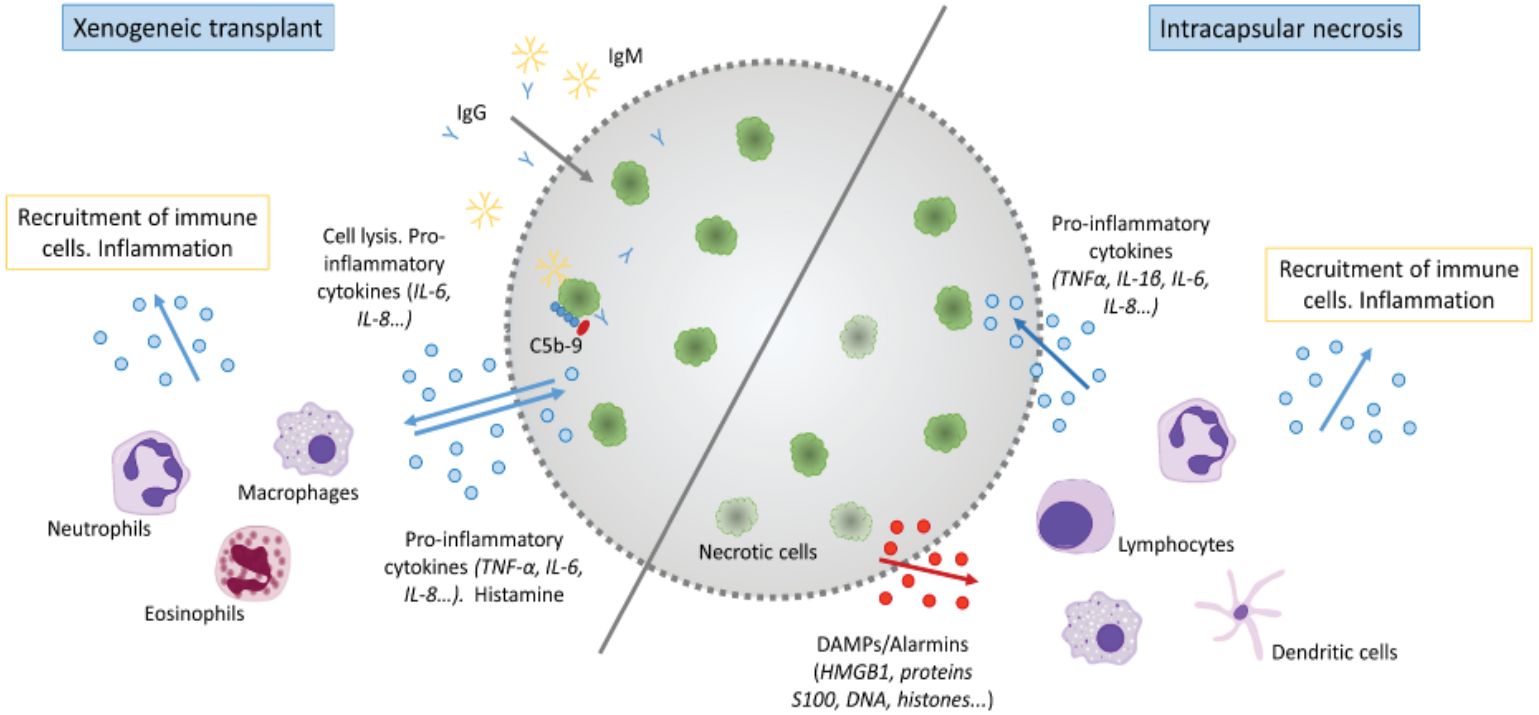

Figure 4. Pro-inflamatory molecule secretion from the microcapsules activates the immune response in different scenarios. Xenogeneic transplant. Some antibodies are able to enter the capsule or contact the encapsulated cells located in the most superficial layers of the implant. These antibodies recognize sequences that are not present in the host species, such as the Gal carbohydrate in the case of primates, and this leads to the activation of complement pathways. This activation produces direct cell lysis and the release of molecules that promote inflammation and the recruitment of immune cells, such as neutrophils, to the implant site. The recruited cells release small cytokines that can cross the microcapsule membrane and damage the encapsulated cells. In more advanced phases, fibrotic processes appear, which could end up isolating the implant and compromising the supply of nutrients and oxygen to the interior of the capsule. **Intracapsular necrosis.** Necrotic cells release the so-called DAMPs or alarmins , such as high-mobility group box-1 (HMGB1), heat shock proteins (HSPs), S100 proteins, DNA/RNA fragments etc., to the extracellular fluid. These small molecules can diffuse outside the microcapsules and activate cells of the immune system, such as macrophages, dendritic cells, neutrophils or lymphocytes, binding PRRs, such as TLRs. These cells, in response, will secrete pro-inflammatory cytokines, such as IL-1β, IL-6, interleukin-8 (IL-8), or TNF-α, which will produce inflammation and recruit more immune cells to the area. These molecules can enter the microcapsules and damage the encapsulated cells. If the situation persists over time, the adaptive immune response may be activated.

MSCs have demonstrated to be very suitable for their use in cell encapsulation systems, due to their hypoimmunogenic and immunomodulatory characteristics [116-118]. These cells inhibit immune responses by secreting cytokines and soluble growth factors that produce a local immunosuppressive effect in the surrounding cells. In recent studies, efforts have focused on analyzing the behavior of immortalized MSCs, genetically modified to secrete erythropoietin (EPO), for the treatment of anemia [45,119-121]. In addition, their benefits have also been evaluated in hepatic pathologies [122,123], as an alternative to porcine hepatocytes [124,125]. Moreover, MSCs not only are a very interesting option as a secretory cell [45,120], but also as a co-encapsulated auxiliary cell [126-129]. In a recent study, pancreatic islets and MSCs were co-encapsulated in alginate and PEG microcapsules and implanted into the intraperitoneal space of a diabetic mouse model [130]. The results showed that MSCs interact with N-cadherin and increase insulin secretion, in addition to providing structural support to the islets, improving their viability and functionality.

2.3. Microcapsule size and shape

The optimal size for cell microencapsulation systems remains a matter of debate. On the one hand, it is evident that a larger capsule size could be an obstacle for the diffusion of nutrients and oxygen. This would lead the encapsulated cells to situations of hypoxia and cell death, as well as to slower responses to the stimuli from their environment [131]. In fact, in a recent study, it was suggested that, in the case of pancreatic islets, the maximum distance between these and the extracapsular fluid should not be more than 100 μm, to allow adequate exchange of nutrients and oxygen [132].

Therefore, many have been the studies aimed at obtaining smaller capsules. Coaxial air flow and flow focusing technologies were presented as attractive alternatives to the usual methods of making microcapsules by means of electrostatic dripping, making it possible to manufacture capsules of 100-200 μm in diameter, that allow for more complicated routes of administration, such as intracranial administration or even intravitreal [133,134]. Furthermore, trying to reduce the size of the capsules as much as possible, in recent years nanoencapsulation strategies

have also been evaluated — such as conformal coating or layer-by-layer coating —, especially for the immunoprotection of the islets of Langerhans [117].

Conformal coating is a form of non-spherical encapsulation that reduces the diffusion distance and the volume of the implant [135]. However, the process often involves multiple steps that can cause damage to the encapsulated cells, and a conclusion has not yet been reached regarding whether these type of coatings are thick enough for their use in clinical practice [136,137]. Some studies [138] have suggested that the conformal coating has a lower immunoprotective capacity, compared to hydrogel microcapsules, but in recent years several new strategies have demonstrated the potential of this technology [139-141].

In case of layer-by-layer coatings, layers of polymers of opposite charges alternate on the surface of a group of cells, decreasing the biomaterial/cell ratio and thus improving the diffusion. In theory, this strategy should improve some of the most characteristic limitations of conformal coatings, such as inadequate mechanical stability or limited immunoprotection. Layer-by-layer coatings have been evaluated in several studies in rodents [142-144] and in a recent study in non-human primates, encapsulated pancreatic islets with 3 layers of PEG had 100% survival during 150 days after xenotransplantation — with immunosuppressive treatment —[145,146].

However, the polymers used to nanoencapsulate therapeutic cells are usually less biocompatible than other hydrogels normally used in the field of cell microencapsulation. Furthermore, the shape and roughness of the implant surface produce notable differences in the immune response that it causes. Therefore, in nanoencapsulation, it might be interesting to add a second type of coating that attenuates the shapes and complements the system [147].

On the other hand, and in opposition to the idea of reducing size as much as possible, Veiseh *et al.* published a complete study analyzing the influence of the size of the alginate microspheres (containing or not Langerhans islets) in rodents and non-human primates. Their conclusions, validated also with other materials such as ceramics, metals and plastics, indicated that the larger microspheres (1.5 mm) had a smaller number of immune system cells and fibrotic processes in all cases [148] **(Figure 5)**. This has led to an opinion division among the experts in the field [22].

In fact, some of them have criticized that the study did not take into account the degree of purity of the alginate used, one of the factors considered key to predict the expected inflammatory response [149].

2.4. Implant site and administration procedure

The choice of a suitable implant site can greatly determine its biocompatibility and viability. Ideally, this space should be large enough to accommodate the required number of microcapsules and easily accessible for implant removal. Likewise, the neovacularization of the implant must be favored, while the immune response must be limited to avoid an excessive fibrotic response that may condition the supply of nutrients and oxygen to the microencapsulated cells. In this sense, when a systemic effect is pursued, the intraperitoneal and subcutaneous cavities appear as simple and minimally invasive routes [32,150]. In fact, most of the studies with pancreatic islets have focused on the intraperitoneal route, despite the high activity of macrophages and the need for larger numbers of cells compared to other areas [151]. However, the neovascularization capacity in these two pathways is not sufficient in some cases, resulting in inadequate therapeutic molecule release pharmacokinetics and a shortage of nutrients and oxygen for encapsulated cells, especially when pancreatic islets are used [21,147]. In this case, the hepatic and renal subcapsular cavities are considered to have some advantages over the intraperitoneal or the subcutaneous spaces [151,152].

In recent years, preserving the benefits of the intraperitoneal route but improving the disadvantages, in some studies the surgery to create an omental pouch has been proposed. This surgery can ensure a space large enough to accommodate the necessary number of microcapsules, with greater vascularization and improving one of the main problems of biped hosts: the aggregation of the spheres in the lower part of the peritoneum, which increases the shortage of nutrients and oxygen to the implant. This strategy has demonstrated its long-term benefits, keeping diabetic rodents in normoglycemia [153]. More recently, Bochenek *et al.* described the implantation of allogeneic pancreatic cells encapsulated in alginate beads in a similar omental pouch in non-human primates [24] **(Figure 6)**.

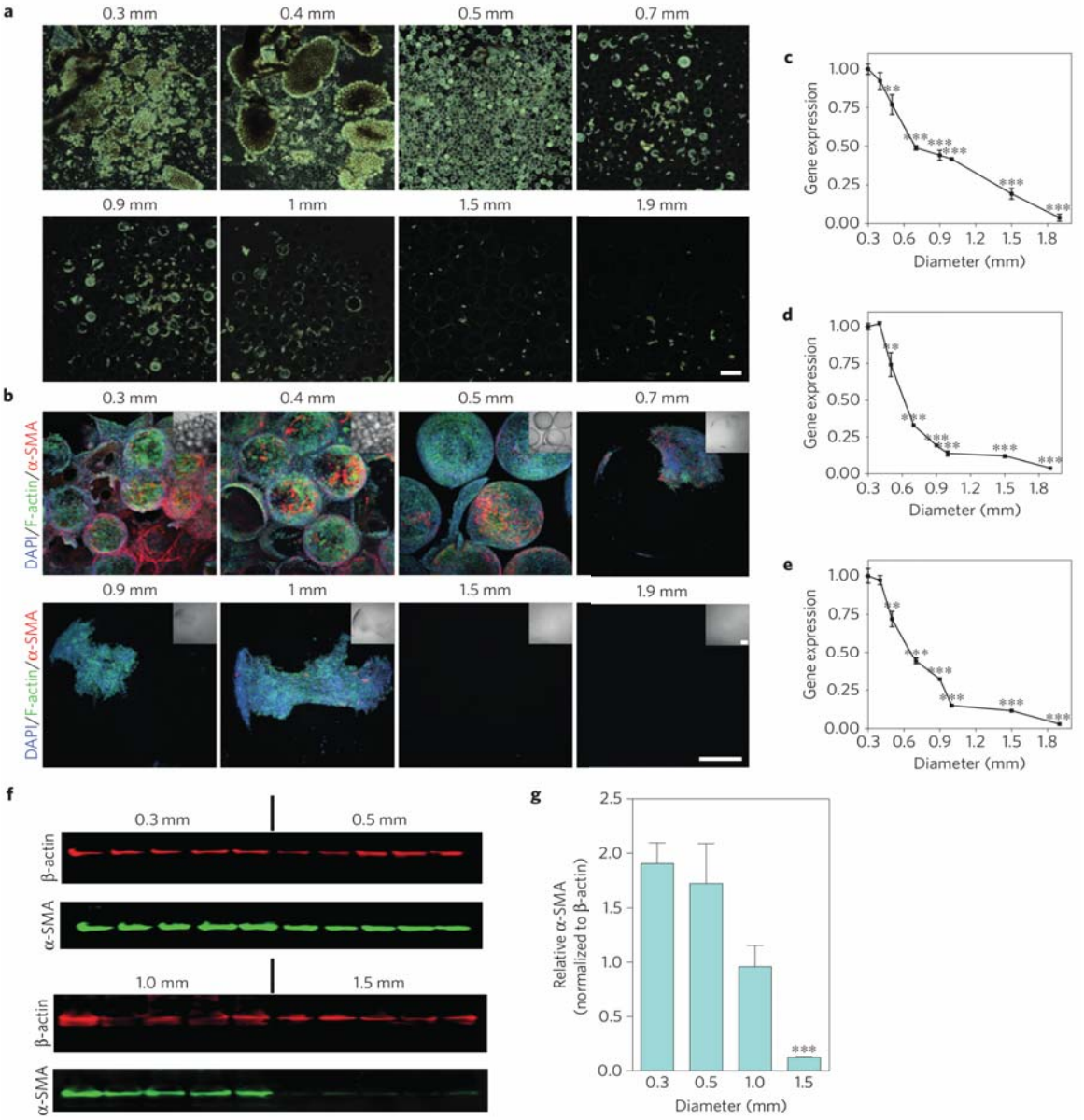

Figure 5. Increasing alginate sphere size results in reduced cellular deposition and fibrosis formation on the spheres. SLG20 alginate spheres (0.5ml in volume) of different sizes (0.3, 0.4, 0.5, 0.6, 0.7, 1, 1.5 and 1.9 mm) were implanted into the intraperitoneal space of C57BL/6 mice, where they were retained for 14 days and analyzed for degree of fibrosis upon retrieval. **a** Dark phase contrast images obtained from retrieved spheres reveal a significant decrease in level of cellular overgrowth with increase in sphere size; scale bar = 2mm. **b** Z-stacked confocal images of retrieved spheres immunofluorescence stained with DAPI (highlighting cellular nuclei), phalloidin (highlighting F-actin) and α-Smooth Muscle Actin (α-SMA, myofibroblast cells); Scale bar = 300 μm. **c** q-PCR based expression analysis of fibrotic markers α-SMA, **d** collagen 1a1 and **e** collagen 1a2 directly on the 8 various sized (0.3, 0.4, 0.5, 0.7, 0.9, 1, 1.5, 1.9 mm) spheres plotted normalized to relative expression levels on 300 μm sized spheres. **f** Semi-quantitative western-blot analysis of α-SMA expression in cell overgrowth from on microspheres (1-5 labeling of bands corresponds to individual mice). **g** Plot of analyzed band intensities from western blot images shown in **f.** Error bars, mean ± SEM. N = 5 mice per treatment. All experiments were performed at least three times. qPCR and western blot statistical analysis; one-way ANOVA with Bonferroni multiple comparison correction *:$p < 0.05$, **: $p < 0.001$, and ***: $p < 0.0001$. Reprinted from ref. [148] with permission from Springer Nature.

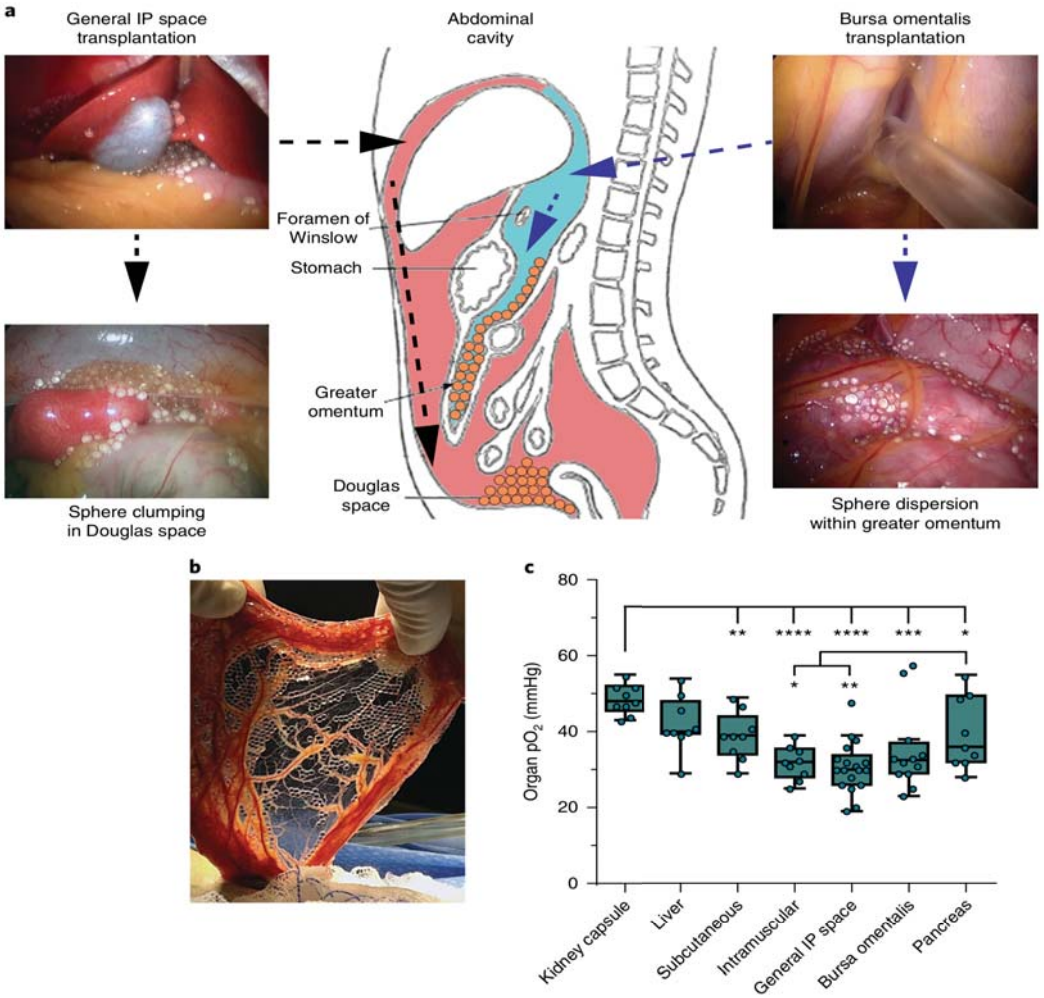

Figure 6. Transplantation method (general IP space VS. bursa omentalis) causes differential spatial distribution of the Z1-Y15 alginate spheres post-implantation. a General intraperitoneal space transplantation: Z1-Y15 spheres were laparoscopically distributed around the left and right medial lobes of the liver within the intraperitoneal space (pink) (I). At 1-month post-implantation, the non-fibrosed spheres had settled and clumped within the Douglas space (II). Bursa omentalis transplantation: the stomach was lifted with a laparoscopic grasper and a small incision was made into an avascular section of the gastrocoli ligament. The Z1-Y15 spheres were then infused into the bursa omentalis (blue) (III). At 1-month post-implantation, the Z1-Y15 spheres remained spatially dispersed within the bilayer of the greater omentum (IV). A schematic of the two transplantation methods provides the location of the anatomical sites and a summary of the spatial distribution of the Z1-Y15 spheres during the 1-month retrievals (center). The general IP space transplantation was repeated independently for n = 10 NHP and the bursa omentalis transplantation for n = 7 with resultant similar spatial distributions. **b** The greater omentum was extracted through the supra umbilical midline incision at 1 month and shows translucent, unattached Z1-Y15 spheres with encapsulated allogeneic islets within the omental tissue bilayer. **c** Partial oxygen pressures (pO2) of various transplantation sites that have been previously investigated for encapsulated islet transplantation. The kidney capsule has the highest pO2 measurements compared to the other anatomical sites. The intramuscular space (rectus abdominis) and general IP space have lower pO2 compared to the pancreas, liver, subcutaneous and kidney capsule. The bursa omentalis site was not found to be statistically significantly different than the pancreas or the general IP space. (* $p < 0.05$; one-way analysis of variance (ANOVA) with Fisher´s LSD for multiple comparisons; 3 steady-state measurements were taken for each anatomical site from the same primate; n = 3 NHP; box and whisker with median, upper and lower quartile ranges, outliers, 1.5 x IQR, individual data points overlaid). Reprinted from ref. [24] with permission from Springer Nature.

Regarding the renal subcapsular space, although the vascularization in this area is greater than in other areas, the space is more limited and it is difficult to administer the necessary large implant volumes. As a mere example, in a study carried out in 7 macaca fascicularis xenotransplanted in the renal subcapsular space with microencapsulated pancreatic islets, porcine C-peptide was detectable in 2 of the animals for 60 days after administration [154].

Finally, regarding the subcutaneous route, some authors argue that it may still be attractive due to some remarkable advantages such as being less invasive, allowing the easy monitoring and retrieval of the implant and showing a lower immunogenic activity [21].

On the other hand, when a local release of the therapeutic molecule is sought, the administration must be carried out near the target tissue. Clear examples of this are the eye [155] or CNS [156], in which the natural barriers prevent the systemic administration. These two routes are considered to be immune-privileged and thus lower immunological responses are expected after implantation. Another situation that requires local administration is when the objective of the microencapsulated cells is the conversion of a prodrug into an active molecule, exclusively near a tumor, to avoid the adverse events derived from a systemic exposure [157].

In any case, the viability of the implant will largely depend on the lack of any fibrotic capsule that could isolate the encapsulated cells. In order to reduce the fibrotic response, some groups have described the benefits of concomitant administration of immunosuppressive molecules locally or temporarily, just a few days after implantation. The incorporation of drugs, such as ketoprofen or dexamethasone within the microcapsules has been tested in several studies, in which the fibrotic response has been reduced [158-160]. More recently, the CXCL12 molecule was co-encapsulated together with SC-β derived from hPSCs, with the aim of reducing the fibrotic pericapsular response, in the absence of systemic or local immunosuppressive treatments. CXCL12 produced an increase in insulin secretion by the encapsulated cells and the implant remained viable for more than 150 days in immunocompetent mice [161]. The same strategy was also used in non-human primates (n = 4) but the results are still preliminary [162].

3. BIOSAFETY: DOSE CONTROL, MONITORIZATION AND EXTRACTION

Once the implant has been placed, real-time monitoring of its location and correct operation can give us valuable information. The exact location of the microcapsules can be determined by cellular labeling with fluorescent dyes or radiolabels [163,164], traditional imaging systems, such as ultrasounds [165] or, more commonly, by high resolution and contrast magnetic resonance imaging (MRI) [166-170]. There are different types of contrast materials that can be used with these techniques. One of the most studied examples are the superparamagnetic iron oxide nanoparticles (SPIO) [171].

It is also possible to detect microcapsules by X-ray, if we encapsulate contrast agents such as barium sulfate or bismuth sulfide, which make them opaque [172]. In one study, a method based on gold nanoparticles was developed as a contrast agent to monitor alginate microcapsules by X-ray and micro-CT [173] techniques. The same group demonstrated that it is possible to detect alginate microcapsules both in vitro and in vivo, through low exposure to X-rays, if they are coated with gold nanoparticles [174]. On the other hand, different groups have found other innovative ways to monitor implanted microcapsules. For example, researchers have recently developed a type of microcapsule with intrinsic capacity for *in vivo* imaging by incorporating genipin into its own design [175]. Taking advantage of the natural fluorescence of this compound, they demonstrated the linear correlation between the implanted microcapsule volume and the signal emitted by the microcapsules for several weeks. Thus, through this strategy, it is possible to assess the actual injected dose — volume of microcapsules — after administration and monitor the position of the implant over time, which improves in a remarkable manner the biosafety and efficacy of the therapy **(Figure 7).**

Molecular imaging techniques not only allow us to monitor the exact location of the implant, but also to simultaneously confirm the viability and functionality of the encapsulated cells by including reporter genes that emit fluorescent and/or bioluminescent signals [176-178]. These techniques provide us with quantitative and real-time information, in a non-invasive way. Recently, Spanoudaki *et al.* combined

fluorine MRI and unsupervised machine learning to monitor over time the spatial arrangement and the oxygen content of implants encapsulating pancreatic islets *in vivo* [179].

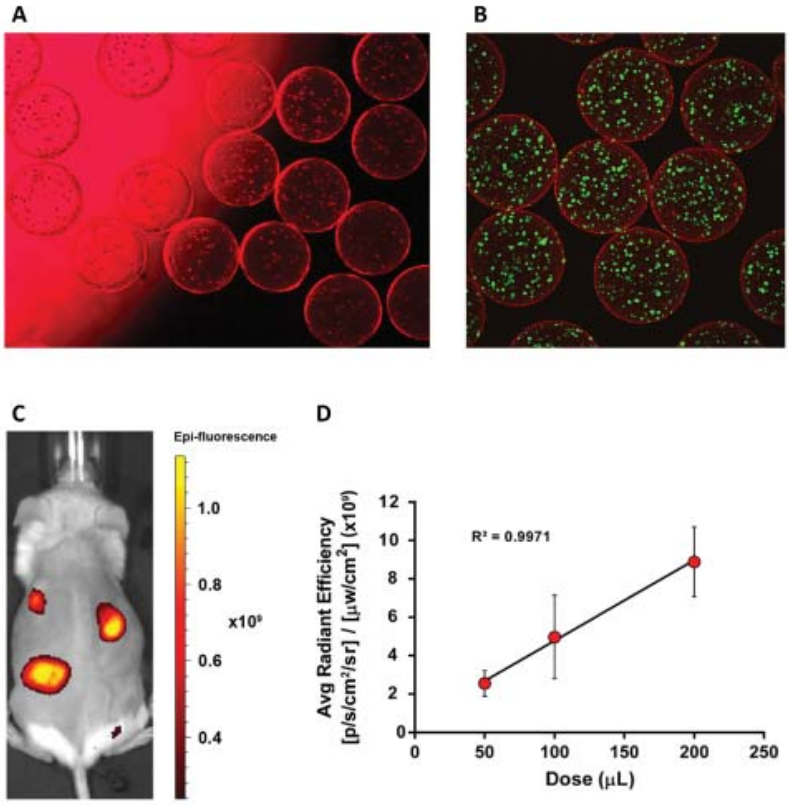

Figure 7. Monitoring implantable immunoisolation devises with intrinsic fluorescence of genipin. **A** Representative epifluorescence micrograph. **B** Representative confocal fluorescence image of cells encapsulated in genipin-cross-linked double poly-L-Lysine membrane (GDP) microcapsules and probed with LIVE/DEAD viability kit (Green, living cells; Red, dead cells) 14 days after encapsulation. **C** Representative image of a mouse 21 days after injection of GDP microcapsules. The fluorescence from the microcapsules was imaged with 570 nm excitation and 620 nm emission. Scale bar denotes range of photons displayed on a pseudocolor scale with yellow and dark red denoting highest and lowest values, respectively. **D** Graph displays dose-dependent response of average radiant efficiency for GDP microcapsules. Reprinted from ref. [175], Copyright 2018, with permission from John Wiley and Sons.

Regarding biosafety, another critical point may occur at the end of the therapy, or in an event where significant adverse effects are detected. In these situations, a system that allows us to ensure a total inactivation and/or removal of the implant can be necessary. For such aim, one of the main strategies is the inclusion of suicide genes into the genome of the encapsulated cells [180-182]. The enzyme-activated prodrug mechanism, thymidine kinase/ganciclovir system that targets actively dividing cells is the most frequently studied gene therapy strategy [182]. However,

these strategy could present some disadvantages when the encapsulated cells are in a slowly dividing state. In order to improve this problem, Wong *et al.* equipped glial cell-derived neurotrophic factor (GDNF)-secreting cells with a proliferation independent Tet-on regulated pro-caspase 8 apoptotic gene switch for a safer ocular drug delivery [183,184].

Recently, Delcassian *et al.* developed functionalized iron oxide nanoparticle-loaded alginate microcapsules that enabled graft retrieval under an applied magnetic field [185]. In addition, this system facilitates graft localization via MRI. These capsules containing islets were evaluated both *in vitro* and *in vivo*, in immunocompetent diabetic mice, and they were able to restore normoglycemia for at least 6 weeks. The application of a magnetic field for 90 s, 24h after implantation, allowed the retrieval of up to 94% of the transplant volume.

On the other hand, there is the possibility of introducing the microcapsules in a physical support that prevents their dispersion. These retention elements can be, for example, cements based on calcium phosphate or hydrogels of different composition. Acarregui *et al.* managed to improve the administration, retention and extraction of the APA microcapsules, administering them in injectable or preformed alginate hydrogels. Likewise, this system significantly reduced the post-implant inflammation that normally occurs in the first days after administration [160].

Finally, in some cases, in order to avoid the need to remove the implant after treatment, biodegradable systems that can be eliminated when necessary could be the best option [186].

The field of synthetic biology has opened new perspectives for cell microencapsulation technologies. Using genetic engineering techniques, it is possible to reprogram the metabolic activities of eukaryotic cells so that they produce the therapeutic molecule at the right time. The secretion can be activated by a specific inducer or even in direct response to the needs of the patient [187-189] — when working with more advanced systems —, capable of interpreting and reacting to various pathophysiological stimuli [190,191]. Taking control over the therapeutic molecule expression levels allows us to administer the necessary dose, increasing the efficacy and minimizing adverse events.

Finally, when these functionalities are incorporated into encapsulated cells, an adequate control over the system is mandatory, avoiding possible genetic construct-transfers to the host's cells or checking that these systems do not interfere with the metabolic processes of the host.

4. CONCLUDING REMARKS AND FUTURE PROSPECTS

The clinical application of cell microencapsulation technologies has remained elusive for decades, even if the first clinical trials took place more than 20 years ago [192]. One of the most limiting factors slowing their development is the great variability between the protocols used. This, together with the lack of detail in the descriptions of the materials and processes used, makes the comparison between systems and the extraction of solid conclusions very complicated.

In recent years, the improvements made in the alginate — either by optimized purification protocols [14-17] or the recent proposals to modify its chemical structure [23] — and the emergence of stem cell therapies, have greatly improved key biocompatibility issues, taking the technology an step forward in terms of efficacy.

In the upcoming years, cell microencapsulation technologies are expected to finally reach the market, but their success will depend on their ability to meet the strict regulations applied to cellular therapies and the possibility to set up large-scale practices that allow the safe and efficient production of the microcapsules. Even if there are still some aspects that need to be optimized, the extensive work carried out to date, in terms of improving key aspects such as efficacy and biosafety, have taken cell microencapsulation technologies closer than ever to the clinical practice.

5. ACKNOWLEDGEMENTS

Authors gratefully acknowledge the ICTS "NANBIOSIS", specifically by the Drug Formulation Unit (U10) of the CIBER-BBN at the University of Basque Country UPV/EHU in Vitoria-Gasteiz. Tania B. Lopez-Mendez thanks the Basque Government (Department of Education, Universities and Research) for the Ph.D. fellowship.

6. DECLARATION OF INTEREST

The authors declare no competing financial interest.

7. REFERENCES

[1] Gonzalez-Pujana A, Santos E, Orive G, Pedraz JL, Hernandez RM. Cell microencapsulation technology: Current vision of its therapeutic potential through the administration routes. J Drug Deliv Sci Tec 2017; DOI: 10.1016/j.jddst.2017.03.028

[2] Farina M, Alexander JF, Thekkedath U, Ferrari M, Grattoni A. Cell encapsulation: Overcoming barriers in cell transplantation in diabetes and beyond. Adv Drug Deliv Rev 2019; DOI: S0169-409X(18)30080-2

[3] Orive G, Santos E, Pedraz JL, Hernandez RM. Application of cell encapsulation for controlled delivery of biological therapeutics. Adv Drug Deliv Rev 2014; DOI: 10.1016/j.addr.2013.07.009

[4] Orive G, Santos E, Poncelet D, Hernández RM, Pedraz JL, Wahlberg LU et al. Cell encapsulation: technical and clinical advances. Trends Pharmacol Sci 2015; DOI: 10.1016/j.tips.2015.05.003)

[5] Rokstad AM, Lacik I, de Vos P, Strand BL. Advances in biocompatibility and physico-chemical characterization of microspheres for cell encapsulation. Adv Drug Deliv Rev 2014; DOI: 10.1016/j.addr.2013.07.010

[6] Olabisi RM. Cell microencapsulation with synthetic polymers. J Biomed Mater Res A 2015; DOI: 10.1002/jbm.a.35205

[7] de Vos P, Lazarjani HA, Poncelet D, Faas MM. Polymers in cell encapsulation from an enveloped cell perspective. Adv Drug Deliv Rev 2014; DOI: 10.1016/j.addr.2013.11.005

[8] Lee KY and Mooney DJ. Alginate: properties and biomedical applications. Prog Polym Sci 2012; DOI: 10.1016/j.progpolymsci.2011.06.003

[9] Tam SK, Dusseault J, Bilodeau S, Langlois G, Halle JP, Yahia L. Factors influencing alginate gel biocompatibility. J Biomed Mater Res A 2011; DOI: 10.1002/jbm.a.33047

[10] Tam SK, Dusseault J, Polizu S, Menard M, Halle JP, Yahia L. Impact of residual contamination on the biofunctional properties of purified alginates used for cell encapsulation. Biomaterials 2006; DOI: S0142-9612(05)00796-9

[11] Paredes-Juarez GA, de Haan BJ, Faas MM, de Vos P. A Technology Platform to Test the Efficacy of Purification of Alginate. Materials 2014; DOI: 10.3390/ma7032087

[12] Krishnan R, Ko D, Foster CE,3rd, Liu W, Smink AM, de Haan B et al. Immunological Challenges Facing Translation of Alginate Encapsulated Porcine Islet Xenotransplantation to Human Clinical Trials. Methods Mol Biol 2017; DOI: 10.1007/978-1-4939-6364-5_24

[13] Dorrington MG and Fraser IDC. NF-kappaB Signaling in Macrophages: Dynamics,

Crosstalk, and Signal Integration. Front Immunol 2019; DOI: 10.3389/fimmu.2019.00705

[14] Klock G, Frank H, Houben R, Zekorn T, Horcher A, Siebers U et al. Production of purified alginates suitable for use in immunoisolated transplantation. Appl Microbiol Biotechnol 1994; DOI: 10.1007/bf00173321

[15] De Vos P, De Haan BJ, Wolters GH, Strubbe JH, Van Schilfgaarde R. Improved biocompatibility but limited graft survival after purification of alginate for microencapsulation of pancreatic islets. Diabetologia 1997; DOI: 10.1007/s001250050673

[16] Prokop A and Wang TG. Purification of polymers used for fabrication of an immunoisolation barrier. Ann N Y Acad Sci 1997; DOI: 10.1111/j.1749-6632.1997.tb52197.x

[17] Sondermeijer HP, Witkowski P, Woodland D, Seki T, Aangenendt FJ, van der Laarse A et al. Optimization of alginate purification using polyvinylidene difluoride membrane filtration: Effects on immunogenicity and biocompatibility of three-dimensional alginate scaffolds. J Biomater Appl 2016; DOI: 0885328216645952

[18] Menard M, Dusseault J, Langlois G, Baille WE, Tam SK, Yahia L et al. Role of protein contaminants in the immunogenicity of alginates. J Biomed Mater Res B Appl Biomater 2010; DOI: 10.1002/jbm.b.31570

[19] Paredes-Juarez GA, de Haan BJ, Faas MM, de Vos P. The role of pathogen-associated molecular patterns in inflammatory responses against alginate based microcapsules. J Control Release 2013; DOI: 10.1016/j.jconrel.2013.09.009

[20] Kim AR, Hwang JH, Kim HM, Kim HN, Song JE, Yang YI et al. Reduction of inflammatory reaction in the use of purified alginate microcapsules. J Biomater Sci Polym Ed 2013; DOI: 10.1080/09205063.2012.735100

[21] Vaithilingam V, Bal S, Tuch BE. Encapsulated Islet Transplantation: Where Do We Stand?. Rev Diabet Stud 2017; DOI: 10.1900/RDS.2017.14.51

[22] Calafiore R. Microencapsulation for cell therapy of type 1 diabetes mellitus: The interplay between common beliefs, prejudices and real progress. J Diabetes Investig 2018; DOI: 10.1111/jdi.12788

[23] Vegas AJ, Veiseh O, Doloff JC, Ma M, Tam HH, Bratlie K et al. Combinatorial hydrogel library enables identification of materials that mitigate the foreign body response in primates. Nat Biotechnol 2016; DOI: 10.1038/nbt.3462

[24] Bochenek MA, Veiseh O, Vegas AJ, McGarrigle JJ, Qi M, Marchese E et al. Alginate encapsulation as long-term immune protection of allogeneic pancreatic islet cells transplanted into the omental bursa of macaques. Nat Biomed Eng 2018; DOI: 10.1038/s41551-018-0275-1

[25] Liu Q, Chiu A, Wang LH, An D, Zhong M, Smink AM et al. Zwitterionically modified alginates mitigate cellular overgrowth for cell encapsulation. Nat Commun 2019; DOI: 10.1038/s41467-019-13238-7

[26] Morch YA, Donati I, Strand BL, Skjak-Braek G. Effect of Ca2+, Ba2+, and Sr2+ on

alginate microbeads. Biomacromolecules 2006; DOI: 10.1021/bm060010d

[27] Basta G, Montanucci P, Luca G, Boselli C, Noya G, Barbaro B et al. Long-term metabolic and immunological follow-up of nonimmunosuppressed patients with type 1 diabetes treated with microencapsulated islet allografts: four cases. Diabetes Care 2011; DOI: 10.2337/dc11-0731

[28] Robles L, Storrs R, Lamb M, Alexander M, Lakey JR. Current status of islet encapsulation. Cell Transplant 2014; DOI: 10.3727/096368913X670949

[29] Morch YA, Qi M, Gundersen PO, Formo K, Lacik I, Skjak-Braek G et al. Binding and leakage of barium in alginate microbeads. J Biomed Mater Res A 2012; DOI: 10.1002/jbm.a.34237

[30] Zimmermann H, Hillgartner M, Manz B, Feilen P, Brunnenmeier F, Leinfelder U et al. Fabrication of homogeneously cross-linked, functional alginate microcapsules validated by NMR-, CLSM- and AFM-imaging. Biomaterials 2003; DOI: S0142961202006397

[31] Thanos CG, Bintz BE, Bell WJ, Qian H, Schneider PA, MacArthur DH et al. Intraperitoneal stability of alginate-polyornithine microcapsules in rats: an FTIR and SEM analysis. Biomaterials 2006; DOI: S0142-9612(06)00131-1

[32] Thanos CG, Bintz BE, Emerich DF. Stability of alginate-polyornithine microcapsules is profoundly dependent on the site of transplantation. J Biomed Mater Res A 2007; DOI: 10.1002/jbm.a.31033

[33] Gattas-Asfura KM, Fraker CA, Stabler CL. Covalent stabilization of alginate hydrogel beads via Staudinger ligation: assessment of poly(ethylene glycol) and alginate cross-linkers. J Biomed Mater Res A 2011; DOI: 10.1002/jbm.a.33162

[34] Hall KK, Gattas-Asfura KM, Stabler CL. Microencapsulation of islets within alginate/poly(ethylene glycol) gels cross-linked via Staudinger ligation. Acta Biomater 2011; DOI: 10.1016/j.actbio.2010.07.016

[35] Sun JY, Zhao X, Illeperuma WR, Chaudhuri O, Oh KH, Mooney DJ et al. Highly stretchable and tough hydrogels. Nature 2012; DOI: 10.1038/nature11409

[36] Szabo L, Gonelle-Gispert C, Montanari E, Noverraz F, Bornet A, Buhler LH et al. Cross-Reactive Alginate Derivatives for the Production of Dual Ionic–Covalent Hydrogel Microspheres Presenting Tunable Properties for Cell Microencapsulation. ACS Appl Polym Mater 2019; DOI: 10.1021/acsapm.9b00139

[37] Somo SI, Langert K, Yang CY, Vaicik MK, Ibarra V, Appel AA et al. Synthesis and evaluation of dual crosslinked alginate microbeads. Acta Biomater 2018; DOI: S1742-7061(17)30674-8

[38] Llacua A, de Haan BJ, Smink SA, de Vos P. Extracellular matrix components supporting human islet function in alginate-based immunoprotective microcapsules for treatment of diabetes. J Biomed Mater Res A 2016; DOI: 10.1002/jbm.a.35706

[39] Llacua LA, de Haan BJ, de Vos P. Laminin and collagen IV inclusion in immunoisolating

microcapsules reduces cytokine-mediated cell death in human pancreatic islets. J Tissue Eng Regen Med 2018; DOI: 10.1002/term.2472

[40] Llacua LA, Faas MM, de Vos P. Extracellular matrix molecules and their potential contribution to the function of transplanted pancreatic islets. Diabetologia 2018; DOI: 10.1007/s00125-017-4524-8

[41] Llacua LA, Hoek A, de Haan BJ, de Vos P. Collagen type VI interaction improves human islet survival in immunoisolating microcapsules for treatment of diabetes. Islets 2018; DOI: 10.1080/19382014.2017.1420449

[42] Santos E, Garate A, Pedraz JL, Orive G, Hernandez RM. The synergistic effects of the RGD density and the microenvironment on the behavior of encapsulated cells: in vitro and in vivo direct comparative study. J Biomed Mater Res A 2014; DOI: 10.1002/jbm.a.35073

[43] Sayyar B, Dodd M, Marquez-Curtis L, Janowska-Wieczorek A, Hortelano G. Cell-matrix Interactions of Factor IX (FIX)-engineered human mesenchymal stromal cells encapsulated in RGD-alginate vs. fibrinogen-alginate microcapsules. Artif Cells Nanomed Biotechnol 2014; DOI: 10.3109/21691401.2013.794354

[44] Garate A, Santos E, Pedraz JL, Hernández RM, Orive G. Evaluation of different RGD ligand densities in the development of cell-based drug delivery systems. J Drug Target 2015; DOI: 10.3109/1061186X.2015.1020428

[45] Garate A, Ciriza J, Casado JG, Blazquez R, Pedraz JL, Orive G et al. Assessment of the Behavior of Mesenchymal Stem Cells Immobilized in Biomimetic Alginate Microcapsules. Mol Pharm 2015; DOI: 10.1021/acs.molpharmaceut.5b00419

[46] Gonzalez-Pujana A, Santos-Vizcaino E, García-Hernando M, Hernaez-Estrada B, de Pancorbo M,M., Benito-Lopez F et al. Extracellular matrix protein microarray-based biosensor with single cell resolution: Integrin profiling and characterization of cell-biomaterial interactions. Sensors Actuators B: Chem 2019; DOI: 10.1016/j.snb.2019.126954

[47] Canibano-Hernandez A, Saenz Del Burgo L, Espona-Noguera A, Orive G, Hernandez RM, Ciriza J et al. Hyaluronic acid enhances cell survival of encapsulated insulin-producing cells in alginate-based microcapsules. Int J Pharm 2019; DOI: S0378-5173(18)30980-3

[48] Cañibano-Hernández A, Saenz Del Burgo L, Espona-Noguera A, Orive G, Hernández RM, Ciriza J et al. Alginate Microcapsules Incorporating Hyaluronic Acid Recreate Closer in Vivo Environment for Mesenchymal Stem Cells. Mol Pharm 2017; DOI: 10.1021/acs.molpharmaceut.7b00295

[49] Cañibano-Hernández A, Saenz Del Burgo L, Espona-Noguera A, Orive G, Hernández RM, Ciriza J et al. Hyaluronic Acid Promotes Differentiation of Mesenchymal Stem Cells from Different Sources toward Pancreatic Progenitors within Three-Dimensional Alginate Matrixes. Mol Pharm 2019; DOI: 10.1021/acs.molpharmaceut.8b01126

[50] de Vos P, Bucko M, Gemeiner P, Navratil M, Svitel J, Faas M et al. Multiscale requirements for bioencapsulation in medicine and biotechnology. Biomaterials 2009; DOI:

10.1016/j.biomaterials.2009.01.014

[51] Chick WL, Perna JJ, Lauris V, Low D, Galletti PM, Panol G et al. Artificial pancreas using living beta cells: effects on glucose homeostasis in diabetic rats. Science 1977; DOI: 10.1126/science.407649

[52] Orive G, Hernandez RM, Gascon AR, Igartua M, Pedraz JL. Development and optimisation of alginate-PMCG-alginate microcapsules for cell immobilisation. Int J Pharm 2003; DOI: S0378517303002011

[53] Haque T, Chen H, Ouyang W, Martoni C, Lawuyi B, Urbanska AM et al. In vitro study of alginate-chitosan microcapsules: an alternative to liver cell transplants for the treatment of liver failure. Biotechnol Lett 2005; DOI: 10.1007/s10529-005-0687-3

[54] Ponce S, Orive G, Hernandez R, Gascon AR, Pedraz JL, de Haan BJ et al. Chemistry and the biological response against immunoisolating alginate-polycation capsules of different composition. Biomaterials 2006; DOI: S0142-9612(06)00432-7

[55] Kendall WF,Jr and Opara EC. Polymeric Materials for Perm-Selective Coating of Alginate Microbeads. Methods Mol Biol 2017; DOI: 10.1007/978-1-4939-6364-5_7

[56] Hajifathaliha F, Mahboubi A, Nematollahi L, Mohit E, Bolourchian N. Comparison of different cationic polymers efficacy in fabrication of alginate multilayer microcapsules. Asian J Pharm Sci 2020; DOI: 10.1016/j.ajps.2018.11.007

[57] Rokstad AM, Brekke OL, Steinkjer B, Ryan L, Kollarikova G, Strand BL et al. Alginate microbeads are complement compatible, in contrast to polycation containing microcapsules, as revealed in a human whole blood model. Acta Biomater 2011; DOI: 10.1016/j.actbio.2011.03.011

[58] Tam SK, Bilodeau S, Dusseault J, Langlois G, Halle JP, Yahia LH. Biocompatibility and physicochemical characteristics of alginate-polycation microcapsules. Acta Biomater 2011; DOI: 10.1016/j.actbio.2010.12.006

[59] Rokstad AM, Brekke OL, Steinkjer B, Ryan L, Kollarikova G, Strand BL et al. The induction of cytokines by polycation containing microspheres by a complement dependent mechanism. Biomaterials 2013; DOI: 10.1016/j.biomaterials.2012.10.012

[60] Tam SK, Dusseault J, Polizu S, Menard M, Halle JP, Yahia L. Physicochemical model of alginate-poly-L-lysine microcapsules defined at the micrometric/nanometric scale using ATR-FTIR, XPS, and ToF-SIMS. Biomaterials 2005; DOI: S0142-9612(05)00387-X

[61] van Hoogmoed CG, Busscher HJ, de Vos P. Fourier transform infrared spectroscopy studies of alginate-PLL capsules with varying compositions. J Biomed Mater Res A 2003; DOI: 10.1002/jbm.a.10086

[62] de Vos P, Spasojevic M, de Haan BJ, Faas MM. The association between in vivo physicochemical changes and inflammatory responses against alginate based microcapsules. Biomaterials 2012; DOI: 10.1016/j.biomaterials.2012.04.039

[63] You JO, Park SB, Park HY, Haam S, Chung CH, Kim WS. Preparation of regular sized

Ca-alginate microspheres using membrane emulsification method. J Microencapsul 2001; DOI: 10.1080/02652040010018128

[64] Lekka M, Sainz-Serp D, Kulik AJ, Wandrey C. Hydrogel microspheres: influence of chemical composition on surface morphology, local elastic properties, and bulk mechanical characteristics. Langmuir 2004; DOI: 10.1021/la048389h

[65] Arifin DR, Long CM, Gilad AA, Alric C, Roux S, Tillement O et al. Trimodal gadolinium-gold microcapsules containing pancreatic islet cells restore normoglycemia in diabetic mice and can be tracked by using US, CT, and positive-contrast MR imaging. Radiology 2011; DOI: 10.1148/radiol.11101608

[66] Hillberg AL, Kathirgamanathan K, Lam JB, Law LY, Garkavenko O, Elliott RB. Improving alginate-poly-L-ornithine-alginate capsule biocompatibility through genipin crosslinking. J Biomed Mater Res B Appl Biomater 2013; DOI: 10.1002/jbm.b.32835

[67] Hillberg AL, Oudshoorn M, Lam JB, Kathirgamanathan K. Encapsulation of porcine pancreatic islets within an immunoprotective capsule comprising methacrylated glycol chitosan and alginate. J Biomed Mater Res B Appl Biomater 2015; DOI: 10.1002/jbm.b.33185

[68] Virumbrales-Muñoz M, Santos-Vizcaino E, Paz L, Gallardo-Moreno A, Orive G, Hernandez RM et al. Force spectroscopy-based simultaneous topographical and mechanical characterization to study polymer-to-polymer interactions in coated alginate microspheres. Sci Rep 2019; DOI: 10.1038/s41598-019-56547-z

[69] Zheng J, Xie H, Yu W, Tan M, Gong F, Liu X et al. Enhancement of surface graft density of MPEG on alginate/chitosan hydrogel microcapsules for protein repellency. Langmuir 2012; DOI: 10.1021/la302615t

[70] Spasojevic M, Paredes-Juarez GA, Vorenkamp J, de Haan BJ, Schouten AJ, de Vos P. Reduction of the inflammatory responses against alginate-poly-L-lysine microcapsules by anti-biofouling surfaces of PEG-b-PLL diblock copolymers. PLoS One 2014; DOI: 10.1371/journal.pone.0109837

[71] Spasojevic M, Bhujbal S, Paredes G, de Haan BJ, Schouten AJ, de Vos P. Considerations in binding diblock copolymers on hydrophilic alginate beads for providing an immunoprotective membrane. J Biomed Mater Res A 2014; DOI: 10.1002/jbm.a.34863

[72] Villa C, Manzoli V, Abreu MM, Verheyen CA, Seskin M, Najjar M et al. Effects of Composition of Alginate-Polyethylene Glycol Microcapsules and Transplant Site on Encapsulated Islet Graft Outcomes in Mice. Transplantation 2017; DOI: 10.1097/TP.0000000000001454

[73] Park HS, Kim JW, Lee SH, Yang HK, Ham DS, Sun CL et al. Antifibrotic effect of rapamycin containing polyethylene glycol-coated alginate microcapsule in islet xenotransplantation. J Tissue Eng Regen Med 2017; DOI: 10.1002/term.2029

[74] Vaithilingam V, Kollarikova G, Qi M, Larsson R, Lacik I, Formo K et al. Beneficial effects of coating alginate microcapsules with macromolecular heparin conjugates-in vitro

and in vivo study. Tissue Eng Part A 2014; DOI: 10.1089/ten.TEA.2013.0254

[75] Chen T, Yuan J, Duncanson S, Hibert ML, Kodish BC, Mylavaganam G et al. Alginate encapsulant incorporating CXCL12 supports long-term allo- and xenoislet transplantation without systemic immune suppression. Am J Transplant 2015; DOI: 10.1111/ajt.13049

[76] Yang HK, Ham DS, Park HS, Rhee M, You YH, Kim MJ et al. Long-term Efficacy and Biocompatibility of Encapsulated Islet Transplantation With Chitosan-Coated Alginate Capsules in Mice and Canine Models of Diabetes. Transplantation 2016; DOI: 10.1097/TP.0000000000000927

[77] Arlov O, Skjak-Braek G, Rokstad AM. Sulfated alginate microspheres associate with factor H and dampen the inflammatory cytokine response. Acta Biomater 2016; DOI: S1742-7061(16)30292-6

[78] Su J, Hu BH, Lowe WL,Jr, Kaufman DB, Messersmith PB. Anti-inflammatory peptide-functionalized hydrogels for insulin-secreting cell encapsulation. Biomaterials 2010; DOI: 10.1016/j.biomaterials.2009.09.045

[79] Wang T, Lacik I, Brissova M, Anilkumar AV, Prokop A, Hunkeler D et al. An encapsulation system for the immunoisolation of pancreatic islets. Nat Biotechnol 1997; DOI: 10.1038/nbt0497-358

[80] Cha C, Kim SY, Cao L, Kong H. Decoupled control of stiffness and permeability with a cell-encapsulating poly(ethylene glycol) dimethacrylate hydrogel. Biomaterials 2010; DOI: 10.1016/j.biomaterials.2010.02.059

[81] Bhujbal SV, de Haan B, Niclou SP, de Vos P. A novel multilayer immunoisolating encapsulation system overcoming protrusion of cells. Sci Rep 2014; DOI: 10.1038/srep06856

[82] Johnson MA, Kleinberger R, Abu Helal A, Latchminarine N, Ayyash A, Shi S et al. Quantifying cellular protrusion in alginate capsules with covalently crosslinked shells. J Microencapsul 2019; DOI: 10.1080/02652048.2019.1618404

[83] Montanucci P, Cari L, Basta G, Pescara T, Riccardi C, Nocentini G et al. Engineered Alginate Microcapsules for Molecular Therapy Through Biologic Secreting Cells. Tissue Eng Part C Methods 2019; DOI: 10.1089/ten.TEC.2018.0329

[84] Ekser B, Cooper DKC, Tector AJ. The need for xenotransplantation as a source of organs and cells for clinical transplantation. Int J Surg 2015; DOI: S1743-9191(15)00349-0

[85] Duvivier-Kali VF, Omer A, Parent RJ, O'Neil JJ, Weir GC. Complete protection of islets against allorejection and autoimmunity by a simple barium-alginate membrane. Diabetes 2001; DOI: 10.2337/diabetes.50.8.1698

[86] Tector AJ, Mosser M, Tector M, Bach J. The Possible Role of Anti-Neu5Gc as an Obstacle in Xenotransplantation. Front Immunol 2020; DOI: 10.3389/fimmu.2020.00622

[87] Dufrane D and Gianello P. Pig islet for xenotransplantation in human: structural and physiological compatibility for human clinical application. Transplant Rev 2012; DOI: 10.1016/j.trre.2011.07.004

[88] Sachet M, Liang YY, Oehler R. The immune response to secondary necrotic cells. Apoptosis 2017; DOI: 10.1007/s10495-017-1413-z

[89] Komatsu H, Kandeel F, Mullen Y. Impact of Oxygen on Pancreatic Islet Survival. Pancreas 2018; DOI: 10.1097/MPA.0000000000001050

[90] Ashimova A, Yegorov S, Negmetzhanov B, Hortelano G. Cell Encapsulation Within Alginate Microcapsules: Immunological Challenges and Outlook. Front Bioeng Biotechnol 2019; DOI: 10.3389/fbioe.2019.00380

[91] Paredes-Juarez GA, Sahasrabudhe NM, Tjoelker RS, de Haan BJ, Engelse MA, de Koning EJP et al. DAMP production by human islets under low oxygen and nutrients in the presence or absence of an immunoisolating-capsule and necrostatin-1. Sci Rep 2015; DOI: 10.1038/srep14623

[92] Papas KK, De Leon H, Suszynski TM, Johnson RC. Oxygenation strategies for encapsulated islet and beta cell transplants. Adv Drug Deliv Rev 2019; DOI: S0169-409X(19)30052-3

[93] Cristea D, Krishtul S, Kuppusamy P, Baruch L, Machluf M, Blank A. New approach to measuring oxygen diffusion and consumption in encapsulated living cells, based on electron spin resonance microscopy. Acta Biomater 2020; DOI: S1742-7061(19)30711-1

[94] Moya ML, Garfinkel MR, Liu X, Lucas S, Opara EC, Greisler HP et al. Fibroblast growth factor-1 (FGF-1) loaded microbeads enhance local capillary neovascularization. J Surg Res 2010; DOI: 10.1016/j.jss.2009.06.003

[95] Pareta R, McQuilling JP, Sittadjody S, Jenkins R, Bowden S, Orlando G et al. Long-term function of islets encapsulated in a redesigned alginate microcapsule construct in omentum pouches of immune-competent diabetic rats. Pancreas 2014; DOI: 10.1097/MPA.0000000000000107

[96] Marchioli G, Luca AD, de Koning E, Engelse M, Van Blitterswijk CA, Karperien M et al. Hybrid Polycaprolactone/Alginate Scaffolds Functionalized with VEGF to Promote de Novo Vessel Formation for the Transplantation of Islets of Langerhans. Adv Healthc Mater 2016; DOI: 10.1002/adhm.201600058

[97] Yin N, Han Y, Xu H, Gao Y, Yi T, Yao J et al. VEGF-conjugated alginate hydrogel prompt angiogenesis and improve pancreatic islet engraftment and function in type 1 diabetes. Mater Sci Eng C Mater Biol Appl 2016; DOI: S0928-4931(15)30540-3

[98] Pepper AR, Gala-Lopez B, Pawlick R, Merani S, Kin T, Shapiro AM. A prevascularized subcutaneous device-less site for islet and cellular transplantation. Nat Biotechnol 2015; DOI: 10.1038/nbt.3211

[99] Tomei AA. Engineering Confined and Prevascularized Sites for Islet Transplantation. Transplantation 2018; DOI: 10.1097/TP.0000000000002290

[100] Takahashi K and Yamanaka S. Induction of pluripotent stem cells from mouse embryonic and adult fibroblast cultures by defined factors. Cell 2006; DOI: S0092-8674(06)00976-7

[101] Horiguchi I, Chowdhury MM, Sakai Y, Tabata Y. Proliferation, morphology, and pluripotency of mouse induced pluripotent stem cells in three different types of alginate beads for mass production. Biotechnol Prog 2014; DOI: 10.1002/btpr.1891

[102] Takahashi K, Tanabe K, Ohnuki M, Narita M, Ichisaka T, Tomoda K et al. Induction of pluripotent stem cells from adult human fibroblasts by defined factors. Cell 2007; DOI: S0092-8674(07)01471-7

[103] Kroon E, Martinson LA, Kadoya K, Bang AG, Kelly OG, Eliazer S et al. Pancreatic endoderm derived from human embryonic stem cells generates glucose-responsive insulin-secreting cells in vivo. Nat Biotechnol 2008; DOI: 10.1038/nbt1393

[104] Chayosumrit M, Tuch B, Sidhu K. Alginate microcapsule for propagation and directed differentiation of hESCs to definitive endoderm. Biomaterials 2010; DOI: 10.1016/j.biomaterials.2009.09.071

[105] Richardson T, Kumta PN, Banerjee I. Alginate encapsulation of human embryonic stem cells to enhance directed differentiation to pancreatic islet-like cells. Tissue Eng Part A 2014; DOI: 10.1089/ten.TEA.2013.0659

[106] Pagliuca FW, Millman JR, Gurtler M, Segel M, Van Dervort A, Ryu JH et al. Generation of functional human pancreatic beta cells in vitro. Cell 2014; DOI: 10.1016/j.cell.2014.09.040

[107] Rezania A, Bruin JE, Arora P, Rubin A, Batushansky I, Asadi A et al. Reversal of diabetes with insulin-producing cells derived in vitro from human pluripotent stem cells. Nat Biotechnol 2014; DOI: 10.1038/nbt.3033

[108] Richardson T, Barner S, Candiello J, Kumta PN, Banerjee I. Capsule stiffness regulates the efficiency of pancreatic differentiation of human embryonic stem cells. Acta Biomater 2016; DOI: 10.1016/j.actbio.2016.02.025

[109] Millman JR, Xie C, Van Dervort A, Gurtler M, Pagliuca FW, Melton DA. Generation of stem cell-derived beta-cells from patients with type 1 diabetes. Nat Commun 2016; DOI: 10.1038/ncomms11463

[110] Ma H, Wert KJ, Shvartsman D, Melton DA, Jaenisch R. Establishment of human pluripotent stem cell-derived pancreatic beta-like cells in the mouse pancreas. Proc Natl Acad Sci USA 2018; DOI: 10.1073/pnas.1702059115

[111] Vegas AJ, Veiseh O, Gurtler M, Millman JR, Pagliuca FW, Bader AR et al. Long-term glycemic control using polymer-encapsulated human stem cell-derived beta cells in immune-competent mice. Nat Med 2016; DOI: 10.1038/nm.4030

[112] Nair GG, Liu JS, Russ HA, Tran S, Saxton MS, Chen R et al. Recapitulating endocrine cell clustering in culture promotes maturation of human stem-cell-derived beta cells. Nat Cell Biol 2019; DOI: 10.1038/s41556-018-0271-4

[113] Chun SY, Mack DL, Moorefield E, Oh SH, Kwon TG, Pettenati MJ et al. Pdx1 and controlled culture conditions induced differentiation of human amniotic fluid-derived stem cells to insulin-producing clusters. J Tissue Eng Regen Med 2015; DOI: 10.1002/term.1631

[114] Chandra V, Swetha G, Muthyala S, Jaiswal AK, Bellare JR, Nair PD et al. Islet-like cell aggregates generated from human adipose tissue derived stem cells ameliorate experimental diabetes in mice. PLoS One 2011; DOI: 10.1371/journal.pone.0020615

[115] Montanucci P, Pescara T, Alunno A, Bistoni O, Basta G, Calafiore R. Remission of hyperglycemia in spontaneously diabetic NOD mice upon transplant of microencapsulated human umbilical cord Wharton jelly-derived mesenchymal stem cells (hUCMS). Xenotransplantation 2019; DOI: 10.1111/xen.12476

[116] Zanotti L, Sarukhan A, Dander E, Castor M, Cibella J, Soldani C et al. Encapsulated mesenchymal stem cells for in vivo immunomodulation. Leukemia 2013; DOI: 10.1038/leu.2012.202

[117] Mao AS, Özkale B, Shah NJ, Vining KH, Descombes T, Zhang L et al. Programmable microencapsulation for enhanced mesenchymal stem cell persistence and immunomodulation. Proc Natl Acad Sci USA 2019; DOI: 10.1073/pnas.1819415116

[118] Fath-Bayati L and Ai J. Assessment of mesenchymal stem cell effect on foreign body response induced by intraperitoneally implanted alginate spheres. J Biomed Mater Res A 2020; DOI: 10.1002/jbm.a.36795

[119] Gurruchaga H, Ciriza J, Saenz del Burgo L, Rodriguez-Madoz JR, Santos E, Prosper F et al. Cryopreservation of microencapsulated murine mesenchymal stem cells genetically engineered to secrete erythropoietin. Int J Pharm 2015; DOI: 10.1016/j.ijpharm.2015.02.047

[120] Lopez-Mendez TB, Santos-Vizcaino E, Blanco FJ, Pedraz JL, Hernandez RM, Orive G. Improved control over MSCs behavior within 3D matrices by using different cell loads in both in vitro and in vivo environments. Int J Pharm 2017; DOI: S0378-5173(17)30869-4

[121] Gonzalez-Pujana A, Rementeria A, Blanco FJ, Igartua M, Pedraz JL, Santos-Vizcaino E et al. The role of osmolarity adjusting agents in the regulation of encapsulated cell behavior to provide a safer and more predictable delivery of therapeutics. Drug Deliv 2017; DOI: 10.1080/10717544.2017.1391894

[122] Liu ZC and Chang TM. Intrasplenic transplantation of bioencapsulated mesenchymal stem cells improves the recovery rates of 90% partial hepatectomized rats. Stem Cells Int. 2012; DOI: 10.1155/2012/697094

[123] Meier RP, Mahou R, Morel P, Meyer J, Montanari E, Muller YD et al. Microencapsulated human mesenchymal stem cells decrease liver fibrosis in mice. J Hepatol 2015; DOI: 10.1016/j.jhep.2014.10.030

[124] Diekmann S, Glockner P, Bader A. The influence of different cultivation conditions on the metabolic functionality of encapsulated primary hepatocytes. Int J Artif Organs 2007; DOI: 10.1177/039139880703000303

[125] Harm S, Stroble K, Hartmann J, Falkenhagen D. Alginate-encapsulated human hepatoma C3A cells for use in a bioartificial liver device - the hybrid-MDS. Int J Artif Organs 2009; DOI: 49D3145D-793D-4022-9DF3-56D48E5C874A

[126] Ito T, Itakura S, Todorov I, Rawson J, Asari S, Shintaku J et al. Mesenchymal stem cell and islet co-transplantation promotes graft revascularization and function. Transplantation 2010; DOI: 10.1097/tp.0b013e3181db09c4

[127] Longoni B, Szilagyi E, Quaranta P, Paoli GT, Tripodi S, Urbani S et al. Mesenchymal stem cells prevent acute rejection and prolong graft function in pancreatic islet transplantation. Diabetes Technol Ther 2010; DOI: 10.1089/dia.2009.0154

[128] Kerby A, Jones ES, Jones PM, King AJ. Co-transplantation of islets with mesenchymal stem cells in microcapsules demonstrates graft outcome can be improved in an isolated-graft model of islet transplantation in mice. Cytotherapy 2013; DOI: 10.1016/j.jcyt.2012.10.018

[129] Vaithilingam V, Evans MDM, Lewy DM, Bean PA, Bal S, Tuch BE. Co-encapsulation and co-transplantation of mesenchymal stem cells reduces pericapsular fibrosis and improves encapsulated islet survival and function when allografted. Sci Rep 2017; DOI: 10.1038/s41598-017-10359-1

[130] Montanari E, Meier RPH, Mahou R, Seebach JD, Wandrey C, Gerber-Lemaire S et al. Multipotent mesenchymal stromal cells enhance insulin secretion from human islets via N-cadherin interaction and prolong function of transplanted encapsulated islets in mice. Stem Cell Res Ther 2017; DOI: 10.1186/s13287-017-0646-7

[131] Buchwald P, Tamayo-Garcia A, Manzoli V, Tomei AA, Stabler CL. Glucose-stimulated insulin release: Parallel perifusion studies of free and hydrogel encapsulated human pancreatic islets. Biotechnol Bioeng 2018; DOI: 10.1002/bit.26442

[132] Iwata H, Arima Y, Tsutsui Y. Design of Bioartificial Pancreases From the Standpoint of Oxygen Supply. Artif Organs 2018; DOI: 10.1111/aor.13106

[133] Kontturi LS, Yliperttula M, Toivanen P, Maatta A, Maatta AM, Urtti A. A laboratory-scale device for the straightforward production of uniform, small sized cell microcapsules with long-term cell viability. J Control Release 2011; DOI: 10.1016/j.jconrel.2011.03.005

[134] Santos E, Orive G, Calvo A, Catena R, Fernandez-Robredo P, Layana AG et al. Optimization of 100 mum alginate-poly-L-lysine-alginate capsules for intravitreous administration. J Control Release 2012; DOI: 10.1016/j.jconrel.2011.09.079

[135] Teramura Y and Iwata H. Bioartificial pancreas: Microencapsulation and conformal coating of islet of Langerhans. Adv Drug Deliv Rev 2010; DOI: 10.1016/j.addr.2010.01.005

[136] Calafiore R. Alginate microcapsules for pancreatic islet cell graft immunoprotection: struggle and progress towards the final cure for type 1 diabetes mellitus. Expert Opin Biol Ther 2003; DOI: 10.1517/14712598.3.2.201

[137] Basta G and Calafiore R. Immunoisolation of pancreatic islet grafts with no recipient's immunosuppression: actual and future perspectives. Curr Diab Rep 2011; DOI: 10.1007/s11892-011-0219-6

[138] Basta G, Sarchielli P, Luca G, Racanicchi L, Nastruzzi C, Guido L et al. Optimized parameters for microencapsulation of pancreatic islet cells: an in vitro study clueing on islet

graft immunoprotection in type 1 diabetes mellitus. Transpl Immunol. 2004; DOI: 10.1016/j.trim.2004.10.003

[139] Lou S, Zhang X, Zhang J, Deng J, Kong D, Li C. Pancreatic islet surface bioengineering with a heparin-incorporated starPEG nanofilm. Mater Sci Eng C Mater Biol Appl 2017; DOI: S0928-4931(17)30819-6

[140] Giraldo JA, Molano RD, Rengifo HR, Fotino C, Gattas-Asfura KM, Pileggi A et al. The impact of cell surface PEGylation and short-course immunotherapy on islet graft survival in an allogeneic murine model. Acta Biomater 2017; DOI: S1742-7061(16)30656-0

[141] Manzoli V, Villa C, Bayer AL, Morales LC, Molano RD, Torrente Y et al. Immunoisolation of murine islet allografts in vascularized sites through conformal coating with polyethylene glycol. Am J Transplant 2018; DOI: 10.1111/ajt.14547

[142] Zhi ZL, Kerby A, King AJ, Jones PM, Pickup JC. Nano-scale encapsulation enhances allograft survival and function of islets transplanted in a mouse model of diabetes. Diabetologia 2012; DOI: 10.1007/s00125-011-2431-y

[143] Dong H, Fahmy TM, Metcalfe SM, Morton SL, Dong X, Inverardi L et al. Immuno-isolation of pancreatic islet allografts using pegylated nanotherapy leads to long-term normoglycemia in full MHC mismatch recipient mice. PLoS One 2012; DOI: 10.1371/journal.pone.0050265

[144] Pham-Hua D, Padgett LE, Xue B, Anderson B, Zeiger M, Barra JM et al. Islet encapsulation with polyphenol coatings decreases pro-inflammatory chemokine synthesis and T cell trafficking. Biomaterials 2017; DOI: S0142-9612(17)30131-X

[145] Haque MR, Jeong JH, Byun Y. Combination strategy of multi-layered surface camouflage using hyperbranched polyethylene glycol and immunosuppressive drugs for the prevention of immune reactions against transplanted porcine islets. Biomaterials 2016; DOI: S0142-9612(16)00053-3

[146] Haque MR, Kim J, Park H, Lee HS, Lee KW, Al-Hilal TA et al. Xenotransplantation of layer-by-layer encapsulated non-human primate islets with a specified immunosuppressive drug protocol. J Control Release 2017; DOI: S0168-3659(17)30540-0

[147] Calafiore R and Basta G. Clinical application of microencapsulated islets: actual prospectives on progress and challenges. Adv Drug Deliv Rev 2014; DOI: 10.1016/j.addr.2013.09.020

[148] Veiseh O, Doloff JC, Ma M, Vegas AJ, Tam HH, Bader AR et al. Size- and shape-dependent foreign body immune response to materials implanted in rodents and non-human primates. Nat Mater 2015; DOI: 10.1038/nmat4290

[149] Hu S and de Vos P. Polymeric Approaches to Reduce Tissue Responses Against Devices Applied for Islet-Cell Encapsulation. Front Bioeng Biotechnol 2019; DOI: 10.3389/fbioe.2019.00134

[150] Dufrane D, Steenberghe M, Goebbels RM, Saliez A, Guiot Y, Gianello P. The influence

of implantation site on the biocompatibility and survival of alginate encapsulated pig islets in rats. Biomaterials 2006; DOI: S0142-9612(06)00087-1

[151] De Vos P, Wolters GH, Fritschy WM, Van Schilfgaarde R. Obstacles in the application of microencapsulation in islet transplantation. Int J Artif Organs 1993; 16(4):205-12

[152] Iwata H, Kobayashi K, Takagi T, Oka T, Yang H, Amemiya H et al. Feasibility of agarose microbeads with xenogeneic islets as a bioartificial pancreas. J Biomed Mater Res 1994; DOI: 10.1002/jbm.820280905

[153] Kobayashi T, Aomatsu Y, Iwata H, Kin T, Kanehiro H, Hisanga M et al. Survival of microencapsulated islets at 400 days posttransplantation in the omental pouch of NOD mice. Cell Transplant 2006; DOI: 10.3727/000000006783981954

[154] Dufrane D, Goebbels RM, Saliez A, Guiot Y, Gianello P. Six-month survival of microencapsulated pig islets and alginate biocompatibility in primates: proof of concept. Transplantation 2006; DOI: 10.1097/01.tp.0000208610.75997.20

[155] Orive G, Santos-Vizcaino E, Pedraz JL, Hernandez RM, Vela Ramirez JE, Dolatshahi-Pirouz A et al. 3D cell-laden polymers to release bioactive products in the eye. Prog Retin Eye Res 2019; DOI: S1350-9462(18)30025-9

[156] López-Méndez, T, Murua A, Pedraz JL, Hernandez RM, Orive G. Cell encapsulation technology: an alternative biotechnological platform for the treatment of Central Nervous System diseases. Bioencapsulation of Living Cells for Diverse Medical Applications. Bentham Science Publishers; 2012, p. 102-152.

[157] Lohr JM, Haas SL, Kroger JC, Friess HM, Hoft R, Goretzki PE et al. Encapsulated cells expressing a chemotherapeutic activating enzyme allow the targeting of subtoxic chemotherapy and are safe and efficacious: data from two clinical trials in pancreatic cancer. Pharmaceutics 2014; DOI: 10.3390/pharmaceutics6030447

[158] Ricci M, Blasi P, Giovagnoli S, Rossi C, Macchiarulo G, Luca G et al. Ketoprofen controlled release from composite microcapsules for cell encapsulation: effect on post-transplant acute inflammation. J Control Release 2005; DOI: S0168-3659(05)00292-0

[159] Bunger CM, Tiefenbach B, Jahnke A, Gerlach C, Freier T, Schmitz KP et al. Deletion of the tissue response against alginate-pll capsules by temporary release of co-encapsulated steroids. Biomaterials 2005; DOI: S0142-9612(04)00668-4

[160] Acarregui A, Herran E, Igartua M, Blanco FJ, Pedraz JL, Orive G et al. Multifunctional hydrogel-based scaffold for improving the functionality of encapsulated therapeutic cells and reducing inflammatory response. Acta Biomater 2014; DOI: 10.1016/j.actbio.2014.06.038

[161] Alagpulinsa DA, Cao JJL, Driscoll RK, Sirbulescu RF, Penson MFE, Sremac M et al. Alginate-microencapsulation of human stem cell-derived beta cells with CXCL12 prolongs their survival and function in immunocompetent mice without systemic immunosuppression. Am J Transplant 2019; DOI: 10.1111/ajt.15308

[162] Sremac M, Lei J, Penson MFE, Schuetz C, Lakey JRT, Papas KK et al. Preliminary

Studies of the Impact of CXCL12 on the Foreign Body Reaction to Pancreatic Islets Microencapsulated in Alginate in Nonhuman Primates. Transplant Direct 2019; DOI: 10.1097/TXD.0000000000000890

[163] Balhuizen A, Massa S, Mathijs I, Turatsinze JV, De Vos J, Demine S et al. A nanobody-based tracer targeting DPP6 for non-invasive imaging of human pancreatic endocrine cells. Sci Rep 2017; DOI: 10.1038/s41598-017-15417-2

[164] El-Kawy O,A. and García-Horsman J,A. 99mTc-labeled glimepiride as a tracer for targeting pancreatic β-cells mass: preparation and preclinical evaluation. J Radioanal Nucl Ch 2017; 10.1007/s10967-017-5615-1

[165] Barnett BP, Arepally A, Stuber M, Arifin DR, Kraitchman DL, Bulte JW. Synthesis of magnetic resonance-, X-ray- and ultrasound-visible alginate microcapsules for immunoisolation and noninvasive imaging of cellular therapeutics. Nat Protoc 2011; DOI: 10.1038/nprot.2011.352

[166] Gomez-Mauricio RG, Acarregui A, Sánchez-Margallo FM, Crisóstomo V, Gallo I, Hernández RM et al. A preliminary approach to the repair of myocardial infarction using adipose tissue-derived stem cells encapsulated in magnetic resonance-labelled alginate microspheres in a porcine model. Eur J Pharm Biopharm 2013; DOI: 10.1016/j.ejpb.2012.11.028

[167] Vaithilingam V, Yim MM, Foster JL, Stait-Gardner T, Oberholzer J, Tuch BE. Noninvasive Tracking of Encapsulated Insulin Producing Cells Labelled with Magnetic Microspheres by Magnetic Resonance Imaging. J Diabetes Res 2016; DOI: 10.1155/2016/6165893

[168] Zhang ZQ and Song SC. Thermosensitive/superparamagnetic iron oxide nanoparticle-loaded nanocapsule hydrogels for multiple cancer hyperthermia. Biomaterials 2016; DOI: S0142-9612(16)30401-X

[169] Adams C, Israel LL, Ostrovsky S, Taylor A, Poptani H, Lellouche JP et al. Development of Multifunctional Magnetic Nanoparticles for Genetic Engineering and Tracking of Neural Stem Cells Adv Healthc Mater 2016; DOI: 10.1002/adhm.201500885

[170] Sarkis S, Silencieux F, Markwick KE, Fortin M, Hoesli CA. Magnetic Resonance Imaging of Alginate Beads Containing Pancreatic Beta Cells and Paramagnetic Nanoparticles. ACS Biomater Sci Eng 2017; DOI: 10.1021/acsbiomaterials.7b00404

[171] Long CM and Bulte JW. In vivo tracking of cellular therapeutics using magnetic resonance imaging. Expert Opin Biol Ther 2009; DOI: 10.1517/14712590802715723

[172] Barnett BP, Kraitchman DL, Lauzon C, Magee CA, Walczak P, Gilson WD et al. Radiopaque alginate microcapsules for X-ray visualization and immunoprotection of cellular therapeutics. Mol Pharm 2006; DOI: 10.1021/mp060056l

[173] Astolfo A, Qie F, Kibleur A, Hao X, Menk RH, Arfelli F et al. A simple way to track single gold-loaded alginate microcapsules using x-ray CT in small animal longitudinal studies. Nanomedicine 2014; DOI: 10.1016/j.nano.2014.06.008

[174] Qie F, Astolfo A, Wickramaratna M, Behe M, Evans MD, Hughes TC et al. Self-assembled gold coating enhances X-ray imaging of alginate microcapsules. Nanoscale 2015; DOI: 10.1039/c4nr06692h

[175] Santos-Vizcaino E, Haley H, Gonzalez-Pujana A, Orive G, Hernandez RM, Luker GD et al. Monitoring implantable immunoisolation devices with intrinsic fluorescence of genipin. J Biophotonics 2019; DOI: 10.1002/jbio.201800170

[176] Olabisi RM, Lazard ZW, Franco CL, Hall MA, Kwon SK, Sevick-Muraca EM et al. Hydrogel microsphere encapsulation of a cell-based gene therapy system increases cell survival of injected cells, transgene expression, and bone volume in a model of heterotopic ossification. Tissue Eng Part A 2010; DOI: 10.1089/ten.TEA.2010.0234

[177] Catena R, Santos E, Orive G, Hernández RM, Pedraz JL, Calvo A. Improvement of the monitoring and biosafety of encapsulated cells using the SFGNESTGL triple reporter system. J Control Release 2010; DOI: 10.1016/j.jconrel.2010.05.018

[178] Kauer TM, Figueiredo JL, Hingtgen S, Shah K. Encapsulated therapeutic stem cells implanted in the tumor resection cavity induce cell death in gliomas. Nat Neurosci 2011; DOI: 10.1038/nn.3019

[179] Spanoudaki V, Doloff JC, Huang W, Norcross SR, Farah S, Langer R et al. Simultaneous spatiotemporal tracking and oxygen sensing of transient implants in vivo using hot-spot MRI and machine learning. Proc Natl Acad Sci USA 2019; DOI: 10.1073/pnas.1815909116

[180] Kobayashi K, Yasuhara T, Agari T, Muraoka K, Kameda M, Ji Yuan W et al. Control of dopamine-secretion by Tet-Off system in an in vivo model of parkinsonian rat. Brain Res 2006; DOI: S0006-8993(06)01158-9

[181] Di Stasi A, Tey SK, Dotti G, Fujita Y, Kennedy-Nasser A, Martinez C et al. Inducible apoptosis as a safety switch for adoptive cell therapy. N Engl J Med 2011; DOI: 10.1056/NEJMoa1106152

[182] Santos E, Larzabal L, Calvo A, Orive G, Pedraz JL, Hernandez RM. Inactivation of encapsulated cells and their therapeutic effects by means of TGL triple-fusion reporter/biosafety gene. Biomaterials 2013; DOI: 10.1016/j.biomaterials.2012.10.076

[183] Carlotti F, Zaldumbide A, Martin P, Boulukos KE, Hoeben RC, Pognonec P. Development of an inducible suicide gene system based on human caspase 8. Cancer Gene Ther 2005; DOI: 10.1038/sj.cgt.7700825

[184] Wong FSY, Tsang KK, Chu AMW, Chan BP, Yao KM, Lo ACY. Injectable cell-encapsulating composite alginate-collagen platform with inducible termination switch for safer ocular drug delivery. Biomaterials 2019; DOI: 10.1016/j.biomaterials.2019.01.032

[185] Delcassian D, Luzhansky I, Spanoudaki V, Bochenek M, McGladrigan C, Nguyen A et al. Magnetic Retrieval of Encapsulated Beta Cell Transplants from Diabetic Mice Using Dual-Function MRI Visible and Retrievable Microcapsules. Adv Mater 2020; DOI: 10.1002/adma.201904502

[186] He H, Luedke E, Zhang X, Yu B, Schmitt A, McClarren B et al. A naonoporous cell-therapy device with controllable biodegradation for long-term drug release. J Control Release 2013; DOI: 10.1016/j.jconrel.2012.11.020

[187] de Guzman RC, Ereifej ES, Broadrick KM, Rogers RA, VandeVord PJ. Alginate-matrigel microencapsulated Schwann cells for inducible secretion of glial cell line derived neurotrophic factor. J Microencapsul 2008; DOI: 10.1080/02652040802054745

[188] Ortner V, Kaspar C, Halter C, Töllner L, Mykhaylyk O, Walzer J et al. Magnetic field-controlled gene expression in encapsulated cells. J Control Release 2012; DOI: 10.1016/j.jconrel.2011.12.006

[189] Chang H, Kim P, Cho H, Yum S, Choi Y, Son Y et al. Inducible HGF-secreting Human Umbilical Cord Blood-derived MSCs Produced via TALEN-mediated Genome Editing Promoted Angiogenesis. Mol Ther 2016; DOI: 10.1038/mt.2016.120

[190] Weber W and Fussenegger M. Emerging biomedical applications of synthetic biology. Nat Rev Genet 2011; DOI: 10.1038/nrg3094

[191] Gubeli RJ, Burger K, Weber W. Synthetic biology for mammalian cell technology and materials sciences. Biotechnol Adv 2013; DOI: 10.1016/j.biotechadv.2012.01.007

[192] Soon-Shiong P, Heintz RE, Merideth N, Yao QX, Yao Z, Zheng T et al. Insulin independence in a type 1 diabetic patient after encapsulated islet transplantation. Lancet 1994; DOI: S0140-6736(94)90067-1

[193] Gifford R, Kehoe JJ, Barnes SL, Kornilayev BA, Alterman MA, Wilson GS. Protein interactions with subcutaneously implanted biosensors. Biomaterials 2006; DOI: S0142-9612(05)01059-8

[194] Brodbeck WG and Anderson JM. Giant cell formation and function. Curr Opin Hematol 2009; DOI: 10.1097/MOH.0b013e32831ac52e

[195] Rodriguez A, Meyerson H, Anderson JM. Quantitative in vivo cytokine analysis at synthetic biomaterial implant sites. J Biomed Mater Res A 2009; DOI: 10.1002/jbm.a.31939

[196] Anderson JM, Rodriguez A, Chang DT. Foreign body reaction to biomaterials. Semin Immunol 2008; DOI: S1044-5323(07)00096-6

[197] Kastellorizios M, Papadimitrakopoulos F, Burgess DJ. Prevention of foreign body reaction in a pre-clinical large animal model. J Control Release 2015; DOI: 10.1016/j.jconrel.2015.01.03

2

Introduction
Chapter 2

CELL MICROENCAPSULATION TECHNOLOGIES FOR SUSTAINED DRUG DELIVERY: CLINICAL TRIALS AND COMPANIES

Tania B. Lopez-Mendez[1,2], Edorta Santos-Vizcaino[1,2], Jose Luis Pedraz[1,2], Rosa Maria Hernandez[1,2*], Gorka Orive[1,2,3,4*]

[1]NanoBioCel Group, School of Pharmacy, University of the Basque Country (UPV/EHU), Paseo de la Universidad, 7, 01006, Vitoria-Gasteiz, Spain.

[2]Biomedical Research Networking Center in Bioengineering, Biomaterials and Nanomedicine (CIBER-BBN), Instituto de Salud Carlos III, C/Monforte de Lemos 3-5, 28029 Madrid, Spain

[3]University Institute for Regenerative Medicine and Oral Implantology - UIRMI (UPV/EHU-Fundación Eduardo Anitua); BTI Biotechnology Institute, Vitoria-Gasteiz, (Spain).

[4]Singapore Eye Research Institute, The Academia, 20 College Road, Discovery Tower, Singapore.

Under revision in: Drug Discovery Today (2020)

*Corresponding authors: Orive G (gorka.orive@ehu.eus)
Hernandez RM (rosa.hernandez@ehu.eus)

ABSTRACT

In recent years, cell microencapsulation technology has taken one step further, mainly driven by recent advances in the use of stem cells or the optimization of biomaterials. Old challenges have been addressed from new perspectives, and systems developed and improved for decades are now being transferred to the market by novel startups and consolidated companies. These products are mainly intended for the treatment of diabetes mellitus, but also cancer, central nervous system disorders or lysosomal diseases, among others. This review aims to analyze the results obtained in the clinical trials carried out to date and to define the global key players that will lead the cell microencapsulation market to bring this technology to the clinic in the upcoming years.

Keywords: Cell encapsulation, clinical trials, market, companies, biomaterials, drug delivery.

1. INTRODUCTION

Experts estimate that the market of cell encapsulation technologies, with a current value of about 250 million dollars (USD), will reach a value of approximately 303 million dollars by 2024 [1]. Several key areas are included in this market, such as regenerative medicine, cell transplants, encapsulation of probiotics or controlled-release medications.

The growth of the market is mainly due to the increase in the incidence of several of the target diseases of these therapies, the advances and the greater knowledge in the technologies, the increase in both private and public investments, and the acceptance and understanding of these possible therapies by society. However, the still high manufacturing costs, the limited availability of high-quality raw materials and the existence, in some cases, of alternative therapies, are expected to contain such growth in the coming years.

Among all the applications related to cell encapsulation, the sustained release of drugs is the one that currently produces the greatest benefits. Moreover, this trend is expected to continue in the coming years, mainly thanks to the latest technological advances and the use of increasingly biocompatible and affordable materials. In fact, three of the five most influential companies in the field of cell encapsulation today — Viacyte, Inc., Neurotech Pharmaceuticals, Inc. and Living Cell Technologies Ltd. (LCT) —, focus their efforts on developing systems for the sustained release of therapeutic molecules from live encapsulated cells.

In these systems, cells producing molecules of therapeutic interest are immobilized in biocompatible materials that are usually surrounded by a semipermeable polymeric membrane. The capsule prevents the passage of high molecular weight molecules — such as antibodies and other agents of the immune system —, protecting the cells from the host's immune response, while allowing the release of the therapeutic molecule of interest. In this way, different sustained release profiles of the therapeutic molecule — synthesized *de novo* — can be obtained without the need for immunosuppressive treatments, thus avoiding some of the adverse events associated with transplantation of cells and organs [2]. Traditionally, the market is divided between the devices considered "micro" and "macro".

On the one hand, we find cell macroencapsulation systems in which the cells are located in relatively large diffusion chambers with semipermeable properties. These devices can have different shapes, such as discs, flat sheets or hollow fibers. The application of cell macroencapsulation devices have shown very good results in vivo, demonstrating an undeniable therapeutic potential [3]. However, macrocapsules are characterized by a relatively small surface to volume ratio, which is probably their worst disadvantage. This implies the need for large amounts of nutrients and oxygen to achieve an adequate diffusion into the chamber and limits the amount of cells that can be encapsulated without creating necrotic nuclei in the innermost and inaccessible areas. However, they also have the advantage of allowing the implant to be removed easily in the event of adverse effects or loss of function **(Box 1)**.

Cell microencapsulation, comprising spherical particles between approximately 100 and 1500 μm in diameter, represents a very interesting alternative, greatly improving the surface to volume ratio and increasing the diffusion of nutrients and oxygen inside the capsules. Both natural and synthetic polymers have been tested for cell microencapsulation technologies, but alginate is by far the most widely used. This polysaccharide allows relatively smooth encapsulation processes, going from sol to gel when it reacts with divalent ions — such as Ca^{+2} and Ba^{+2} — and forming hydrogels with a high water content and biocompatibility. The hydrogel matrices are typically reinforced by means of polycations-based coatings, which provide the microcapsule with enhanced mechanical properties and more controlled permeability.

First *in vivo* studies with microencapsulated pancreatic islets were already carried out by Lim and Sum in the 80s [4], and during the following decades, type 1 diabetes mellitus (T1D) has persisted as the main target pathology. However, this versatile strategy has also been used for applications as diverse as myocardial regeneration, anemia, liver pathologies, different cancer types, neurodegenerative diseases or as a therapeutic alternative in severe hypoparathyroidism [5]. Nevertheless, its clinical application has remained elusive mainly due to biocompatibility issues that usually leads to fibrosis and implant failure.

Box 1. Highlights in cell macroencapsulation market

Relying on cell macroencapsulation technologies, all the following companies have their products in advanced stages of development. Cell micro and macroencapsulation technologies are expected to share the market because they have the same basis and very similar applications. Some of these macroencapsulation systems do not confer immunoprotection to the encapsulated cells and, thus, concomitant immunosuppressive treatments are needed. The combination of both micro and macro strategies could lead to very interesting synergies.

Viacyte, Inc. [1] (before Novocell, Inc.): The company differentiates hESCs into pancreatic islet precursors (PEC-01 cells) and places them within 2 products: PEC-Direct™ (VC-02), with no immunoprotective capacity and PEC-Encap™ (VC-01) with the Encaptra® immunoprotective system. Both strategies are currently in phase I/II clinical trials with T1D and type 2 diabetes mellitus (T2D) patients. ViaCyte and **CRISPR Therapeutics** formed a partnership to use gene-editing technology to create an immune-evasive version of a pluripotent stem cell line (in pre-clinical stages) potentially eliminating the need for immunosuppressants.

Neurotech Pharmaceuticals, Inc. [2] Its device, the NT-501 Encapsulated Cell Therapy (NT-501 ECT), for intravitreal ocular implantation, consists of human cells genetically modified to produce the ciliary neurotrophic factor (CNTF), encapsulated in a macro-system made with medical grade plastics. It is currently being evaluated in phase II/III clinical trials for different ocular diseases.

Sernova Corp. [3] Its Cell Pouch System® (vascularized implantable device) is already being tested in the first phase I/II clinical trials for the treatment of T1D and at pre-clinical level for other pathologies, such as hemophilia A or thyroid disease. The company patented, under the name of Sertolin®, the co-culture of pancreatic islets with Sertoli cells. The system does not confer immunoprotection but the company announced it will combine micro and macroencapsulation systems to improve this aspect.

Beta-O2 technologies Ltd. [4] The β Air technology (βAir Bio-artificial Pancreas device; βAir BAP), consisting of islets of Langerhans immunoprotected in alginate hydrogels, includes an exogenous source of oxygen. The company is currently developing a second-generation device, with stem cell derived beta cell clusters, that is expected to reach clinical trials in the near future.

Seraxis Inc. [5] The company has a line of iPSCs aimed at producing fully differentiated pancreatic islets. The strategy consists on encapsulating these cells in their immunoprotective SeraGraft® macrodevice to implant them in T1D patients. They are currently seeking funding to start clinical trials.

Defymed. [6] The spin off from the European Center for Diabetes Studies signed a strategic collaboration with Semma Therapeutics, with the intention of encapsulating the **Semma Therapeutics'** stem cell-derived insulin-producing cells in their MailPan® system. Pre-clinical studies are currently underway for diabetes, but also for hemophilia A and obesity.

Gloriana Therapeutics Inc. [7] (before NsGene). Its EC-NGF (encapsulated cell device secreting nerve growth factor) macrodevice has been tested, in a phase I clinical trial, for the treatment of Alzheimer's disease (AD). The company is also developing a second system, the EC-GDNF (encapsulated cell device secreting glial cell-derived neurotrophic factor), for the treatment of PD and for temporal lobe intractable epilepsy.

In recent years, driven by recent advances in related disciplines, old challenges have been addressed from totally new perspectives, taking cell microencapsulation technology one step further. On the one hand, some groups have focused their efforts on optimizing the purification protocols of the alginate [6-8] to eliminate the endotoxins, proteins and polyphenols that trigger immune responses and that are known to be key factors in implant viability. On the other hand, chemical modifications of the alginates are proving to be a promising option to reduce the immunological reactions against the implant [9-11]. Triazole-containing alginate analogues, identified by Vegas *et al.*, are a representative example of the latter, as they have demonstrated to significantly reduce foreign body response, inhibiting macrophage recognition and fibrosis formation [9,10,12]. Moreover, recently Veiseh *et al*. [13] suggested that the size of the microcapsules could be a determinant factor for implant biocompatibility, but this conclusion generated debate among the experts in the field [8].

Regarding the selected cell type, it differs depending on the target pathology. In some cases, working with allogeneic or xenogeneic primary cells may be the safest option, exploiting the natural productive capacity of the selected cell type. However, the sources of allogenic cells are usually limited and using non-human cells is normally associated with stronger immunological reactions against the implant, related to xenogeneic epitopes. In recent years, the possibility of obtaining the desired cell type from pluripotent stem cells (hPSCs) —either embryonic stem

cells (hESCs) or induced pluripotent stem cells (iPSC)— has opened a recently unthinkable world of possibilities, which are already being explored, with promising results [12,14,15].

2. CELL MICROENCAPSULATION COMPANIES AND CLINICAL TRIALS

Cell microencapsulation technologies were first tested in humans in 1994, by Soon Shiong *et al*. In this study, a diabetic patient on immunosuppressive treatment received a first intraperitoneal infusion of islets (10,000IEQ/kg) encapsulated in PLL-APA microcapsules — alginate microbeads, coated with poly-L-Lysine (PLL) and a second layer of alginate to increase their biocompatibility — and another 5000IEQ/kg, 6 months later [16]. The patient remained insulin independent for 9 months after implantation, with stable blood glucose levels. This first encouraging clinical trial laid the groundwork for those coming in the following years, mostly for the treatment of insulin-dependent diabetes **(Table 1)**.

Nowadays, **Living Cell Technologies Limited (LCT)** [17] is one of the most advanced companies when it comes to cell microencapsulation therapies for the sustained release of therapeutic molecules **(Figure 1)**. Its Immupel® technology, consists of alginate spheres, crosslinked with Ca^{+2} and coated with Poly-L-Ornithine (PLO) and a second layer of alginate (APA-PLO). This strategy is similar to the one used by Prof. Calafiore and his group (Perugia, Italy), probably because they collaborated and shared their technologies in the 1990s [8]. Initially, LCT focused on the development of DIABECELL as a treatment for patients with T1D. After initial phase I/II trials, LCT began a collaboration with the company **Otsuka Pharmaceutical Factory, Inc. (OPF)** [18], founding the company **Diatranz Otsuka Limited (DOL)** [19]. In 2014, DOL authorized OPF to continue the development of the product in the USA and Japan. Later on, in January 2018, LCT sold its participation in DOL to OPF, so the latter will continue with the development of DIABECELL. OPF and LCT are currently in negotiations to divide the commercialization of DIABECELL in different countries.

Table 1. Clinical trials with cell microencapsulation technologies

Researcher/company	Strategy	Immunosuppression	Results	Phase	Ref.
Diabetes mellitus					
Soong-Shiong *et al.* (1994)	Allogeneic islets in APA microcapsules, implanted in the peritoneum.	Yes	The patient remained exogenous insulin-independent and with controlled blood glucose levels for 9 months.	I/II	[1]
Novocell (now Viacyte) (2005-2007)	Human pancreatic islets, with conformal PEG coating, implanted subcutaneously.	Low dose of cycloporine in the first 12h	It was not possible to eliminate the need of exogenous insulin in any of the 2 treated patients. C-peptide levels were maintained at lower levels than expected.	I/II	[2]
Calafiore *et al.* (2006-2011)	Allogeneic islets in APA microcapsules, implanted intraperitonally.	No	Lower exogenous insulin requirements for 3 years. No significant adverse events were detected. 7 years later, the patients went back to the initial exogenous insulin requirements.	I/II	[3,4]
Living Cell Technologies (LCT) (2007)	Porcine pancreatic islets in APA microcapsules, implanted in the peritoneum (xenogeneic transplant).	No	30% reduction in the need for exogenous insulin after 12 weeks, with return to baseline after 49 weeks. After 9.5 years, the microcapsules were explanted and found to contain viable islets that still produced insulin.	I/II	[5]
Living Cell Technologies (LCT) (2009-2014)	Porcine pancreatic islets in APA microcapsules, implanted in the peritoneum (xenogeneic transplant). DIABECELL®	No	Better control of hypoglycaemic episodes. No notable adverse effects were detected. Significant decrease in HbA1c. Exogenous insulin dose reduction in some cases. No independence from exogenous insulin.	I/II	[6-8]
Tuch *et al.* (2009)	Allogeneic islets in Ba^{2+}-cross-linked microbeads, implanted in the peritoneum.	No	The need for exogenous insulin was not reduced and the glycaemic control was not improved. No notable adverse effects were detected, but after 16 months, necrotic tissue was reported around the microbeads.	I	[9]
Jacobs-Tulleneers-thevissen *et al.* (2013)	Allogeneic islets in Ba^{2+}/Ca^{2+} -cross-linked microbeads, implanted in the peritoneum.	Yes, due to a previous islet intraportal transplant.	During 12 weeks, higher levels of C-peptide were detected in the bloodstream of the patients, but after 3 months of follow-up, the need for exogenous insulin was not reduced.	II	[10]

Traumatic brain injury					
Heile and Brinker (2011)	Allogeneic MSCs, transfected to produce GLP-1, immobilized in alginate microcapsules and implanted in the intracranial cavity, in the space resulting from the removal of the hematoma (brain trauma).	No	After 2 weeks of treatment, the implant was removed. No notable adverse effects due to treatment or surgical intervention were detected.	I/II	[11]
Parkinson's disease					
Living Cell Technologies (LCT) (2012-2020)	Porcine ChP cells in PLO-APA microcapsules, implanted in the intracranial cavity (xenogeneic transplant). NTCELL®	No	Positive biosafety results gave the green light to a second phase IIb clinical trial.	I/II	[12]
Living Cell Technologies (LCT) (2016-2019)	Porcine ChP cells in PLO-APA microcapsules, implanted in the intracranial cavity (xenogeneic transplant). NTCELL®	No	Results indicate that there is a dose-dependent behaviour and that patients who received 80 NTCELL capsules show significant improvements, compared to placebo, even after 2 years. Higher doses show inflammation in the surrounding tissue, with no significant improvement.	II	[13,14]
Pancreatic cancer					
Löhr *et al.* Salmons *et al.* (1999-2003)	CYP2B1-secreting allogenic 293 cells, immobilized in cellulose-sulfate microcapsules and implanted in blood vessels near the pancreatic tumour.	No	In a first phase I/II clinical trial with a 1g/m^2/day dose of ifosfamide, the median survival rate of patients was doubled and only one patient suffered treatment-related adverse effects.	I/II	[15-18]
Löhr *et al.* (2014)	CYP2B1-secreting allogenic 293 cells, immobilized in cellulose-sulfate microcapsules and implanted in blood vessels near the pancreatic tumour.	No	In a second phase II trial, the ifosfamide dose was increased to 2g/m^2/day. The results showed greater severe adverse effects but the efficacy profile was similar.	II	[18]
Severe hypoparathyroidism					
Hasse *et al.* (1997)	Human parathyroid cells, in Ba^{2+}-cross-linked alginate beads. 20 microbeads implanted in the arm of two patients.	No	Daily calcium and vitamin D needs were halved in both cases.	I/II	[19]

Cabane *et al.* (2009)	Human parathyroid cells, in Ba^{2+}-cross-linked alginate beads. 23 microbeads implanted in the arm and 40 in the leg.	No	The functionality of the implant was maintained for at least 20 months, with no the need of intravenous calcium administration.	I/II	[20]
Yucesan *et al.* (2019)	Human parathyroid cells, in alginate beads, implanted in the omental tissue.	No	No severe adverse events were detected during the intervention. Significant increases in parathyroid hormone were detected in the patient's blood.	I/II	[21]

DIABECELL consists of xenotransplantation of porcine pancreatic islets, immobilized in APA-PLOs. In the first clinical trial with this technology (LCT), microencapsulated porcine islets (15000IEQ/kg) were implanted in the peritoneal cavity of a 41-year-old Caucasian male with T1D, with no immunosuppressive treatments [20]. After 3 months, his exogenous insulin needs were reduced by 30% and C-peptide levels (indicative of functional pancreatic islets) remained detectable for 11 months. However, after those first months, it was necessary to go back to the pre-transplant doses of exogenous insulin. The patient was followed for a long period of time and, after nine and a half years, the researchers performed a laparoscopy in which they detected opaque nodules in the mesentery and omentum, with no indicators of fibrosis in the peritoneum. The biopsy of these nodules showed intact microcapsules with some live cells that secreted small amounts of insulin when stimulated with glucose *in vitro*.

To date, a total of 46 patients have received pancreatic islets in the peritoneal cavity, in two phase I/IIa and one phase IIb trials with DIABECELL [21-23]. In these studies, a dose range of 5,000, 10,000, 15,000 and 20,000 IEQ/kg [24] was tested. The results obtained have led DOL and OPF to begin preparations for future phase III clinical trials **(Figure 2)**.

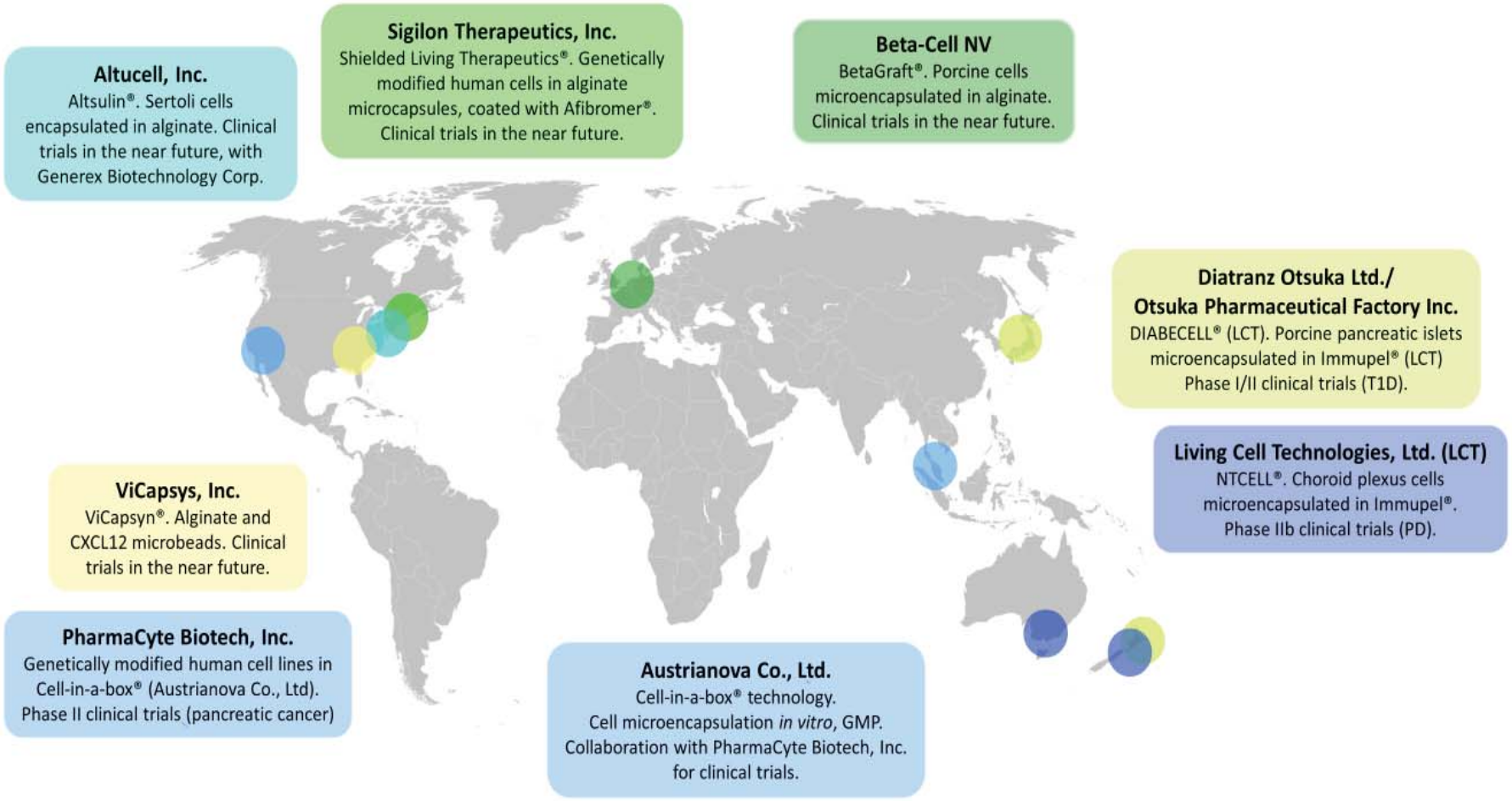

Figure 1. Cell microencapsulation companies around the world, in July 2020. CXC12: C-X-C motif chemokine 12; GMP: Good Manufacturing Practice; T1D: Type 1 diabetes mellitus; PD: Parkinson's disease.

Regarding LCT, it is now focused on the application of its Immupel® technology for the implantation of porcine choroidal plexus (ChP) cells, intracranially, for the treatment of different pathologies of the central nervous system (CNS) (NTCELL). Their first phase I/IIa clinical trial included 4 patients with Parkinson's disease (PD), who received a xenogeneic transplant of ChP cells, microencapsulated in APA-PLOs [25]. The good results obtained in terms of safety, gave the green light to a second phase IIb clinical trial (randomized, double-blind), with 18 patients with PD [26]. The first reported results after 26 weeks, were not able to demonstrate efficacy against placebo, but confirmed the previous biosafety results. However, one year after implantation, the results showed a statistically significant improvement over placebo in patients who received 40 or 80 NTCELL capsules in the putamen, on both sides of the brain. These results were measured using the "Unified Parkinson's Disease Rating Scale". This improvement was maintained, in the group of patients who received 80 NTCELL capsules, at 18 and 24 months after implantation. In the patients who received 120 capsules, there were no significant differences in efficacy compared to placebo. The authors hypothesized that this outcome could have been related to the detected inflammation [27]. After 2 years of studies, LCT considered the criteria of dose-dependent efficacy and safety to be met, and is therefore studying potential partnerships with other companies (maybe out-licensing NTCELL) to fund phase III clinical trials.

Heile and Brinker carried out another clinical trial testing the intracranial administration of microcapsules. This approach consisted in the administration of allogeneic mesenchymal stromal cells (MSCs) microencapsulated in alginate microspheres for the release of the glucagon-1-like peptide (GLP-1), an anti-inflammatory and neuroprotective factor [28]. The microbeads were administered locally, contained in a manually sutured polypropylene "bag", after removal of the hematoma in patients with traumatic brain injury. The implant was removed after 2 weeks of treatment. In this phase I/II clinical trial, no adverse events derived from the treatment or the surgical intervention were detected.

Altucell, Inc. [29] is also a very promising company since, despite its relatively short business career, the team in charge has the remarkable experience of

the laboratory led by Prof. Calafiore, in Italy. Pioneers for decades in the production of alginate microcapsules — especially for the treatment of T1D — its technology has been proven in numerous *in vitro* and *in vivo* studies [30-33] and in the first clinical trial with microencapsulated pancreatic islets without immunosuppressive treatment. In this first phase I trial with 4 patients, the group from the University of Perugia implanted microencapsulated allogeneic human islets intraperitoneally and followed them for 6 years [34,35]. The formulation consisted of APA-PLOs of ultra-pure alginate, cross-linked with Ca^{+2}. During the study, no anti-mayor histocompatibility complex I/II (anti-MHC I/II) or anti-glutamic acid decarboxylase 65 (anti-GAD65) antibodies, nor antibodies against islets were detected. Therefore, it was concluded that microencapsulation managed to protect the islets, even without immunosuppressive treatment. Although measuring efficacy was not one of the main objectives of the study, it should be mentioned that the administration of exogenous insulin decreased for some patients and its use could be temporarily canceled in one. In one of the patients, part of the implant was placed in a more superficial layer than the peritoneum and a cyst was formed around it, causing the death of the microencapsulated cells.

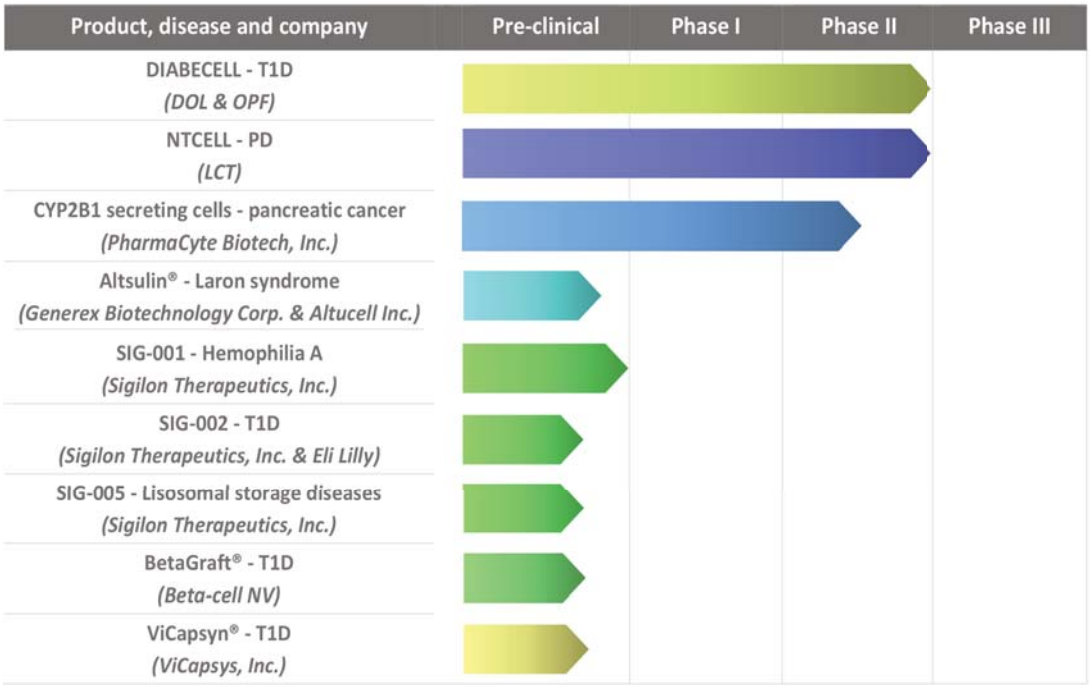

Figure 2. Development stages of most advanced cell microencapsulation products, July 2020. T1D: Type 1 diabetes mellitus; PD: Parkinson's disease.

At the end of 2019, **Generex Biotechnology Corp.** [36] announced its future acquisition of 51% of **Altucell, Inc.** and its intentions to carry out the first clinical trial of the product Altsulin®, elaborated with Sertoli cells encapsulated in alginate microcapsules, for patients with Laron syndrome. The study will be designed to demonstrate the long-term safety of this product, the *in vivo* release of insulin-like growth factor-1 (IGF-1) and the possibility of recovering the implant by surgery at the end of treatment. In addition to Altsulin®, Altucell Inc. has 2 other patents: Altucap®, an alginate ultra-purification process, and Altustem®, stem cell-derived myofibroblasts, isolated from human umbilical cord Wharton jelly.

In addition to those previously mentioned, to date 3 other clinical trials have been performed for the treatment of T1D using cell microencapsulation technologies. In the first one, Tuch *et al.* administered human islets in alginate and Ba^{+2} microspheres, intraperitoneally infused (178000IEQ/infusion) to 4 patients with T1D ("The Seaweed Diabetes Trial") [37]. No immunosuppressive treatment was used but the patients received an anti-inflammatory agent and antioxidants. Two of the participants received only one infusion of microbeads, another one received 2 infusions —10 months apart —, and the last one received a total of 4 infusions over 7 months. The need for exogenous insulin was not reduced, the glycemic control did not improve significantly and, unlike in other clinical trials, anti-GAD and cytotoxic antibodies were detected in this study. A laparoscopy performed on the patient who received the most infusions of islets revealed that the microbeads were intact but, surrounded by fibrotic tissue, causing the necrosis of the encapsulated islets.

In another clinical trial, by Jacobs-Tulleneers-Thevissen *et al.*, allogeneic pancreatic islets — immobilized in alginate microbeads, cross-linked with Ca^{+2} or Ba^{+2} — were administered intraperitoneally to a woman with T1D (300000 IEQ) [38]. The patient had been receiving immunosuppressive therapy for 5 years related to a previous intraportal administration of islets. Exogenous insulin requirements did not decrease after implantation but no cytotoxic antibodies were detected. A laparoscopy performed 3 months after the administration concluded that most of the microsbeads were aggregated, surrounded by fibrotic tissue and that they only contained cellular debris.

In addition, even though it is not a classical microencapsulation approach per se, in 2005, Novocell (now Viacyte, Inc.) carried out a first phase I/II clinical trial with human pancreatic islets protected with a conformal PEG coating and implanted subcutaneously [39]. The results were not satisfactory since none of the two treated patients managed to remain independent of exogenous insulin and blood C-peptide levels remained below expectations throughout the study.

Another interesting company is **PharmaCyte Biotech, Inc.** [40]. This company develops microencapsulation-based therapies for housing human cell lines genetically modified to produce the desired therapeutic molecule. Its main therapeutic targets are focused on the treatment of different cancer types and T1D. PharmaCyte Biotech, Inc. has purchased the rights to use Cell-in-a-box® technology from **Austrianova Co., Ltd.** [41]. This technology deals with the microencapsulation of different cell types in cellulose sulfate beads and has been tested, for years, at the preclinical level [42] and in 2 phase I/II clinical trials [43-46]. In these latter cases, microencapsulated cells that overexpressed cytochrome P450 2B1 (CYP2B1) — which metabolizes the cytotoxic agent ifosfamide, transforming it into its active metabolites — were implanted in patients with pancreatic cancer. Normally, this conversion occurs in the liver and the active metabolites circulate through the bloodstream to the tumor, thus limiting the exposure of tumor cells to the active agent and increasing the risk of adverse effects. By placing the microencapsulated cells close to the area to be treated, a much more focused therapy is obtained, so better results are expected with lower doses. In a first phase I/II clinical trial with a 1 g/m^2/day dose of ifosfamide, the median survival of patients was doubled and only one of the patients suffered treatment-related adverse effects [43-45]. In a second phase II trial, the ifosfamide dose was increased to 2 g/m^2/day. The results showed greater severe adverse effects but the efficacy profile was similar [46]. Now, PharmaCyte Biotech, Inc. will be in charge of continuing with these promising clinical trials and are currently conducting the tests required by the regulatory agencies to begin a phase IIb clinical trial as soon as possible.

Another company with great potential in the field of cell microencapsulation for drug delivery is **Sigilon Therapeutics, Inc.** [47] founded in 2016 by Flagship

Pioneering and Professors Robert Langer and Daniel Anderson, from the Massachusetts Institute of Technology (MIT). Their proposal focuses on the Shielded Living Therapeutics® platform, which consists of genetically modified human cells immobilized and immunoprotected in spheres of approximately 1 mm in diameter. The latter are composed of Afibromer®, patented modified alginates that help this platform to go unnoticed by the immune system components, that are the result of years of studies both *in vitro* and *in vivo* [9,10,12,13]. Although clinical trials have not yet started, they are expected to begin in the coming months and will cover various pathologies such as hemophilia, lysosomal pathologies or T1D. In March 2020, the company announced it completed a Series B financing and thus the imminent start of the first clinical trial of their SIG-001 product – which received Orphan Drug Designation from the U.S. Food and Drug Administration (FDA) - for hemophilia A. For T1D, it is important to mention the association of Sigilon Therapeutics with the Pharmaceutical giant **Eli Lilly** [48], which will conduct the clinical trials when the technology is ready.

There are also other companies in very advanced stages of preclinical development, that may start their own clinical trials in the coming years. **Beta-cell NV** [49] is one of those examples, with its BetaGraft® technology, that consists of porcine islets microencapsulated in alginate for the treatment of T1D. Also **ViCapsys, Inc.** [50], recently introduced the ViCapsyn® technology, microbeads of 200-600 μm in diameter made with alginate and incorporating the C-X-C motif chemokine 12 (CXCL12). This molecule has been shown to selectively repel effector T cells while continuing to recruit and retain immune-suppressive regulatory T cells, to play a role in reducing inflammatory responses at sites of injury, to promote healing through the recruitment of endothelial progenitor cells and to act as a prosurvival signal for beta cells [51]. ViCapsyn® technology has been tested in preclinical studies on rodents and non-human primates, where it has been shown to reduce fibrotic processes compared to alginate beads without CXCL12 [51-53].

Finally, cell microencapsulation has also been studied for the treatment of severe postsurgical hypoparathyroidism. In a first clinical trial, Hasse *et al*. immobilized human parathyroid cells in Ba^{+2}-crosslinked alginate microbeads and

administered them to two patients, implanting them in the brachioradialis muscle. Daily calcium and vitamin D needs were halved in both cases and the use of immunosuppressive treatments was not necessary [54].

A few years later, Cabane et al. used a similar strategy —human parathyroid cells immobilized in Ba^{+2}-crosslinked alginate microbeads— to treat a patient in need of intravenous calcium administration due to severe hypoparathyroidism. The implant remained viable for at least 20 months and the patient did not need intravenous calcium administration during that time [55].

Very recently, Yucesan *et al.* administered human parathyroid cells, immobilized in alginate beads, to a 37-year-old woman [56]. The implant was placed in the omental tissue and, for one year, the levels of calcium, parathyroid hormone and phosphorus in the blood were analyzed. No notable adverse effects were detected during the treatment. Calcium and parathyroid hormone levels were significantly higher after implantation and remained elevated throughout the year of the study.

3. CONCLUSIONS

Cell microencapsulation technologies present clear advantages when a sustained and controlled release of the therapeutic molecule is required for long periods of time. Using living cells that respond to the host's biological stimuli by secreting the right amount of the active substance, at the right time, goes far beyond the classic treatments that are used today for the diseases that are postulated as targets for these types of systems, such as diabetes or different metabolic disorders. All the products we have discussed here are in advanced stages of development, some of them being tested in clinical trials. It is expected that several of them will reach the market in the coming years, but first it will be necessary to set up large-scale practices that allow the safe and efficient production of the microcapsule batches, that must also comply with strict regulatory aspects to be applied in the clinic. In addition, the success of these therapies based on cell microencapsulation technologies will also depend on whether they show an advantageous cost-effectiveness relationship compared to other technologies with which they will share the market, such as cell macroencapsulation systems or totally different approaches, like non-cellular

sustained release carriers or gene therapies, for example. In any case, all indicators suggest that finally the promises and expectations regarding cell microencapsulation technologies, postponed for decades, are closer than ever to becoming a reality. In upcoming years, the systems described here may improve the lives of patients with chronic pathologies and insufficient and/or highly uncomfortable treatments.

4. ACKNOWLEDGEMENTS

Authors gratefully acknowledge the ICTS "NANBIOSIS", specifically by the Drug Formulation Unit (U10) of the CIBER-BBN at the University of Basque Country UPV/EHU in Vitoria-Gasteiz. Tania B. Lopez-Mendez thanks the Basque Government (Department of Education, Universities and Research) for the Ph.D. fellowship.

5. DECLARATION OF INTEREST

The authors declare no competing financial interest.

6. REFERENCES

[1] Live cell encapsulation market forecast to 2024, https://www.marketsandmarkets.com/Market-Reports/live-cell-encapsulation-technology-market-218019375.html; 2020 [accessed 24 July 2020].

[2] Ashimova A, Yegorov S, Negmetzhanov B, Hortelano G. Cell Encapsulation Within Alginate Microcapsules: Immunological Challenges and Outlook. Front Bioeng Biotechnol 2019; DOI: 10.3389/fbioe.2019.00380 (https://www.frontiersin.org/)

[3] Farina M, Alexander JF, Thekkedath U, Ferrari M, Grattoni A. Cell encapsulation: Overcoming barriers in cell transplantation in diabetes and beyond. Adv Drug Deliv Rev 2019; DOI: S0169-409X(18)30080-2 (https://www.journals.elsevier.com/advanced-drug-delivery-reviews)

[4] Lim F and Sun AM. Microencapsulated islets as bioartificial endocrine pancreas. Science 1980; DOI: 10.1126/science.6776628 (https://www.sciencemag.org/)

[5] Gonzalez-Pujana A, Santos E, Orive G, Pedraz JL, Hernandez RM. Cell microencapsulation technology: Current vision of its therapeutic potential through the administration routes. J Drug Deliv Sci Tec 2017; DOI: 10.1016/j.jddst.2017.03.028 (https://www.sciencedirect.

com/journal/journal-of-drug-delivery-science-and-technology)

[6] Paredes-Juarez GA, de Haan BJ, Faas MM, de Vos P. A Technology platform to test the efficacy of purification of alginate. Materials 2014; DOI: 10.3390/ma7032087 (https://www.mdpi.com/journal/materials)

[7] Sondermeijer HP, Witkowski P, Woodland D, Seki T, Aangenendt FJ, van der Laarse A et al. Optimization of alginate purification using polyvinylidene difluoride membrane filtration: Effects on immunogenicity and biocompatibility of three-dimensional alginate scaffolds. J Biomater Appl 2016; DOI: 0885328216645952 (https://journals.sagepub.com/home/jba)

[8] Calafiore R. Microencapsulation for cell therapy of type 1 diabetes mellitus: The interplay between common beliefs, prejudices and real progress. J Diabetes Investig 2018; DOI: 10.1111/jdi.12788 (https://onlinelibrary.wiley.com/journal/20401124)

[9] Vegas AJ, Veiseh O, Doloff JC, Ma M, Tam HH, Bratlie K et al. Combinatorial hydrogel library enables identification of materials that mitigate the foreign body response in primates. Nat Biotechnol 2016; DOI: 10.1038/nbt.3462 (https://www.nature.com/nbt/)

[10] Bochenek MA, Veiseh O, Vegas AJ, McGarrigle JJ, Qi M, Marchese E et al. Alginate encapsulation as long-term immune protection of allogeneic pancreatic islet cells transplanted into the omental bursa of macaques. Nat Biomed Eng 2018; DOI: 10.1038/s41551-018-0275-1 (https://www.nature.com/natbiomedeng/)

[11] Liu Q, Chiu A, Wang LH, An D, Zhong M, Smink AM et al. Zwitterionically modified alginates mitigate cellular overgrowth for cell encapsulation. Nat Commun 2019; DOI: 10.1038/s41467-019-13238-7 (https://www.nature.com/ncomms/)

[12] Vegas AJ, Veiseh O, Gurtler M, Millman JR, Pagliuca FW, Bader AR et al. Long-term glycemic control using polymer-encapsulated human stem cell-derived beta cells in immune-competent mice. Nat Med 2016; DOI: 10.1038/nm.4030 (https://www.nature.com/nm/)

[13] Veiseh O, Doloff JC, Ma M, Vegas AJ, Tam HH, Bader AR et al. Size- and shape-dependent foreign body immune response to materials implanted in rodents and non-human primates. Nat Mater 2015; DOI: 10.1038/nmat4290 (https://www.nature.com/nmat/)

[14] Millman JR, Xie C, Van Dervort A, Gurtler M, Pagliuca FW, Melton DA. Generation of stem cell-derived beta-cells from patients with type 1 diabetes. Nat Commun 2016; DOI: 10.1038/ncomms11463 (https://www.nature.com/ncomms/)

[15] Montanucci P, Pescara T, Alunno A, Bistoni O, Basta G, Calafiore R. Remission of hyperglycemia in spontaneously diabetic NOD mice upon transplant of microencapsulated human umbilical cord Wharton jelly-derived mesenchymal stem cells (hUCMS). Xenotransplantation 2019; DOI: 10.1111/xen.12476 (https://onlinelibrary.wiley.com/journal/13993089)

[16] Soon-Shiong P, Heintz RE, Merideth N, Yao QX, Yao Z, Zheng T et al. Insulin independence in a type 1 diabetic patient after encapsulated islet transplantation. Lancet 1994; DOI: S0140-6736(94)90067-1 (https://www.thelancet.com/)

[17] Living Cell Technologies Limited (LCT), https://lctglobal.com/; 2020 [accessed 24 July 2020].

[18] Otsuka Pharmaceutical Factory, Inc. (OPF), www.otsukakj.jp/en; 2020 [accessed 24 July 2020].

[19] Diatranz Otsuka Limited (DOL), http://dolglobal.com/; 2020 [accessed 24 July 2020].

[20] Elliott RB, Escobar L, Tan PL, Muzina M, Zwain S, Buchanan C. Live encapsulated porcine islets from a type 1 diabetic patient 9.5 yr after xenotransplantation. Xenotransplantation 2007; DOI: XEN384 (https://onlinelibrary.wiley.com/journal/13993089)

[21] Open-label Investigation of the Safety and Effectiveness of DIABECELL(R) in Patients With Type I Diabetes Mellitus, https://clinicaltrials.gov/ct2/show/NCT00940173?term=NCT00940173&draw=2&rank=1; 2020 [accessed 24 July 2020].

[22] Open-label Investigation of the Safety and Effectiveness of DIABECELL in Patients With Type 1 Diabetes Mellitus, https://clinicaltrials.gov/ct2/show/NCT01739829?term=NCT01739829&draw=2&rank=1; 2020 [accessed 24 July 2020].

[23] Open-label Investigation of the Safety and Efficacy of DIABECELL in Patients With Type 1 Diabetes Mellitus, https://clinicaltrials.gov/ct2/show/NCT01736228?term=NCT01736228&draw=2&rank=1; 2020 [accessed 24 July 2020].

[24] Matsumoto S, Abalovich A, Wechsler C, Wynyard S, Elliott RB. Clinical Benefit of Islet Xenotransplantation for the Treatment of Type 1 Diabetes. EBioMedicine 2016; DOI: S2352-3964(16)30389-9 (https://www.thelancet.com/journals/ebiom/home)

[25] Open-label Investigation of the Safety and Clinical Effects of NTCELL in Patients With Parkinson's Disease, https://clinicaltrials.gov/ct2/show/NCT01734733?term=NCT01734733&draw=2&rank=1; 2020 [accessed 24 July 2020].

[26] Investigation of the Safety and Efficacy of NTCELL [Immunoprotected (Alginate-Encapsulated) Porcine Choroid Plexus Cells for Xenotransplantation] in Patients With Parkinson's Disease, https://clinicaltrials.gov/ct2/show/NCT02683629?term=NCT02683629&draw=2&rank=1; 2020 [accessed 24 July 2020].

[27] Snow B, Mulroy E, Bok A, Simpson M, Smith A, Taylor K et al. A phase IIb, randomised, double-blind, placebo-controlled, dose-ranging investigation of the safety and efficacy of NTCELL((R)) [immunoprotected (alginate-encapsulated) porcine choroid plexus cells for xenotransplantation] in patients with Parkinson's disease. Parkinsonism Relat Disord 2019; DOI: S1353-8020(18)30500-5 (https://www.journals.elsevier.com/parkinsonism-and-related-disorders)

[28] Heile A and Brinker T. Clinical translation of stem cell therapy in traumatic brain injury: the potential of encapsulated mesenchymal cell biodelivery of glucagon-like peptide-1. Dialogues Clin Neurosci 2011; 13(3): 279-86.

[29] Altucell, Inc., https://altucell.com/; 2020 [accessed 24 July 2020].

[30] Calafiore R, Basta G, Luca G, Boselli C, Bufalari A, Bufalari A et al. Transplantation of

pancreatic islets contained in minimal volume microcapsules in diabetic high mammalians. Ann N Y Acad Sci 1999; DOI: 10.1111/j.1749-6632.1999.tb08506.x (https://nyaspubs.onlinelibrary.wiley.com/journal/17496632)

[31] Basta G, Sarchielli P, Luca G, Racanicchi L, Nastruzzi C, Guido L et al. Optimized parameters for microencapsulation of pancreatic islet cells: an in vitro study clueing on islet graft immunoprotection in type 1 diabetes mellitus. Transpl Immunol 2004; DOI: 10.1016/j.trim.2004.10.003 (https://www.journals.elsevier.com/transplant-immunology)

[32] Elliott RB, Escobar L, Tan PLJ, Garkavenko O, Calafiore R, Basta P et al. Intraperitoneal alginate-encapsulated neonatal porcine islets in a placebo-controlled study with 16 diabetic cynomolgus primates. Transplant Proc 2005; DOI: 10.1016/j.transproceed.2005.09.038 (https://www.sciencedirect.com/journal/transplantation-proceedings)

[33] Thanos CG, Calafiore R, Basta G, Bintz BE, Bell WJ, Hudak J et al. Formulating the alginate-polyornithine biocapsule for prolonged stability: evaluation of composition and manufacturing technique. J Biomed Mater Res A 2007; DOI: 10.1002/jbm.a.31472 (https://onlinelibrary.wiley.com/journal/15524965)

[34] Calafiore R, Basta G, Luca G, Lemmi A, Montanucci MP, Calabrese G et al. Microencapsulated pancreatic islet allografts into nonimmunosuppressed patients with type 1 diabetes: first two cases. Diabetes Care 2006; DOI: 29/1/137 (https://care.diabetesjournals.org/)

[35] Basta G, Montanucci P, Luca G, Boselli C, Noya G, Barbaro B et al. Long-term metabolic and immunological follow-up of nonimmunosuppressed patients with type 1 diabetes treated with microencapsulated islet allografts: four cases. Diabetes Care 2011; DOI: 10.2337/dc11-0731 (https://care.diabetesjournals.org/)

[36] Generex Biotechnology Corp., https://generex.com/index.html; 2020 [accessed 24 July 2020].

[37] Tuch BE, Keogh GW, Williams LJ, Wu W, Foster JL, Vaithilingam V et al. Safety and viability of microencapsulated human islets transplanted into diabetic humans. Diabetes Care 2009; DOI: 10.2337/dc09-0744 (https://care.diabetesjournals.org/)

[38] Jacobs-Tulleneers-Thevissen D, Chintinne M, Ling Z, Gillard P, Schoonjans L, Delvaux G et al. Sustained function of alginate-encapsulated human islet cell implants in the peritoneal cavity of mice leading to a pilot study in a type 1 diabetic patient. Diabetologia 2013; DOI: 10.1007/s00125-013-2906-0 (https://diabetologia-journal.org/)

[39] Safety and Efficacy of PEG-Encapsulated Islet Allografts Implanted in Type I Diabetic Recipients, https://clinicaltrials.gov/ct2/show/NCT00260234?term=NCT00260234&draw=2&rank=1; 2020 [accessed 24 July 2020].

[40] PharmaCyte Biotech, Inc., https://pharmacyte.com/; 2020 [accessed 24 July 2020].

[41] Austrianova Co., Ltd., https://austrianova.com/; 2020 [accessed 24 July 2020].

[42] Salmons B and Gunzburg WH. Release characteristics of cellulose sulphate capsules

and production of cytokines from encapsulated cells. Int J Pharm 2018; DOI: S0378-5173(18)30438-1 (https://www.sciencedirect.com/journal/international-journal-of-pharmaceutics)

[43] Lohr M, Bago ZT, Bergmeister H, Ceijna M, Freund M, Gelbmann W et al. Cell therapy using microencapsulated 293 cells transfected with a gene construct expressing CYP2B1, an ifosfamide converting enzyme, instilled intra-arterially in patients with advanced-stage pancreatic carcinoma: a phase I/II study. J Mol Med 1999; DOI: 10.1007/s001090050366 (https://www.springer.com/journal/109)

[44] Lohr M, Hoffmeyer A, Kroger J, Freund M, Hain J, Holle A et al. Microencapsulated cell-mediated treatment of inoperable pancreatic carcinoma. Lancet 2001; DOI: S0140673600047498 (https://www.thelancet.com/)

[45] Salmons B, Lohr M, Gunzburg WH. Treatment of inoperable pancreatic carcinoma using a cell-based local chemotherapy: results of a phase I/II clinical trial. J Gastroenterol 2003; 38 Suppl 15:78-84.

[46] Lohr JM, Haas SL, Kroger JC, Friess HM, Hoft R, Goretzki PE et al. Encapsulated cells expressing a chemotherapeutic activating enzyme allow the targeting of subtoxic chemotherapy and are safe and efficacious: data from two clinical trials in pancreatic cancer. Pharmaceutics 2014; DOI: 10.3390/pharmaceutics6030447 (https://www.mdpi.com/journal/pharmaceutics)

[47] Sigilon Therapeutics, Inc., https://sigilon.com/; 2020 [accessed 24 July 2020].

[48] Eli Lilly, https://www.lilly.com/; 2020 [accessed 24 July 2020].

[49] Beta-cell NV, https://www.beta-cell.com/; 2020 [accessed 24 July 2020].

[50] ViCapsys, Inc., https://vicapsys.com/; 2020 [accessed 24 July 2020].

[51] Sremac M, Lei J, Penson MFE, Schuetz C, Lakey JRT, Papas KK et al. Preliminary Studies of the Impact of CXCL12 on the Foreign Body Reaction to Pancreatic Islets Microencapsulated in Alginate in Nonhuman Primates. Transplant Direct 2019; DOI: 10.1097/TXD.0000000000000890 (https://journals.lww.com/transplantationdirect/pages/default.aspx)

[52] Chen T, Yuan J, Duncanson S, Hibert ML, Kodish BC, Mylavaganam G et al. Alginate encapsulant incorporating CXCL12 supports long-term allo- and xenoislet transplantation without systemic immune suppression. Am J Transplant 2015; DOI: 10.1111/ajt.13049 (https://onlinelibrary.wiley.com/journal/16006143)

[53] Alagpulinsa DA, Cao JJL, Driscoll RK, Sirbulescu RF, Penson MFE, Sremac M et al. Alginate-microencapsulation of human stem cell-derived beta cells with CXCL12 prolongs their survival and function in immunocompetent mice without systemic immunosuppression. Am J Transplant 2019; DOI: 10.1111/ajt.15308 (https://onlinelibrary.wiley.com/journal/16006143)

[54] Hasse C, Klock G, Schlosser A, Zimmermann U, Rothmund M. Parathyroid

allotransplantation without immunosuppression. Lancet 1997; DOI: S0140-6736(05)62473-7 (https://www.thelancet.com/)

[55] Cabane P, Gac P, Amat J, Pineda P, Rossi R, Caviedes R et al. Allotransplant of microencapsulated parathyroid tissue in severe postsurgical hypoparathyroidism: a case report. Transplant Proc 2009; DOI: 10.1016/j.transproceed.2009.06.211 (https://www.journals.elsevier.com/transplantation-proceedings)

[56] Yucesan E, Basoglu H, Goncu B, Akbas F, Ersoy YE, Aysan E. Microencapsulated parathyroid allotransplantation in the omental tissue. Artif Organs 2019; DOI: 10.1111/aor.13475 (https://onlinelibrary.wiley.com/journal/15251594)

[57] Viacyte, Inc., https://viacyte.com/; 2020 [accessed 24 July 2020].

[58] Neurotech Pharmaceuticals, Inc., https://www.neurotechusa.com/; 2020 [accessed 24 July 2020].

[59] Sernova Corp., https://sernova.com/; 2020 [accessed 24 July 2020].

[60] Beta-O2 technologies Ltd., https://beta-o2.com/; 2020 [accessed 24 July 2020].

[61] Seraxis Inc., https://seraxis.com/; 2020 [accessed 24 July 2020].

[62] Defymed, https://defymed.com/; 2020 [accessed 24 July 2020].

[63] Gloriana Therapeutics Inc., https://glorianatx.com/; 2020 [accessed 24 July 2020].

OBJECTIVES

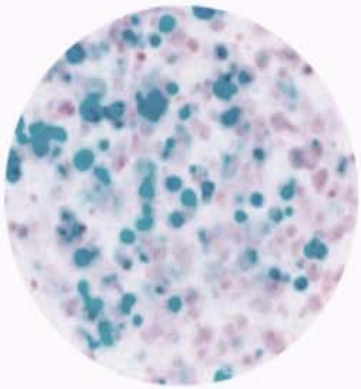

OBJECTIVES

Cell microencapsulation systems for the sustained delivery of therapeutic molecules have shown wide applicability in pathologies with very diverse characteristics, such as diabetes mellitus, cancer, anemia, hemophilia B or pathologies of the central nervous system, among others. The results obtained in the various clinical trials carried out to date make clear the advantages and potential applications of this promising technology. However, there are still aspects that need to be improved. In the last years, researchers have directed efforts towards trying to solve some of the key aspects that still limit efficacy (closely related to the biocompatibility of the implant) and biosafety, the two major criteria that must be satisfied to reach the clinical practice.

The main objective of this doctoral thesis was to address two of the most critical aspects, related to biocompatibility and biosafety, which still need to be optimized, working with cells that present suitable characteristics for reducing the immunological reaction against the implant and designing tools that allow an adequate dose control. More specifically, the following objectives were defined:

1. To analyze the behavior of genetically modified multipotent mesenchymal stromal cells (D1-MSCs), that present hypoimmunogenic and immunomodulatory characteristics, encapsulated in 3D alginate microcapsules, in terms of viability, metabolism, proliferation and erythropoietin secretion.

2. To analyze the influence of different D1-MSC-loads in alginate-based cell microencapsulation systems, in both *in vitro* and *in vivo* environments.

3. To design a complete and user-friendly mathematical model that allows accurate dose control in cell/drug delivery hydrogel particulate systems.

4. To experimentally validate the designed mathematical model with the complex example of cell microencapsulation technologies for sustained drug delivery.

EXPERIMENTAL SECTION

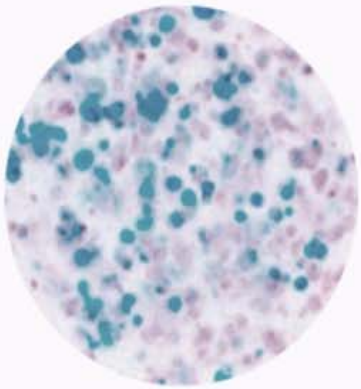

4

Experimental section
Chapter 1

IMPROVED CONTROL OVER MSCs BEHAVIOR WITHIN 3D MATRICES BY USING DIFFERENT CELL LOADS IN BOTH *IN VITRO* AND *IN VIVO* ENVIRONMENTS

Tania B. Lopez-Mendez[1,2], Edorta Santos-Vizcaino[1,2], Francisco Javier Blanco[3], Jose Luis Pedraz[1,2], Rosa Maria Hernandez[1,2], Gorka Orive[1,2*]

[1]NanoBioCel Group, School of Pharmacy, University of the Basque Country (UPV/EHU), Paseo de la Universidad, 7, 01006, Vitoria-Gasteiz, Spain.

[2]Biomedical Research Networking Center in Bioengineering, Biomaterials and Nanomedicine (CIBER-BBN), Instituto de Salud Carlos III, C/Monforte de Lemos 3-5, 28029 Madrid, Spain

[3]CIBER-BBN-Bioscaff Cartílago, INIBIC Institute for Biomedical research, 15006, A Coruña, Spain.

Published in: International Journal of Pharmaceutics (2017);
DOI: 10.1016/j.ijpharm.2017.09.014

*Corresponding author: Orive G (gorka.orive@ehu.eus)

ABSTRACT

The combination of multipotent mesenchymal stromal cells (MSCs) and different biomaterials has led to enormous advances in cell-based therapies, among which cell microencapsulation technologies are included. In the present work, we have studied the influence of different cell densities on the behavior of erythropoietin (EPO)-secreting MSCs immobilized in alginate microcapsules for their use as drug delivery systems. *In vitro* studies showed a more sustained and controlled EPO-secretion in groups with higher cell densities, which may be related to a more balanced renewal of the encapsulated cells, while low and intermediate densities gave rise to a continuous increase of both the number of cells and the EPO secretion levels. However, *in vivo* studies depicted a completely different scenario. Here the higher levels of cell proliferation led to a rapid space saturation and oxygen depletion of the capsule core, which eventually resulted in implant failure for the highest cell loads. On the contrary, lower cell densities showed a longer lasting release with a steadily increasing secretion profile. In conclusion, these results demonstrate how the final outcome of a cell-based drug delivery system may be tuned by just modifying the initial cell load, always taking into account the surrounding microenvironment.

Keywords: Cell encapsulation, efficacy, biosafety, biocompatibility, biomaterial, alginate.

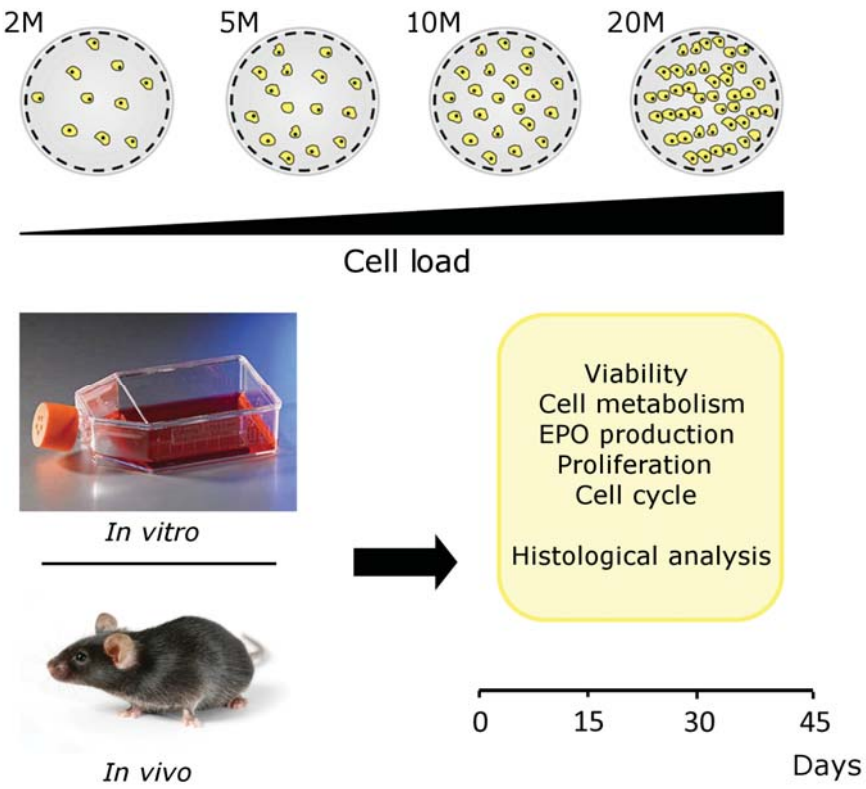

Graphical abstract. Schematic illustration of the main design of the study. For 45 days, 4 different groups of microcapsules (CL2, CL5, CL10 and CL20) were tested, both *in vitro* and *in vivo*, for cell viability, metabolism, proliferation, cell cycle and EPO secretion. Histological analyses were also performed in order to confirm the results obtained in other tests.

1. INTRODUCTION

Over the last decades, a significant effort has been directed to create artificial three-dimensional (3D) scaffolds that can hold, carry and protect cells from the external environment in order to develop several cell-therapy strategies, some of which are currently being used both for drug and cell delivery purposes [1-4]. Cell microencapsulation represents one of the strategies that aim to overcome the present difficulties related to whole organ graft rejection and the side-effects associated with the use of immunomodulatory protocols or immunosuppressive drugs. This approach can be used to release proteins and morphogens for long-periods of time, becoming an interesting platform for several chronic diseases [5-7].

Since the first approach carried out more than 30 years ago with the encapsulation of pancreatic islets in alginate microcapsules [8], this strategy has provided a wide range of promising therapeutic treatments for different kinds of diseases, such as diabetes, bone and cartilage defects, cancer, heart failure, anemia or central nervous system pathologies. Furthermore, to date some clinical trials have been conducted with promising results [7,9-12].

In recent years, the use of stem cells has generated a great impact on tissue engineering field, providing benefits impossible to achieve with other cell types. Pluripotent mesenchymal stromal cells (MSCs) can be extracted from adult individuals and have the ability to differentiate into various cell types such as chondrocytes, osteocytes or adipocytes, among others. MSCs present characteristics of hypo-immunogenicity (due to the lack in expression of mayor histocompatibility complex (MHC) class II and most of the classical costimulatory molecules [13,14] and immunomodulation, regulating the adaptive and innate immune systems. The occurrence of MSCs-mediated immunosuppression occurs via cell-cell contact, but also by the production of extracellular vesicles, including exosomes, and a multitude of cytokines and growth factors, that also induce the endogenous repair mechanisms of the surrounding tissues [15-19].

The combination of MSCs with biomaterials such as alginate offers the possibility of modifying some of their differentiation characteristics to suit the desired therapeutic goal [20-23]. However, sustained release systems based on the

combination of MSCs with non-degradable materials are also showing promising results. Mesenchymal stem cells are sometimes used as a support for other cells [24,25], but they can be used as well for their natural secretome or as genetically modified cells to secrete the therapeutic molecule of interest [26-29]. Surprisingly, cell lines are not commonly studied, even if they present some clear advantages over primary cells when designing this type of sustained release systems [30-33].

The choice of a cell that presents suitable properties for its use in this type of systems is critical but, once selected, it is also essential to recreate the optimal conditions for it within the microcapsule since, as a living organism, the environment to which they are exposed may vary their behavior substantially. In this regard, factors such as cell-cell (through direct contact or via soluble factors) and/or cell-material interactions play a critical role. The selected cell load is a key point for both types of interactions, as it increases or decreases them, based on the chosen cell/material ratio. Likewise, the ratio can affect the diffusion of nutrients, waste, oxygen or therapeutic products.

In this study, we genetically modified D1 multipotent mesenchymal stromal cells (D1-MSCs) to secrete erythropoietin (EPO) and encapsulated them in 3D alginate microcapsules with different cell loads, in order to analyze the influence of cell density for this type of cell in microencapsulation systems. The viability, metabolism, proliferation and EPO secretion of microencapsulated D1-MSCs were first evaluated *in vitro* and then microcapsules were implanted in an allogenic animal model to assess the differences caused by the enriched environment found *in vivo*.

2. MATERIALS AND METHODS

2.1. Cell culture

D1-MSCs were purchased from ATCC (ATCC® CRL12424™). Cells were genetically modified with the lentiviral vector pSIN-EF2-Epo-Pur to express EPO [32] and further grown and selected in Dulbecco´s modified Eagle´s medium (DMEM) (ATCC 30-2002) supplemented with 10% fetal bovine serum (FBS), 1% penicillin/streptomycin and 12.5 μg/mL puromycin solution. Cells were plated in

T-flasks, maintained at 37 ºC in a 5% $C0_2$/95% air atmosphere and passaged every 2-3 days. Reagents were purchased from Gibco (Life technologies, Spain).

2.2. Cell microencapsulation procedure

Ultra pure low-viscosity high guluronic acid alginate (UPLVG) was purchased from FMC Biopolymer, Norway. D1-MSCs genetically modified to release EPO were incorporated into 3D alginate-poly-l-lysine-alginate (APA) microcapsules using an electrostatic droplet generator with brief modifications of the procedure designed by Lim and Sun [8]. Briefly, cells were harvested from monolayer cultures using trypsin-EDTA (Life technologies), filtered through a 40 μm pore mesh and suspended in a solution of 1.5% (w/v) sodium alginate in phosphate buffered saline (PBS), at $2*10^6$, $5*10^6$, $10*10^6$ and $20*10^6$ cells/ml density (CL2, CL5, CL10 and CL20). These suspensions were extruded in a sterile syringe through a 0.35 mm needle at a 5.9 mL/h flow rate using a peristaltic pump. The resulting alginate particles were collected in a 55mM $CaCl_2$ solution and maintained under agitation for 15 min after the end of the process to ensure complete gelation of all the beads. Then, beads were suspended in 0.05% PLL solution for 5 min, washed twice with 10 mL of mannitol 1% and coated again with another layer of 0.1% alginate for 5 min. Poly-l-lysine (PLL hidrobromide Mw 15 000–30 000 Da) was obtained from Sigma Aldrich. All the solutions were prepared with milli-Q water and the pH and osmolarity values were adjusted to 7.4 (HEPES buffer) and 270 mosm/L (mannitol), respectively. All the process was carried out under aseptic conditions at room temperature, and resulting microcapsules were cultured in complete medium at 37 ºC in a 5 % $C0_2$/95% air atmosphere standard incubator.

2.3. Microcapsule morphology observation

Regular observation of the microcapsule morphology was performed throughout the study in order to detect any deterioration or damage. For that purpose, a Nikon TSM microscope model was selected.

2.4. Cell metabolism assessment

Metabolic activity was determined on the basis of tetrazolium production using the Cell Counting Kit-8 (CCK-8) (Sigma Aldrich). For all samples, this assay was performed on days 1, 15, 30 and 45. Concisely, 100 μL of microcapsule suspension per well were inoculated in a 96-well plate, followed by addition of 10 uL of CCK-8. After 4 h incubation, color development was read at 450 nm using a Tecan M200 microplate reader. All values were corrected with the reference wavelength at 690 nm and normalized against the mean value of three blank wells (only cell culture medium). Data were shown as mean ± S.D of seven independent samples for each group, divided by the initial number of cells loaded in each group in order to make results comparable.

2.5. EPO secretion of encapsulated D1-MSC

Supernatants of all groups were assayed in triplicate by using Quantikine IVD Human Erythropoietin ELISA Kit purchased from R&D Systems (Minneapolis, MN). Standards were run in duplicate according to the procedure specified in the kit. The volume of microcapsules needed for each group was adjusted in each case in order to obtain the same number of cells in all groups. The calculations were made taking into account the quantity of cells/mL in the initial cell-alginate suspension, and the needed number of microcapsules for each group were used for the assay, always maintaining the same number of cells, in order to normalize the results and make them comparable. Microcapsules were washed twice with phosphate buffered saline and placed on cell culture plates with complete growth medium, for a 24 h period. Then, supernatants were collected and stored at -80ºC until the last day of the study, when ELISA assay was performed. Results were expressed as mean ± S.D.

2.6. Viability of encapsulated D1-MSCs

To assess the viability, cells entrapped into APA microcapsules were dyed with the LIVE/DEAD kit (Life technologies) following manufacturer's indications. After 30 min, fluorescence micrographs were taken using an epi-fluorescence

microscope (Nikon TSM). To quantify the number of living cells, enclosed cells were firstly de-encapsulated with alginate lyase (0.5 mg/mL) (Sigma Aldrich), and stained with LIVE/DEAD kit (Life technologies). Incubation of microcapsules with alginate lyase is a widely used method that allows total de-encapsulation of cells without affecting their viability [31,34]. After 20 min incubation at room temperature protected from light, cells were counted by flow cytometry on a FACSCalibur cytometer (BD Biosciences, San Jose, CA), using Trucount Tubes (BD). All samples were assayed in triplicate for all groups, and obtained values are shown as mean of 3 independent samples ± S.D per study group. The number of living cells obtained for the day 1 was considered as 100% in each group, and all values were expressed in function of this percentage.

2.7. *In vivo* study: Microcapsule implantation and microcapsule retrieval to evaluate explanted encapsulated cells

Animal studies were carried out according to the ethical guidelines established by our Institutions, under an approved animal protocol (CEEA/369/2014/HERNANDEZ MARTÍN). Adult female C57BL/6J mice were anesthetized by isoflurane inhalation, and implanted subcutaneously with a total volume of 300 µL of cell-loaded microcapsules (CL2 $2*10^6$; CL5 $5*10^6$; CL10 $10*10^6$; CL20 $20*10^6$cells/mL) suspended in PBS using a 20-gauge catheter (Nipro; Nissho Corp, Belgium). Animals were housed in specific pathogen free facility under controlled temperature and humidity with a standardized 12 h light/dark cycle and had access to food and water ad libitum.

At days 15, 30 and 45 after implantation, 3 animals from each group were sacrificed and capsules were explanted. Microcapsule recovery was easy, and more than 90% in all cases, as most microcapsules could be found aggregated and surrounded by newly formed vascularized tissue [35]. Samples of explants and surrounding tissue were taken for histological analysis (Hematoxilin-eosin staining and Ki-67 immunohistochemistry). The rest of the explants were disaggregated in order to release the microcapsules immobilized in them. Briefly, a mix of collagenase H (2 mg/mL) and hyaluronidase (1 mg/mL) (Sigma, St. Louis, USA) was prepared

using DMEM. This enzyme solution was filtered-sterilized prior to use. Using 50 mL tubes, 5-6 mL of disaggregation solution was added to each microcapsule aggregate and incubated in a shaker bath at 37 ºC for 4 h at 100 rpm. Once the surrounding tissue was digested, the solution in the tubes was filtered using 40 µm pore size filters to recover tissue-free capsules. The aforementioned cell metabolism and viability assays, EPO secretion quantification and cell proliferation analysis were performed with the explanted microcapsules, following the same procedures used *in vitro*.

2.8. Proliferation and cell cycle of encapsulated D1-MSCs: comparison between *in vitro* and *in vivo*

30 days after the encapsulation, in order to assess the proliferation of encapsulated D1-MSCs, microcapsules from both the *in vitro* and the *in vivo* studies were exposed for 48 h to the thymidine analogue, 5-bromo-2´-deoxyuridine (BrdU), which is incorporated to the new synthesized DNA during replication. The volume of microcapsules needed for each group was adjusted in each case in order to obtain the same number of cells in all groups (normalized comparable results). After the exposure, enclosed cells were de-encapsulated with alginate lyase (0.5 mg/mL) (Sigma Aldrich) and fixed for intracellular labelling with the fluorescent intercalator 7-Aminoactinomycin D (7AAD) for DNA staining and anti-BrdU antibody for BrdU detection. All the process was carried out using a BD Pharmingen FITC BrdU flow kit (Cat. No 559619) and following manufacturer's instructions with brief modifications for making it more adequate for the analysis of encapsulated cells. For the assay a FACSCalibur cytometer (BD Biosciences, San Jose, CA) was used. All values are shown as mean of independent experiments ± S.D per study group.

2.9. Histological analysis of microcapsules and surrounding tissue

Proliferation behavior was also assessed by immunohistochemistry in order to confirm the results obtained in previous experiments. Microcapsules from both *in vitro* and *in vivo* studies were fixed in 4% paraformaldehyde solution, embedded in paraffin, sectioned and stained for hematoxylin-eosin and Ki67 (peroxidase catalyzed

reaction). *In vitro*, some capsules from each group were taken at days 15, 30 and 45. *In vivo*, at days 15, 30 and 45 after implantation, three animals from each group were sacrificed, and the implants were retrieved and fixed in a 4% paraformaldehyde solution for histological analyses. Serial horizontal cryostat sections (14 μm) were processed for both stainings. Photographic images were taken using a Nikon D-60. Histological analyses were performed in a blind way by two different pathologists and for each group.

Randomly taken slides were used to count the number of positively stained cells for Ki-67 per capsule, and the results were normalized against the total number of counted capsules per slide.

2.10. Statistical analysis

Data are presented as mean ± S.D. One-way ANOVA and post-hoc test were used in multiple comparisons. The Bonferroni or Tamhane post-hoc test was applied according to the result of the Levene test of homogeneity of variances. In viability studies, Student`s T-Test was selected for the comparison between days 30 and 45. In the case of non-normally distributed data, Mann-Whitney U non-parametric analysis was used. All statistical computations were performed using SPSS 20 (SPSS, Inc., Chicago, IL).

3. RESULTS

3.1. Microcapsule morphology after the encapsulation process

All batches of microcapsules, both *in vitro* and *in vivo*, showed spherical morphology and homogeneous size distribution (diameter 450-480 μm) **(Figures 1 and 2)**. There were no broken or damaged capsules.

3.2. Cell metabolism of encapsulated D1-MSCs

The results obtained from cell metabolism assays showed a general upward trend for all groups throughout the study. The data shown in **Figure 1A** was

represented dividing the absorbance values by the initial number of cells in each group, in order to make them comparable. The highest values were observed in the group of CL2 in which the upward slope was steeper until day 45, followed by the rest of the groups, in load ascending order, to the group of the highest cell load, which presented nearly constant values in all the measurements. Significant differences between CL2 and the rest of the groups were observed, at day 30 ($P<0.01$) and the following differences at day 45: CL2 and CL5, $P<0.01$; CL2 and CL10 or CL20, $P<0.001$; CL20 and CL5, $P<0.01$ and CL20 and CL10, $P<0.05$. Differences between CL2 and CL20 were described in the graph.

3.3. EPO secretion of encapsulated D1-MSCs

EPO secretion of encapsulated cells **(Figure 1B)** was measured in order to analyze the influence of cell load in the ability of D1-MSCs to produce the therapeutic factor. As in cell metabolism assays, the obtained values were divided by the number of cells per group to make them comparable. In this case, we also observed a general upward trend in all groups that was, once again, more evident in those with the smaller cell loads, being nearly constant in the group of CL20. Significant differences were detected during the study: At day 1 between CL2 and CL10 or CL20 ($P<0.05$); at day 15, between CL5 or CL10 and CL2 or CL 20 ($P<0.05$) and between CL2 and CL20 ($P<0.001$); and at days 30 and 45, between CL5 or CL10 and CL2 or CL20 ($P<0.01$) and between CL2 and CL20 ($P<0.001$). There were not statistical differences between CL5 and CL10 during the study. Differences between CL2 and CL20 were described in the graph.

3.4. Viability of encapsulated D1-MSCs

Cell viability of encapsulated cells was assayed using a LIVE/DEAD kit, which stains the dead cells in red and the living ones in green, and analyzing the outcome both via flow cytometry (quantitative results) and with microscopic observations (qualitative results).

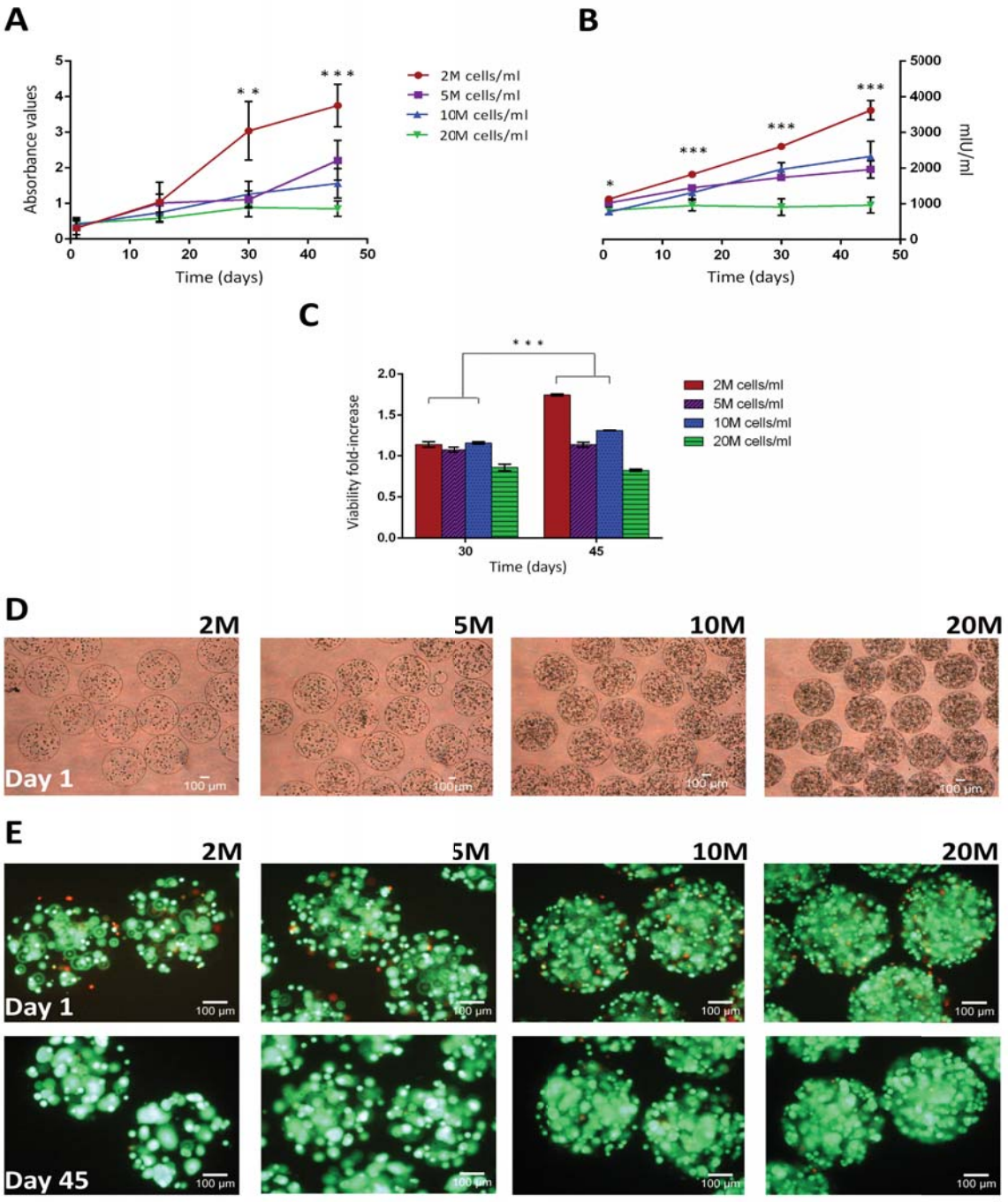

Figure 1. Results obtained for *in vitro* studies. Cell metabolism **(A)** and EPO secretion **(B)** at days 1, 15, 30 and 45. Statistical differences (ANOVA) between CL2 and CL20 are described in the graphs. For cell metabolism assay, results were divided by the number of cells per group in order to make them comparable. For the ELISA assay, a different number of microcapsules was used for each group, with the same final number of cells in all cases. EPO secretion graph represents EPO mlU in a mL of the collected supernatant, for each group (different number of microcapsules, same number of cells). Cell viability **(C)** at days 30 and 45. The percentage of living cells obtained for day 0 was considered as 100% in each microcapsule group, and all values were expressed in function of this percentage. Statistical analysis (T-Test) showed differences between days 30 and 45 for CL2 and CL10 (***). For all the graphs, bar graphs symbolize the mean ± SD. Statistical significance *$p < 0.05$, **$p < 0.01$, and ***$p < 0.001$. **D** Microcapsule morphology at day 1. **E** Fluorescence micrographs with LIVE/DEAD staining of the entrapped cells within the APA microcapsules at days 1 and 45.

Results obtained by flow cytometry **(Figure 1C)** demonstrated the high percentages of living cells inside the microcapsules throughout the study. The values are presented normalized against day 1, considered as 100% for all groups. The shape of the graph agrees with that observed in cell metabolism and EPO secretion assays, as they also show a general upward trend in all the groups except the one of CL20, which remains constant over 45 days. Differences between days 30 and 45 were significant for CL2 and CL10 groups ($P<0.001$), according to T-test statistical analysis.

Data obtained by microscopy images provided further evidence on our observations. Fluorescence micrographs collected by day 45 demonstrated the high viability of cells encapsulated in all batches of microcapsules maintaining the green fluorescence of living cells even at the end of the study **(Figure 1E)**. Likewise, there was an evident increase in the number of living cells per capsule, for all groups of microcapsules, during the study.

3.5. Encapsulated cell metabolism, viability and EPO secretion *in vivo*

In a second set of experiments, the same types of microcapsules that were previously evaluated *in vitro* were subcutaneously implanted in mice to observe the effects of different cell loads *in vivo*. At day 15, 30 and 45, the microcapsules were retrieved to further evaluate the immobilized cells.

Figures 2A and **2B** show the results obtained for cell metabolism **(2A)** and EPO secretion **(2B)** *in vivo*. In both cases, a general upward trend can be observed in the beginning of the study for all groups but, in the last day of the study, the values of all groups fell down dramatically to reach even values of zero in the group of the highest cell load. The group of CL2 is the only one that maintained, by day 45, more constant values for cell metabolism and even higher ones for the secretion of the therapeutic molecule.

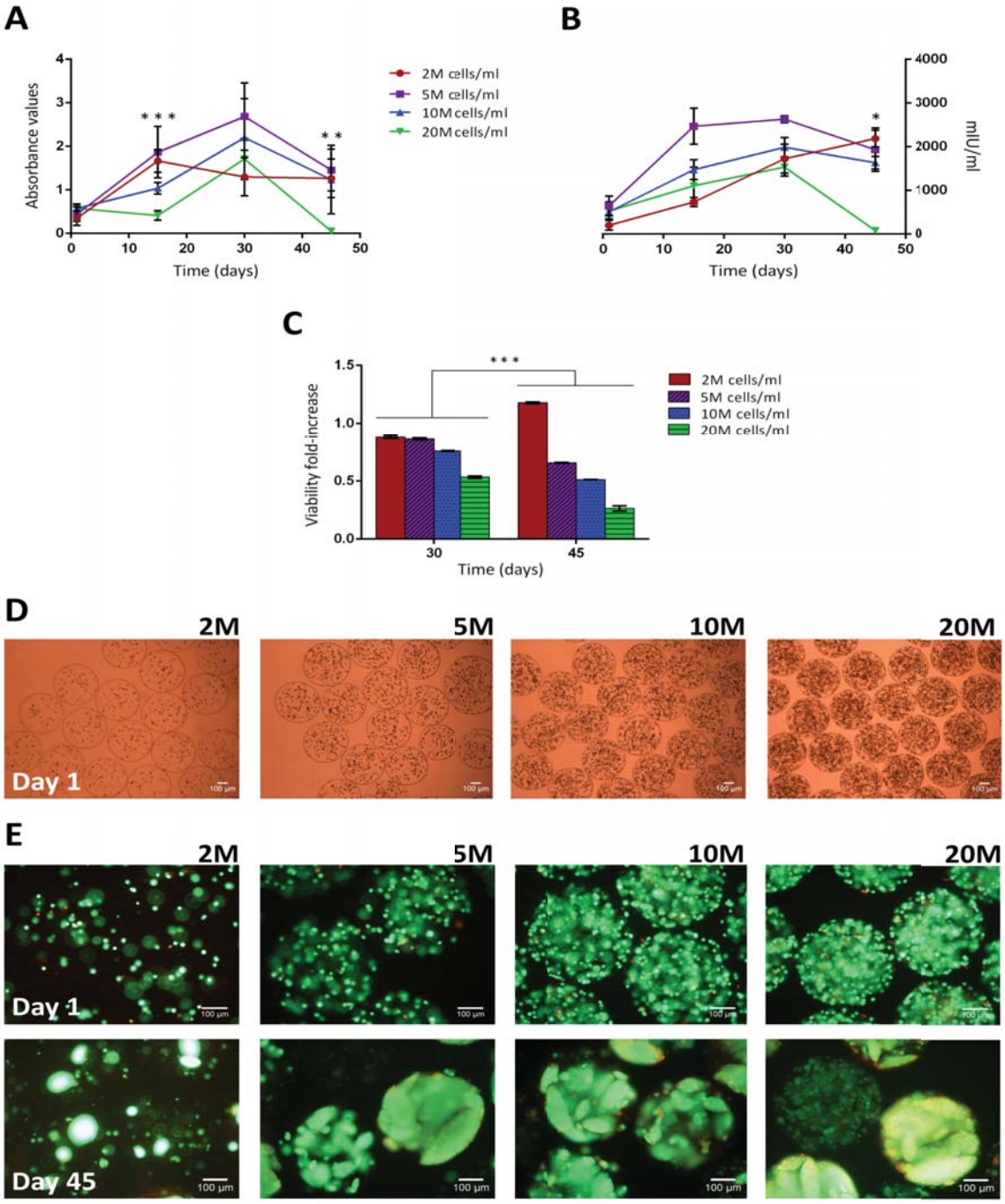

Figure 2. Results obtained for *in vivo* studies. Cell metabolism **(A)** and EPO secretion **(B)** at days 1, 15, 30 and 45. Statistical differences (ANOVA) between CL2 and CL20 are described in the graphs. For cell metabolism assay, results were divided by the number of cells per group in order to make them comparable. For the ELISA assay, a different number of microcapsules was used for each group, with the same final number of cells in all cases. EPO secretion graph represents EPO mlU in a mL of the collected supernatant, for each group (different number of microcapsules, same number of cells). Cell viability **(C)** at days 30 and 45. The percentage of living cells obtained for day 0 was considered as 100% in each microcapsule group, and all values were expressed in function of this percentage. Statistical analysis (T-Test) showed differences between days 30 and 45 for all groups. For all the graphs, bar graphs symbolize the mean ± SD. Statistical significance *$p < 0.05$, **$p < 0.01$, and ***$p < 0.001$. **D** Microcapsule morphology at day 1. **E** Fluorescence micrographs with LIVE/DEAD staining of the entrapped cells within the APA microcapsules at days 1 and 45.

In cell metabolism experiments, significant differences were detected at day 15 in the following cases: between CL2 and CL10, ($P<0.01$); CL2 and CL20, ($P<0.001$); CL5 and CL20, ($P<0.01$) and CL10 and CL20, ($P<0.001$). At day 30, there were significant differences only between CL2 and CL5 and, at day 45, between CL2 and CL20 ($P<0.01$), CL5 ($P<0.01$) and CL10 ($P<0.05$). For EPO secretion values, there were statistical differences (ANOVA) between CL5 and CL20 ($P<0.05$) at day 30 and between CL2 and CL10 ($P<0.05$) or CL20 ($P<0.05$) at day 45. Significant statistical differences between the groups of CL2 and CL20 were highlighted in the graphs.

LIVE/DEAD staining of the explanted cells also showed a different trend in viability percentages for all groups over the study, when compared to those obtained in vitro **(Figure 2C)**. In flow cytometry results, groups of lower cell loads maintained or even increased cell viability values, while higher cell load group´s values, especially CL20´s, dropped down at the end of the assay. According to T-test statistical analysis, there were significant differences between days 30 and 45 for all groups ($P<0.01$).

In the photographs taken using the same staining, it is possible to note that, even if cell viability seems to be high throughout the study, the behavior of the cells appears to be totally different, especially due to the apparition of some cell aggregates by day 45, with evident signs of central necrosis (see histological analysis below), which leads us to consider possible differences in cell cycle and proliferation patterns when implanted *in vivo* **(Figure 2E)**.

3.6. Proliferation behavior and cell cycle of encapsulated D1-MSCs both *in vitro* and *in vivo*

With the aim of elucidating potential differences in cell cycle and proliferation between in vitro and *in vivo* studies, several complementary assays were carried out in order to develop a global idea about which was exactly the cell behavior, in that regard, for both cases.

First, at day 30, cell cycle and cell proliferation were analyzed by flow cytometry using 7AAD and BrdU. 7AAD is a molecule that stains all the DNA of the cell in red and allows us to determine in which phase of the cycle is it (when replicating, the quantity of DNA is doubled). Secondly, when cells are cultured with labelling medium that contains BrdU, this pyrimidine analogue is incorporated in place of thymidine into the newly synthesized DNA of proliferating cells and gives us the opportunity to detect those cells via flow cytometry **(Figure 3A)**. The combination of 48h exposure of the encapsulated cells to BrdU and the 7AAD DNA staining, allowed us to distinguish 4 clearly different populations: 1- Negative for BrdU uptake and G_0/G_1 for cell cycle (no cell proliferation); 2- Positive for BrdU uptake and G_0/G_1 (cell cycle completed, cell division finished); 3-Positive for BrdU and M/G_2 (DNA replication with or without nuclear division, no cytoplasm division); 4- Negative for BrdU uptake and M/G_2 (DNA replicated but not in the last 48h, cell cycle delayed or blocked) **(Figure 3B)**.

A representative sample of the obtained cytometry plots is presented in **Figure 3C** where clear differences between the results of *in vitro* and *in vivo* studies can be observed. *In vitro*, the most notable cell population was the one in which cells were in M/G_2 phases of the cell cycle but their genetic material had not been replicated in the last 48h, when exposed to BrdU. Therefore, it could be said that those cells slowed or blocked their cell cycle and, for some reason, cytoplasm division was not completed. It seems as there were some kind of restrictions for cell cycle to be completed. However, *in vivo*, this population was much smaller and there was a much more remarkable one: cells that had replicated their DNA during those 48h, incorporating BrdU, and finally completed the cell division, going back to G_0/G_1 phases with the incorporated Thymidine analogue in their DNA. Interestingly, the microenvironment to which cells are exposed seems to be more decisive for cell behavior than the selected cell load.

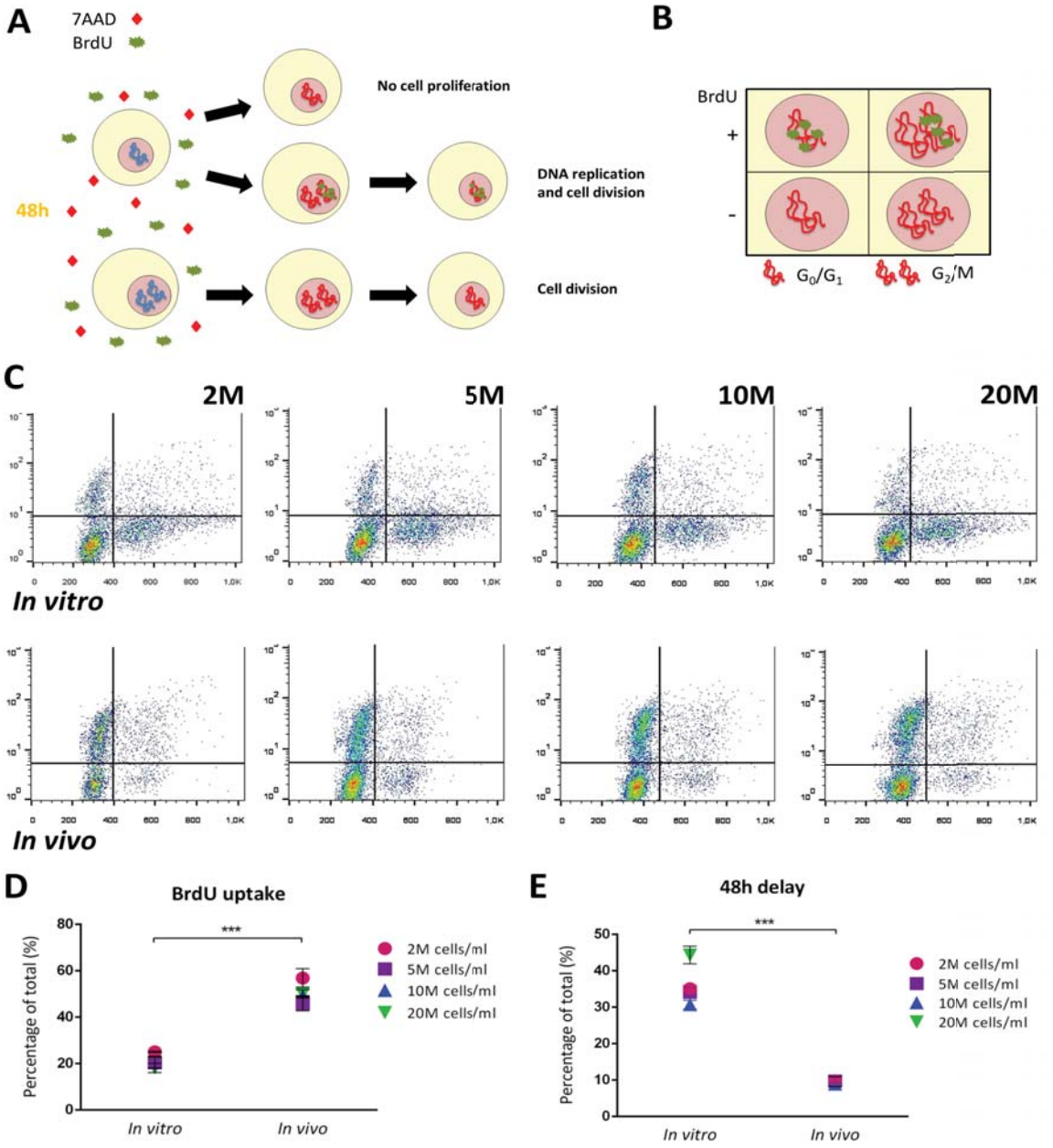

Figure 3. Cell cycle and proliferation analysis of microencapsulated cells, both *in vitro* and *in vivo*. **A** Cells were exposed for 48h to the thymidine analogue, 5-bromo-2´-deoxyuridine (BrdU), which is incorporated to the new synthesized DNA during replication. After the exposure, all the samples were fixed for intracellular labelling with the fluorescent intercalator 7-Aminoactinomycin D (7AAD) for DNA staining and anti-BrdU antibody for BrdU detection. 7AAD stains all the DNA, regardless of the cell cycle phase, while BrdU is only incorporated during the DNA replication. **B** Scheme of the 4 different populations that can be found after 48 h cell exposure to BrdU and 7AAD. **C** Flow cytometry dot plots of CL2, CL5, CL10 and CL20 groups, both *in vitro* and *in vivo*, after BrdU+7AAD test. The 4 populations correspond to the ones described in **B**. **D** and **E**. Comparison between *in vitro* and *in vivo* cell proliferation behavior. The number of cells positive for BrdU (D) was higher in the *in vivo* for all groups (***) (Mann-Whitney U test) while the population of cells in M/G2 phases without incorporation of BrdU in the last 48 h (48 h delay in cell cycle) (E) was higher *in vitro* for all groups (***) (Mann-Whitney U test). There were no statistical differences between cell load groups in neither cases (ANOVA). Bar graphs symbolize the mean ± SD. Statistical significance *$p < 0.05$, **$p < 0.01$, and ***$p < 0.001$.

With the aim of analyzing in detail the differences observed between in vitro and *in vivo* populations, in **Figures 3D** and **3E**, the percentage of cells that had incorporated BrdU to their DNA during those 48h **(Figure 3D)** and the number of cells that had been in M/G_2 phases during the same period of time (with replicated DNA but without completing cell division, cell cycle blocked) **(Figure 3E)** were plotted. From these graphs, it is possible to deduce that the absolutely different environmental conditions found *in vitro* or *in vivo* drastically changed cell proliferation behaviors that, however, seem to be less dependent on different cell densities. The Mann-Whitney U statistical test conducted in both analysis showed significant differences ($P < 0.01$) between the results obtained *in vitro* and *in vivo*, for both populations. In the other hand, ANOVA analysis between groups for *in vitro* and *in vivo* studies separately determined that there were no significant differences associated to cell load modifications.

3.7. Histological analysis of microcapsules and surrounding tissue

Cell proliferation was also evaluated via indirect peroxidase immunohistochemistry for Ki-67, at 15, 30 and 45 days. **Figure 4A** shows a comparison between the results obtained *in vitro* and *in vivo* throughout the study.

In the beginning of the *in vitro* study, highly undifferentiated cells were observed inside the microcapsules in all groups (morphological observation). From day 30, cell proliferation became faster in all groups, with values greater than 10% in some cases (positive for Ki-67) and the appearance of central necrosis in some microcapsules. By day 45, the proliferation rate remained very pronounced in the first three groups (CL2, CL5 and CL10) but not on the CL20 one, in which some simple flat or cubical morphologies could be seen. These results agree with those obtained in other studies (metabolism, production, etc.).

Regarding the *in vivo* studies, at day 15 after implantation, cells of undifferentiated morphology were observed inside the microcapsules, but also some empty capsules in the CL2 group, where the initial number of cells per capsule was lower. From the beginning of the study, a rapid cell growth was detected in CL10 and CL20 groups, with a proliferation rate greater than 50% (positive for Ki-67) and

a high mitotic index. Like in the *in vitro* studies, by the last day, it was possible to observe some morphological changes, especially in the CL20 group but, in this case, the morphology seemed mostly chondroblastic.

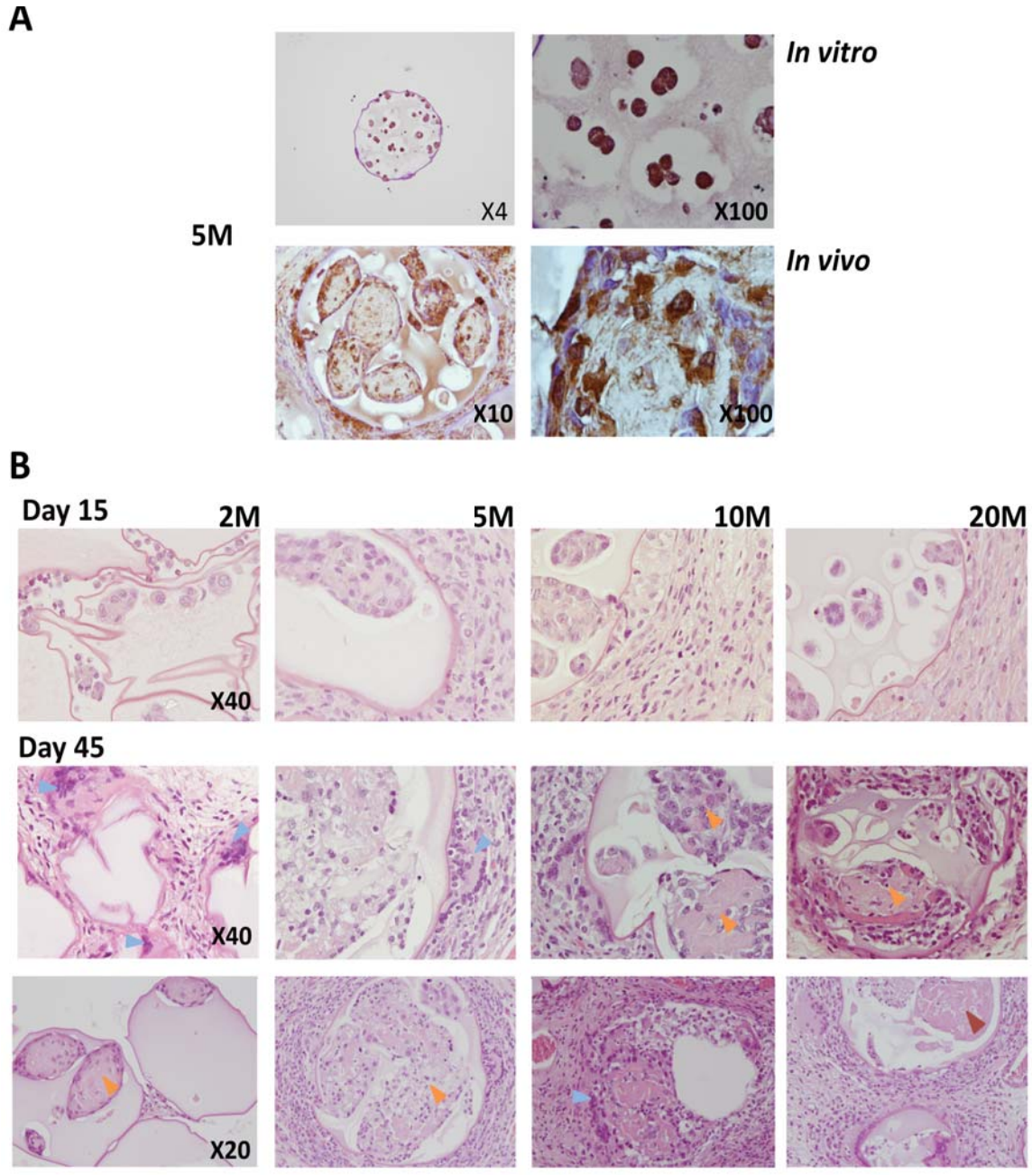

Figure 4. Histological analysis of the microcapsules and their environment. A Ki-67 staining of both *in vitro* and *in vivo* microcapsules. An example of the proliferation behavior of the same cell load (CL5) shows evident differences between the 2 situations. **B** Hematoxylin and eosin staining of *in vivo* explants, at days 15 and 45. Arrows show: in blue, multinucleated histiocytes around the microcapsules; in orange, high proliferation areas and in red, intramicrocapsular necrosis.

Regardless the group, the number of Ki-67-positive cells were always higher in the *in vivo* study. This result agrees with that obtained in cell cycle analysis and BrdU uptake at day 30, in which a much faster proliferation was described.

In vivo, the observation of the explants at days 15, 30 and 45, with hematoxylin-eosin staining, allowed us to better understand intracapsular cell behavior. In **figure 4B**, it is possible to detect cellular aggregates in all groups, at day 45, and even intramicrocapsular necrosis, especially in the higher cell load groups. This clear progression from excessive proliferation to intracapsular necrosis could explain the final drop observed previously in viability, metabolism and EPO secretion in some of the groups and the implant failure reported, for CL20 group at day 45. Histological analyses of the surrounding tissue showed also some inflammatory infiltrates of eosinophils and neutrophils in the beginning and the formation of multinucleated histiocytes, more linked to chronic immune responses, in the following weeks and principally in the higher cell load groups, as intracapsular necrosis progressed.

4. DISCUSSION

Cell microencapsulation systems represent an attractive tool to enable the local and controlled delivery of therapeutic molecules but there are still some aspects that must be optimized in order to translate this technology to the clinical practice [36]. Selecting a suitable cell type is one of these points and, in this regard, MSCs present very good characteristics for their use in this type of systems, but their suitability may vary substantially depending on the environment to which they get exposed once implanted. The selected cell load is a key point for factors such as cell-cell and/or cell-material interactions, as the chosen cell/material ratio directly increases or decreases them. It also can affect the diffusion of nutrients, waste, oxygen or therapeutic products.

The objective of this study was to describe the influence of different cell loads on cell microencapsulation systems incorporating MSC-D1 for the sustained release of therapeutic factors. In this regard, the extensive battery of tests selected and the comparison of the results obtained both *in vitro* and *in vivo* gave us comprehensive and relevant information that will help in future related studies.

In previous studies carried out at our laboratory using the same D1-MSCs, it has been demonstrated that the genetic modification of this cell line, with pSIN-EF2-Epo-Pur vector, to secrete EPO or it´s encapsulation into APA microcapsules does not significantly alter cell phenotype or it´s differentiation capacity [31,32].

Tests of cellular metabolism and production of EPO *in vitro* **(Figure 1A and 1B)** resulted in a general upward trend for all groups that showed steeper slopes in the lower cell load groups and remained practically constant in the CL20 group. Given that all the results have been presented normalized by the total number of encapsulated cells in each group at baseline, it is possible to make a direct comparison and say that lower cell load groups allow a greater increase in both parameters. The percentages of cell viability throughout the study **(Figure 1C)** also allow us to associate these increases in metabolism and production of EPO with a greater number of living cells in more advanced points of the study in groups of lower cell loads. The viability percentages for the CL20 group, however, were constant until the end of the study, which is consistent with the results obtained in the other two tests. Photographs taken by fluorescence microscopy **(Figure 1E)** showed good cell viability until the last day of the study and no evidence of cell aggregates. Given that there is cell proliferation and this remains very similar between groups, as discussed later, it seems that in the CL20 group, levels of proliferation and cell death keep a balance of constant renewal. In contrast, we find that the group CL2 does increase the levels of cellular metabolism and production of the therapeutic molecule, probably due to a decrease in the percentage of cell death during the study.

The explanation to these phenomena may be associated with one of the following reasons: on the one hand, a better balance in cell renewal could be explained by the fact that, with increased cell load there will be more cell-cell interactions that produce inhibition of cell proliferation [37]. Furthermore, it is possible that in the microcapsules of low cell densities the access of the cells to nutrients and oxygen would be easier than in the opposite case where perhaps the cells located in the innermost areas of the microcapsule could suffer a reduced flow of those elements [38]. Either way, in view of these first *in vitro* results, perhaps we could conclude that higher cell loads could result more appropriate for sustained release systems

based on the immobilization of cells, in order to achieve a more constant release of the therapeutic factor.

Interestingly, the fact that so different cell behavior profiles can be obtained by just varying the initial cell load, could be determinant also when this type of matrices are used as bioreactors for 3D cultures *in vitro* [39-45]. In such cases, it appears that selecting a suitable initial cell density will greatly influence the final growth and proliferation results of the encapsulated cells.

The *in vivo* study results show a different scenario. Assays in cell metabolism **(Figure 2A)** and EPO-secretion **(Figure 2C)** showed a general upward trend in the early phases of the study but, in both graphs, perhaps the most remarkable feature is the turning point that exists around day 30, in which most groups seem to reach a maximum point after which all values decrease. The only group that does not follow this trend is CL2, which remains more or less constant in the case of cellular metabolism and even increases the secretion of EPO. The percentages of viability throughout the study **(Figure 2C)** reported higher percentages of cell death *in vivo* that become very high at the end of the study for the CL20 group and noticeable for intermediate groups, but which, however, remain at low values in the group of the lowest cell load. Taking into account all this information, it can be deduced that, even if viability percentages dropped in the end of the study, the total number of cells in all groups seem to increase until the end, rising the values for cell metabolism and EPO secretion at first and producing the accumulation of dead cells inside the capsule in the end of the study, when all the values dropped down. The only exception was the case of CL2 in which the percentages of living cells increase until the last moment, explaining the values obtained in tests of metabolism and production of EPO for that group.

The images obtained by fluorescence microscopy with calcein-ethidium **(Figure 2E)** showed good viability until the end of the study, with the appearance of some capsules of reduced viability in the group of CL20, at day 45. The most notable feature on these photographs is probably the aggregates that can be seen, for all groups but especially for CL20, in the end of the study, which made us assume a high proliferative activity and the possible appearance of necrosis in the inner part of

the microcapsules and the cell aggregates, which would explain the final decrease in all the parameters.

Given that all tests led us to draw the levels of proliferation as the main difference between the *in vitro* and *in vivo*, we decided to analyze this parameter in a more exhaustive way. We analyzed, for all groups at day 30, existing patterns of proliferation within the microcapsules, both by cell cycle analysis and BrdU uptake **(Figures 3A and 3B)**. The cytometry results **(Figure 3C)** showed, *in vitro*, a remarkable population of cells that had a double copy of their DNA but which nevertheless had not completed the cell division in the last 48 hours, which seemed to indicate some kind of arrest of the cell cycle in M/G_2, perhaps by insufficient cell signaling, lack of space inside the microcapsule and/or error detection in G_2 to mitosis checkpoint. Problems that stop the cell cycle in this point, such as inadequate cell size or morphology, are usually reversible once the problem disappears [46]. *In vivo*, however, this population barely existed but the one corresponding to cells that had completed the full cell cycle in the past 48 hours gained importance, with the incorporation of the BrdU molecule during the synthesis of new DNA and a single copy of their genetic material. It is possible that the enriched environment in which the implanted cells were placed, would have enhanced this rapid cell proliferation [47]. In the other hand, pH and osmolarity changes microcapsules face *in vivo* could affect the physicochemical characteristics of the nucleus of the capsules, leading to a softer alginate matrix which has a direct impact in cell behavior [48].

The results obtained for BrdU uptake and cell cycle were exposed in **3D** and **3E graphs**, making a comparison between the *in vitro* and *in vivo*, of the corresponding cell numbers for these populations and clearly significant statistical differences between *in vitro* and *in vivo*, but not between the groups, were found. It seems that proliferation patterns remain constant regardless of the number of encapsulated cells.

With the intention of corroborating what had been observed in these analyses, another study was performed by immunohistochemistry, where levels of Ki-67 were assessed; both *in vitro* and *in vivo* **(Figure 4A)**. The levels for all groups were higher always in the *in vivo* study, reaching values of 50% and causing the appearance

of central necrosis in many of the microcapsules, while *in vitro* the proliferation percentages were maintained around 10% for all groups. This histological analysis allowed us to observe the center of the microcapsules, and to clarify the reason why a total failure of the implant had happened at the end of the study *in vivo* **(Figure 4B)**. While the images obtained by fluorescence microscopy showed the appearance of cell aggregates, it was necessary to make cuts at different levels inside the capsules, to analyze more closely the necrosis that was taking place in the central points and that was more difficult to detect by photographs of the capsular surface.

In the observation of the surrounding tissue of the explants *in vivo*, we could observe signs of the foreign body response against the implant [49], with an initial acute phase characterized by infiltration of neutrophils and eosinophils, followed by the appearance of multinucleated histiocytes and the development of granulomas in some cases. The immunomodulatory capacity of these cells is widely described [19,50], also in previous studies carried out with MSCs enclosed in similar encapsulation devices [51-53], but in this case, the high proliferation rates observed and the presence of necrosis from an early point of the *in vivo* study could alter the normal properties of these cells and produce a higher release of proinflammatory molecules, such as DAMPs (cytosolic proteins, pieces of genetic material etc.), from the implant to the environment, which are described to trigger substantially the host immune response [54-57].

At the end of the study, it was possible to detect some morphological changes in some of the encapsulated cells, to simple flat or cubic morphologies in the CL20 group *in vitro*, and to what seemed chondroblastic morphology *in vivo*. In this sense, it is interesting to highlight that differentiation phenomena and the resulting morphologies vary dramatically depending on the environment in which the cells are found. In this regard, there is some controversy over the degree of differentiation that usually occurs in this type of implant and its consequences [31,58]. For these EPO secreting D1-MSC, our group have already published a full study about their differentiation behavior both *in vitro*, being exposed to differentiation mediums, and subcutaneously implanted *in vivo* and how this affects their capacity to secrete EPO [31]. The results showed these cells were able to differentiate inside

the microcapsules, in vitro, towards specific lineages, when exposed to different culture mediums, while maintaining their capacity to secrete EPO. After 30 days *in vivo*, however, the phenotype of MSCs (CD29+, CD44+, CD45−, CD73+, CD105+, SCA-I+) was preserved in all conditions assayed. We could expect a similar behavior in this study as the same cells are exposed to the same conditions, thus probably the morphological changes observed in the histological analysis would correspond with early stages of differentiation in a reduced group of cells.

Therefore, in the view of these results, we could hypothesize that the enriched environment found *in vivo*, lead to much higher proliferation rates and the rapid increase of the cell load in all groups, but especially in those with higher cell densities. As the study progressed, however, the percentage of viability dropped, particularly in the group of CL20, with an increased accumulation of dead cells within the microcapsules and the central necrosis phenomenon, probably caused by lack of nutrients, oxygen and space for the innermost cells. As the days passed, the situation of high proliferation and accumulation of dead cells was maintained until reaching its peak around day 30 in most groups. From there, the levels of proliferation did not seem able to keep the number of living cells, making the percentage of cell viability drop in the 3 groups with higher cell densities and that led to a decrease in metabolism levels and erythropoietin production. The CL2 group was the only one that did not maintain this trend and this could be due to the low initial cell load that left more space for cell growth. This trend in charts of metabolism, production and cell viability, leads us to speculate on a similar progression for all groups, with a slower chronology in groups with lower cell density.

5. CONCLUSION

This study shows how the variation of a single factor, cell load in this case, can have a great impact on the behavior of a line of MSCs immobilized in a 3D matrix, and how these changes can significantly alter the functionality of the implant. *In vitro*, the choice of the most appropriate cell load should be made based on the desired application, ranging from a more sustained and constant proliferation and EPO release to a more or less pronounced increase over time. The enriched

environment found *in vivo*, however, sharply increases cell proliferation which leads to a totally different scenario inside the microcapsules.

6. ACKNOWLEDGEMENTS

Authors would like to thank Dr Felipe Prosper at the University Clinic of Navarra (CUN) for his assistance on the development of the lentiviral vector pSIN-EF2-Epo-Pur. Authors also gratefully acknowledge the support to research in cell microencapsulation from the Basque Government (IT 907-16) and the intellectual and technical assistance from the ICTS "NANBIOSIS", more specifically by the Drug Formulation Unit (U10) of the CIBER in Bioengineering, Biomaterials & Nanomedicine (CIBER-BBN). T. B. Lopez-Mendez thanks the Basque Government (Department of Education, Universities and Research) for the Ph.D. fellowship.

7. DECLARATION OF INTEREST

The authors declare no competing financial interest.

8. REFERENCES

[1] Chang TM. Semipermeable Microcapsules. Science 1964; DOI: 10.1126/science.146.3643.524

[2] Chick WL, Like AA, Lauris V. Beta cell culture on synthetic capillaries: an artificial endocrine pancreas. Science 1975; DOI: 10.1126/science.187.4179.847

[3] Langer R and Vacanti JP. Tissue engineering. Science 1993; DOI: 10.1126/science.8493529

[4] Khademhosseini A and Langer R. A decade of progress in tissue engineering. Nat Protoc 2016. DOI: 10.1038/nprot.2016.123

[5] Orive G, Hernandez RM, Gascon AR, Calafiore R, Chang TM, De Vos P et al. Cell encapsulation: promise and progress. Nat Med 2003; DOI: 10.1038/nm0103-104

[6] Orive G, Hernandez RM, Rodriguez Gascon A, Calafiore R, Chang TM, de Vos P et al. History, challenges and perspectives of cell microencapsulation. Trends Biotechnol 2004; DOI: S0167779903003111

[7] Orive G, Santos E, Pedraz JL, Hernandez RM. Application of cell encapsulation for controlled delivery of biological therapeutics. Adv Drug Deliv Rev 2014; DOI: 10.1016/j.addr.2013.07.009

[8] Lim F and Sun AM. Microencapsulated islets as bioartificial endocrine pancreas. Science 1980; DOI: 10.1126/science.6776628

[9] López-Méndez, T, Murua A, Pedraz JL, Hernandez RM, Orive G. Cell encapsulation technology: an alternative biotechnological platform for the treatment of Central Nervous System diseases. Bioencapsulation of Living Cells for Diverse Medical Applications. Bentham Science Publishers; 2012, p. 102-152

[10] Acarregui A, Orive G, Pedraz JL, Hernandez RM. Therapeutic applications of encapsulated cells. Methods Mol Biol 2013; DOI: 10.1007/978-1-62703-550-7_23

[11] Gurruchaga H, Saenz del Burgo L, Ciriza J, Orive G, Hernandez RM, Pedraz JL. Advances in cell encapsulation technology and its application in drug delivery. Expert Opin Drug Deliv 2015; DOI: 10.1517/17425247.2015.1001362

[12] Orive G, Santos E, Poncelet D, Hernández RM, Pedraz JL, Wahlberg LU et al. Cell encapsulation: technical and clinical advances. Trends Pharmacol Sci 2015; DOI: 10.1016/j.tips.2015.05.003

[13] Ankrum JA, Ong JF, Karp JM. Mesenchymal stem cells: immune evasive, not immune privileged. Nat Biotechnol 2014; DOI: 10.1038/nbt.2816

[14] Faiella W and Atoui R. Immunotolerant Properties of Mesenchymal Stem Cells: Updated Review. Stem Cells Int 2016; DOI: 10.1155/2016/1859567

[15] Abdi R, Fiorina P, Adra CN, Atkinson M, Sayegh MH. Immunomodulation by mesenchymal stem cells: a potential therapeutic strategy for type 1 diabetes. Diabetes 2008; DOI: 10.2337/db08-0180

[16] Hoogduijn MJ, Popp F, Verbeek R, Masoodi M, Nicolaou A, Baan C et al. The immunomodulatory properties of mesenchymal stem cells and their use for immunotherapy. Int Immunopharmacol 2010; DOI: 10.1016/j.intimp.2010.06.019

[17] Ranganath SH, Levy O, Inamdar MS, Karp JM. Harnessing the mesenchymal stem cell secretome for the treatment of cardiovascular disease. Cell Stem Cell 2012; DOI: 10.1016/j.stem.2012.02.005

[18] Shi Y, Su J, Roberts AI, Shou P, Rabson AB, Ren G. How mesenchymal stem cells interact with tissue immune responses. Trends Immunol 2012; DOI: 10.1016/j.it.2011.11.004

[19] Gao F, Chiu SM, Motan DA, Zhang Z, Chen L, Ji HL et al. Mesenchymal stem cells and immunomodulation: current status and future prospects. Cell Death Dis 2016; DOI: 10.1038/cddis.2015.327

[20] Wen Q, Zhou C, Luo W, Zhou M, Ma L. Pro-osteogenic effects of fibrin glue in treatment of avascular necrosis of the femoral head in vivo by hepatocyte growth factor-transgenic mesenchymal stem cells. J Transl Med 2014; DOI: 10.1186/1479-5876-12-114

[21] Li YY, Cheng HW, Cheung KMC, Chan D, Chan BP. Mesenchymal stem cell-collagen microspheres for articular cartilage repair: Cell density and differentiation status 2014; DOI: 10.1016/j.actbio.2014.01.002

[22] Moshaverinia A, Chen C, Xu X, Akiyama K, Ansari S, Zadeh HH et al. Bone regeneration potential of stem cells derived from periodontal ligament or gingival tissue sources encapsulated in RGD-modified alginate scaffold. Tissue Eng Part A 2014; DOI: 10.1089/ten.TEA.2013.0229

[23] Trouche E, Girod Fullana S, Mias C, Ceccaldi C, Tortosa F, Seguelas MH et al. Evaluation of alginate microspheres for mesenchymal stem cell engraftment on solid organ. Cell Transplant 2010; DOI: 10.3727/096368910X514297

[24] Kerby A, Jones ES, Jones PM, King AJ. Co-transplantation of islets with mesenchymal stem cells in microcapsules demonstrates graft outcome can be improved in an isolated-graft model of islet transplantation in mice. Cytotherapy 2013; DOI: 10.1016/j.jcyt.2012.10.018

[25] Shi XL, Zhang Y, Gu JY, Ding YT. Coencapsulation of hepatocytes with bone marrow mesenchymal stem cells improves hepatocyte-specific functions. Transplantation 2009; DOI: 10.1097/TP.0b013e3181bc288b

[26] Hu J, Li H, Chi G, Yang Z, Zhao Y, Liu W et al. IL-1RA gene-transfected bone marrow-derived mesenchymal stem cells in APA microcapsules could alleviate rheumatoid arthritis. Int J Clin Exp Med 2015; 8(1): 706-13.

[27] Han Y, Tao R, Han Y, Sun T, Chai J, Xu G et al. Microencapsulated VEGF gene–modified umbilical cord mesenchymal stromal cells promote the vascularization of tissue-engineered dermis: an experimental study. Cytotherapy 2014; DOI: 10.1016/j.jcyt.2013.10.014

[28] Barminko J, Kim JH, Otsuka S, Gray A, Schloss R, Grumet M et al. Encapsulated mesenchymal stromal cells for in vivo transplantation. Biotechnol Bioeng 2011; DOI: 10.1002/bit.23233

[29] Landazuri N, Levit RD, Joseph G, Ortega-Legaspi JM, Flores CA, Weiss D et al. Alginate microencapsulation of human mesenchymal stem cells as a strategy to enhance paracrine-mediated vascular recovery after hindlimb ischaemia. J Tissue Eng Regen Med 2016; DOI: 10.1002/term.1680

[30] Attia N, Santos E, Abdelmouty H, Arafa S, Zohdy N, Hernandez RM et al. Behaviour and ultrastructure of human bone marrow-derived mesenchymal stem cells immobilised in alginate-poly-l-lysine-alginate microcapsules. J Microencapsul 2014; DOI: 10.3109/02652048.2014.898706

[31] Garate A, Ciriza J, Casado JG, Blazquez R, Pedraz JL, Orive G et al. Assessment of the behavior of mesenchymal stem cells immobilized in biomimetic alginate microcapsules. Mol Pharm 2015; DOI: 10.1021/acs.molpharmaceut.5b00419

[32] Gurruchaga H, Ciriza J, Saenz del Burgo L, Rodriguez-Madoz JR, Santos E, Prosper F et al. Cryopreservation of microencapsulated murine mesenchymal stem cells genetically engineered to secrete erythropoietin. Int J Pharm 2015; DOI: 10.1016/j.ijpharm.2015.02.047

[33] Sanz-Nogues C, Horan J, Thompson K, Howard L, Ryan G, Kassem M et al. Inefficiency in macromolecular transport of SCS-based microcapsules affects viability of primary human

mesenchymal stem cells but not of immortalized cells. J Biomed Mater Res A 2015; DOI: 10.1002/jbm.a.35493

[34] Breguet V, von Stockar U, Marison IW. Characterization of alginate lyase activity on liquid, gelled, and complexed states of alginate. Biotechnol Prog 2007; DOI: 10.1021/bp070150e

[35] Murua A, Orive G, Hernandez RM, Pedraz JL. Xenogeneic transplantation of erythropoietin-secreting cells immobilized in microcapsules using transient immunosuppression. J Control Release 2009; DOI: 10.1016/j.jconrel.2009.04.009

[36] Santos E, Pedraz JL, Hernandez RM, Orive G. Therapeutic cell encapsulation: ten steps towards clinical translation. J Control Release 2013; DOI: 10.1016/j.jconrel.2013.04.015

[37] McClatchey AI and Yap AS. Contact inhibition (of proliferation) redux. Curr Opin Cell Biol 2012; DOI: 10.1016/j.ceb.2012.06.009

[38] Park SJ, Shin S, Koo OJ, Moon JH, Jang G, Ahn C et al. Functional improvement of porcine neonatal pancreatic cell clusters via conformal encapsulation using an air-driven encapsulator. Exp Mol Med 2012; DOI: 10.3858/emm.2012.44.1.001

[39] Kim J, Sachdev P, Sidhu K. Alginate microcapsule as a 3D platform for the efficient differentiation of human embryonic stem cells to dopamine neurons. Stem Cell Res 2013; DOI: 10.1016/j.scr.2013.06.005

[40] Forsey RW, Tare R, Oreffo RO, Chaudhuri JB. Perfusion bioreactor studies of chondrocyte growth in alginate-chitosan capsules. Biotechnol Appl Biochem 2012; DOI: 10.1002/bab.1009

[41] Zhao S, Agarwal P, Rao W, Huang H, Zhang R, Liu Z et al. Coaxial electrospray of liquid core-hydrogel shell microcapsules for encapsulation and miniaturized 3D culture of pluripotent stem cells. Integr Biol 2014; DOI: 10.1039/c4ib00100a

[42] Foster NC, Henstock JR, Reinwald Y, El Haj AJ. Dynamic 3D culture: models of chondrogenesis and endochondral ossification. Birth Defects Res C Embryo Today 2015; DOI: 10.1002/bdrc.21088

[43] Dorati R, Genta I, Ferrari M, Vigone G, Merico V, Garagna S et al. Formulation and stability evaluation of 3D alginate beads potentially useful for cumulus-oocyte complexes culture. J Microencapsul 2016; DOI: 10.3109/02652048.2015.1134691

[44] Kingsley DM, Dias AD, Corr DT. Microcapsules and 3D customizable shelled microenvironments from laser direct-written microbeads. Biotechnol Bioeng 2016; DOI: 10.1002/bit.25987

[45] Domejean H, de la Motte Saint Pierre,M., Funfak A, Atrux-Tallau N, Alessandri K, Nassoy P et al. Controlled production of sub-millimeter liquid core hydrogel capsules for parallelized 3D cell culture. Lab Chip 2016; DOI: 10.1039/c6lc00848h

[46] Rhind N and Russell P. Signaling pathways that regulate cell division. Cold Spring Harb Perspect Biol 2012; DOI: 10.1101/cshperspect.a005942

[47] Rodrigues M, Griffith LG, Wells A. Growth factor regulation of proliferation and survival of multipotential stromal cells. Stem Cell Res Ther 2010. DOI: 10.1186/scrt32

[48] Garate A, Murua A, Orive G, Hernandez RM, Pedraz JL. Stem cells in alginate bioscaffolds. Ther Deliv 2012; DOI: 10.4155/tde.12.53.

[49] Kastellorizios M, Tipnis N, Burgess DJ. Foreign body reaction to subcutaneous implants. Adv Exp Med Biol 2015; DOI: 10.1007/978-3-319-18603-0_6

[50] Kyurkchiev D, Bochev I, Ivanova-Todorova E, Mourdjeva M, Oreshkova T, Belemezova K et al. Secretion of immunoregulatory cytokines by mesenchymal stem cells. World J Stem Cells 2014; DOI: 10.4252/wjsc.v6.i5.552

[51] Goren A, Dahan N, Goren E, Baruch L, Machluf M. Encapsulated human mesenchymal stem cells: a unique hypoimmunogenic platform for long-term cellular therapy. FASEB J 2010; DOI: 10.1096/fj.09-131888

[52] Meier RP, Mahou R, Morel P, Meyer J, Montanari E, Muller YD et al. Microencapsulated human mesenchymal stem cells decrease liver fibrosis in mice. J Hepatol 2015; DOI: 10.1016/j.jhep.2014.10.030

[53] Zanotti L, Sarukhan A, Dander E, Castor M, Cibella J, Soldani C et al. Encapsulated mesenchymal stem cells for in vivo immunomodulation. Leukemia 2013; DOI: 10.1038/leu.2012.202

[54] Pittman K and Kubes P. Damage-associated molecular patterns control neutrophil recruitment. J Innate Immun 2013; DOI: 10.1159/000347132

[55] Hirsiger S, Simmen HP, Werner CM, Wanner GA, Rittirsch D. Danger signals activating the immune response after trauma. Mediators Inflamm 2012; DOI: 10.1155/2012/315941

[56] Kaczmarek A, Vandenabeele P, Krysko DV. Necroptosis: the release of damage-associated molecular patterns and its physiological relevance. Immunity 2013; DOI: 10.1016/j.immuni.2013.02.003

[57] Tang D, Kang R, Coyne CB, Zeh HJ, Lotze MT. PAMPs and DAMPs: signal 0s that spur autophagy and immunity. Immunol Rev 2012; DOI: 10.1111/j.1600-065X.2012.01146.x

[58] Wilson JL, Najia MA, Saeed R, McDevitt TC. Alginate encapsulation parameters influence the differentiation of microencapsulated embryonic stem cell aggregates. Biotechnol Bioeng 2014; DOI: 10.1002/bit.25121

5

Experimental section
Chapter 2

MATHEMATICAL MODELING FOR ACCURATE DOSE CONTROL IN SPHERICAL HYDROGEL DRUG/CELL DELIVERY SYSTEMS

Tania B. Lopez-Mendez[1,2], Edorta Santos-Vizcaino[1,2], Christopher W. MacMinn[3], Bertrand Thibault[4], Amaia Molinuevo[5], Jose Luis Pedraz[1,2], Gorka Orive[1,2,6,7], Rosa Maria Hernandez[1,2*]

[1]NanoBioCel Group, School of Pharmacy, University of the Basque Country (UPV/EHU), Paseo de la Universidad, 7, 01006, Vitoria-Gasteiz, Spain.

[2]Biomedical Research Networking Center in Bioengineering, Biomaterials and Nanomedicine (CIBER-BBN), Instituto de Salud Carlos III, C/Monforte de Lemos 3-5, 28029 Madrid, Spain

[3]Department of Engineering Science, University of Oxford, Oxford OX1 3PJ, United Kingdom

[4]Department of Mechanical Engineering and Materials Science, Yale University, New Haven, Connecticut 06520, USA

[5]Biodonostia Health Research Institute, Group of Environmental Epidemiology and Child Development, Paseo Doctor Begiristain s/n, 20014, San Sebastian, Spain

[6]University Institute for Regenerative Medicine and Oral Implantology - UIRMI (UPV/EHU-Fundación Eduardo Anitua); BTI Biotechnology Institute, Vitoria-Gasteiz, (Spain).

[7]Singapore Eye Research Institute, The Academia, 20 College Road, Discovery Tower, Singapore.

*Corresponding author: Hernandez RM (rosa.hernandez@ehu.eus)

ABSTRACT

When hydrogel spherical microparticles are used as part of biotechnological systems, the number of spheres contained in a defined pelleted volume is directly related to the dose administered to the patients. However, this relationship usually is not a straightforward deduction, especially when the active ingredients are not the spheres themselves, but a molecule encapsulated into the hydrogel or synthetized by entrapped cells. The physical-mechanical properties of the spheres or the shape and size of the container we use to measure the volume, among others, are determinant variables that influence the administered dose. Despite the complexity involved, dose control is a critical factor that must be defined in order to ensure safe and effective treatments. Here we describe a complete, simple and practical mathematical model that allows for the easy calculation of a number of cells or a quantity of drug in a single sphere (cells/sphere; drug/sphere), a number of spheres in a given volume of pelleted spheres (spheres/V_s) and a number of cells or a quantity of drug in that volume of pelleted spheres (cells/V_s; drug/V_s). The model only relies on end-point measurements of the particle-elaboration process, but taking into account complex intermediate phenomena, making it easily applicable in a wide range of hydrogel-based particulate systems. The model is validated using the most common cell microencapsulation elaboration protocols, because this example represents one of the most complex and demanding scenarios with the secretion of therapeutic molecules from cells entrapped into hydrogel microparticles,

Keywords: Mathematical model, simulation, hydrogel deformable spheres, microparticle, cell delivery, drug delivery.

1. INTRODUCTION

Hydrogel-based microparticles have been studied for the delivery of small molecule drugs, lipids, polymers and nanoparticles, allowing the design of different complex release profiles, relying on diffusion, polymer degradation or using responsive polymers properties to trigger the release of the molecules [1-3]. Besides, when chronic treatments are needed, cell microencapsulation technologies for sustained bioactive molecule release, permits the controlled drug release synthesized de novo by the entrapped cells, which remain protected from the host immune response [4,5]. Moreover, hydrogels provide a unique and tunable 3D environment for cell expansion when tailored cell growth, proliferation or differentiation conditions are needed [6], or for the administration of *in vitro* preseeded cells, turning particles into cell delivery systems [7].

In spite of the wide range of applications being tested for hydrogel microparticles, all these systems share some common behaviors in terms of physical-mechanical characteristics, as long as they can be cataloged as spheres within a narrow size and density values. It is generally accepted that systems containing microparticles above 10 μm in diameter can be distinguished from other particulate matter, such as colloids, because they experience stronger gravitational forces relative to thermal forces and the influence of the Van der Waals interaction loses its importance due to the appearance of friction [8]. In consequence, hydrogel microparticles can be found either as free-floating particles in solution or, and more commonly, in jammed state [9].

When hydrogel spherical microparticles are used as part of biotechnological systems, the number of spheres contained in a defined pelleted volume is directly related to the dose administered to the patients. However, this relationship usually is not a straightforward deduction, especially when the active ingredients are not the spheres themselves, but a molecule encapsulated into the hydrogel or synthetized by entrapped cells. For example, when particles are allowed to settle down by gravity, the individual particles reach a stable mechanical equilibrium with their local neighbors [10]. In a random configuration of particles, empty regions appear naturally making it heterogeneous and the force network providing the stability of

the system is nonuniform [11]. This process may include also different levels of sphere deformation and shape modification depending on their physical-mechanical properties (density, elasticity, stiffness etc.). Small perturbations such as tapping or shearing [12] can move the particles and lead to the evolution from one jammed state to another, generally more compact state [10], where a global minimum is reached.

Despite the complexity involved, dose control is a critical factor that must be defined in order to ensure safe and effective treatments. Controlling the therapeutic dose is crucial to avoid problems such as intoxication of the patient or inefficacy of the treatment, especially when working with narrow therapeutic index drugs. Therefore, particulate systems require as powerful as user-friendly tools that allow researchers to calculate the number of spherical hydrogel microparticles in a given volume, and going a step further, the quantity of drug or cells immobilized in that volume of particles. Dosing based in standard volume units is sometimes the only acceptable option and in other cases, it could substantially reduce the cost and difficulty of product application and dosing errors that could result from a more complex counting system.

The objective of this work is to present a useful mathematical model as a simple and practical way of making calculations for different hydrogel-based monodisperse spherical microparticles. Here we use the example of cell microencapsulation technologies for the description of the equations **(Box 1)**. This is because, aside from involving different bead elaboration protocols and after-gelling modifications, they represent some of the most complex and demanding scenarios with the secretion of therapeutic molecules from cells entrapped into hydrogel microparticles, which need a complete and well-defined model. In order to confirm the adequacy and usefulness of the mathematical model, in the present study we conduct several experiments, testing the most common elaboration protocols for cell microencapsulation systems.

2. MATERIALS AND METHODS

2.1. Mathematical model description

The parameter definition is directly related to the elaboration procedure of

the microspheres. As mentioned before, this procedure varies widely depending on the type of microparticle, the application or the selected elaboration protocol in every case. The mathematical model described here only takes into account end-point measurements, shared generally by hydrogel spherical microparticles, loaded or not with drugs or cells, making it possible to obtain accurate results in very different situations.

Box 1. Principles of cell microencapsulation technologies for drug delivery purposes

Cell microencapsulation strategy is based on the immobilization of cells that produce therapeutically interesting molecules in particles between 100 and 1500 μm in diameter, approximately. The particles are elaborated with biocompatible materials that prevent the passage of high molecular weight molecules, antibodies and other components of the immune system, protecting these cells from the host's immune response and from the mechanical stress that may occur when the implant is placed in the selected tissue. In addition, the capsule must allow the bidirectional diffusion of nutrients, oxygen and cellular debris; control the sustained release of *de novo* synthesized therapeutic factors inside the microcapsules; and provide cells with a suitable environment that improves and controls its viability and proliferation. This technology also suppresses, or at least reduces, the chronic administration of immunosuppressive agents, avoiding some of the adverse events associated with organ and tissue transplantation. Cell encapsulation systems have shown wide applicability in pathologies with very diverse characteristics, such as diabetes mellitus (DM), anemia, cancer or pathologies of the central nervous system (CNS), among others. They are especially convenient for pathologies in which a strictly controlled long-term release of the therapeutic molecule is necessary [5].

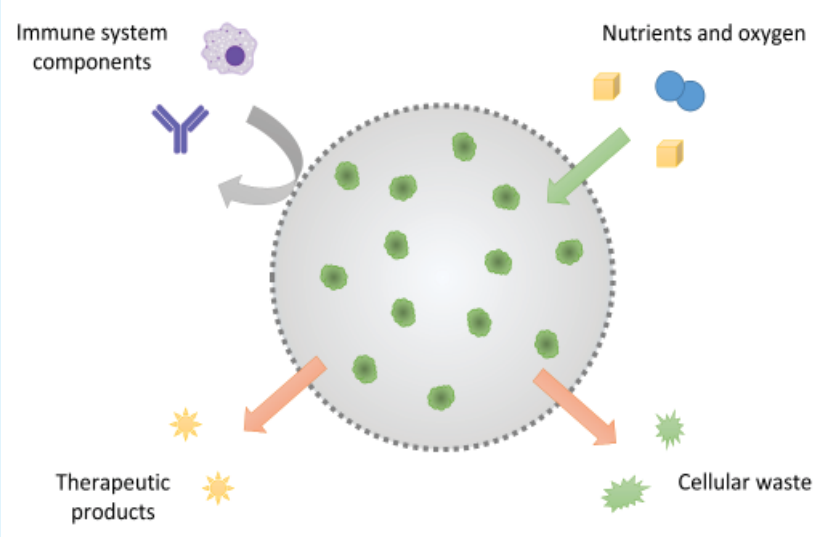

All the protocols begin with the elaboration of the hydrogel microspheres. When cells (cell load, **CL**) or drug load (drug load, **DL**) are needed for the application, these are usually mixed with the polymer, prior to sphere formation **(Figure 1)**. Then, this mix is transformed into spherical microparticles, following different procedures, such as emulsification, dripping and gelation, spray drying, electrospraying or supercritical fluid mixing, among others.

Sometimes these spheres (unmodified spheres, **USs)** are the final product, ready to be administered. However, many applications require after-formation elaboration steps, such as, volume changing exposure to different media or functional coatings (for controlled drug release or cell microencapsulation technologies, for example). It is important to note that these secondary steps do not change the initial cell or drug load per sphere, just the final volume and maybe the physical-mechanical characteristics of the microparticles. We will name these resulting spheres (USs with volume changes) as "modified spheres" (modified spheres, **MSs**), regardless of the followed procedure.

Taking into account these end point products, we designated a minimum number of parameters that would include all the possible variables and would lead us to confidently establish a relationship between a quantity of drug (or number of cells in this case), a number of particles and the volume occupied by them **(Figure 2A)**:

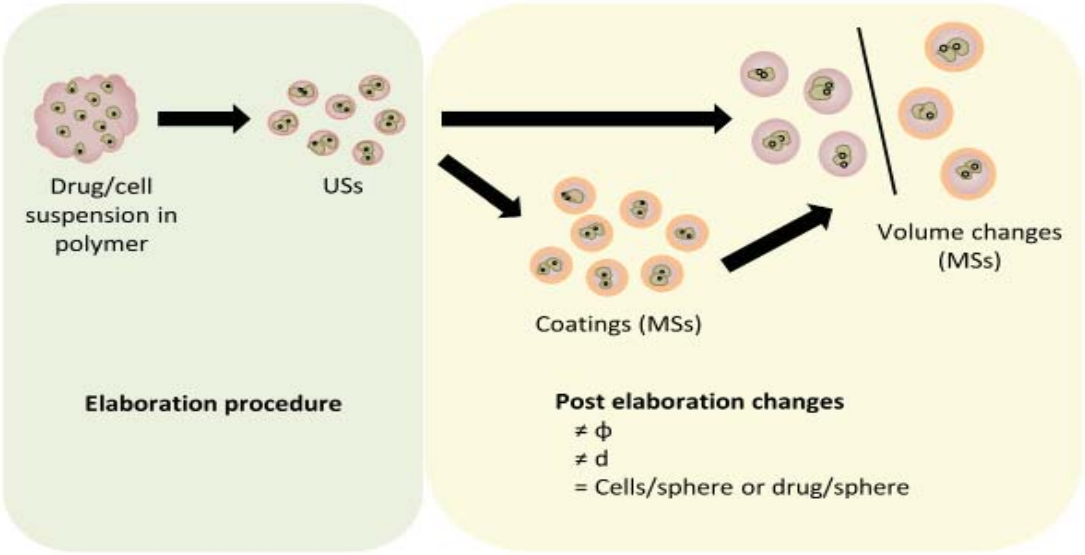

Figure 1. General scheme of hydrogel microparticle elaboration steps and the main final and intermediate products. USs: Unmodified spheres (without post-elaboration modifications); MSs: modified spheres (after coatings or volume changes); ϕ: packing fraction; d: diameter.

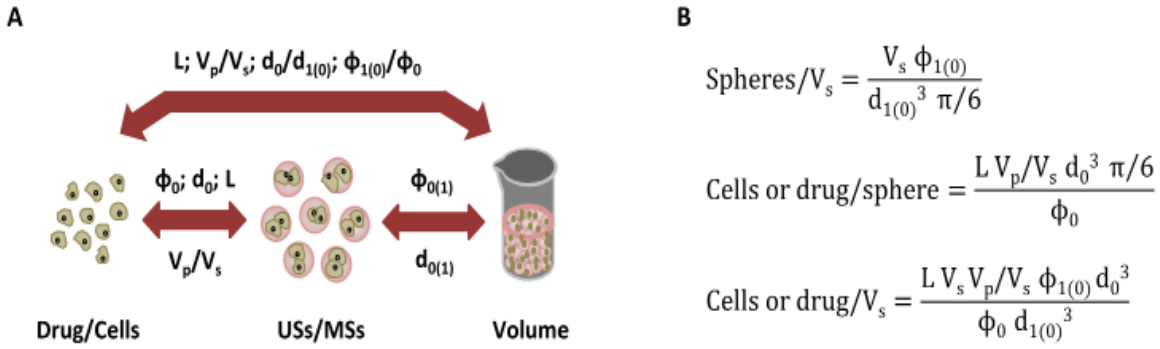

Figure 2. Mathematical model definition. A. Parameter relationship between a quantity of drug or cells, a number of microspheres and the volume occupied by them. **B.** Mathematical formulas for spheres/V_S, cells or drug/sphere and cells or drug/V_S. ϕ_0=Packing fraction of the unmodified spheres (USs); ϕ_1=Packing fraction of the modified spheres (MSs); L=initial drug/cell load (cells or drug in 1m3 of polymer); d_0= Diameter of the USs; d_1= Final diameter of the MSs; V_p/V_S= The ratio between a volume of drug/cell suspension in a polymer and the volume occupied by the USs formed with that volume of mixture; V_S= Volume of spheres. All the units are in SI (diameters in m and volume in m3).

- Initial cell or drug load (**L**): The mass of drug or the number of cells included in 1 m3 of polymer volume (kg/m3 or n/m3).

- **V_p/V_s**: The ratio between a volume of drug or cell suspension in a polymer (pre-spheres volume, **V_p**) and the volume occupied by the pelleted USs formed with that volume of mixture (pelleted sphere volume, **V_s**). It involves, for example, the volume increase related to the packing fraction (ϕ) of the new formed spheres and the volume changes caused by shrinking or swelling of the polymer due to sphere elaborating procedures (no units).

- **d_0**: Diameter of USs (m).

- **d_1:** Diameter of MSs (m), after all the elaborations steps (including coatings or volume changes after exposure to different media).

- **ϕ_0:** Packing fraction in USs pellets (no units).

- **ϕ_1:** Packing fraction in MSs pellets (no units).

Once these parameters have been calculated, they will remain constant as long as there are no significant changes in the protocol (polymer, elaboration technique, environmental conditions, etc.). Thus, some of the parameters could be checked just from time to time when working with the same protocols. However, fixing the size of the particles for every batch could be interesting as

small changes in diameter length lead to significant volume changes and all the elaboration techniques face an intrinsic variability.

Taking into account the selection and definition of the parameters needed to describe the elaboration process, it is possible to create a mathematical definition for each of the following relationships:

- The number of spheres in a pelleted volume of spheres (Spheres/V_s): It depends on the diameter and the packing fraction of the USs or MSs, d_0 and ϕ_0 or d_1 and ϕ_1 respectively.

- The quantity of drug or the number of cells in a single sphere (drug/sphere or cells/sphere): In this case, it is only necessary to determine the drug or cell load in a single US, as all the subsequent volume modifications will not affect this number (the value will be the same in all the MSs too).

The quantity of drug or the number of cells in a single US would be L divided by the number of particles elaborated with the same volume of the initial suspension (or drug and polymer blend). Hence, it would depend on the diameter and packing fraction of the USs obtained right after the elaboration process (without further modifications), d_0 and ϕ_0 respectively, and the V_p/V_s ratio.

- The quantity of drug or the number of cells in a volume of pelleted spheres (drug/V_s or cells/V_s): It is necessary to consider the initial load, L, the V_p/V_s ratio, the initial diameter of the USs (d_0), the final diameter after volume modifications and/or coatings (d_1) and the packing fractions of USs and MSs, ϕ_0 and ϕ_1 respectively.

Based on these descriptions, it is possible to design mathematical equations that link those three concepts **(Figure 2B)**. The model can be used in every case were these six values can be calculated, regardless of the elaboration protocol. L is usually chosen, based on the needs of the faced application. The V_p/V_s ratio is normally easy to measure, letting the microparticles elaborated with a known volume of polymer solution settle down into a graduated container. Finally, just a microcospe is needed for measuring both the d_0 and the d_1. Probably, ϕ_0 and ϕ_1 are the most difficult ones to be exactly calculated but the possible results oscillate in a very narrow range of values when working with hydrogels (described later) and, in this work, we

estimated those values based on hydrogel sphere arrangement simulations, making them applicable in a wide range of situations.

2.2. Simulations

The following simulations were performed, using MATLAB®, to obtain useful packing fraction values for hydrogel microspheres (based on different container shapes and sizes, sphere diameters and sphere numbers): Tested for $100<N<5000$ (number of spheres) and $0.2<d<4$ mm (d of the spheres)

- Simulation with 1.5 mL Eppendorf tube (Eppendorf AG, #0030.120.086) cone measures (container): Internal radius of the spherical cap (R): 1.75 mm; Inner half angle of the cone (α): 0.167 rad.
- Simulation with 15 mL Corning tube (Merk, #CLS430055) cone measures (container): Internal radius of the spherical cap (R): 2.4 mm; Inner half-angle of the cone (α): 0.227 rad
- Simulation with 1.5 mL Eppendorf tube cylinder measures (container): Internal radius of the cylinder (R): 4.45 mm.
- Simulation with 15 mL Corning tube cylinder measures (container): Internal radius of the cylinder (R) 7.37 mm

A custom code based on the discrete element method (DEM) was used, in which the particles interact via linear Hookean springs with stiffness 200 kg/s^2 (equivalent to a Young's modulus of ~600 kPa). Particles were sedimented in an effective background fluid (viscosity of 0.001 $Pa\text{-}s$, same as water) by subjecting them to Stokes drag. The fluid density was taken to be that of water (1000 kg/m^3) and the particle density to be 1200 kg/m^3.

The shape of the simulated particles was always maintained spherical and smooth (no friction between the spheres) and the rest of the physical-mechanical properties were kept constant. No electrostatic charges or interactions were simulated. Prior to the selection of the suitest particle density value (1200 kg/m^3) for the simulations, the influence of the density was tested in a range of 1-1.5 on the ratio of sphere density to fluid density (ρ_s/ρ_f).

The initial configuration for each simulation was random in two ways. First, we randomly selected the desired number of particle diameters from a truncated Gaussian distribution of sizes with a 5% of standard deviation. Second, we scattered these particles randomly within the container before allowing them to settle to the bottom. For every condition, 5 different sphere random arrangements were tested in order to analyze the intrinsic variability of the procedure.

2.3. Validation of the mathematical model

For the validation of the previously described mathematical model, a representative sample of the most used cell microencapsulation technologies was chosen, because we considered it to be a complex scenario were a well defined model is necessary for the correct calculation of the cells and USs or MSs contained in a given volume.

The elaboration procedure normally includes dropping an alginate-cells mixture over a $BaCl_2$ or $CaCl_2$ bath that crosslinks the alginate, creating USs (alginate beads) of a suitable size for the selected application **(Supplementary discussion)**. After that, many protocols include subsequent coating steps to elaborate what is known as microcapsules (MCs), polymer-coated beads with more restricted permeability that improves the protection of the encapsulated cells from the host's immune response. All these after-gelling steps or all the size changes related to a water/ion exchange that occurs when the beads are placed in different media do not change the number of cells/sphere, and for the application of the mathematical model, we can consider all the obtained final products, also the MCs, as MSs.

All the selected particle types were elaborated and, for every batch, the number of cells/sphere, sphere/V_s and cells/V_s were experimentally determined. In parallel, the V_p/V_s ratio and the d_0 and d_1 diameter values were measured. These values and the ϕ_0 and ϕ_1 ones predicted from the simulations were substituted into the formulas for the calculation of the theoretical values for cells/sphere, sphere/V_s and cells/V_s. The expected variability associated to the theoretical values was calculated as the combination of all the possible measurement errors associated to the individual parameters included into the formulas. The adequacy of the mathematical

model and its ability to predict the experimentally obtained values were evaluated by comparing the experimental and theoretical values **(Figure 3)**.

During the whole validation study, some of the variables were maintained constant:

- Polymer type of the spherical matrices: LVG alginate (PRONOVATM, #4200001)
- Initial number of cells in the suspension of alginate (CL): 5 x 10^6 cells/mL of alginate
- Types, concentrations and availability of other ions and/or cross-linkers in solution that may interfere in the gelation and/or coating processes.
- Temperature

2.1.1. Cell culture

Murine C_2C_{12} myoblasts derived from the skeletal leg muscle of an adult C3H mouse and genetically engineered to secrete murine Erythropoietin (EPO) were grown in Dulbecco's modified Eagle medium (DMEM) supplemented with 10% fetal bovine serum (FBS), L-glutamine to a final concentration of 2 mM, 4.5 g/L glucose, and 1% antibiotic/antimycotic solution. Cultures were plated in T-flasks, maintained at 37 °C in a humidified 5% CO_2/95% air atmosphere standard incubator, and were passaged every 2-3 days. All reagents were purchased from Gibco (Thermo Fisher Scientific, Spain).

2.1.2. Tested elaboration protocols

In order to validate the above described mathematical model, some of the most used elaboration protocols for cell microencapsulation systems were selected. For the experimental measurements, the following USs and MSs (including different types of MCs) were prepared **(Figure 4)**:

- Ca^{+2}-alginate USs (Ca^{+2} as crosslinker): 2 sizes of ~ 400 μm (d_0) and ~ 150 μm (d_0), **US400** and **US150**, respectively.

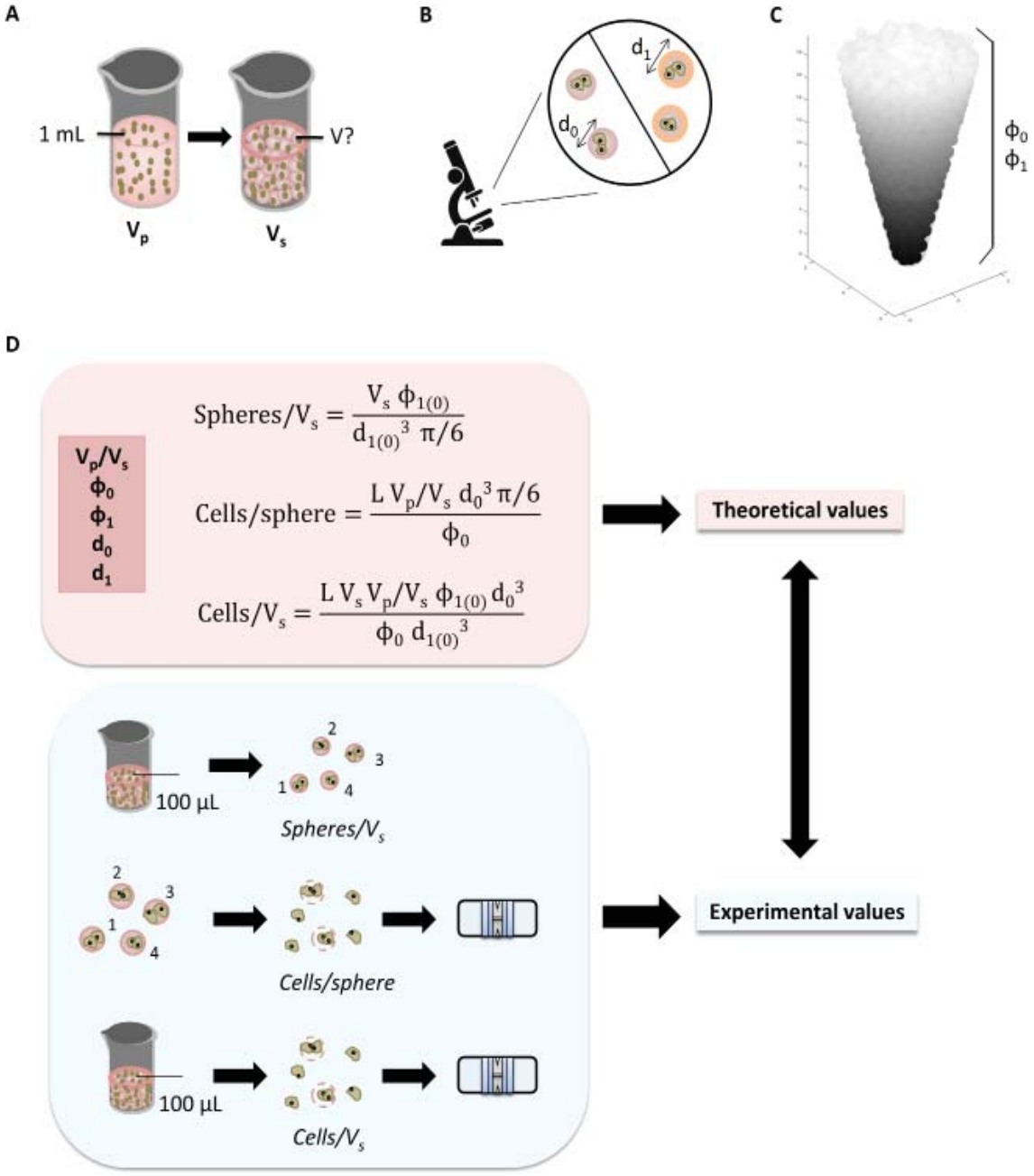

Figure 3. Mathematical model validation. A-C Obtaining the parameters. **A.** V_p/V_s ratio: The ratio between a volume of drug/cell suspension in a polymer (pre-spheres volume, Vp) and the volume occupied by the unmodified spheres (USs) formed with that volume of mixture (sphere volume, V_s). **B.** Diameters of the USs and the modified spheres (MSs), d_0 and d_1 respectively, were measured using and inverted microscope and the image processing package Fiji-Image J. **C.** Packing fraction of the USs and the MSs, ϕ_0 and ϕ_1 respectively, were calculated from computational simulations. **D** Various alginate cell microencapsulation protocols were selected for the validation of the mathematical model. In every case, the experimental values for spheres/V_s, cells/sphere and cells/V_s were calculated and compared to the corresponding ones obtained from the theoretical mathematical expressions. For the experimental calculation of spheres/V_s, we counted the number of spheres contained in a known volume of spheres (V_s); a few spheres were counted and enzymatically digested when measuring cells/sphere; and for the calculation of cells/V_s, a known volume of spheres was digested in order to count the entrapped cells.

First, a C_2C_{12} myoblast cell line suspension was prepared in 1.5% alginate. A precise volume of 2.5 mL of this suspension was dropped into a solution of 100 mM $CaCl_2$. The newly formed beads were allowed to gel for 10 min. Two different droppers were used for the elaboration of the beads: an electrostatic dropper for the biggest beads and a Cellena® dropper (Ingeniatrics technologies, Spain), based on flow focusing technology, for the 150 μm ones.

- Ca^{+2}-alginate MSs (Ca^{+2} as crosslinker): 2 sizes of ~ 550 μm (d_1) and ~ 230 μm (d_1), **MS(swollen)550** and **MS(swollen)230**, respectively.

Some of the alginate USs were exposed for 30 seconds to a chelating solution in order to change the diameter and the mechanical properties of the beads.

- Ca_{+2}-alginate-PLL MCs (Ca_{+2} as crosslinker): 2 sizes of ~ 480 μm (d_1) and ~ 170 μm (d_1) and Ca^{+2}-alginate-PLO MCs (Ca^{+2} as crosslinker) of ~ 450 μm (d_1), **MS(PLL)480**, **MS(PLL)170** and **MS(PLO)450**, respectively.

After the elaboration of the alginate USs, two different coatings were performed, with poly-l-lysine (PLL) or poly-l-ornithine (PLO) in order to elaborate MCs. In both cases, a second coating of alginate was added on top of the other. The aim of this second coating is to mask the positive charges of the non-bounded PLL or PLO molecules that could trigger an immune response against the microcapsules, and is widely used in cell microencapsulation protocols.

For PLL coating, the USs were suspended, for 5 min, into a solution of 0.05% PLL and for PLO coating into a solution of 0.1% PLO for 10 min. For the second coating, a solution of 0.1% alginate was used for 5 min in both cases.

- Ca^{+2}-alginate-PLL liquefied-core MCs: (Ca^{+2} as crosslinker): ~ 500 μm (d_1), **MS(PLL+LiqCore)500**.

For core liquefaction, some MS(PLL)480 were suspended, for 1 min, in a 1% citrate solution.

- Ba^{+2}-alginate USs (Ba^{+2} as crosslinker): 2 sizes of ~ 350 μm (d_0) and ~ 140 μm (d_0), **BaUS350** and **BaUS140**, respectively.

The exact same procedure used for the elaboration of US400 and US150 was followed but changing the $CaCl_2$ solution for a 50 mM $BaCl_2$ solution. The

sizes of the USs crosslinked with barium are usually smaller when all the parameters are maintained constant as the barium shows higher affinity for the alginate chains and the process associated to the crosslinking of the alginate shows higher loses of water [13].

- Ca^{+2}-alginate USs (Ca^{+2} as crosslinker) of larger size: ~ 2300 μm (d_0), **US2300**.

In order to force the limits of the model, this one last group was included in the validation, even if they cannot be considered microparticles due to their size. The elaboration procedure was the one used for the normal alginate USs but, in this case, the pre-gelled alginate solution was extruded through a needle of larger diameter and without electrostatic cutting of the solution to make the beads larger (the formation of the drops was only dependent on the gravity force).

All the solutions were elaborated with 1% mannitol in milli Q water, filtered with a 0.22 μm filter and conserved at 4 ºC in aseptic conditions. All the coatings and culture media changes of the USs were done right after the gelling process. A mannitol 1% solution was used after every coating to wash the extra polymer that was not attached to the bead's surface. Different coating times were used for different polymers in order to assure a total coating. All the USs were maintained in their own crosslinking solution and the MSs were maintained in standard culture media.

2.1.3. Simulations applicability

In order to check the applicability of the packing fraction simulations, an easy density test was performed with USs and MSs of different sizes. Single particles were allowed to settle from the top of a 50 mL Corning tube (Merck, # CLS430829), containing phosphate buffered saline (PBS) (Thermo Fisher Scientific #10010023). The descent of the spheres was recorded to calculate the velocity of the movement and, finally the approximate density of the spheres was deduced.

All the containers used for the experimental tests (Eppendorf tubes and Corning tubes) had similar measures to the ones simulated with MATLAB®.

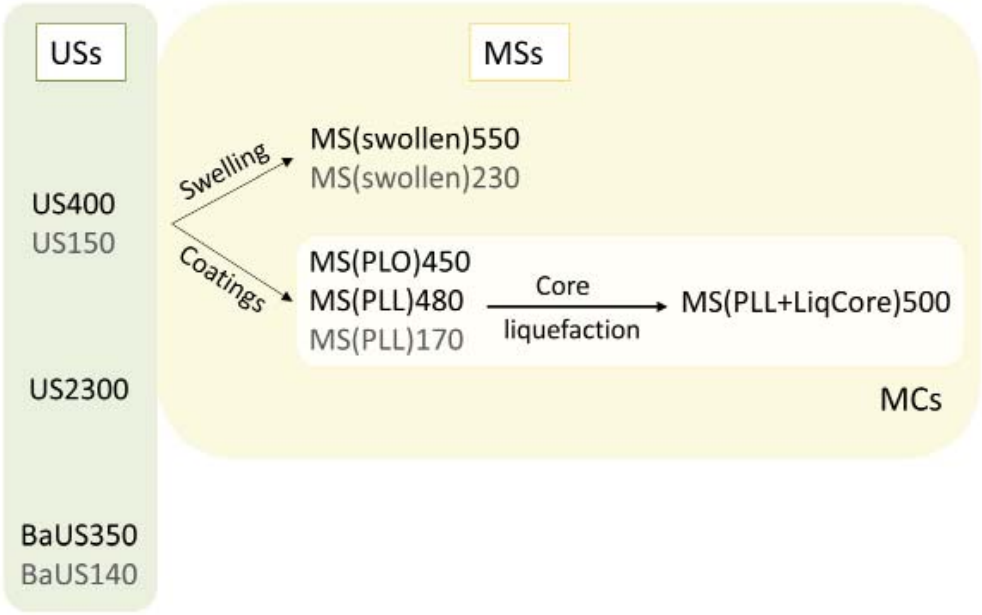

Figure 4. Scheme of selected unmodified sphere (USs) and modified sphere (MSs) types, including microcapsules (MCs), for validation of the mathematical model.

2.1.4. Microsphere diameter measurement

A representative sample of every batch was selected and 20 different diameters were measured using an inverted microscope (Nikon TSM). The mean value and the standard deviation (SD) were calculated.

2.1.5. Dosing procedures

In order to obtain a similar packing fraction in all cases, the spheres were transferred to the tube where the volume was going to be measured (following volumetric marks), always maintaining them into a liquid ($BaCl_2$/$CaCl_2$ solution for USs and cell culture media for MSs), and after that, the same steps were followed in every case:

- Wait until no evident changes in pelleted volume were seen for 5 min.
- Soft agitation to improve the packing density.
- Wait until no evident changes in pelleted volume were seen for 5 min.
- If needed, remove excess supernatant to leave empty volume in the tube.
- Add more spheres.

- Repeat all the steps until the wanted dosing volume was reached.
- Remove the liquid above the spheres.

These dosing procedures were carried out in 1.5 mL Eppendorf tubes and 15 mL Corning tubes. Both of them widely used tubes by scientists working in biomedical sciences.

2.1.6. V_p/V_s calculation

A precise volume of 2.5 mL of the cell suspension in alginate was dropped into a bath of 100 mM $CaCl_2$ or 50 mM $BaCl_2$. 10 min after the last drops, all resulting USs were carefully collected on a 15 mL tube, following previously described dosing procedures, to measure the volume occupied by the pelleted USs resulted from the gelation of those 2.5 mL of pre-gelled cell suspension. In the case of the largest USs (~ 2300 μm d_0), the dropped volume was 2 mL.

2.1.7. Spheres/V_s measurement

After the dosing procedure, the supernatant of the pelleted microspheres was removed using a micropipette and 1 mL of the same fluid was added to resuspend the known volume of spheres. After strong agitation, a representative sample of 100 μL (liquid+suspended spheres) was taken and diluted. The particles contained in that volume were counted using an LEICA TCS SP2 AOBS microscope and the image processing package Fiji-Image J. The number was then extrapolated to the total volume, taking into account all the performed dilutions. For every batch, 3 different pellets of 100 μL were measured and from every measure 3 separated dilutions were counted under the microscope. In order to detect differences in the packing fraction related to larger sphere numbers, also for every batch, pellets of 500, 1000 and 1500 μL were measured and for every measure 3 separated dilutions were counted under the microscope. In case of BaUS140, only the 100 and 500 μL sediments were measured.

2.1.8. Cells/V_S measurement

After the dosing procedure, the supernatant of the microspheres was removed using a micropipette and 1 mL of 1% alginate lyase dissolved in cell culture medium was added to resuspend the known volume of spheres. After a 15 min incubation at 37 ºC, the process was mechanically aided by gently pipetting to break all the remaining pieces of alginate. A sample of the cellular suspension was used for counting the number of cells/mL using a cell counter (TC20 automated cell counter, Bio-Rad). For every batch, 3 different pellets of 100 μL were measured and from every sample 3 separated quantifications were made in the cell counter. It was not possible to quantify the number of cells/V_S in BaUS140 and BaUS350 due to the difficulty to enzymatically digest the gelled particles.

2.1.9. Cells/sphere measurement

An exact number of USs, counted by inverted microscope, was placed in an Eppendorf tube, the supernatant of the sedimented beads was removed using a micropipette and 1 mL of a solution of 1% alginate lyase in culture medium was added to resuspend the known number of spheres. After 15 min of incubation at 37ºC, the process was mechanically aided by gently pipetting to break all the remaining pieces of alginate. A sample of the cellular suspension was used for counting the number of cells/mL using a cell counter. For every batch, 3 different pellets were measured and from every measure 3 separated quantifications were made in the cell counter. In case of the largest spheres (~ 2300 μm d_0), the number of particles to be digested was directly counted by bare eye (no need for microscopy techniques).

The number of cells immobilized in BaUS140 was determined directly counting the cells entrapped into the beads using an inverted microscope (the alginate hydrogel is transparent), as they were not easy to digest enzymatically. In the case of BaUS350, the number of cells/sphere increases dramatically with the size of the bead, making it impossible to count the cells in this way.

2.1.10. Goodness of fit analysis

Pearson correlation coefficient (PCC) was used to analyze the correlation between theoretical and experimental data obtained for spheres/V_S, cells/V_S and cells/sphere. Data was analyzed as a whole and segmented by particle type and, in case of spheres/V_S, also by jammed dose volume (100 µL, 500 µL, 1000 µL and 1500 µL).

On the other hand, Kolmogorov-Smirnov (if n>50) and Shapiro-Wilk (if n<50) tests were applied in order to analyze the normality of the data. The median values of both theoretical and experimental results were directly compared using the nonparametric Mann-Whitney-Wilcoxon test. Data was analyzed as a whole and segmented by particle type and, in case of spheres/V_S, also by jammed dose volume.

All statistical computations were performed using R-4.0.2 software.

3. RESULTS

3.1. Simulations

All the parameters necessary for the application of the model are, in general, easy to measure. However, the packing fraction of both the USs and the MSs could be more complex. In this work, we selected four container types, a range of sphere diameter sizes and different numbers of spheres and we performed different simulations to obtain useful packing fraction values for hydrogel microspheres.

3.1.1. Robustness of the simulations

In order to make the simulations as useful as possible, the selected container shapes included a 1.5 mL Eppendorf tube cone and cylinder and a 15 mL Corning tube cone and cylinder **(Figure 5A)**, because these tubes are very commonly used by the scientist in the field.

For running the simulations, sphere diameter mean sizes between 0.2 and 4 mm were selected. In order to make the results more comparable to the experimentally expected ones, a 5% standard deviation was included in all cases. **Figure 5B** shows

a truncated Gauss distribution of a mean sphere diameter size of 0.5 mm with a 5% polydispersity. In all measurements, for the desired number of spheres, the needed diameter sizes were randomly selected from similar distributions in every case.

In addition, we analyzed the influence of the hydrogel density on the packing fraction for the purpose of determining a range of sphere density values in which the simulations may be applicable. **Figure 5C** shows the results for sphere sediment height measurements tested for ρ_s/ρ_f values, ranging from 1 to 1.5. The number of spheres and their diameter was kept constant for comparison. Within the range tested, the obtained values for the h of the sphere sediment are constant and stable, meaning that the expected packing fraction would also be very similar if no other parameters are changed.

With higher sphere density values, the resultant downwards force (from the combination of gravity, friction and the buoyant force and, to a lesser extent the interparticle forces) would increase and in case of hydrogel deformable spheres, it could produce the squishing of the spheres and the reduction of the h of the sediment [14]. In this case, density values contained in the tested range does not seem to significantly change de compression of the hydrogel spheres, as the h values in all cases are very similar. Moreover, a small variability related to changes in the density of the spheres would probably be overwhelmed by variation due to the random initial configuration of the spheres (see below).

Presumably, materials with similar densities to the tested ones (probably even with slight variations), which include particulate hydrogels for a wide range of applications, would behave in the same way when working with a similar numbers of spheres [15]. If higher numbers of spheres are used, changes in the density values would probably generate more noticeable variations in h, as the spheres at the bottom of the container would support the higher weight of the spheres on top. However, the results in that case are not easy to predict, as the pressure at the bottom of a granular material with high h is not proportional to the h of the sediment [16]. In that case, the squishing of the spheres would also depend on the elasticity of the hydrogel, mainly defined by its Poisson ratio and Young modulus.

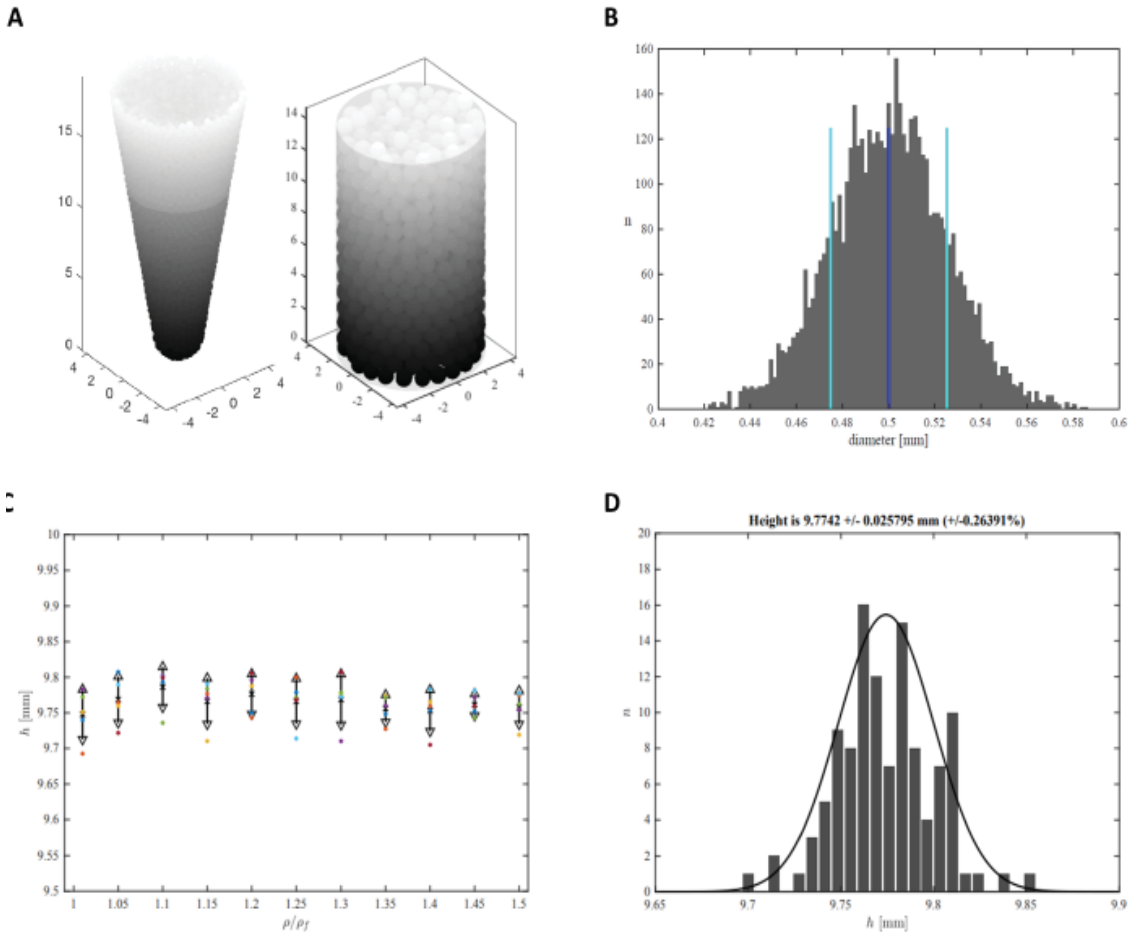

Figure 5. A. Representative examples of computational simulations, both in conical and cylindrical shape containers **B.** Example of truncated Gaussian distribution for sphere diameter size with a mean value of 0.5 mm and a standard deviation of 5 %. **C.** Graphical representation of sediment height values obtained for a tested range of sphere density values. **D.** Histogram representing the variability in sphere sediment height due to the different initial random arrangement of spheres.

Furthermore, in order to analyze the intrinsic variability of the procedure, for every condition, 5 independent simulations were carried out, just changing the initial random arrangements of the spheres before settling down to the bottom of the container. The histogram in **Figure 5D** shows an example of this variability in the sediment height, for spheres of 0.5 mm.

3.1.2. Best fit functions

For every condition, we chose a sphere diameter size (with a 5% polydispersity), a number of spheres and a type of container, and tests were ran five times in random initial particle arrangements. In this way, we obtained the height of

every sediment of particles. Finally, a relationship between the measured sediment height values and corresponding volume was defined. **Figures 6A** and **6B** show the results obtained for the simulations with the 15 mL Corning tube and the 1.5 mL Eppendorf tube shapes, respectively. In every condition, we determined the best fit function for ϕ (d, N) and a mathematical equation for the calculation of V as a function of h.

For the calculation of V as a function of h, the fit functions seem to reproduce the right h to within about 0.5% in most cases.

The fit functions seem to reproduce the right packing fraction to within 1% in most cases, which is comparable to the variation between different configurations for the same conditions.

For the 15 mL Corning tube, the packing fraction appears to be around 0.61 in all cases tested, with slightly smaller values for the spheres of smaller diameters, as long as N>1000. In case of the 1.5 mL Eppendorf tube, the reported packing fraction values seem to vary depending on the diameter size of the spheres. The biggest spheres, with diameters around 2.2 mm showed packing fraction values of not even 0.57, while spheres of 0.2 mm formed pellets of packing fraction values higher than 0.60. Thus, packing fraction values does not seem to strongly depend on sphere diameter sizes, until they get bigger enough and approach the diameter of the container. In both cases, in Corning and Eppendorf tubes, the packing fraction values observed for N<1000 represent the range were the number of spheres is still not enough to form a proper sediment and the spheres pack in the conical part of the containers, where the particles are expected to arrange differently.

No significant deformation of the spheres is expected mainly due to the importance of the buoyant force in neutralizing the effects of gravity [14]. At this "jamming transition point" of deformable frictionless spheres, the packing fraction reaches values which have been associated with the random close packing (RCP) [17] (generally accepted to be around 0.635 [18-20]) when the number of spheres is high enough. Therefore, in case of the 15 mL Corning tube, the obtained values around 0.61 totally agree with the expected results for deformable spheres contained into a fluid of similar density.

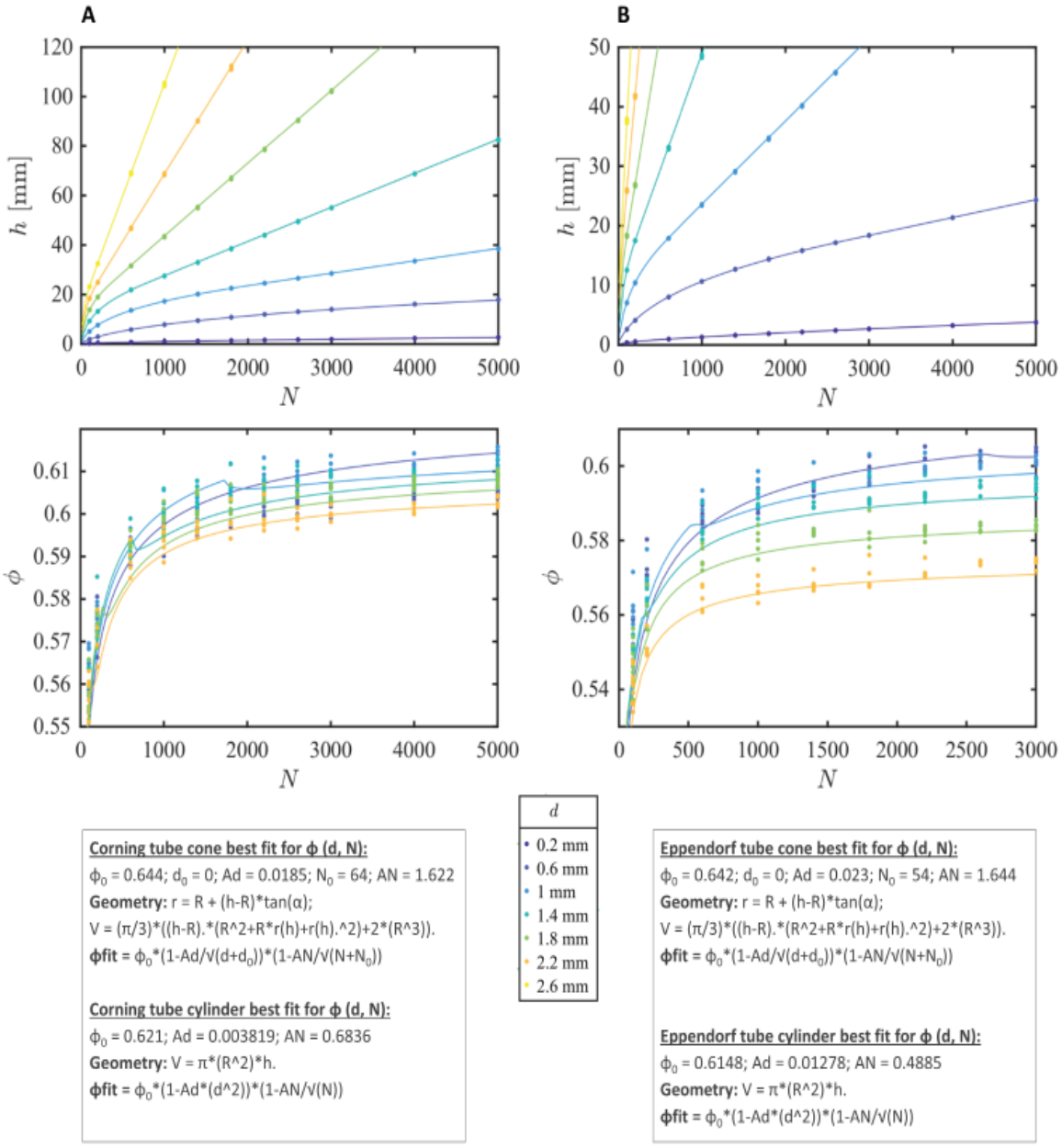

Figure 6. Results for computational simulations. Results for computational simulations in 15 mL Corning tubes **(A)** and in 1.5 mL Eppendorf tubes **(B)**. Graphs show the results obtained for the height and packing fraction of a pelleted number of spheres, for different diameter sizes. The best fit functions for both the conical and cylindrical parts of the tube and the mathematical equation for the calculation of V in function of h are also described below. The best fit functions represented on the graphs are a combination of both tube parts (cone and cylinder).

The packing fraction is also influenced by the size distribution, the shape of the container and the size of the spheres relative to the size of the container, being the latter the most determinant. High sphere to container diameter ratios generate abnormal sphere arrangements due to the lack of space, while smaller ratios of 0.06 or

less [21], tend to standard packing fraction values, with different arrangements next to the container walls (the wall effect [22,23]). The geometry of the container does influence the results to some degree, but the effect is weak as long as the particles are small relative to the diameter of the container and the number of particles is relatively large. In case of the Eppendorf tube geometry, the influence of the sphere diameter size, relative to the diameter of the container, can be clearly appreciated on the graphs.

For all simulations, a 5% polydispersity in particle size was included in order to make the results more realistic and applicable to experimentally obtained batches of microspheres. For particle elaboration procedures generating high size variability between same-batch particles, we would probably find notable changes in packing fraction values, as higher differences between the largest and the smallest sphere sizes result in higher packing fraction values, up to a maximum, where values higher than 0.8 can be observed [24].

In the simulations, we decided to consider as negligible the possible electrostatic interactions between the spheres, or the spheres and the container walls, and the roughness of the sphere surface. Being microparticles surrounded by a fluid, which usually contains different electrolytes and charged molecules [25] and taking into account that the materials used for the containers are usually inert and smooth, the effect of these variables are commonly not strong enough to significantly influence the final packing fraction values.

The packing fraction values would probably be similar when granular materials of comparable physical-mechanical properties are tested, as long as the number of particles is high enough and the ratio of sphere to container diameters allows for a normal arrangement of the spheres, with mild wall effects. However, high diameter polydispersity, strong electrostatic interactions between the particles or very rough sphere surfaces, among others, could significantly alter the obtained results. In addition, sediments made of very high particle numbers would presumably behave differently, probably with noticeable particle deformations.

3.2. Validation of the mathematical model

For the validation of the previously described mathematical model, a representative sample of the most used cell microencapsulation protocols was chosen.

First, all the batches were elaborated. For every batch, the number of cells/sphere, spheres/V_S and cells/V_S were experimentally determined (experimental values). In parallel, the V_p/V_S ratio and the d_0 and d_1 diameter values were measured. These values and the ϕ_0 and ϕ_1 ones predicted from the simulations were substituted into the formulas for the calculation of the theoretical values for cells/sphere, spheres/V_S and cells/V_S. The adequacy of the mathematical model and its ability to predict the experimentally obtained values was evaluated by comparing the experimental and theoretical results **(Supplementary material 1)**.

Before the calculation of the theoretical cells/sphere, cells/V_S and spheres/V_S with the packing fraction values obtained from the simulations, we checked their applicability in this specific case, taking into account the density of the alginate beads and the adequacy of the containers used for the measurements **(Supplementary discussion)**. For all the dosing procedures, Eppendorf and Corning tubes were used, with the same measures as the simulated containers. In addition, the density values of all the spheres were found to be between 1.002 and 1.006 times the density of the fluid, which falls within the tested range of ρ_s/ρ_f ratios.

Figure 7 shows the comparison between the obtained experimental and theoretical results for spheres/V_S, where V_S = 100 µL, 500 µL, 1000 µL and 1500 µL. **Figure 8A** and **8B** show the comparison between the results obtained theoretically and experimentally for cells/V_S (when V_S = 100 µL) and cells/sphere, respectively. Kolmogorov-Smirnov (if $n>50$) and Shapiro-Wilk (if $n<50$) tests confirmed that the all data follows a non-normal distribution so nonparametric Mann-Whitney-Wilcoxon test was applied to compare the median experimental and theoretical values **(Supplementary material 2)**. All the tests were carried out taking into account all the data or segmenting it by particle type or by volume (in case of spheres/V_S). No significant differences were detected, in any of the three formulas, between the theoretical and experimental median values.

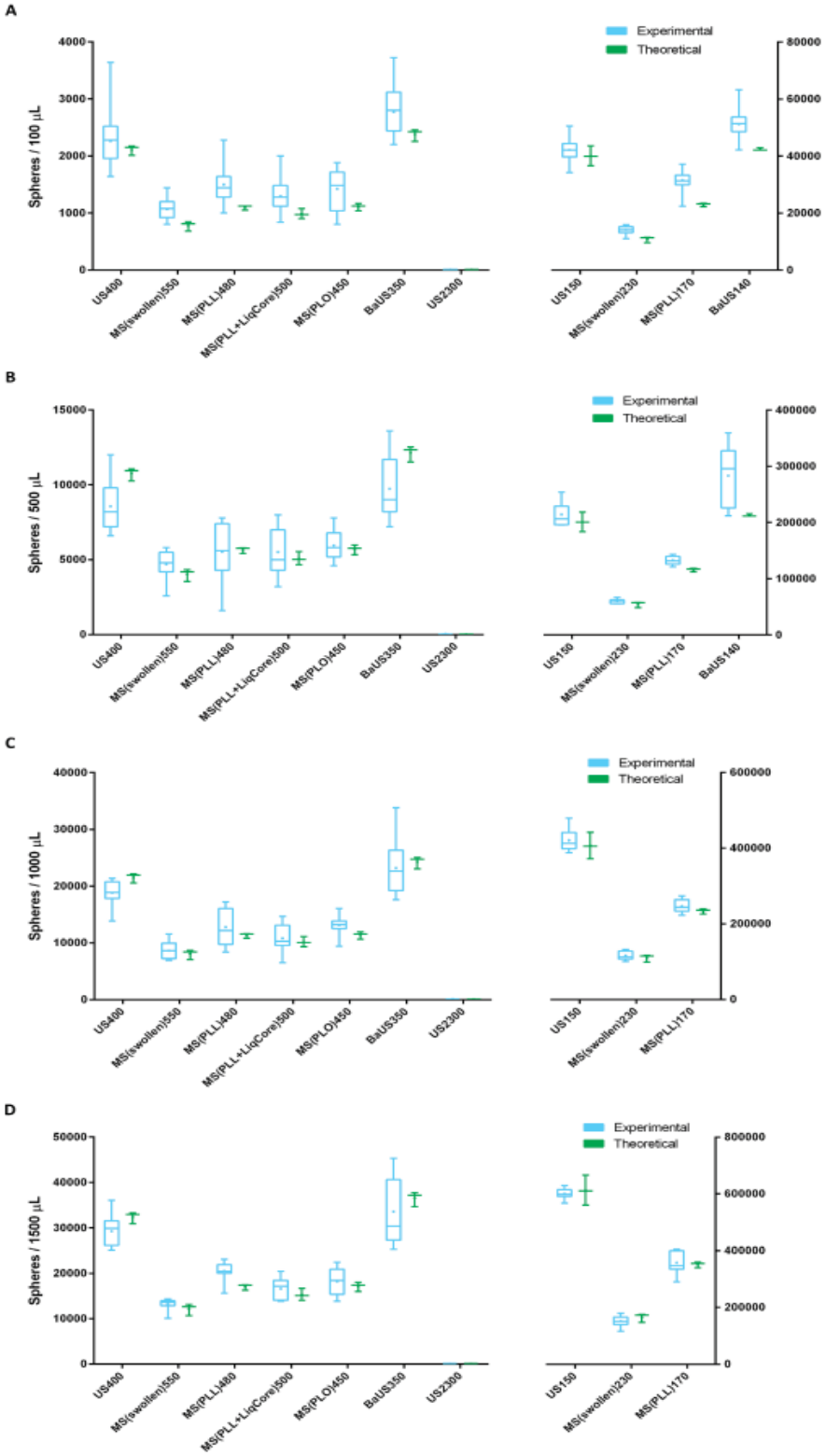

Figure 7. Experimental and theoretical results obtained for spheres/V_S, when V_S = 100 µL (A), 500 µL (B), 1000 µL (C) and 1500 µL (D). Due to the different scales, two Y-axes are displayed on the box plots. Left and right Y-axes show the scale for the spheres of diameters bigger or equal to 400 µm and smaller or equal to 230 µm, respectively. The mean value is plotted with a dot in every case. Mann-Whitney-Wilcoxon test showed no significant differences between the theoretical and the experimental median values in any case.

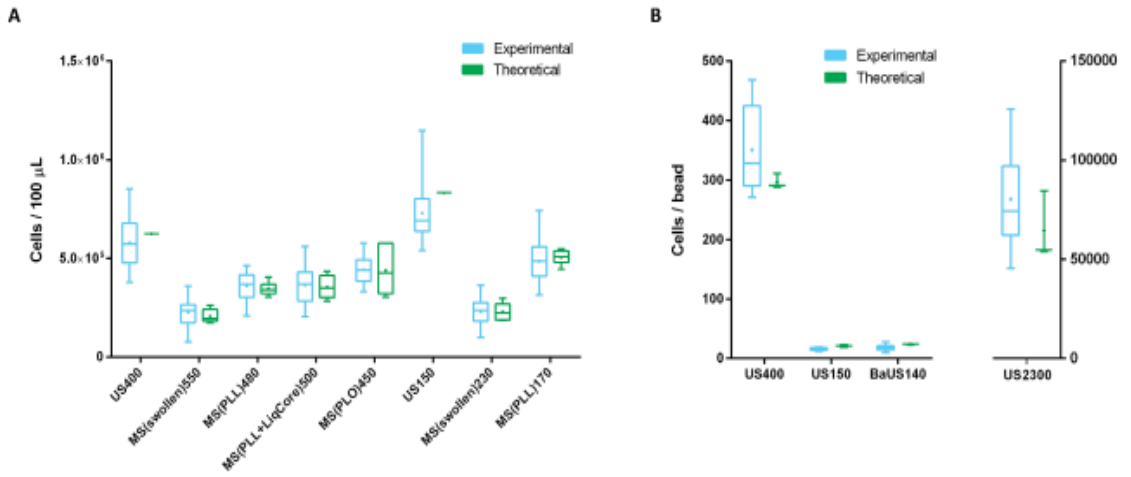

Figure 8. Experimental and theoretical results obtained for cells/V_S (V_S = 100 µL) (A) and cells/sphere (B). Due to the different scales, two Y-axes are displayed on the cells/sphere box plot. Left Y-axis shows the scale for the spheres of diameters smaller or equal to 400 µm and right Y-axis shows the scale for spheres of 2300 µm of diameter. The mean value is plotted with a dot in every case. Mann-Whitney-Wilcoxon test showed no significant differences between the theoretical and the experimental median values in any case.

In order to check the linear correlation between the theoretical and experimental results obtained for spheres/V_S, cells/V_S and cells/sphere, Pearson correlation coefficients were analyzed. **Figure 9** shows the correlation between theoretical and experimental values of spheres/V_S, cells/V_S and cells/sphere. Pearson correlation coefficients were close to 1 in all cases ($p<0.001$), proving a positive strong correlation between theoretical and experimental data.

The obtained data shows that the theoretical results match the experimental ones, with a positive strong correlation in all cases, proving the ability of the three formulas to predict the real cells/sphere, spheres/V_S and cells/V_S values.

The variability of the experimental results is relatively high in some cases but it could be expected as the protocols include many steps that imply different sources of error. First of all, the automated cell counting presents an approximate coefficient of variation (CV) of 2.6% [26]. Regarding the diameters of the tested spheres, the polydispersity affects both the effect that the diameter values have on the formulas (which is powered by three), but also the packing fraction values. Also the different sphere arrangements could lead to variability in the number of particles that could fit in a given volume, even if we stablished a soft agitation between waiting times, that helps achieving a more compact jammed state. Moreover, the process needed to

count the encapsulated cells, involves the digestion of the spheres that, depending on the particle type, can be a difficult process.

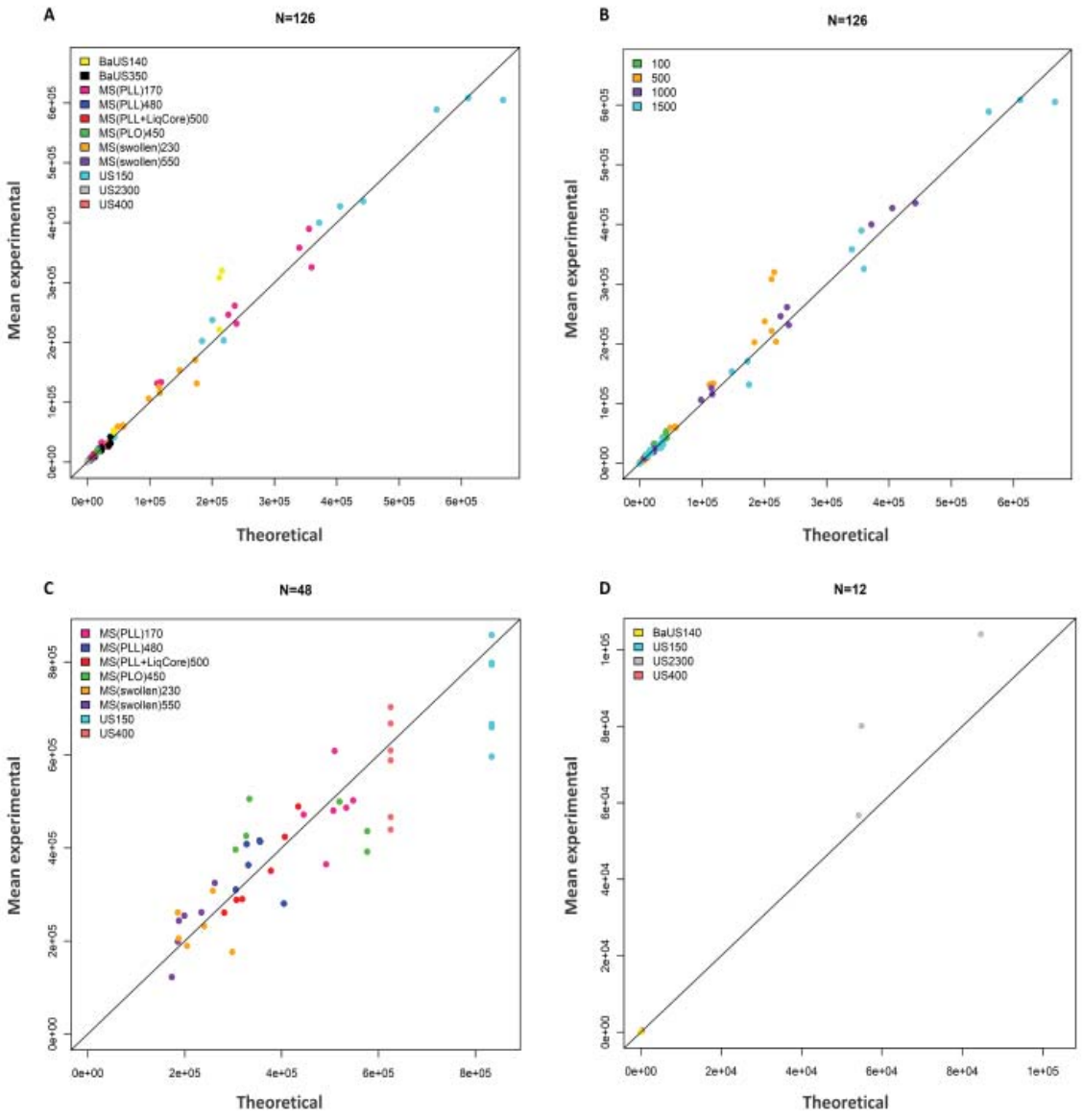

E

	N	cor	p
Spheres/V_S	126	0,992	*<0.001*
Cells/V_S	48	0,899	*<0.001*
Cells/sphere	12	0,992	*<0.001*

Figure 9. Linear correlation analyses between theoretical and experimental data. The results obtained for spheres/V_S were colored based on the different sphere types **(A)** and volumes **(B)**. The results for cells/V_S **(C)** and cells/sphere **(D)** were colored based on the different sphere types. Pearson correlation coefficients were close to 1 in every case and the p values were statistically significant (<0.001) **(E).**

It is important to note that the simulated packing fraction values seem to adequately describe the real values of the alginate sphere batches even if the physical-mechanical characteristics of the real spheres differ from the simulated ones. Alginate beads and MCs are known to present surface roughness and charges, while none of these parameters were included on the simulations. Moreover, the polydispersity of the elaborated batches of microparticles ranged from 2-8% and only a fixed 5% polydispersion was included on the simulations **(supplementary discussion)**. These results confirmed our hypothesis that moderate surface roughness or charges, or common polydispersity in sphere sizes do not notably change packing fraction values, which makes it possible to extrapolate the results obtained from the simulations to different hydrogel spherical microparticles.

4. DISCUSSION AND FINAL CONCLUSIONS

The main objective of this study was to define a simple and practical mathematical model that allows for the easy calculation of cells or drug/sphere, cells or drug/V_s and spheres/V_s in a wide range of hydrogel-based particulate systems. The model can be applied in any case were the described parameters, ϕ_0, ϕ , d_0, d_1 and V_p/V_s can be measured. V_p/V_s, d_0 and d_1 are usually easy to measure. Packing fractions are probably the most difficult to be calculated but the values can be found in a very narrow range as long as a few conditions are met. In our simulations, hydrogel spheres with a similar density to the fluid they are imbibed in are used. It could be expected that spherical particles, surrounded by a fluid were the ρ_s/ρ_f ratio falls within the tested range of 1-1.5 (probably it would be possible to extrapolate the applicability to higher ratios), would generate comparable packing densities, if no other parameters are changed and as long as the ratio of container to sphere size is big enough and the number of spheres are sufficient to form a proper packing density. The mathematical model also takes into account possible volume changes caused by shrinking or swelling of the polymer due to particle-elaborating procedures, which is a very common phenomenon when working with hydrogels. The designed equations take into account all these changes just by end-point measurements, making otherwise complex phenomena, easy to quantify **(Box 2)**.

Caution should be taken when spheres of elevated roughness or electrostatic charges are used, or when the polydispersity of the batches remarkably surpasses the stablished 5%. Anyway, moderate levels of roughness or electrostatic charges do not seem to notably influence the results. These approximate values should not be taken into account neither when very high numbers of spheres are used, as the behavior of the packing fraction could vary with the increase of the packing weight. In addition, we strongly suggest adjusting the diameters for every batch if notable variability is expected, as small changes in this parameter can lead to noticeable differences on the results (diameters are powered by three on the formulas).

Box 1. Advantages of the model

- Improved work-flow.
- Certainty when it comes to analyzing data.
- Predictability and capacity to detect anomalies.
- Removes batch to batch variability derived from swelling processes (normalized results).
- Removes the variability of counting processes.
- Possibility to adjust the dose in narrowed therapeutic ranges.

Altogether, this is intended to become a general standard guide for accurate dose control in spherical hydrogel drug/cell delivery systems. Since all empirical procedures entail an intrinsic variability, the error accumulated through serial procedures may distort the actual values. On the contrary, we demonstrated that the estimated values obtained by the present mathematical model, which include the simulated packing fraction values, represent reliable central points to set as reference for many measurements in the daily clinical or laboratory routine.

5. ACKNOWLEDGEMENTS

Authors gratefully acknowledge the ICTS “NANBIOSIS”, specifically by the Drug Formulation Unit (U10) of the CIBER-BBN at the University of Basque

Country UPV/EHU in Vitoria-Gasteiz. Tania B. Lopez-Mendez thanks the Basque Government (Department of Education, Universities and Research) for the Ph.D. fellowship.

6. DECLARATION OF INTEREST

The authors declare no competing financial interest.

7. REFERENCES

[1] Koetting MC, Guido JF, Gupta M, Zhang A, Peppas NA. pH-responsive and enzymatically-responsive hydrogel microparticles for the oral delivery of therapeutic proteins: Effects of protein size, crosslinking density, and hydrogel degradation on protein delivery. J Control Release 2016; DOI: 10.1016/j.jconrel.2015.11.023

[2] Davoodi P, Ng WC, Srinivasan MP, Wang CH. Codelivery of anti-cancer agents via double-walled polymeric microparticles/injectable hydrogel: A promising approach for treatment of triple negative breast cancer. Biotechnol Bioeng 2017; DOI: 10.1002/bit.26406

[3] Secret E, Kelly SJ, Crannell KE, Andrew JS. Enzyme-responsive hydrogel microparticles for pulmonary drug delivery. ACS Appl Mater Interfaces 2014; DOI: 10.1021/am501754s

[4] Gonzalez-Pujana A, Santos E, Orive G, Pedraz JL, Hernandez RM. Cell microencapsulation technology: Current vision of its therapeutic potential through the administration routes. J Drug Deliv Sci Tec 2017; DOI: 10.1016/j.jddst.2017.03.028

[5] Farina M, Alexander JF, Thekkedath U, Ferrari M, Grattoni A. Cell encapsulation: Overcoming barriers in cell transplantation in diabetes and beyond. Adv Drug Deliv Rev 2019; DOI: S0169-409X(18)30080-2

[6] Lu S, Lee EJ, Lam J, Tabata Y, Mikos AG. Evaluation of Gelatin Microparticles as Adherent-Substrates for Mesenchymal Stem Cells in a Hydrogel Composite. Ann Biomed Eng 2016; DOI: 10.1007/s10439-016-1582-x

[7] Xia B, Krutkramelis K, Oakey J. Oxygen-purged microfluidic device to enhance cell viability in photopolymerized PEG hydrogel microparticles. Biomacromolecules 2016; DOI: 10.1021/acs.biomac.6b00597

[8] Riley L, Schirmer L, Segura T. Granular hydrogels: emergent properties of jammed hydrogel microparticles and their applications in tissue repair and regeneration. Curr Opin Biotechnol 2018; DOI: S0958-1669(18)30137-X

[9] Weeks ER. Soft jammed materials. In: Maruyama S, Tokuyama M, editors. Statistical physics of complex fluids, Tohoku University Press; 2007, chapter 2.

[10] O'Hern CS, Silbert LE, Liu AJ, Nagel SR. Jamming at zero temperature and zero applied

stress: the epitome of disorder. Phys Rev E Stat Nonlin Soft Matter Phys 2003; DOI: 10.1103/PhysRevE.68.011306

[11] Jaeger HM and Nagel SR. Physics of the granular state. Science 1992; DOI: 255/5051/1523

[12] Knight JB, Fandrich CG, Lau CN, Jaeger HM, Nagel SR. Density relaxation in a vibrated granular material. Phys Rev E Stat Phys Plasmas Fluids Relat Interdiscip Topics 1995; DOI: 10.1103/PhysRevE.51.3957

[13] Morch YA, Donati I, Strand BL, Skjak-Braek G. Effect of Ca2+, Ba2+, and Sr2+ on alginate microbeads. Biomacromolecules 2006; DOI: 10.1021/bm060010d

[14] Mukhopadhyay S and Peixinho J. Packings of deformable spheres. Phys Rev E Stat Nonlin Soft Matter Phys 2011; DOI: 10.1103/PhysRevE.84.011302

[15] Ahmed EM. Hydrogel: Preparation, characterization, and applications: A review. J Adv Res 2015; DOI: 10.1016/j.jare.2013.07.006

[16] Sperl M. Experiments on corn pressure in silo cells - translation and comment of Janssen's paper from 1895. Granular matter 2006; DOI: 10.1007/s10035-005-0224-z

[17] van Hecke M. Jamming of soft particles: geometry, mechanics, scaling and isostaticity 2009; DOI: 10.1088/0953-8984/22/3/033101

[18] Visscher WM and Bolsterli M. Random packing of equal and unequal spheres in two and three dimensions. Nature 1972; DOI: 10.1038/239504a0

[19] Jodrey WS and Tory EM. Computer simulation of close random packing of equal spheres. Phys Rev A 1985; DOI: 10.1103/PhysRevA.32.2347

[20] Tobochnik J and Chapin PM. Monte Carlo simulation of hard spheres near random closest packing using spherical boundary conditions. J Chem Phys 1988; DOI: 10.1063/1.454542

[21] An X and Li C. Experiments on densifying packing of equal spheres by two-dimensional vibration. Particuology 2013; DOI: 10.1016/j.partic.2012.06.019

[22] Lachhab T and Weill C. Compression of a soft sphere packing. Eur Phys J B 1999; DOI: 10.1007/s100510050742

[23] Suzuki M, Shinmura T, Iimura K, Hirota M. Study of the wall effect on particle packing structure using X-ray micro computed tomography. Adv Powder Technol 2008; DOI: 10.1163/156855208X293817

[24] Sohn HY and Moreland C. The effect of particle size distribution on packing density. Can J Chem Eng 1968; DOI: 10.1002/cjce.5450460305

[25] Lekka M, Sainz-Serp D, Kulik AJ, Wandrey C. Hydrogel microspheres: influence of chemical composition on surface morphology, local elastic properties, and bulk mechanical characteristics. Langmuir 2004; DOI: 10.1021/la048389h

[26] https://www.bio-rad.com/webroot/web/pdf/lsr/literature/Bulletin_6003.pdf [accessed 30 July 2020]

[27] Chan E, Lim T, Voo W, Pogaku R, Tey BT, Zhang Z. Effect of formulation of alginate

beads on their mechanical behavior and stiffness. Particuology 2011; DOI: 10.1016/j.partic.2010.12.002

[28] Capone SH, Dufresne M, Rechel M, Fleury M, Salsac A, Paullier P et al. Impact of alginate composition: from bead mechanical properties to encapsulated HepG2/C3A cell activities for in vivo implantation. PLOS ONE 2013; DOI: 10.1371/journal.pone.0062032

[29] Loh QL, Wong YY, Choong C. Combinatorial effect of different alginate compositions, polycations, and gelling ions on microcapsule properties. Colloid Polym Sci 2012; DOI: 10.1007/s00396-011-2568-8

[30] de Vos P, Spasojevic M, de Haan BJ, Faas MM. The association between in vivo physicochemical changes and inflammatory responses against alginate based microcapsules. Biomaterials 2012; DOI: 10.1016/j.biomaterials.2012.04.039

[31] Virumbrales-Muñoz M, Santos-Vizcaino E, Paz L, Gallardo-Moreno A, Orive G, Hernandez RM et al. Force spectroscopy-based simultaneous topographical and mechanical characterization to study polymer-to-polymer interactions in coated alginate microspheres. Sci Rep 2019; DOI: 10.1038/s41598-019-56547-z

[32] Hajifathaliha F, Mahboubi A, Nematollahi L, Mohit E, Bolourchian N. Comparison of different cationic polymers efficacy in fabrication of alginate multilayer microcapsules. Asian J Pharm Sci 2020; DOI: 10.1016/j.ajps.2018.11.007

[33] Abbah SA, Lu WW, Peng SL, Aladin DMK, Li ZY, Tam WK et al. Extracellular matrix stability of primary mammalian chondrocytes and intervertebral disc cells cultured in alginate-based microbead hydrogels. Cell Transplant 2008; DOI: 10.3727/096368908787236648

Supplementary discussion. Adequacy of the cell microencapsulaton example

There is still no consensus about which is the most adequate cell microencapsulation protocol and they greatly vary between the different research groups. Today, the materials used include natural (alginate, agarose, collagen, or cellulose, for example) or synthetic (polyethylene glycol (PEG), PLGA or polyvinyl alcohol (PVA), among others) polymers, being the alginate the most widely used. This polysaccharide is able to form hydrogels when it is ionically crosslinked, mainly using barium or calcium as crosslinking agents. Today there is no clear preference between these two ions and its use depends mainly on the protocols adopted in the different research groups.

In some cases, and depending on the application, the beads composed of different biomaterials and cells, are the final product to be administered. However, obtained pore size in most cases is too large and does not present a real barrier against the threats that the implant will face once implanted. Therefore, many groups coat these beads with different polymers to elaborate a semipermeable membrane that transforms de beads into microcapsules (MCs) that filter and control the molecules and cells that can come into contact with the immobilized cells. For the elaboration of this semipermeable membrane, different polymers have been used, such as chitosan, oligo-chitosan or poly(methylene-co-guanidine) (PMCG), but both in preclinical studies and in human trials, the most used molecules are poly-L-lysine (PLL) and poly-L-ornithine (PLO) [5].

This example of cell microencapsulation technologies meets the criteria for the application of the model: It is a granular material in which a relationship between a volume and a number of cells would dramatically improve the dose control and we have the possibility to measure all the needed parameters (d_0, d_1, ϕ_0, ϕ_1 and V_p/V_s). d_0, d_1 and the V_p/V_s values could be directly measured from the batches and the values of ϕ_0 and ϕ_1 were deduced from the simulations. As mentioned before, the simulations aim to be an approximation of the expected packing fraction values, that usually fit in a narrow range, with some assumptions.

Before the calculation of the theoretical cells/sphere, cells/V_S and spheres/V_S with the packing fraction values obtained from the simulations, we checked their applicability in this specific case. Even if it can be deducted from the obtained results that the application of the simulations in this case gives us adequate theoretical values that match the experimental results, there are some clear differences between the real alginate sphere pellets and the simulated ones that should be discussed.

First of all, for the simulations, perfectly spherical and smooth particles were selected, with no surface charge and with a polydispersity of 5%. Actual alginate beads and microcapsules are known to have surface roughness and charge and the size deviation of the alginate spheres in the experimental spheres ranged from 2% to 8%, depending on the batch, which also could affect the packing fraction.

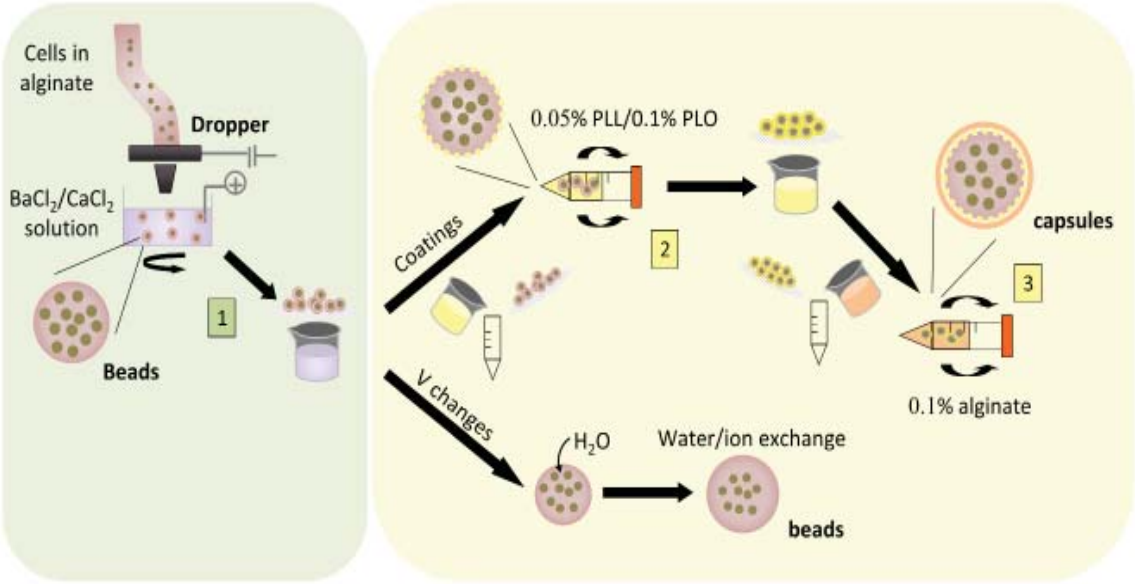

SD 1. General scheme of the most used protocols for the elaboration of cell microencapsulation systems for sustained drug delivery. In a first step, a mix of cells and alginate is extruded through a needle and dropped over a bath of $BaCl_2$ or $CaCl_2$ to form alginate beads (USs). In some protocols, in subsequent steps, these beads are coated with different polymers to reduce the permeability of the system and create the microcapsules (MCs), which can be considered as modified spheres (MSs). Both the USs and the MCs can suffer water/ion exchanges when they are exposed to different media (as soon as they are removed from the first crosslinking bath), changing their size and physical-mechanical properties.

For the simulations, the density values of the spheres and the fluid around were 1200 kg/m^3 and 1000 kg/m^3, respectively. The density of all the tested spheres

was checked before the application of the model as described in the "simulations applicability" section. The values fell within the tested density range, with a ρ_s/ρ_f value ranging from 1 to 1.5, which allowed us to deduce that the behavior of the spheres would be very similar to the one in the simulations.

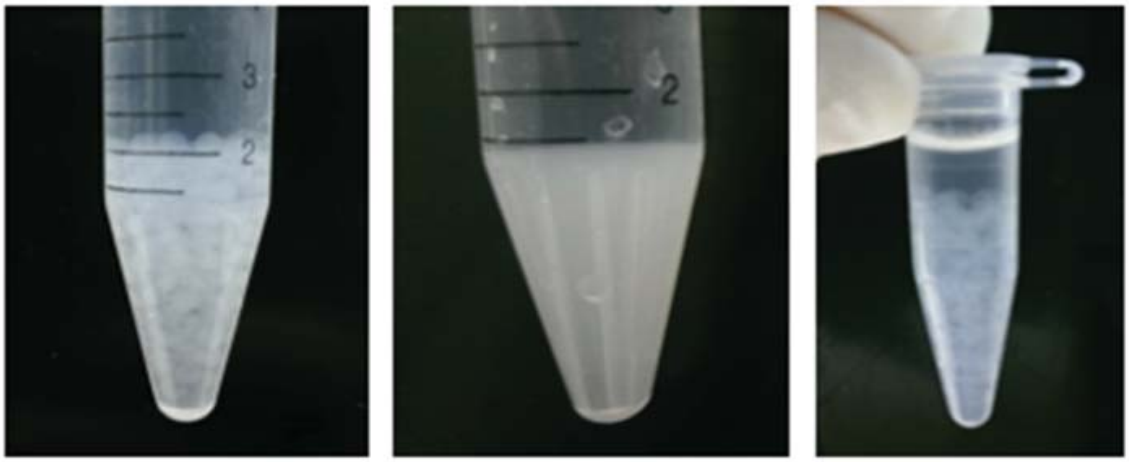

SD2. Dosing procedures in 15 mL Corning tubes and 1.5 mL Eppendorf tubes. The hydrogel spheres, immersed in a fluid, were allowed to settle down to the bottom of the container, in order to measure the volume occupied by them.

With respect to the stiffness, for alginate microspheres, Chang *et al*. [27] described how different alginates (depending on the G/M-block content) or crosslinkers (Ca^{+2}, Ba^{+2}, Cu^{+2} or Sr^{+2}) and their concentrations can influence the stiffness of the spheres. Tested bead stiffness in their study ranged from 250 to 900KPa. In this case, for spheres made of 1.5% alginate with a high content in G-blocks, crosslinked with 100mM $CaCl_2$ a Young modulus of approximately 200KPa is expected and of 400-500KPa for the ones crosslinked with $BaCl_2$. In general, the stiffness of alginate spheres is considered to depend on the degree of crosslinking. More concentrated alginates generate higher cross-linking densities which lead to stiffer beads. Also, it is well accepted that gels made of alginates with higher contents of G-blocks are stronger [13]. The affinity of the crosslinking agent towards the alginate chains is also determinant, with the barium producing stiffer beads than calcium [27]. Finally, the availability of the cations in solution and the alginate chains alters the way in which the alginate gels, as slower crosslinking kinetics usually results in higher crosslinking rates in the inner part of the beads,

giving stronger spheres as a result. A similar phenomenon occurs with beads of different sizes, were smaller diameters allow for more complete crosslinking of the bead core.

The addition of polycation coatings has been described to notably increase the Young modulus of the beads. A 1.7 fold increase in the Young modulus has been reported after the addition of PLL [28] and even higher increases are expected when the coating are made with PLO [29].

For the number of spheres tested, and taking into account the ρ_s/ρ_f ratio no significant deformation of the spheres is expected in this case. With very high numbers of spheres, the stiffness of the beads and MCs would have a greater influence on the packing fraction, as the weight of the spheres would increase the deformation of the particles.

Regarding surface charge of the spheres, zeta-potential studies of the different types of beads and MCs have shown that the surface charge is usually negative for the beads elaborated with alginate. Polycation-coated MCs also show negative surface charges, even without the last alginate coating, as the positive charges are normally neutralized with the negative charges of the alginate molecules [30].

With respect to the surface topography, the Ca^{+2}-alginate beads show more or less smooth surfaces with less than 1nm height [25], even when they are coated with different polycations, with no-significant differences between the peak to walley ratios [31,32]. Ba^{+2}-alginate microbeads have been described to have similar surfaces with some studies pointing to smoother topographies and others to the opposite [25,33].

Taking into account that the density and stiffness values were very similar in both the simulations and the real spheres, and that the measurements were made in Eppendorf and Corning tubes, with big enough container to sphere diameter ratios to allow the formation of proper sediments, we hypothesized that the differences related to surface charge and roughness would be negligible and that the packing fraction values obtained from the simulations would be applicable in this case. The effect of slight surface charge and roughness are commonly not strong enough to significantly influence the final packing fraction values when working with spheres surrounded

by a fluid, which usually contains different electrolytes and charges molecules. The results demonstrated that the simulated packing fraction values allowed us to accurately predict the experimental values, using the presented mathematical model.

A last aspect that must be emphaticized is the fact that the mathematical model also takes into account possible volume changes caused by shrinking or swelling of the polymer due to bead elaborating procedures, which is a very common phenomenon when working with hydrogels. In this case, it is well known that the crosslinking of the alginate produces the shrinking of the beads to a greater or lesser extent, depending on the affinity and concentration of the crosslinker, the concentration of the alginate or the size of the spheres, among others [13]. The designed equations take into account these volume changes just by end-point measurements, making otherwise complex phenomena, easy to quantify.

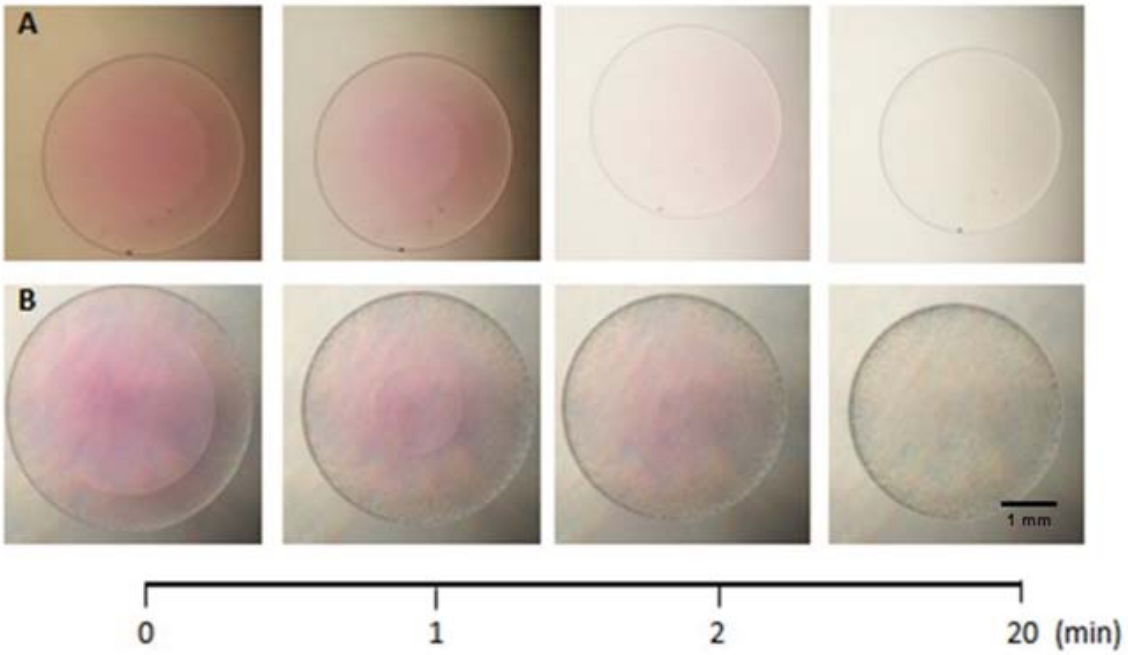

SD3. Gelling process of alginate beads (USs) crosslinked with $CaCl_2$ (A) or $BaCl_2$ (B). The 1.5% alginate solution was prepared in growth media, instead a 1% mannitol solution, in order to obtain a colored solution. The USs were elaborated following the described procedure and the gelling process was recorded under the microscope to visualize the shrinking phenomena associated to the crosslinking of the alginate.

Supplementary material

SM 1. Comparison between theoretical and experimental data. ECo: Eppendorf cone; ECy: Eppendorf tube; d_0: diameters of USs; d_1: diameters of MSs; φ_0: packing fraction of USs; φ_1: packing fraction of MSs.

Spheres/V_S (100 µL)							
Batch	**d_0 (µm) ± SD**	**d_1 (µm) ± SD**	**V (mL) & shape**	**ϕ_0 ± SD**	**ϕ_1 ± SD**	**Spheres/V_s (theor) ± SD**	**Spheres/V_s (exp) ± SD**
US400	375.71 ± 8.45	375.71 ± 8.45	0.1ECo	0.60 ± 0.00023	0.60 ± 0.00023	2147 ± 47	2227 ± 317
	374.43 ± 11.33	374.43 ± 11.33		0.60 ± 0.00023	0.60 ± 0.00023	2170 ± 47	2391 ± 569
	383.83 ± 8.70	383.83 ± 8.70		0.60 ± 0.00024	0.60 ± 0.00024	2012 ± 45	2164 ± 322
MS(swollen)550	375.71 ± 8.45	546.40 ± 9.19	0.1Eco	0.60 ± 0.00023	0.58 ± 0.00056	684 ± 22	1009 ± 141
	374.43 ± 11.33	516.50 ± 17.17		0.60 ± 0.00023	0.59 ± 0.00049	813 ± 25	1164 ± 176
	383.83 ± 8.70	510.43 ± 12.12		0.60 ± 0.00024	0.59 ± 0.00048	843 ± 25	1027 ± 175
MS(PLL)480	384.13 ± 11.72	474.83 ± 16.60	0.1Eco	0.60 ± 0.00024	0.59 ± 0.00040	1052 ± 29	1573 ± 357
	385.39 ± 9.42	464.45 ± 14.65		0.60 ± 0.00025	0.59 ± 0.00038	1126 ± 30	1467 ± 378
	377.42 ± 14.29	464.98 ± 12.56		0.60 ± 0.00023	0.59 ± 0.00038	1122 ± 30	1458 ± 238
MS(PLL+LiqCore)500	384.13 ± 11.72	498.95 ± 18.05	0.1Eco	0.60 ± 0.00024	0,59 ± 0.00046	904 ± 27	1120 ± 235
	385.39 ± 9.42	486.82 ± 22.41		0.60 ± 0.00025	0,59 ± 0.00043	975 ± 28	1200 ± 157
	377.42 ± 14.29	470.91 ± 22.60		0.60 ± 0.00023	0.59 ± 0.00040	1079 ± 30	1564 ± 230
MS(PLO)450	377.05 ± 12.45	477.34 ± 12.29	0.1Eco	0.60 ± 0.00023	0.59 ± 0.00041	1036 ± 29	1467 ± 322
	378.10 ± 23.70	464.76 ± 13.47		0.60 ± 0.00023	0.59 ± 0.00039	1124 ± 31	1253 ± 394
	371.13 ± 11.72	459.33 ± 13.01		0.60 ± 0.00022	0.59 ± 0.00037	1165 ± 31	1556 ± 179
US150	141.95 ± 11.81	141.95 ± 11.81	0.1Eco	0.60 ± 0.00004	0.60 ± 0.00004	39922 ± 685	41227 ± 4306
	146.10 ± 13.02	146.10 ± 13.02		0.60 ± 0.00005	0.60 ± 0.00005	36634 ± 638	42987 ± 3274
	137.86 ± 6.21	137.86 ± 6.21		0.60 ± 0.00004	0.60 ± 0.00004	43551 ± 752	42369 ± 3925
MS(swollen)230	141.95 ± 11.81	215.31 ± 10.40	0.1Eco	0.60 ± 0.00004	0.60 ± 0.00008	11497 ± 199	14289 ± 1613
	146.10 ± 13.02	216.28 ± 11.40		0.60 ± 0.00005	0.60 ± 0.00008	11342 ± 197	14267 ± 965
	137.86 ± 6.21	227.88 ± 11.68		0.60 ± 0.00004	0.60 ± 0.00009	9698 ± 168	13796 ± 1216
MS(PLL)170	141.95 ± 11.81	169.39 ± 6.62	0.1Eco	0.60 ± 0.00004	0.60 ± 0.00006	23565 ± 406	29502 ± 3944
	146.10 ± 13.02	172.59 ± 6.60		0.60 ± 0.00005	0.60 ± 0.00006	22283 ± 386	32316 ± 2400
	137.86 ± 6.21	170.05 ± 5.65		0.60 ± 0.00004	0.60 ± 0.00006	23292 ± 406	32987 ± 2166
BaUS350	361.04 ± 10.28	361.04 ± 10.28	0.1Eco	0.60 ± 0.00021	0.60 ± 0.00021	2423 ± 51	2889 ± 329
	359.32 ± 15.18	359.32 ± 15.18		0.60 ± 0.00021	0.60 ± 0.00021	2458 ± 51	2698 ± 464
	369.49 ± 10.88	369.49 ± 10.88		0.60 ± 0.00022	0.60 ± 0.00022	2259 ± 48	2724 ± 386
BaUS140	138.51 ± 6.32	138.51 ± 6.32	0.1Eco	0.60 ± 0.00004	0.60 ± 0.00004	42951 ± 734	53644 ± 3474
	139.41 ± 8.82	139.41 ± 8.82		0.60 ± 0.00004	0.60 ± 0.00004	42123 ± 727	51956 ± 6304
	139.37 ± 4.99	139.37 ± 4.99		0.60 ± 0.00004	0.60 ± 0.00004	42163 ± 728	48124 ± 3386
US2300	2188.75 ± 45.51	2188.75 ± 45.51	0.1Eco	0.50 ± 0.00120	0.50 ± 0.00120	9 ± 1	9 ± 1
	2248.75 ± 72.31	2248.75 ± 72.31		0.50 ± 0.00116	0.50 ± 0.00116	8 ± 1	8 ± 1
	2623.75 ± 94.76	2623.75 ± 94.76		0.50 ± 0.00092	0.50 ± 0.00092	5 ± 1	5 ± 0

Spheres/V_S (500 µL)							
Batch	**d_0 (µm) ± SD**	**d_1 (µm) ± SD**	**V (mL) & shape**	**ϕ_0 ± SD**	**ϕ_1 ± SD**	**Spheres/V_s (theor) ± SD**	**Spheres/V_s (exp) ± SD**
US400	375.71 ± 8.45	375.71 ± 8.45	0.5Eco	0.61 ± 0.00010	0.61 ± 0.00010	10952 ± 125	9333 ± 4888
	374.43 ± 11.33	374.43 ± 11.33		0.61 ± 0.00010	0.61 ± 0.00010	11064 ± 123	8400 ± 3816
	383.83 ± 8.70	383.83 ± 8.70		0.61 ± 0.00010	0.61 ± 0.00010	10270 ± 119	8000 ± 2117
MS(swollen)550	375.71 ± 8.45	546.40 ± 9.19	0.5Eco	0.61 ± 0.00010	0.60 ± 0.00021	3541 ± 58	3867 ± 2274
	374.43 ± 11.33	516.50 ± 17.17		0.61 ± 0.00010	0.61 ± 0.00019	4198 ± 64	5200 ± 1200
	383.83 ± 8.70	510.43 ± 12.12		0.61 ± 0.00010	0.61 ± 0.00018	4351 ± 66	5000 ± 1600
MS(PLL)480	384.13 ± 11.72	474.83 ± 16.60	0.5Eco	0.61 ± 0.00010	0.61 ± 0.00016	5412 ± 77	6800 ± 2227
	385.39 ± 9.42	464.45 ± 14.65		0.61 ± 0.00010	0.61 ± 0.00015	5786 ± 80	3400 ± 3274
	377.42 ± 14.29	464.98 ± 12.56		0.61 ± 0.00010	0.61 ± 0.00015	5766 ± 80	6400 ± 2800
MS(PLL+LiqCore)500	384.13 ± 11.72	498.95 ± 18.05	0.5Eco	0.61 ± 0.00010	0,61 ± 0.00017	4660 ± 69	6733 ± 3402
	385.39 ± 9.42	486.82 ± 22.41		0.61 ± 0.00010	0,61 ± 0.00017	5020 ± 73	4333 ± 1973
	377.42 ± 14.29	470.91 ± 22.60		0.61 ± 0.00010	0.61 ± 0.00016	5549 ± 78	5467 ± 2948
MS(PLO)450	377.05 ± 12.45	477.34 ± 12.29	0.5Eco	0.61 ± 0.00010	0.61 ± 0.00016	5327 ± 76	6467 ± 1222
	378.10 ± 23.70	464.76 ± 13.47		0.61 ± 0.00010	0.61 ± 0.00015	5774 ± 80	5667 ± 231
	371.13 ± 11.72	459.33 ± 13.01		0.61 ± 0.00009	0.61 ± 0.00015	5982 ± 82	5733 ± 3585
US150	141.95 ± 11.81	141.95 ± 11.81	0.5ECo	0.60 ± 0.00005	0.60 ± 0.00005	200528 ± 1832	237600 ± 31493
	146.10 ± 13.02	146.10 ± 13.02		0.60 ± 0.00004	0.60 ± 0.00004	184050 ± 1658	202467 ± 12029
	137.86 ± 6.21	137.86 ± 6.21		0.60 ± 0.00005	0.60 ± 0.00005	218714 ± 1990	203467 ± 24846
MS(swollen)230	141.95 ± 11.81	215.31 ± 10.40	0.5ECo	0.60 ± 0.00005	0.61 ± 0.00002	57981 ± 524	59533 ± 12601
	146.10 ± 13.02	216.28 ± 11.40		0.60 ± 0.00004	0.61 ± 0.00002	57202 ± 514	61533 ± 3402
	137.86 ± 6.21	227.88 ± 11.68		0.60 ± 0.00005	0.61 ± 0.00002	48943 ± 440	59600 ± 6657
MS(PLL)170	141.95 ± 11.81	169.39 ± 6.62	0.5Eco	0.60 ± 0.00005	0.60 ± 0.00003	118529 ± 1067	133600 ± 12126
	146.10 ± 13.02	172.59 ± 6.60		0.60 ± 0.00004	0.60 ± 0.00003	112100 ± 1016	131867 ± 22476
	137.86 ± 6.21	170.05 ± 5.65		0.60 ± 0.00005	0.60 ± 0.00003	117161 ± 1064	133267 ± 16455
BaUS350	361.04 ± 10.28	361.04 ± 10.28	0.5Eco	0.61 ± 0.00009	0.61 ± 0.00009	12344 ± 133	8667 ± 1665
	359.32 ± 15.18	359.32 ± 15.18		0.61 ± 0.00009	0.61 ± 0.00009	12522 ± 134	10400 ± 6400
	369.49 ± 10.88	369.49 ± 10.88		0.61 ± 0.00009	0.61 ± 0.00009	11515 ± 126	10133 ± 5001
BaUS140	138.51 ± 6.32	138.51 ± 6.32	0.5Eco	0.60 ± 0.00005	0.60 ± 0.00005	215705 ± 1956	320067 ± 97393
	139.41 ± 8.82	139.41 ± 8.82		0.60 ± 0.00005	0.60 ± 0.00005	211554 ± 1941	308267 ± 24417
	139.37 ± 4.99	139.37 ± 4.99		0.60 ± 0.00005	0.60 ± 0.00005	211755 ± 1919	221467 ± 20033
US2300	2188.75 ± 45.51	2188.75 ± 45.51	0.5ECo	0.53 ± 0.00631	0.53 ± 0.00631	48 ± 3	60
	2248.75 ± 72.31	2248.75 ± 72.31		0.53 ± 0.00692	0.53 ± 0.00692	44 ± 3	50
	2623.75 ± 94.76	2623.75 ± 94.76		0.52 ± 0.01121	0.52 ± 0.01121	27 ± 2	29

Spheres/V_S (1000 µL)							
Batch	**d_0 (µm) ± SD**	**d_1 (µm) ± SD**	**V (mL) & shape**	**ϕ_0 ± SD**	**ϕ_1 ± SD**	**Spheres/V_s (theor) ± SD**	**Spheres/V_s (exp) ± SD**
US400	375.71 ± 8.45	375.71 ± 8.45	05Eco	0.61 ± 0.00002	0.61 ± 0.00002	21951 ± 127	19250 ± 3208
	374.43 ± 11.33	374.43 ± 11.33	+	0.61 ± 0.00002	0.61 ± 0.00002	22176 ± 128	18970 ± 2859
	383.83 ± 8.70	383.83 ± 8.70	0.5ECy	0.61 ± 0.00002	0.61 ± 0.00002	20583 ± 124	18270 ± 7869
MS(swollen)550	375.71 ± 8.45	546.40 ± 9.19	05Eco	0.61 ± 0.00002	0.61 ± 0.00003	7097 ± 61	8680 ± 5011
	374.43 ± 11.33	516.50 ± 17.17	+	0.61 ± 0.00002	0.61 ± 0.00003	8413 ± 69	8820 ± 420
	383.83 ± 8.70	510.43 ± 12.12	0.5ECy	0.61 ± 0.00002	0.61 ± 0.00003	8719 ± 70	8470 ± 4249
MS(PLL)480	384.13 ± 11.72	474.83 ± 16.60	05Eco	0.61 ± 0.00002	0.61 ± 0.00002	10844 ± 80	12670 ± 8652
	385.39 ± 9.42	464.45 ± 14.65	+	0.61 ± 0.00002	0.61 ± 0.00002	11592 ± 84	12250 ± 2733
	377.42 ± 14.29	464.98 ± 12.56	0.5ECy	0.61 ± 0.00002	0.61 ± 0.00002	11552 ± 85	13510 ± 9050
MS(PLL+LiqCore)500	384.13 ± 11.72	498.95 ± 18.05	05Eco	0.61 ± 0.00002	0,61 ± 0.00003	9338 ± 72	10150 ± 8340
	385.39 ± 9.42	486.82 ± 22.41	+	0.61 ± 0.00002	0,61 ± 0.00002	10058 ± 77	10850 ± 1590
	377.42 ± 14.29	470.91 ± 22.60	0.5ECy	0.61 ± 0.00002	0.61 ± 0.00002	11119 ± 82	11480 ± 5218
MS(PLO)450	377.05 ± 12.45	477.34 ± 12.29	05Eco	0.61 ± 0.00002	0.61 ± 0.00002	10673 ± 80	13090 ± 1697
	378.10 ± 23.70	464.76 ± 13.47	+	0.61 ± 0.00002	0.61 ± 0.00002	11568 ± 84	12040 ± 4607
	371.13 ± 11.72	459.33 ± 13.01	0.5ECy	0.61 ± 0.00002	0.61 ± 0.00002	11985 ± 85	14227 ± 3183
US150	141.95 ± 11.81	141.95 ± 11.81	05Eco	0.61 ± 0.00003	0.61 ± 0.00003	405524 ± 1921	427420 ± 49404
	146.10 ± 13.02	146.10 ± 13.02	+	0.61 ± 0.00003	0.61 ± 0.00003	372045 ± 1737	399840 ± 25056
	137.86 ± 6.21	137.86 ± 6.21	0.5ECy	0.61 ± 0.00003	0.61 ± 0.00003	442494 ± 2085	435820 ± 77958
MS(swollen)230	141.95 ± 11.81	215.31 ± 10.40	05Eco	0.61 ± 0.00003	0.61 ± 0.00002	116650 ± 550	115710 ± 20278
	146.10 ± 13.02	216.28 ± 11.40	+	0.61 ± 0.00003	0.61 ± 0.00002	115076 ± 546	126000 ± 14628
	137.86 ± 6.21	227.88 ± 11.68	0.5ECy	0.61 ± 0.00003	0.61 ± 0.00002	98412 ± 458	106190 ± 10291
MS(PLL)170	141.95 ± 11.81	169.39 ± 6.62	05Eco	0.61 ± 0.00003	0.61 ± 0.00003	239118 ± 1136	231490 ± 15728
	146.10 ± 13.02	172.59 ± 6.60	+	0.61 ± 0.00003	0.61 ± 0.00003	226094 ± 1064	246400 ± 27045
	137.86 ± 6.21	170.05 ± 5.65	0.5ECy	0.61 ± 0.00003	0.61 ± 0.00003	236347 ± 1114	261310 ± 31358
BaUS350	361.04 ± 10.28	361.04 ± 10.28	05Eco	0.61 ± 0.00002	0.61 ± 0.00002	24743 ± 140	25620 ± 3438
	359.32 ± 15.18	359.32 ± 15.18	+	0.61 ± 0.00002	0.61 ± 0.00002	25101 ± 141	24710 ± 16548
	369.49 ± 10.88	369.49 ± 10.88	0.5ECy	0.61 ± 0.00002	0.61 ± 0.00002	23081 ± 133	19320 ± 420
US2300	2188.75 ± 45.51	2188.75 ± 45.51	05Eco	0.53 ± 0.00084	0.53 ± 0.00084	97 ± 3	113
	2248.75 ± 72.31	2248.75 ± 72.31	+	0.53 ± 0.00087	0.53 ± 0.00087	89 ± 3	107
	2623.75 ± 94.76	2623.75 ± 94.76	0.5ECy	0.51 ± 0.00093	0.51 ± 0.00093	54 ± 2	65

Spheres/V_S (1500 µL)							
Batch	**d_0 (µm) ± SD**	**d_1 (µm) ± SD**	**V (mL) & shape**	**ϕ_0 ± SD**	**ϕ_1 ± SD**	**Spheres/V_S (theor) ± SD**	**Spheres/V_S (exp) ± SD**
US400	375.71 ± 8.45	375.71 ± 8.45	0.5Eco	0.61 ± 0.00001	0.61 ± 0.00001	32980 ± 129	32927 ± 6165
	374.43 ± 11.33	374.43 ± 11.33	+	0.61 ± 0.00001	0.61 ± 0.00001	33319 ± 129	25813 ± 1270
	383.83 ± 8.70	383.83 ± 8.70	1ECy	0.61 ± 0.00001	0.61 ± 0.00001	30925 ± 124	28967 ± 4451
MS(swollen)550	375.71 ± 8.45	546.40 ± 9.19	0.5Eco	0.61 ± 0.00001	0.61 ± 0.00002	10670 ± 61	13347 ± 2258
	374.43 ± 11.33	516.50 ± 17.17	+	0.61 ± 0.00001	0.61 ± 0.00002	12646 ± 68	12613 ± 4319
	383.83 ± 8.70	510.43 ± 12.12	1ECy	0.61 ± 0.00001	0.61 ± 0.00001	13105 ± 70	13787 ± 508
MS(PLL)480	384.13 ± 11.72	474.83 ± 16.60	0.5Eco	0.61 ± 0.00001	0.61 ± 0.00001	16297 ± 80	19140 ± 6160
	385.39 ± 9.42	464.45 ± 14.65	+	0.61 ± 0.00001	0.61 ± 0.00001	17420 ± 84	20460 ± 1320
	377.42 ± 14.29	464.98 ± 12.56	1ECy	0.61 ± 0.00001	0.61 ± 0.00001	17360 ± 85	21927 ± 2995
MS(PLL+LiqCore)500	384.13 ± 11.72	498.95 ± 18.05	0.5Eco	0.61 ± 0.00001	0,61 ± 0.00001	14036 ± 74	15620 ± 3911
	385.39 ± 9.42	486.82 ± 22.41	+	0.61 ± 0.00001	0,61 ± 0.00001	15117 ± 77	17380 ± 6644
	377.42 ± 14.29	470.91 ± 22.60	1ECy	0.61 ± 0.00001	0.61 ± 0.00001	16710 ± 81	16793 ± 5100
MS(PLO)450	377.05 ± 12.45	477.34 ± 12.29	0.5Eco	0.61 ± 0.00001	0.61 ± 0.00001	16040 ± 80	20533 ± 3556
	378.10 ± 23.70	464.76 ± 13.47	+	0.61 ± 0.00001	0.61 ± 0.00001	17385 ± 84	16647 ± 4906
	371.13 ± 11.72	459.33 ± 13.01	1ECy	0.61 ± 0.00001	0.61 ± 0.00001	18011 ± 87	17453 ± 7127
US150	141.95 ± 11.81	141.95 ± 11.81	0.5Eco	0.61 ± 0.00001	0.61 ± 0.00001	610650 ± 1922	608593 ± 32280
	146.10 ± 13.02	146.10 ± 13.02	+	0.61 ± 0.00001	0.61 ± 0.00001	560165 ± 1779	588793 ± 37099
	137.86 ± 6.21	137.86 ± 6.21	1ECy	0.61 ± 0.00002	0.61 ± 0.00002	666410 ± 2114	605000 ± 44086
MS(swollen)230	141.95 ± 11.81	215.31 ± 10.40	0.5Eco	0.61 ± 0.00001	0.61 ± 0.00001	175388 ± 541	131707 ± 31730
	146.10 ± 13.02	216.28 ± 11.40	+	0.61 ± 0.00001	0.61 ± 0.00001	173019 ± 541	170720 ± 17824
	137.86 ± 6.21	227.88 ± 11.68	1ECy	0.61 ± 0.00002	0.61 ± 0.00001	147944 ± 464	153633 ± 12981
MS(PLL)170	141.95 ± 11.81	169.39 ± 6.62	0.5Eco	0.61 ± 0.00001	0.61 ± 0.00001	359806 ± 1125	325600 ± 61480
	146.10 ± 13.02	172.59 ± 6.60	+	0.61 ± 0.00001	0.61 ± 0.00001	340185 ± 1063	358087 ± 79388
	137.86 ± 6.21	170.05 ± 5.65	1ECy	0.61 ± 0.00002	0.61 ± 0.00001	355631 ± 1122	389620 ± 40055
BaUS350	361.04 ± 10.28	361.04 ± 10.28	0.5Eco	0.61 ± 0.00001	0.61 ± 0.00001	37175 ± 138	42167 ± 6381
	359.32 ± 15.18	359.32 ± 15.18	+	0.61 ± 0.00001	0.61 ± 0.00001	37712 ± 141	31607 ± 7154
	369.49 ± 10.88	369.49 ± 10.88	1ECy	0.61 ± 0.00001	0.61 ± 0.00001	34677 ± 133	26913 ± 4847
US2300	2188.75 ± 45.51	2188.75 ± 45.51	0.5Eco	0.54 ± 0.00048	0.54 ± 0.00048	148 ± 4	165
	2248.75 ± 72.31	2248.75 ± 72.31	+	0.54 ± 0.00050	0.54 ± 0.00050	136 ± 3	142
	2623.75 ± 94.76	2623.75 ± 94.76	1ECy	0.52 ± 0.00058	0.52 ± 0.00058	83 ± 2	101

Cells/Vs (100 µL)							
Batch	**d_0 (µm) ± SD**	**d_1 (µm) ± SD**	**V (mL) & shape**	**ϕ_0 ± SD**	**ϕ_1 ± SD**	**Cells/V_s (theor) ± SEM**	**Cells/V_s (exp) ± SD**
US400	518.00 ± 21.18	518.00 ± 21.18	0.1ECo	0.59 ± 0.00049	0.59 ± 0.00049	625000 ± 321342	466556 ± 32837
	449.00 ± 12.52	449.00 ± 12.52		0.59 ± 0.00036	0.59 ± 0.00036	625000 ± 181865	609778 ± 122723
	449.50 ± 10.40	449.50 ± 10.40		0.59 ± 0.00036	0.59 ± 0.00036	625000 ± 185727	703000 ± 92738
	415.50 ± 10.99	415.50 ± 10.99		0.59 ± 0.00029	0.59 ± 0.00029	625000 ± 241831	439444 ± 36514
	402.50 ± 6.39	402.50 ± 6.39		0.59 ± 0.00027	0.59 ± 0.00027	625000 ± 140736	588556 ± 49616
	411.00 ± 8.52	411.00 ± 8.52		0.59 ± 0.00029	0.59 ± 0.00029	625000 ± 213478	667778 ± 56251
MS(swollen)550	375.71 ± 8.45	546.40 ± 9.19	0.1Eco	0.60 ± 0.00023	0.58 ± 0.00056	199137 ± 59003	254500 ± 26105
	374.43 ± 11.33	516.50 ± 17.17		0.60 ± 0.00023	0.59 ± 0.00049	234297 ± 112786	261667 ± 31091
	383.83 ± 8.70	510.43 ± 12.12		0.60 ± 0.00024	0.59 ± 0.00048	261935 ± 92993	325000 ± 29086
	415.50 ± 10.99	631.00 ± 19.71		0.59 ± 0.00029	0.58 ± 0.00077	173434 ± 75919	122400 ± 31548
	402.50 ± 6.39	596.00 ± 26.24		0.59 ± 0.00027	0.58 ± 0.00069	187822 ± 70307	243556 ± 8094
	411.00 ± 8.52	610.50 ± 18.77		0.59 ± 0.00027	0.58 ± 0.00072	185826 ± 70362	198778 ± 34593
MS(PLL)480	415.50 ± 10.99	479.00 ± 19.97	0.1Eco	0.59 ± 0.00029	0.59 ± 0.00042	404958 ± 198831	280444 ± 59180
	402.50 ± 6.39	509.00 ± 17.44		0.59 ± 0.00027	0.59 ± 0.00047	305212 ± 105358	310556 ± 41097
	411.00 ± 8.52	494.50 ± 6.86		0.59 ± 0.00029	0.59 ± 0.00045	355367 ± 103552	413889 ± 8908
	384.13 ± 11.72	474.83 ± 16.60		0.60 ± 0.00024	0.59 ± 0.00040	327637 ± 198235	408333 ± 38019
	385.39 ± 9.42	464.45 ± 14.65		0.60 ± 0.00025	0.59 ± 0.00038	354056 ± 127670	416000 ± 35687
	377.42 ± 14.29	464.98 ± 12.56		0.60 ± 0.00023	0.59 ± 0.00038	331110 ± 136649	363500 ± 49070
MS(PLL+LiqCore)500	384.13 ± 11.72	498.95 ± 18.05	0.1Eco	0.60 ± 0.00024	0.59 ± 0.00046	281518 ± 156751	261000 ± 47564
	385.39 ± 9.42	486.82 ± 22.41		0.60 ± 0.00025	0.59 ± 0.00043	306597 ± 124442	288500 ± 67993
	377.42 ± 14.29	470.91 ± 22.60		0.60 ± 0.00023	0.59 ± 0.00040	318523 ± 189634	290167 ± 33748
	497.00 ± 13.09	571.50 ± 13.09		0.59 ± 0.00046	0.58 ± 0.00062	406909 ± 147668	424111 ± 39904
	460.00 ± 9.51	518.00 ± 9.51		0.59 ± 0.00037	0.59 ± 0.00050	434493 ± 151206	489222 ± 58221
	444.00 ± 18.72	523.50 ± 18.72		0.59 ± 0.00034	0.59 ± 0.00051	377544 ± 235105	351000 ± 42002
MS(PLO)450	377.05 ± 12.45	477.34 ± 12.29	0.1Eco	0.60 ± 0.00023	0.59 ± 0.00041	304670 ± 98975	396667 ± 42676
	378.10 ± 23.70	464.76 ± 13.47		0.60 ± 0.00023	0.59 ± 0.00039	333411 ± 283319	505667 ± 47161
	371.13 ± 11.72	459.33 ± 13.01		0.60 ± 0.00022	0.59 ± 0.00037	326614 ± 135050	426222 ± 62565
	440.00 ± 18.64	467.50 ± 11.64		0.59 ± 0.00034	0.59 ± 0.00039	519390 ± 258425	499667 ± 54106
	449.00 ± 9.12	461.00 ± 12.52		0.59 ± 0.00036	0.59 ± 0.00038	576638 ± 196835	391889 ± 27741
	449.50 ± 7.59	461.50 ± 10.40		0.59 ± 0.00036	0.59 ± 0.00038	576687 ± 176044	436222 ± 82171
US150	141.95 ± 11.81	141.95 ± 11.81	0.1Eco	0.60 ± 0.00004	0.60 ± 0.00004	833333 ± 960189	596556 ± 26315
	146.10 ± 13.02	146.10 ± 13.02		0.60 ± 0.00005	0.60 ± 0.00005	833333 ± 918552	798111 ± 113452
	137.86 ± 6.21	137.86 ± 6.21		0.60 ± 0.00004	0.60 ± 0.00004	833333 ± 413465	666444 ± 23633
	152.00 ± 6.96	152.00 ± 6.96		0.60 ± 0.00005	0.60 ± 0.00005	833333 ± 411938	857889 ± 217148
	162.50 ± 7.86	162.50 ± 7.86		0.60 ± 0.00005	0.60 ± 0.00005	833333 ± 839433	659889 ± 76530
	162.00 ± 11.05	162.00 ± 11.05		0.60 ± 0.00005	0.60 ± 0.00005	833333 ± 1153918	794667 ± 70185
MS(swollen)230	141.95 ± 11.81	215.31 ± 10.40	0.1Eco	0.60 ± 0.00004	0.60 ± 0.00008	239994 ± 248037	232000 ± 8544
	146.10 ± 13.02	216.28 ± 11.40		0.60 ± 0.00005	0.60 ± 0.00008	258001 ± 273274	308111 ± 47374
	137.86 ± 6.21	227.88 ± 11.68		0.60 ± 0.00004	0.60 ± 0.00009	185559 ± 105749	261444 ± 32427
	152.00 ± 6.96	243.00 ± 7.33		0.60 ± 0.00005	0.60 ± 0.00010	204705 ± 97064	189689 ± 65958
	162.00 ± 8.34	266.50 ± 12.68		0.60 ± 0.00005	0.60 ± 0.00011	187574 ± 135753	205667 ± 43181
	172.00 ± 6.96	242.50 ± 15.52		0.60 ± 0.00006	0.60 ± 0.00010	297884 ± 217639	176444 ± 49109
MS(PLL)170	141.95 ± 11.81	169.39 ± 6.62	0.1Eco	0.60 ± 0.00004	0.60 ± 0.00006	491887 ± 493172	365000 ± 41587
	146.10 ± 13.02	172.59 ± 6.60		0.60 ± 0.00005	0.60 ± 0.00006	506872 ± 447824	480444 ± 75023
	137.86 ± 6.21	170.05 ± 5.65		0.60 ± 0.00004	0.60 ± 0.00006	445679 ± 216243	471889 ± 81816
	152.00 ± 6.96	176.50 ± 15.31		0.60 ± 0.00005	0.60 ± 0.00006	533427 ± 337782	486667 ± 74923
	162.50 ± 7.86	187.00 ± 6.57		0.60 ± 0.00005	0.60 ± 0.00006	547777 ± 446735	502222 ± 69310
	162.00 ± 11.05	191.00 ± 5.53		0.60 ± 0.00005	0.60 ± 0.00007	509467 ± 545535	608778 ± 65585

Cells/sphere					
Batch	**d_0 (µm) ± SD**	**ϕ_0 ± SD**	**V_p/V_s**	**Cells/sphere (theor) ± SEM**	**Cells/sphere (exp) ± SD**
US400	375.71 ± 8.45	0.60 ± 0.00023	1.25	291 ± 57	343 ± 108
	374.43 ± 11.33	0.60 ± 0.00023		288 ± 70	353 ± 78
	383.83 ± 8.70	0.60 ± 0.00024		311 ± 70	355 ± 57
US150	141.95 ± 11.81	0.60 ± 0.00004	1.67	21 ± 15	16 ± 3
	146.10 ± 13.02	0.60 ± 0.00005		23 ± 16	17 ± 1
	137.86 ± 6.21	0.60 ± 0.00004		19 ± 6	14 ± 1
US2300	2188.75 ± 45.51	0.50 ± 0.00120	0.93	54764 ± 13221	80118 ± 11326
	2248.75 ± 72.31	0.50 ± 0.00116		54063 ± 15591	56696 ± 14272
	2623.75 ± 94.76	0.50 ± 0.00092		84446 ± 28023	104084 ± 20236
BaUS140	138.51 ± 6.32	0.60 ± 0.00004	2	23 ± 9	17 ± 3
	139.41 ± 8.82	0.60 ± 0.00004		24 ± 14	20 ± 3
	139.37 ± 4.99	0.60 ± 0.00004		24 ± 6	17 ± 3

Median [Q1-Q3]		N	Theoretical	Mean Experimental	*p*
Spheres/Vs					
		126	12432.51 [4236.58 - 42753.95]	14011.11 [3983.33 - 50997.78]	*0,735*
Vol (µL)	100	33	2147.27 [1035.5 - 22282.78]	2226.67 [1253.33 - 29502.22]	*0,305*
	500	33	10951.85 [5326.79 - 112100.1]	2226.67 [1253.33 - 29502.22]	*0,849*
	1000	30	16284.21 [10211.83 - 110909.9]	2226.67 [1253.33 - 29502.22]	*0,708*
	1500	30	24468.18 [15347.68 - 166750.6]	2226.67 [1253.33 - 29502.22]	*0,878*
Sphere type	US400	12	15823.73 [8245.04 - 24363.62]	13801.67 [6597.78 - 20890.83]	*0,630*
	MS(swollen)550	12	5724.07 [2866.81 - 9206.44]	6835 [3191.11 - 9768.33]	*0,514*
	MS(PLL)480	12	8314.93 [4340.75 - 12768.39]	9525 [2943.33 - 14917.5]	*0,410*
	MS(PLL+LiqCore)500	12	7443.7 [3765.16 - 11847.85]	8441.67 [3641.11 - 12515]	*0,551*
	MS(PLO)450	12	8327.38 [4286.26 - 12999.03]	9253.33 [4638.89 - 14831.67]	*0,551*
	US150	12	295379.7 [148925.6 - 471912]	318720 [162596.7 - 474063.3]	*0,887*
	MS(swollen)230	12	78196.43 [39581.58 - 124473.4]	83861.67 [48222.22 - 127426.7]	*0,671*
	MS(PLL)170	12	172311.7 [89966.24 - 264384.5]	182545 [107146.7 - 277382.5]	*0,514*
	BaUS350	12	17801.11 [9250.84 - 27494.76]	14860 [7222.22 - 25943.33]	*0,932*
	BaUS140	6	127252.4 [42359.77 - 211704.4]	137555.6 [52377.78 - 286566.7]	*0,180*
	US2300	12	51.21 [22.8 - 91.06]	62.5 [24 - 108.5]	*0,671*
Cells/Vs					
		48	391250.8 [293792.8 - 588765.5]	414944.4 [286486.1 - 503083.3]	*0,858*
Sphere type	US400	6	625000 [625000 - 625000]	599166.7 [497055.6 - 653277.8]	*0,347*
	MS(swollen)550	6	193479.7 [186324.9 - 225507.1]	249027.8 [209972.2 - 259875]	*0,394*
	MS(PLL)480	6	342582.8 [328505.1 - 355039.5]	385916.7 [323791.7 - 412500]	*0,394*
	MS(PLL+LiqCore)500	6	348033.4 [309578.3 - 399567.5]	320583.3 [288916.7 - 405833.3]	*0,818*
	MS(PLO)450	6	426400.2 [328313.5 - 562326.1]	431222.2 [404055.6 - 483805.6]	*1,000*
	US150	6	833333.3 [833333.3 - 833333.3]	730555.6 [661527.8 - 797250]	*0,063*
	MS(swollen)230	6	222349.5 [191857 - 253499.2]	218833.3 [193683.3 - 254083.3]	*0,937*
	MS(PLL)170	6	508169.5 [495633 - 527437.3]	483555.6 [474027.8 - 498333.3]	*0,310*
Cells/sphere					
		12	156.22 [23.19 - 13776.52]	181.89 [17.13 - 14440.36]	*0,590*
Sphere type	US400	3	291.65 [290.15 - 301.43]	352.94 [348.14 - 354.11]	*0,100*
	US150	3	20.92 [20.04 - 21.85]	16.3 [15.25 - 16.75]	*0,100*
	US2300	3	54874.91 [54523.68 - 69746.17]	80118.02 [68406.81 - 92101.23]	*0,400*
	BaUS140	3	23.77 [23.55 - 23.78]	17.25 [17.08 - 18.85]	*0,100*

SM 2. Median experimental and theoretical values, with their interquartile range (Q3-Q1), and Mann-Whitney-Wilcoxon test results for spheres/V_S, cells/V_S and cells/sphere. Median experimental and theoretical values were compared first including all the data and later segmented by sphere type and, in case of spheres/V_S, also by volume. No statistically significant differences were detected in any case.

DISCUSSION

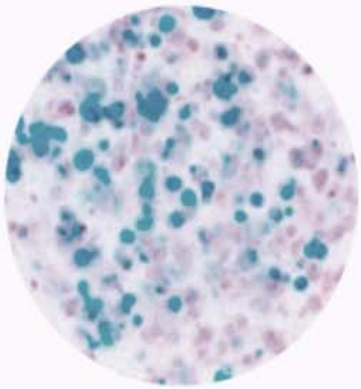

GENERAL DISCUSSION

Cell microencapsulation strategy is based on the immobilization of cells that produce therapeutic molecules in spherical particles between 100 and 1500 μm in diameter, approximately. These systems are capable of immobilizing and protecting living cells, selectively isolating them from their environment while they secrete the therapeutic molecules of interest **(Figure 1)**. The particles are elaborated with biocompatible materials and usually surrounded by a semi-permeable polymeric membrane that prevents the passage of high molecular weight molecules — antibodies and other components of the immune system —, protecting these cells from the host's immune response [1]. In addition, the microcapsule must exert a tight control over the bidirectional diffusion of molecules — entrance of nutrients and oxygen; and release of *de novo* synthesized therapeutic factors and metabolic subproducts —, and provide cells with a suitable environment to enhance and modulate their function. This technology also suppresses, or at least reduces, the chronic administration of immunosuppressive agents, thus avoiding some of the adverse events associated with organ and tissue transplantation [2].

Cell encapsulation systems have shown wide applicability in pathologies with very diverse characteristics, such as diabetes mellitus (DM), cancer, anemia, hemophilia B or pathologies of the central nervous system (CNS), among others [3]. They are especially convenient for pathologies in which maintaining a strict control over the release of the therapeutic molecule is essential.

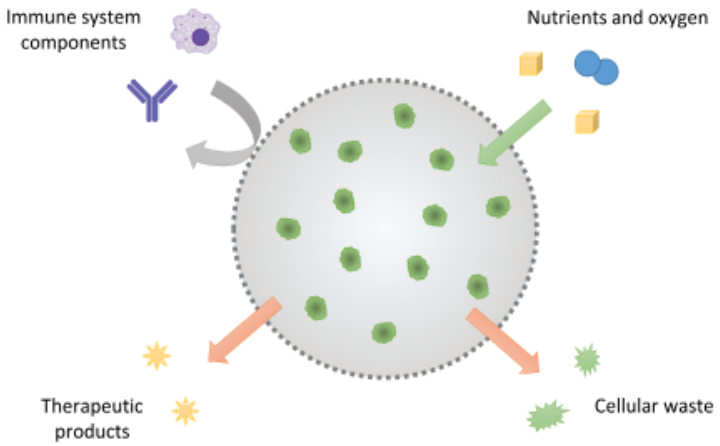

Figure 1. Cell microencapsulation technologies. The microcapsule must allow the bidirectional diffusion of nutrients and oxigen, cellular waste and therapeutic products, while protecting the encapsulated cells from the host immune response.

Among the natural (alginate, agarose, cellulose, etc.) and synthetic (polyethylene glycol (PEG), poly(lactic-co-glycolic acid) (PLGA), polyvinyl alcohol (PVA), etc.) polymers available for the elaboration of the microcapsules, alginate is by far the most widely used, due to its excellent biocompatibility and easy handling [4]. Alginate is a natural anionic polysaccharide that creates three-dimensional structures, going from sol to gel, when it reacts with divalent ions, such as, Ca^{+2} or Ba^{+2}.

In some cases, and depending on the application, the microbeads composed of different biomaterials and cells, are the final product to be administered. However, obtained pore size in most cases is too large and does not present a real barrier against the threats that the implant will face once implanted. Therefore, many groups coat these beads with different polymers to elaborate microcapsules that control the molecules and cells that can come into contact with the immobilized cells. For the elaboration of the semi-permeable membrane, different polymers have been used, such as chitosan, oligo-chitosan or poly(methylene-co-guanidine) (PMCG), but both in preclinical studies and in human trials, the most used molecules are poly-L-lysine (PLL) and poly-L-ornithine (PLO) [5-7].

Today, there is no consensus about which elaboration protocols are the most adequate and their use mainly depends on the preferences of the different research groups.

The results obtained in the various clinical trials carried out to date with this technology, make clear the advantages and potential applications of this promising technology [8-22]. However, there are still aspects that need to be improved so that cell microencapsulation systems can be applied routinely in clinical practice. For this reason, in the last years, researchers have directed efforts towards trying to solve some of the key aspects that still limit efficacy and biosafety, the two major criteria that must be satisfied to reach the clinical practice. Those two concepts are closely related to each other and must be carefully defined and regulated due to their implications regarding patient well-being.

On the one hand, when talking about efficacy of cell microencapsulation, biocompatibility is one of the most important aspects to be considered. It will

determine implant's viability, functionality and durability, becoming in many cases a limiting factor to succeed. The biocompatibility of the implant must be given in 2 directions **(Figure 2)**. From outside to inside, the materials used must protect the immobilized cells, avoiding direct toxicity or the blockage of nutrients and oxygen diffusion. From inside to outside, none of the system components — cells, biomaterials, crosslinking agents, etc. — or procedures used must be toxic for the patient or elicit an immune response in the host. When this occurs, the foreign body reaction can eventually isolate the implant within a fibrotic capsule, thereby preventing the access of essential molecules and leading to graft failure. In addition, the biocompatibility must last over time, since live cell therapies are normally used for long-term treatments [23].

Despite the undeniable improvement occurred in recent decades, the biomaterials and cells that are used today continue to produce, to a greater or lesser extent, an inflammatory response by the host, so searching for suitable components remains a priority. The final performance of the device will depend not only on the biomaterials and cells used, but also on the site of implant, the local application of immunosuppressive drugs, or even the size and shape of the implant.

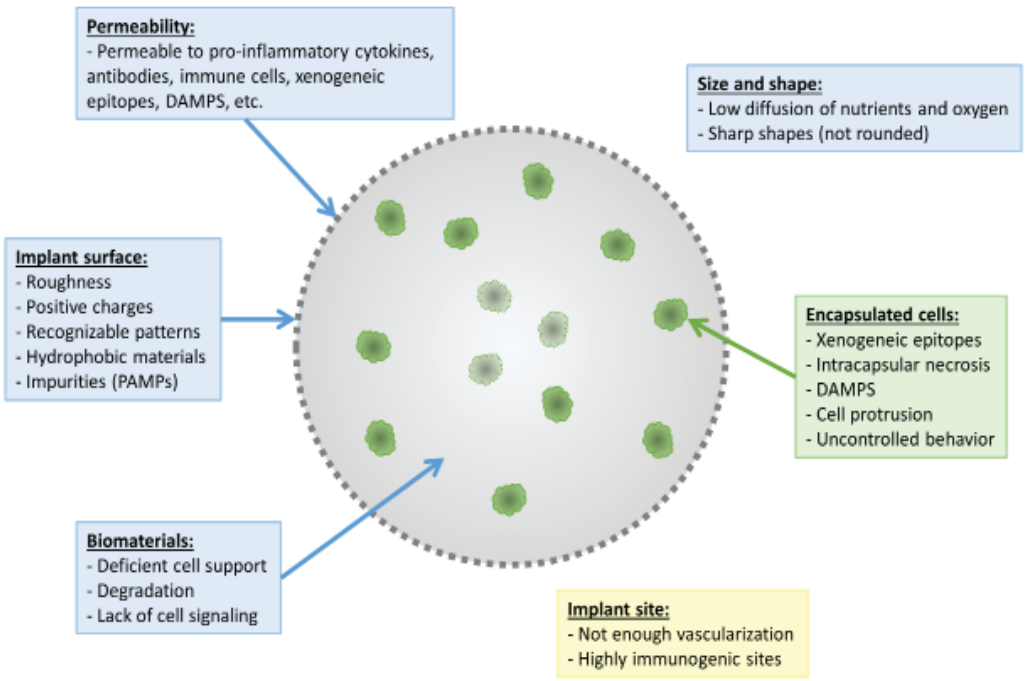

Figure 2. Factors that may compromise implant biocompatibility/biotolerability.

On the other hand, regarding implant biosafety, there are many aspects that should be controlled, especially when working with genetically modified cells. From the moment of implantation, the location of the cells, as well as their viability and secretion of the therapeutic molecule should be kept under control. Likewise, in cases where the duration of the treatment is limited, ideally the system should have an elimination mechanism that does not generate risks or toxic products for the patient [24]. The most advanced systems are also capable of responding in real time to the needs of the patient, secreting the therapeutic molecule of interest at specific time points [25,26]. However, one of the most basic and essential aspects to take into account is the determination of an appropriate dose for the patients and their pathologies. Controlling the therapeutic dose is crucial to avoid problems such as intoxication of the patient or inefficacy of the treatment, especially when working with narrow therapeutic index drugs.

The aim of this doctoral thesis was to address two of the most critical aspects, related to biocompatibility and biosafety, which still need to be optimized, before cell microencapsulation systems can be used routinely in clinical practice. In the first part, the behavior of D1 mesenchymal stromal cells (D1-MSCs) was analyzed, and more specifically the influence of cell load on parameters such as cell viability, proliferation and secretion of the therapeutic molecule, both *in vitro* and *in vivo*. The well-known hypoimmunogenic and immunomodulatory properties of these cells make them excellent candidates for this type of system [27-29].

In the second part, a complete and practical mathematical model was developed, which will allow us to dose the appropriate amount of encapsulated cells, measured by means of a volume of pelleted microparticles, for each specific case. To our knowledge, no similar dose control tool existed to date, despite its critical importance.

Part 1. The influence of different MSC-loads in cell microencapsulation technologies

In the last years, the advances in the field of stem cell use have unlocked an unthinkable potential to be applied in cell microencapsulation systems. Despite

the fact that the use of differentiated allogeneic cells is in many cases the simplest option and the use of xenogeneic cells is increasingly safe, the limited availability of the former and the greater tendency to generate immunological reactions of the latter pose clear disadvantages.

The ability to differentiate human stem cells, from different sources, to obtain the desired cell type or the possibility of reprogramming adult cells to induced pluripotent stem cells (iPSCs) [30,31] have defined the path to a sufficient source of human cells.

In this vein, MSCs can be extracted from adult individuals and have the ability to differentiate into various cell types such as chondrocytes, osteocytes or adipocytes, among others. They have demonstrated to be very convenient for their use in cell encapsulation systems due to their hypoimmunogenic (due to the lack in expression of mayor histocompatibility complex (MHC) class II and most of the classical costimulatory molecules [32,33]) and immunomodulatory characteristics [27-29], that positively influence the biocompatibility of the system. The occurrence of MSCs-mediated immunosuppression occurs via cell-cell contact, but also by the production of extracellular vesicles, including exosomes, and a multitude of cytokines and growth factors, that also induce the endogenous repair mechanisms of the surrounding tissues [34-38].

In recent studies conducted by our group, efforts have focused on analyzing the behavior of immortalized MSCs, genetically modified to secrete erythropoietin (EPO), for the treatment of anemia [39-42]. In addition, their benefits have also been evaluated in hepatic pathologies [43,44], as an alternative to porcine hepatocytes [45,46]. Moreover, MSCs not only are a very interesting option as a secretory cell [39,41], but also as a co-encapsulated auxiliary cell [47-50].

The combination of MSCs with biomaterials such as alginate offers the possibility of modifying some of their differentiation characteristics to suit the desired therapeutic goal [51-54]. However, sustained release systems based on the combination of MSCs with non-degradable materials are also showing promising results. MSCs can be used for their natural secretome or as genetically modified cells to secrete the therapeutic molecule of interest [55-58]. Surprisingly, cell lines,

such as D1-MSCs, are not commonly studied, even if they present some clear advantages over primary cells when designing this type of sustained release systems [39,40,59,60].

The choice of a cell that presents suitable properties for its use in this type of systems is critical but, once selected, it is also essential to recreate the optimal conditions for it within the microcapsule since, as a living organism, the environment to which they are exposed may vary their behavior substantially. In this regard, factors such as cell-cell (through direct contact or via soluble factors) and/or cell-material interactions play a critical role. The selected cell load is a key point for both types of interactions, as it increases or decreases them, based on the chosen cell/material ratio. Likewise, the ratio can affect the diffusion of nutrients, waste, oxygen or therapeutic products.

In this first part, we genetically modified D1-MSCs to secrete EPO and encapsulated them in 3D alginate-PLL microcapsules with different cell loads ($2*10^6$, $5*10^6$, $10*10^6$ and $20*10^6$ cells/mL; CL2, CL5, CL10 and CL20, respectively), in order to analyze the influence of cell density for this type of cell in microencapsulation systems. The viability, metabolism, proliferation and EPO secretion of microencapsulated D1-MSCs were first evaluated *in vitro* and then microcapsules were implanted in an allogenic mouse model to assess the differences caused by the enriched environment found *in vivo* **(Figure 3)**.

Behavior of encapsulated cells was tested first *in vitro*, at days 0, 15, 30 and 45, when cell viability and metabolism and EPO secretion tests were performed. Cellular metabolism and production of EPO **(Figure 4A and 4B)** resulted in a general upward trend for all groups that showed steeper slopes in the lower cell load groups and remained practically constant in the CL20 group. In groups of lower cell loads, cell viability tests **(Figure 4C)** showed greater numbers of live cells in more advanced points of the study. The viability percentages for the CL20 group, however, were constant until the end of the study, which is consistent with the results obtained in the other two tests. Good cell viability and no cell aggregates were also confirmed by fluorescence microscopy **(Figure 4E)**. Taking into account these results, it seems that the CL2 group did increase the levels of cellular metabolism and production of

the therapeutic molecule, probably due to a decrease in the percentage of cell death during the study. In contrast, in the CL20 group, levels of proliferation and cell death seemed to keep a balance of constant renewal.

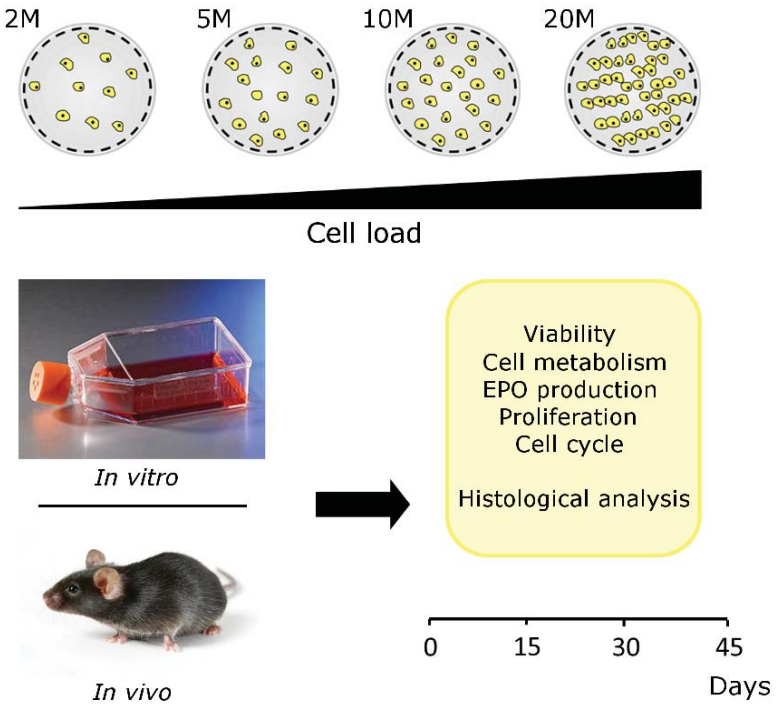

Figure 3. Schematic illustration of the main design of the study. For 45 days, 4 different groups of microcapsules (CL2, CL5, CL10 and CL20) were tested, both *in vitro* and *in vivo*, for cell viability, metabolism, proliferation, cell cycle and EPO secretion. Histological analyses were also performed in order to confirm the results obtained in other tests.

In view of these first *in vitro* results, we concluded that higher cell loads could result more appropriate for sustained release systems based on the immobilization of cells, in order to achieve a more constant release of the therapeutic factor. Probably, with higher cell loads, the arrest of cell proliferation is related to more inhibitory cell-cell interactions [61] and a reduced access to nutrients [62].

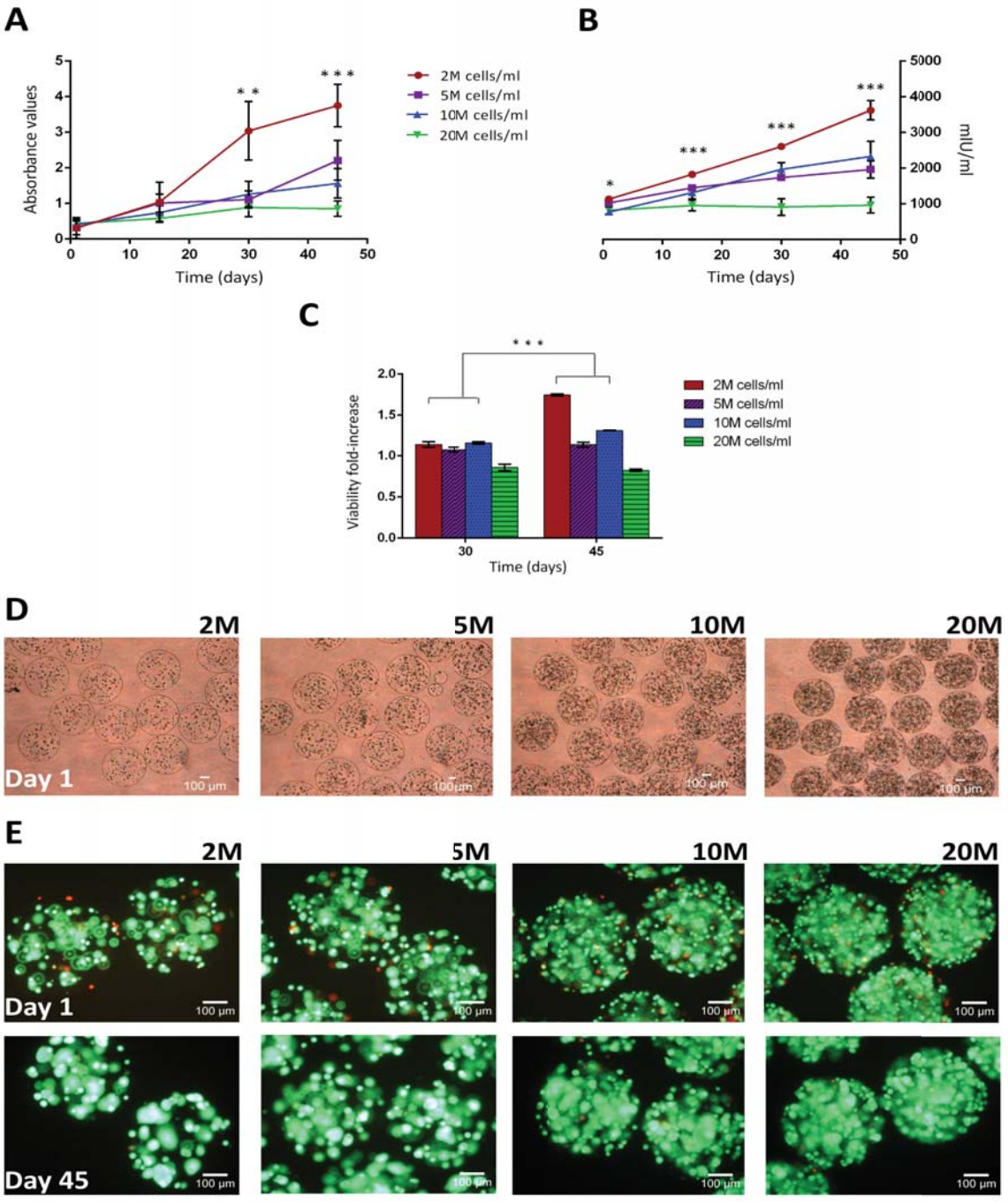

Figure 4. Results obtained for *in vitro* studies. Cell metabolism **(A)** and EPO secretion **(B)** at days 1, 15, 30 and 45. Statistical differences (ANOVA) between CL2 and CL20 are described in the graphs. For cell metabolism assay, results were divided by the number of cells per group in order to make them comparable. For the ELISA assay, a different number of microcapsules was used for each group, with the same final number of cells in all cases. EPO secretion graph represents EPO mlU in a mL of the collected supernatant, for each group (different number of microcapsules, same number of cells). Cell viability **(C)** at days 30 and 45. The percentage of living cells obtained for day 0 was considered as 100% in each microcapsule group, and all values were expressed in function of this percentage. Statistical analysis (T-Test) showed differences between days 30 and 45 for CL2 and CL10 (***). For all the graphs, bar graphs symbolize the mean ± SD. Statistical significance *$p < 0.05$, **$p < 0.01$, and ***$p < 0.001$. **D** Microcapsule morphology at day 1. **E** Fluorescence micrographs with LIVE/DEAD staining of the entrapped cells within the APA microcapsules at days 1 and 45.

However, *in vivo* study results showed a completely different scenario. Assays in cell metabolism **(Figure 5A)** and EPO-secretion **(Figure 5B)**, at days 0, 15, 30 and 45, showed a general upward trend in the early phases of the study but, in both graphs, perhaps the most remarkable feature was the turning point that was documented around day 30, in which most groups seemed to reach a maximum point after which all values decreased. The only group that did not follow this trend was CL2, which remained more or less constant in the case of cellular metabolism and even increased the secretion of EPO. Cell viability assay showed increasing cell death values throughout the study **(Figure 5C)** for all groups, except CL2. Taking into account all this information, it seemed that the total number of cells in all groups increased until the end, rising the values for cell metabolism and EPO secretion at first and producing the accumulation of dead cells inside the capsule in the end of the study, when all the values dropped down. CL2 group was the only exception, in which the percentages of living cells increased until the last moment.

Notably, images obtained by fluorescence microscopy with calcein-ethidium **(Figure 5E)** showed cell aggregates in all groups at the end of the study, but especially in CL20. This fact made us assume the appearance of necrosis in the inner part of the microcapsules, which would explain the final decrease in all the parameters.

Given that all tests led us to draw the levels of proliferation as the main difference between the in vitro and *in vivo*, we decided to analyze this parameter in a more exhaustive way. We analyzed, for all groups at day 30, existing patterns of proliferation within the microcapsules, both by cell cycle analysis (DNA staining) and bromodeoxyuridine (BrdU) uptake. The cytometry results showed, *in vitro*, a remarkable population of cells that had a double copy of their DNA but which nevertheless had not completed the cell division in the last 48 hours, which seemed to indicate some kind of arrest of the cell cycle in M/G_2, perhaps by insufficient cell signaling, lack of space inside the microcapsule and/or error detection in G_2 to mitosis checkpoint [63]. *In vivo,* however, this population barely existed but the one corresponding to cells that had completed the full cell cycle in the past 48 hours gained importance, with the incorporation of the BrdU molecule during the synthesis of new DNA and a single copy of their genetic material.

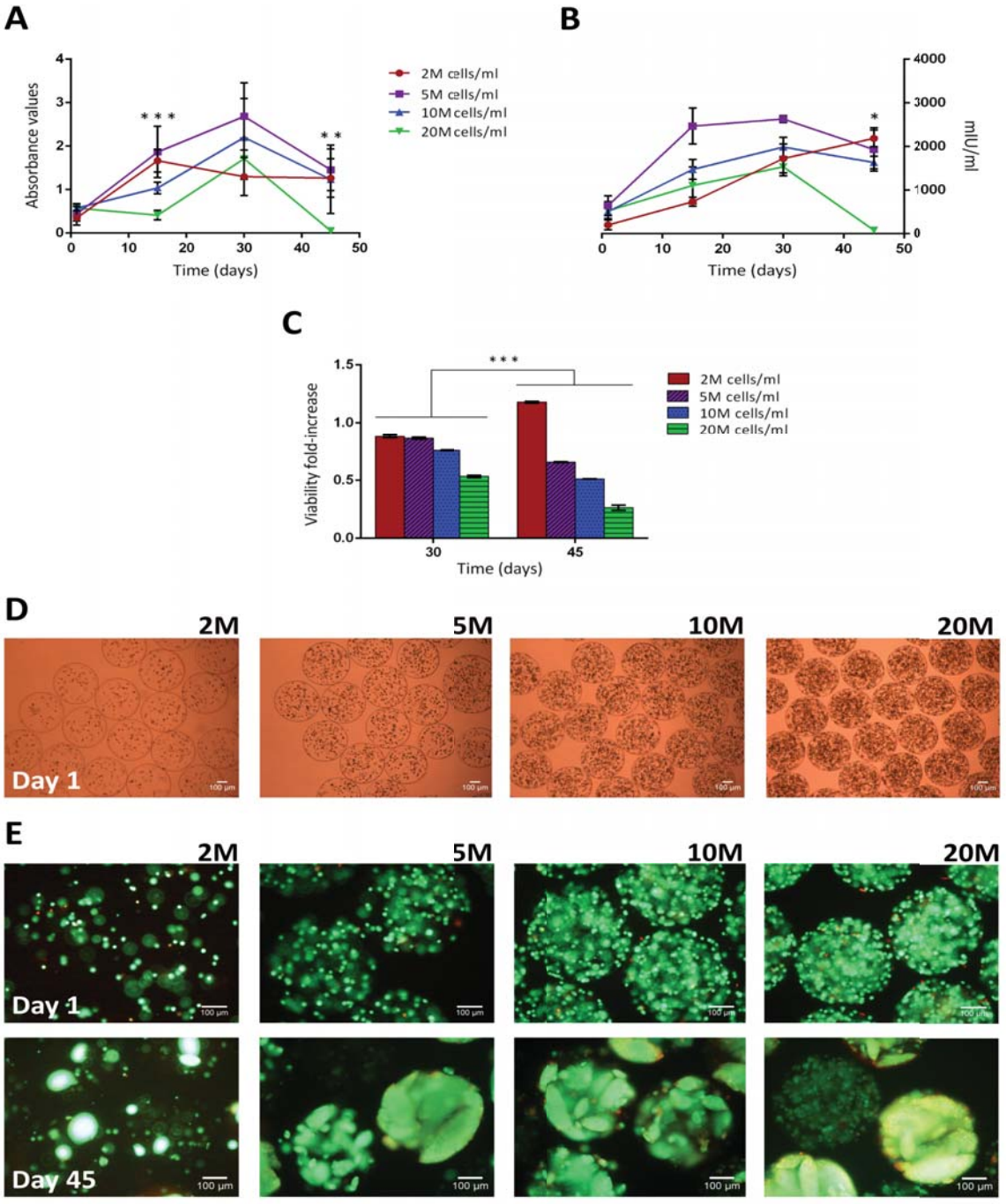

Figure 5. Results obtained for *in vivo* studies. Cell metabolism **(A)** and EPO secretion **(B)** at days 1, 15, 30 and 45. Statistical differences (ANOVA) between CL2 and CL20 are described in the graphs. For cell metabolism assay, results were divided by the number of cells per group in order to make them comparable. For the ELISA assay, a different number of microcapsules was used for each group, with the same final number of cells in all cases. EPO secretion graph represents EPO mlU in a mL of the collected supernatant, for each group (different number of microcapsules, same number of cells). Cell viability **(C)** at days 30 and 45. The percentage of living cells obtained for day 0 was considered as 100% in each microcapsule group, and all values were expressed in function of this percentage. Statistical analysis (T-Test) showed differences between days 30 and 45 for all groups. For all the graphs, bar graphs symbolize the mean ± SD. Statistical significance *$p < 0.05$, **$p < 0.01$, and ***$p < 0.001$. **D** Microcapsule morphology at day 1. **E** Fluorescence micrographs with LIVE/DEAD staining of the entrapped cells within the APA microcapsules at days 1 and 45.

When the number of cells in those populations obtained for BrdU uptake and cell cycle were compared **(Figures 6A and 6B)**, significant statistical differences between *in vitro* and *in vivo* results, but not between the groups, were found. It seems that proliferation patterns remain constant regardless of the number of encapsulated cells.

It is possible that the enriched environment in which the implanted cells were placed, would have enhanced this rapid cell proliferation [64]. In the other hand, pH and osmolarity changes microcapsules faced *in vivo* could affect the physicochemical characteristics of the nucleus of the capsules, leading to a softer alginate matrix which has a direct impact in cell behavior [65].

With the intention of corroborating what had been observed in these analyses, another study was performed by immunohistochemistry, where levels of Ki-67 (a cell proliferation marker) were assessed; both *in vitro* and *in vivo* **(Figure 7A)**. *In vitro*, cell proliferation percentages were maintained around 10% for all groups, while the levels for the *in vivo* study, reached values of 50%, causing the appearance of central necrosis in many of the microcapsules **(Figure 7B)**.

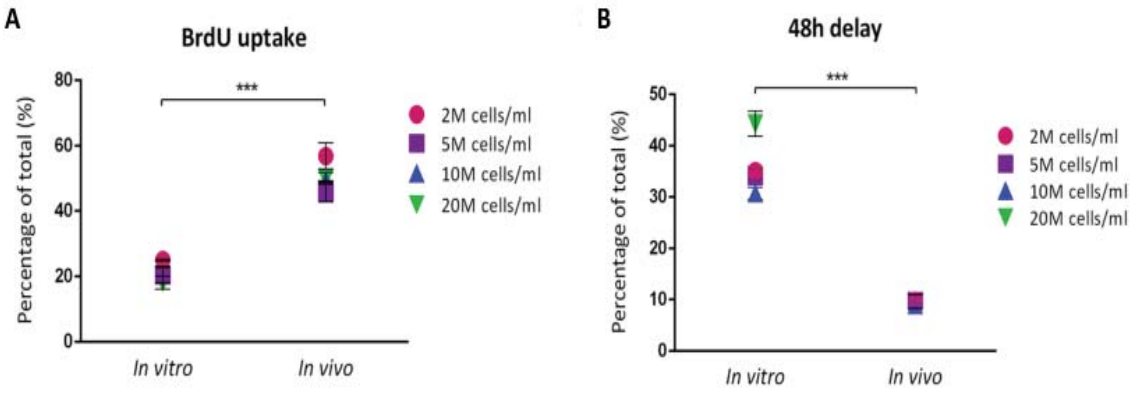

Figure 6. Comparison between *in vitro* and *in vivo* cell proliferation behavior. The number of cells positive for BrdU **(A)** was higher in the *in vivo* for all groups (***) (Mann-Whitney U test) while the population of cells in M/G2 phases without incorporation of BrdU in the last 48 h (48 h delay in cell cycle) **(B)** was higher *in vitro* for all groups (***) (Mann-Whitney U test). There were no statistical differences between cell load groups in neither cases (ANOVA). Bar graphs symbolize the mean ± SD. Statistical significance *$p < 0.05$, **$p < 0.01$, and ***$p < 0.001$.

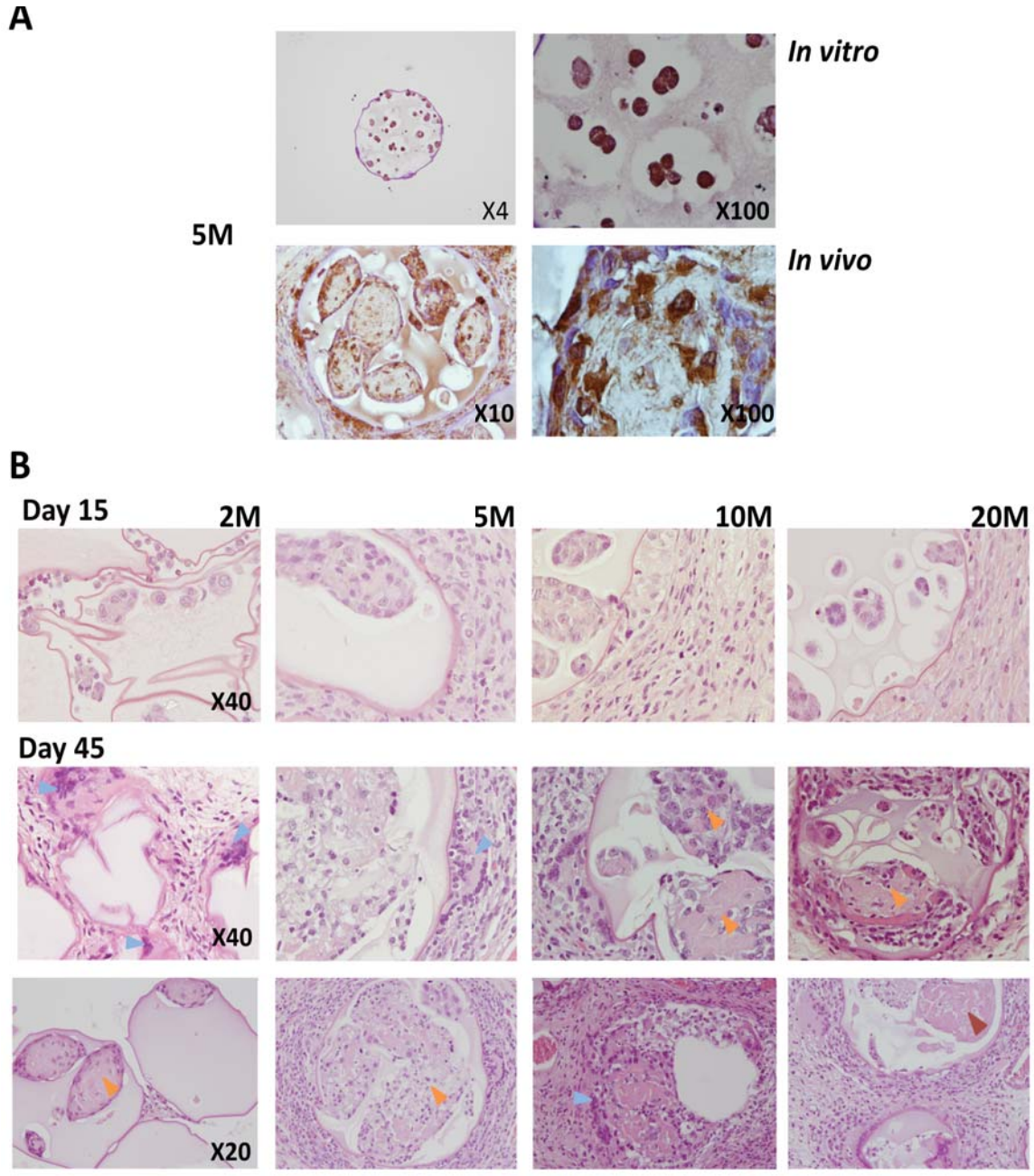

Figure 7. Histological analysis of the microcapsules and their environment. A Ki-67 staining of both *in vitro* and *in vivo* microcapsules. An example of the proliferation behavior of the same cell load (CL5) shows evident differences between the 2 situations. **B** Hematoxylin and eosin staining of *in vivo* explants, at days 15 and 45. Arrows show: in blue, multinucleated histiocytes around the microcapsules; in orange, high proliferation areas and in red, intramicrocapsular necrosis.

In the observation of the surrounding tissue of the explants *in vivo*, we detected signs of foreign body response against the implant [66], with an initial acute phase characterized by infiltration of neutrophils and eosinophils, followed by the appearance of multinucleated histiocytes and the development of granulomas in some cases. The immunomodulatory capacity of these cells is widely described [38,67],

also in previous studies carried out with MSCs enclosed in similar encapsulation devices [27,44,68], but in this case, the high proliferation rates observed and the presence of necrosis from an early point of the *in vivo* study probably altered the normal properties of these cells and produce a higher release of proinflammatory molecules, such as damage-associated molecular patterns (DAMPs) (cytosolic proteins, pieces of genetic material etc.), from the implant to the environment, which are described to trigger substantially the host immune response [69-72].

At the end of the study, it was possible to detect some morphological changes in some of the encapsulated cells, to simple flat or cubic morphologies in the CL20 group *in vitro*, and to what seemed chondroblastic morphology *in vivo*. In this sense, it is interesting to highlight that differentiation phenomena and the resulting morphologies vary dramatically depending on the environment in which the cells are found. In this regard, there is some controversy over the degree of differentiation that usually occurs in this type of implant and its consequences [39,73]. For these EPO secreting D1-MSC, our group published a full study about their differentiation behavior both *in vitro*, being exposed to differentiation mediums, and subcutaneously implanted *in vivo* and how this affects their capacity to secrete EPO [39]. The results showed these cells were able to differentiate inside the microcapsules, *in vitro*, towards specific lineages, when exposed to different culture mediums, while maintaining their capacity to secrete EPO. After 30 days *in vivo*, however, the phenotype of MSCs (CD29+, CD44+, CD45−, CD73+, CD105+, SCA-I+) was preserved in all conditions assayed. We could expect a similar behavior in this study as the same cells were exposed to the same conditions, thus probably the morphological changes observed in the histological analysis would correspond with early stages of differentiation in a reduced group of cells.

As this study clearly pointed out the excessive proliferation observed *in vivo* as the main problem that needed to be solved when working with D1-MSCs, our group conducted later a complete new analysis of how cell behavior can be controlled changing the properties of the matrix of the microcapsules [42]. In this case, two types of osmolarity adjusting agents were chosen for the solutions normally used for the elaboration of the microcapsules. The first set of solutions were elaborated with

175

mannitol (technological set of solutions), like the ones in this doctoral thesis, which can be considered as an inert osmolality adjusting agent, and the second one with electrolytes such as potassium, calcium or phosphates (biological set of solutions). Data showed that these agents interact in the capsule formation process, influencing the alginate crosslinking degree and generating microcapsules with different mechanical properties that influence cell behavior. When technological solutions were employed, microcapsules presented a more permissive matrix, allowing the formation of cell-aggregates that presented necrotic cores, similar to the ones observed in this thesis. Conversely, the use of electrolyte osmolarity adjusting agents, including calcium or sodium, provided the capsule with a suitable crosslinking degree that established a tight control over cell proliferation and enabled an adequate therapeutic regimen *in vivo.*

Therefore, in the view of these results, we concluded that the enriched environment found *in vivo*, led to much higher proliferation rates and the rapid increase of the cell load in all groups, but especially in those with higher cell densities. This situation led to the accumulation of dead cells within the microcapsules and the central necrosis phenomenon, especially in the groups of higher cell loads, probably caused by lack of nutrients, oxygen and space for the innermost cells. The CL2 group was the only one that did not maintain this trend and this could be due to the low initial cell load that left more space for cell growth. In order to better understand the influence of different cell loads on the behavior of the encapsulated D1-MSCs we believe that it would be interesting to analyze it again with a more tight control over cell proliferation, for example using different osmolarity adjusting agents, since the excessive proliferation observed in this study makes it difficult to detect all the differences between the groups.

Part 2. Mathematical modeling for accurate dose control in drug/cell delivery systems

In the second part of this doctoral thesis, we approached another fundamental aspect, related to implant biosafety, that needs to be improved in cell microencapsulation technologies: dose control.

When hydrogel spherical microparticles are used as part of biotechnological systems, the number of spheres contained in a defined pelleted volume is directly related to the dose administered to the patients. However, this relationship usually is not a straightforward deduction, especially when the active ingredients are not the spheres themselves, but a molecule encapsulated into the hydrogel or synthetized by entrapped cells. The physical-mechanical properties of the spheres or the shape and size of the container we use to measure the volume, among others, are determinant variables that influence the administered dose.

Despite the complexity involved, dose control is a critical factor that must be defined in order to ensure safe and effective treatments. Therefore, particulate systems require as powerful as user-friendly tools that allow researchers to calculate the number of spherical hydrogel microparticles in a given volume, and going a step further, the quantity of drug or cells immobilized in that volume of particles. Dosing based in standard volume units is sometimes the only acceptable option and in other cases, it could substantially reduce the cost and difficulty of product application and dosing errors that could result from a more complex counting system.

The objective of this work was to present a useful mathematical model as a simple and practical way of making calculations for different hydrogel-based monodisperse spherical microparticles. The case of cell microencapsulation systems was used as the example to explain the equations but the model could be applied in any other particulate systems where the described parameters can be obtained. In order to confirm the adequacy and usefulness of the mathematical model, we conducted several experiments, testing the most common elaboration protocols for cell microencapsulation systems.

The mathematical model only takes into account end-point measurements, shared generally by hydrogel spherical microparticles, loaded or not with drugs or cells, making it possible to obtain accurate results in very different situations. First of all, we defined the concepts of “unmodified spheres” (USs) as the newly formed spheres, and “modified spheres” (MSs), as spheres with any kind of after-formation elaboration steps, such as, volume changing exposure to different media or functional coatings **(Figure 8)**. It is important to note that these secondary steps do not change

the initial cell or drug load per sphere, just the final volume and maybe the physical-mechanical characteristics of the microparticles.

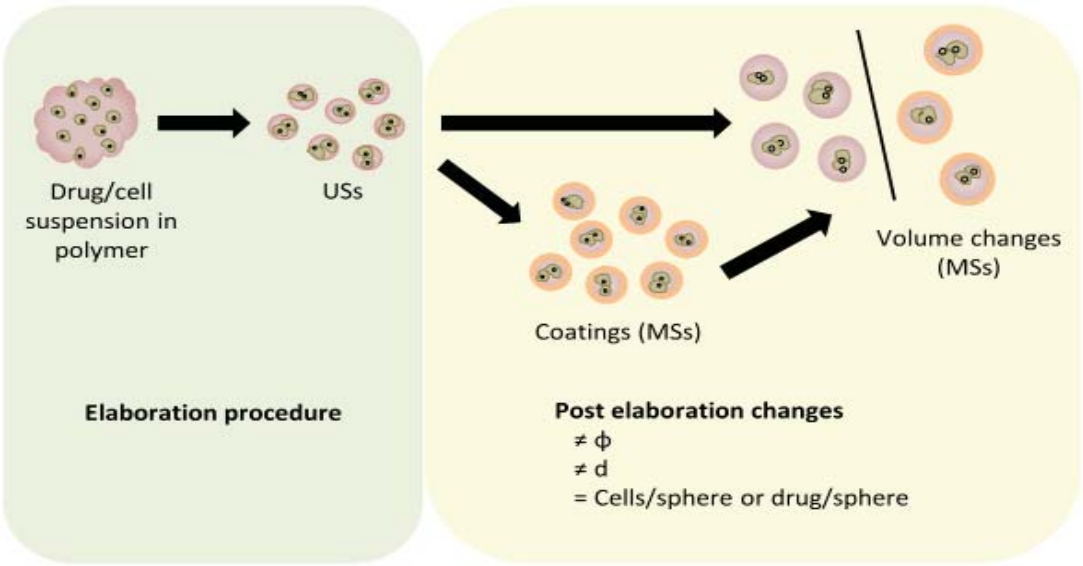

Figure 8. General scheme of hydrogel microparticle elaboration steps and the main final and intermediate products. USs: Unmodified spheres (without post-elaboration modifications); MSs: modified spheres (after coatings or volume changes); ϕ: packing fraction; d: diameter.

Taking into account these end point products, we designated a minimum number of parameters that would include all the possible variables and would lead us to confidently establish a relationship between a quantity of drug (or number of cells in this case), a number of particles and the volume occupied by them **(Figure 9A)**:

- Initial cell or drug load **(L)**: The mass of drug or the number of cells included in 1 m3 of polymer volume (kg/m^3 or n/m^3).

- $\mathbf{V_p/V_s}$: The ratio between a volume of drug or cell suspension in a polymer (pre-spheres volume, $\mathbf{V_p}$) and the volume occupied by the pelleted USs formed with that volume of mixture (pelleted sphere volume, $\mathbf{V_s}$) (no units).

- $\mathbf{d_0}$: Diameter of USs (m).

- $\mathbf{d_1}$**:** Diameter of MSs (m), after all the elaborations steps (including coatings or volume changes after exposure to different media).

- $\boldsymbol{\phi_0}$: Packing fraction in USs pellets (no units).

- $\boldsymbol{\phi_1}$: Packing fraction in MSs pellets (no units).

Taking into account the selection and definition of the parameters needed to describe the elaboration process, it was possible to create mathematical equations to define the number of spheres in a pelleted volume of spheres (spheres/V_S), the quantity of drug or the number of cells in a single sphere (drug/sphere or cells/sphere) and the quantity of drug or the number of cells in a volume of pelleted spheres (drug/V_S or cells/V_S) **(Figure 9B)**.

The model can be used in every case were the described six variables can be calculated, regardless of the elaboration protocol. L is usually chosen, based on the needs of the faced application. The V_p/V_S ratio is normally easy to measure, letting the microparticles elaborated with a known volume of polymer solution settle down into a graduated container. Finally, just a microcospe is needed for measuring both the d_0 and the d_1. Probably, ϕ_0 and ϕ_1 are the most difficult ones to be exactly calculated but the possible results oscillate in a very narrow range of values when working with hydrogels and, in this work, we estimated those values based on hydrogel sphere arrangement simulations, making them applicable in a wide range of situations.

The simulations were performed in MATLAB® and, in order to make them as applicable as possible, different microsphere sizes, numbers and densities were tested in habitually used container shape and sizes (1.5 mL Eppendorf tube and 15 mL Corning tube). The obtained results **(Figure 10)** allowed us to predict the ϕ_0 and ϕ_1 values of different hydrogel sphere pellets.

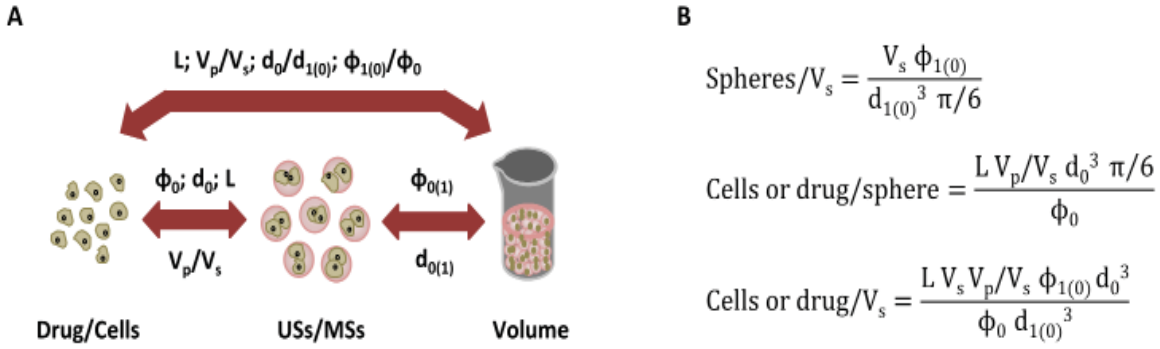

Figure 9. Mathematical model definition. A. Parameter relationship between a quantity of drug or cells, a number of microspheres and the volume occupied by them. **B.** Mathematical formulas for spheres/V_S, cells or drug/sphere and cells or drug/V_S. ϕ_0=Packing fraction of the unmodified spheres (USs); ϕ_1=Packing fraction of the modified spheres (MSs); L=initial drug/cell load (cells or drug in 1m^3 of polymer); d_0= Diameter of the USs; d_1= Final diameter of the MSs; V_p/V_S= The ratio between a volume of drug/cell suspension in a polymer and the volume occupied by the USs formed with that volume of mixture; V_S= Volume of spheres. All the units are in SI (diameters in m and volume in m^3).

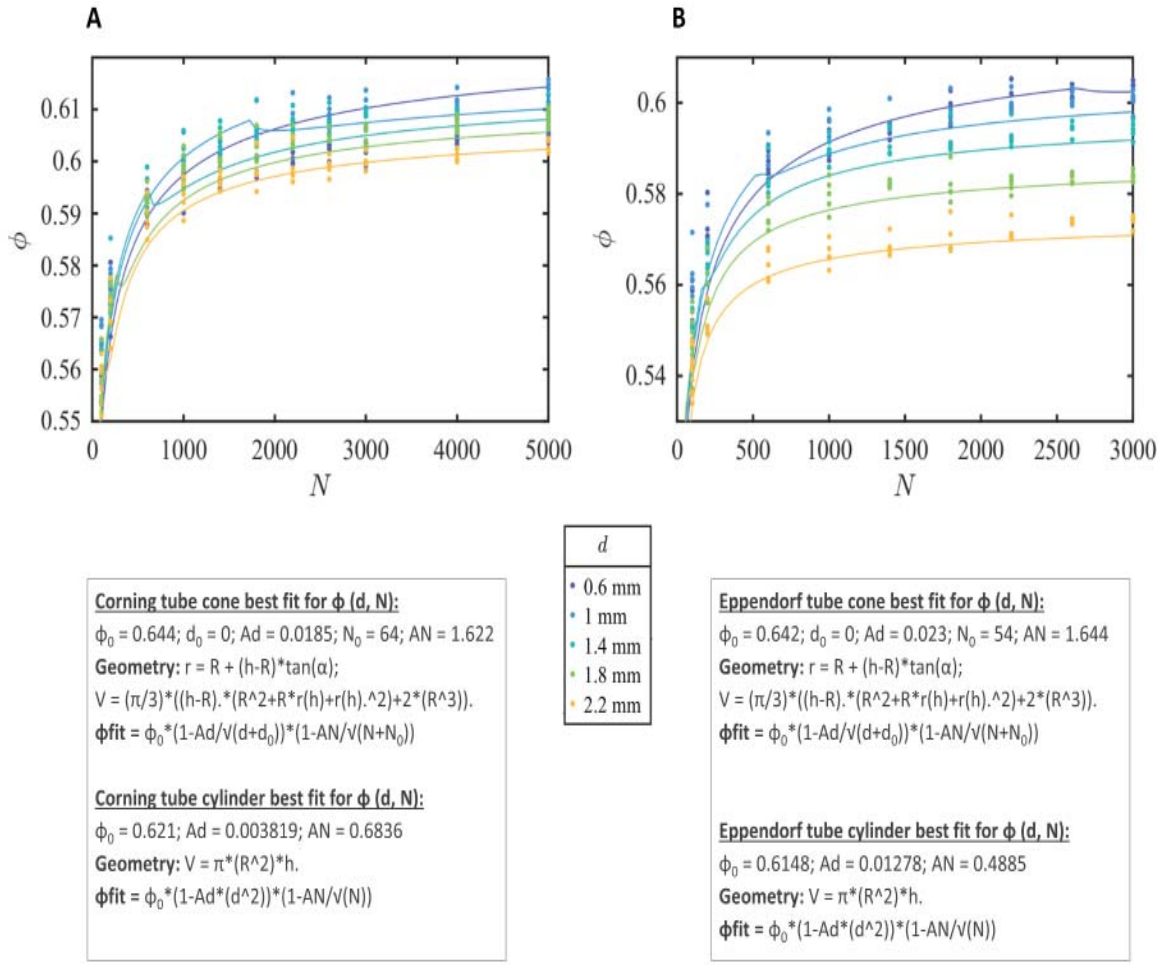

Figure 10. Results for computational simulations. Results for computational simulations in 15 mL Corning tubes **(A)** and 1.5mL Eppendorf tubes **(B)**. Graph shows the results obtained for the packing fraction of a pelleted number of spheres, for different diameter sizes. The best fit functions for both the conical and cylindrical parts of the tube and the mathematical equation for the calculation of V in function of h are also described below. The best fit function represented on the graph is a combination of both tube parts (cone and cylinder).

For the 15 mL Corning tube, the packing fraction appeared to be around 0.61 in all cases tested, with slightly smaller values for the spheres of smaller diameters, as long as N>1000. In case of the 1.5 mL Eppendorf tube, the reported packing fraction values seemed to vary depending on the diameter size of the spheres. The biggest spheres, with diameters around 2.2 mm showed packing fraction values of not even 0.57, while spheres of 0.2 mm formed pellets of packing fraction values higher than 0.60. Thus, packing fraction values did not seem to strongly depend on sphere diameter sizes, until they get bigger enough and approach the diameter of the container. In both cases, in Corning and Eppendorf tubes, the packing fraction

values observed for N<1000 represent the range were the number of spheres is still not enough to form a proper sediment and the spheres pack in the conical part of the containers, where the particles are expected to arrange differently.

No significant deformation of the spheres was expected mainly due to the importance of the buoyant force in neutralizing the effects of gravity [74]. At this "jamming transition point" of deformable frictionless spheres, the packing fraction reaches values which have been associated with the random close packing (RCP) [75] (generally accepted to be around 0.635 [76-78]) when the number of spheres is high enough. Therefore, in case of the 15 mL Corning tube, the obtained values around 0.61 totally agreed with the expected results for deformable spheres contained into a fluid of similar density.

The packing fraction is also influenced by the size distribution, the shape of the container and the size of the spheres relative to the size of the container, being the latter the most determinant. High sphere to container diameter ratios generate abnormal sphere arrangements due to the lack of space, while smaller ratios of 0.06 or less [79], tend to standard packing fraction values, with different arrangements next to the container walls (the wall effect [80,81]). The geometry of the container does influence the results to some degree, but the effect is weak as long as the particles are small relative to the diameter of the container and the number of particles is relatively large. In case of the Eppendorf tube geometry, the influence of the sphere diameter size, relative to the diameter of the container, could be clearly appreciated on the graphs.

For all simulations, a 5% polydispersity in particle size was included in order to make the results more realistic and applicable to experimentally obtained batches of microspheres. For particle elaboration procedures generating high size variability between same-batch particles, we would probably find notable changes in packing fraction values, as higher differences between the largest and the smallest sphere sizes result in higher packing fraction values, up to a maximum, where values higher than 0.8 can be observed [82].

In the simulations, we decided to consider as negligible the possible electrostatic interactions between the spheres, or the spheres and the container walls,

and the roughness of the sphere surface. Being microparticles surrounded by a fluid, which usually contains different electrolytes and charged molecules [83] and taking into account that the materials used for the containers are usually inert and smooth, the effect of these variables are commonly not strong enough to significantly influence the final packing fraction values.

Finally, for the validation of the mathematical model, a representative sample of the most used cell microencapsulation technologies was chosen **(Figure 11):**

- **US400** and **US150**: Ca^{+2}-alginate USs of two different sizes (~ 400 μm (d_0) and ~ 150 μm (d_0)). Alginate beads were elaborated dripping a $5*10^6$ cells/mL alginate solution into a $CaCl_2$ bath that gels the alginate in just a few minutes.

- **MS(swollen)550** and **MS(swollen)230**: Ca^{+2}-alginate MSs of two sizes (~ 550 μm (d_1) and ~ 230 μm (d_1)).Some of the alginate US400 and US150 spheres were exposed for 30 seconds to a chelating solution in order to change the diameter and the mechanical properties of the beads.

- **MS(PLL)480**, **MS(PLL)170** and **MS(PLO)450**: Ca^{+2}-alginate-PLL MCs of 2 sizes (~ 480 μm (d_1) and ~ 170 μm (d_1)) and Ca^{+2}-alginate-PLO microcapsules (MCs) of ~ 450 μm (d_1). After the elaboration of the alginate USs, two different coatings were performed, with PLL or PLO in order to elaborate MCs. In both cases, a second coating of alginate was added on top of the other.

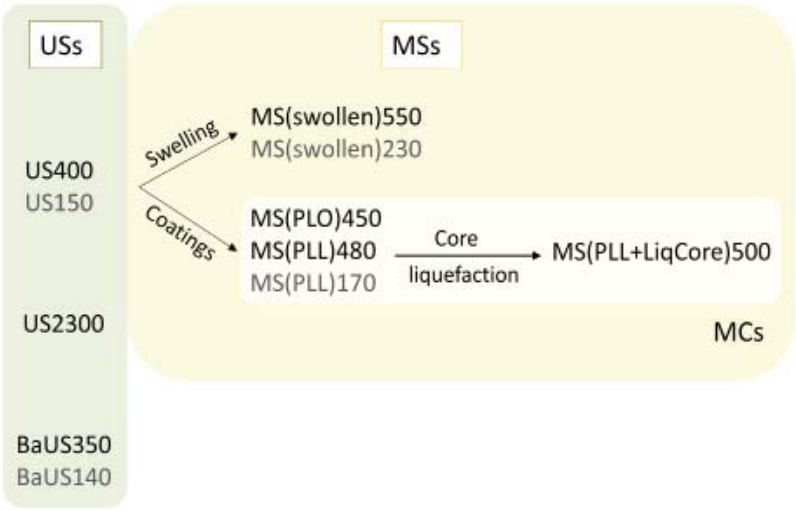

Figure 11. Scheme of selected unmodified sphere (USs) and modified sphere (MSs) types, including microcapsules (MCs), for validation of the mathematical model.

- **MS(PLL+LiqCore)500**: Ca^{+2}-alginate-PLL liquefied-core MCs of ~ 500 μm (d_1). For core liquefaction, some MS(PLL)480 were suspended, for 1 min, in a 1% citrate solution.

- **BaUS350** and **BaUS140**: Ba^{+2}-alginate USs of 2 sizes (~ 350 μm (d_0) and ~ 140 μm (d_0)). The exact same procedure used for the elaboration of US400 and US150 was followed but changing the $CaCl_2$ solution for a 50 mM $BaCl_2$ solution. The sizes of the USs crosslinked with barium are usually smaller when all the parameters are maintained constant as the barium shows higher affinity for the alginate chains and the process associated to the crosslinking of the alginate shows higher loses of water [84].

- **US2300**: Ca+2-alginate USs of a larger size (~ 2300 μm (d_0)). In order to force the limits of the model, this one last group was included in the validation, even if they cannot be considered microparticles due to their size. The elaboration procedure was the one used for the normal alginate USs but, in this case, the pre-gelled alginate solution was extruded through a needle of larger diameter and without electrostatic cutting of the solution to make the beads larger (the formation of the drops was only dependent on the gravity force).

First, all the batches were elaborated. For every batch, the number of cells/sphere, spheres/V_S and cells/V_S were experimentally determined (experimental values). In parallel, the V_p/V_S ratio and the d_0 and d_1 diameter values were measured. These values and the ϕ_0 and ϕ_1 ones predicted from the simulations were substituted into the formulas for the calculation of the theoretical values for cells/sphere, spheres/V_S and cells/V_S. The adequacy of the mathematical model and its ability to predict the experimentally obtained values was evaluated by comparing the experimental and theoretical results **(Figure 12)**.

No significant statistical differences were detected between the theoretical and experimental median values for spheres/V_S (where V_S = 100 μL, 500 μL, 1000 μL and 1500 μL) **(Figure 13)**, cells/V_S **(Figure 14A)**, cells/sphere **(Figure 14B)**.

In order to check the linear correlation between the theoretical and experimental results obtained for spheres/V_S, cells/V_S and cells/sphere, Pearson correlation coefficients were analyzed. The coefficients were close to 1 in all cases ($p<0.001$),

proving a positive strong correlation between theoretical and experimental data **(Figure 15)**.

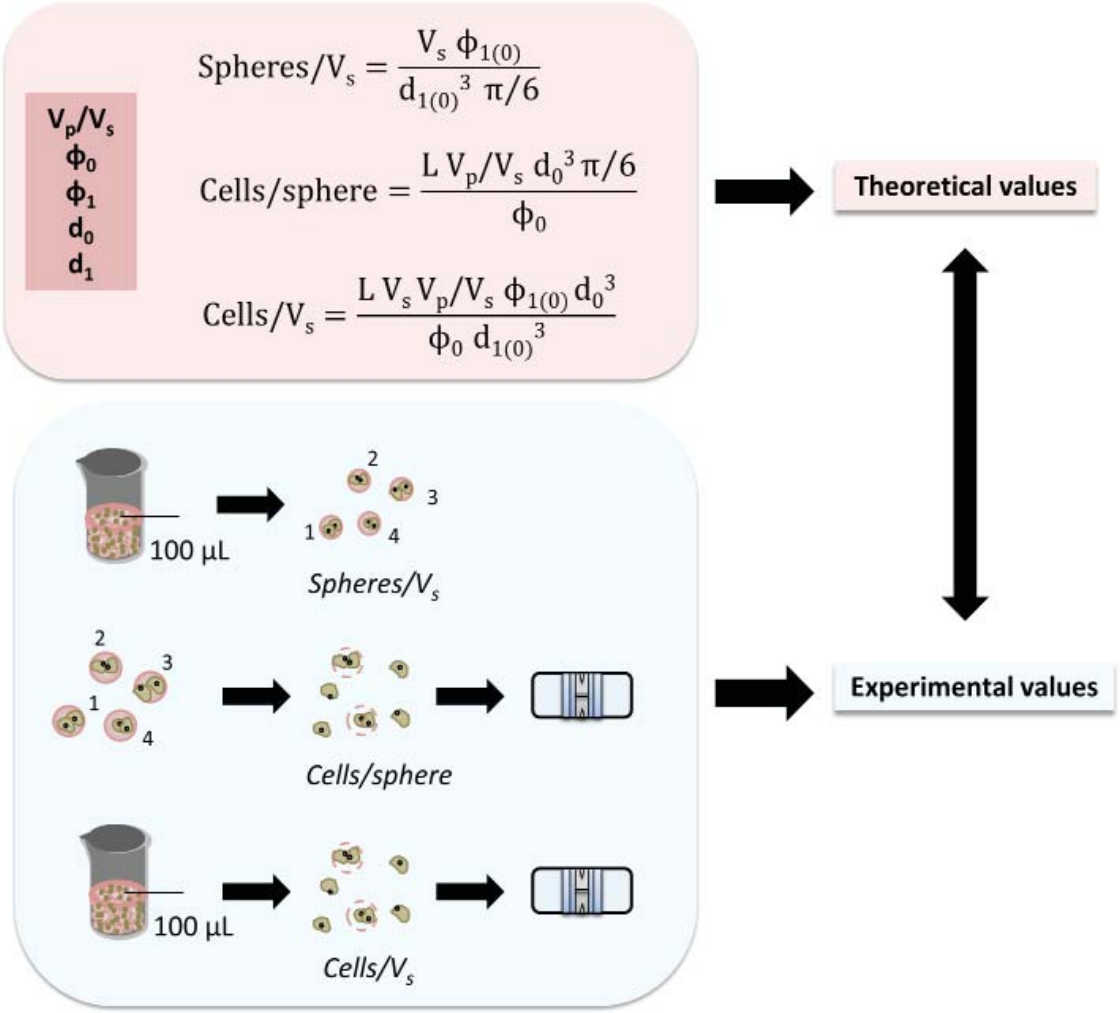

Figure 12. Mathematical model validation. Various alginate cell microencapsulation protocols were selected for the validation of the mathematical model. In every case, the experimental values for spheres/V_S, cells/sphere and cells/V_S were calculated and compared to the corresponding ones obtained from the theoretical mathematical expressions. For the experimental calculation of spheres/V_S, we counted the number of spheres contained in a known volume of spheres (V_S); a few spheres were counted and enzymatically digested when measuring cells/sphere; and for the calculation of cells/V_S, a known volume of spheres was digested in order to count the entrapped cells.

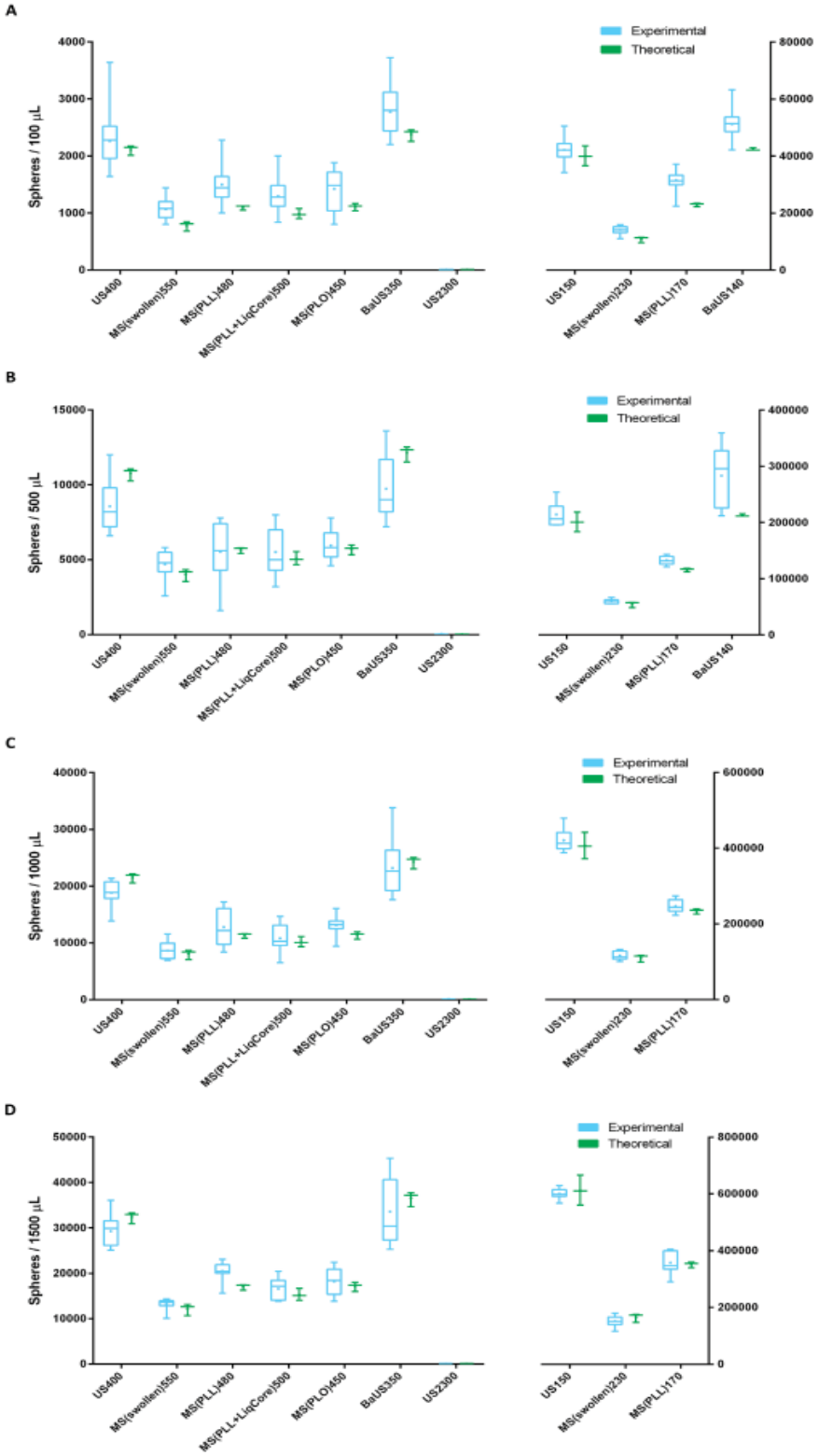

Figure 13. Experimental and theoretical results obtained for spheres/V_S, when V_S = 100 µL (A), 500 µL (B), 1000 µL (C) and 1500 µL (D). Due to the different scales, two Y-axes are displayed on the box plots. Left and right Y-axes show the scale for the spheres of diameters bigger or equal to 400 µm and smaller or equal to 230 µm, respectively. The mean value is plotted with a dot in every case. Mann-Whitney-Wilcoxon test showed no significant differences between the theoretical and the experimental median values in any case.

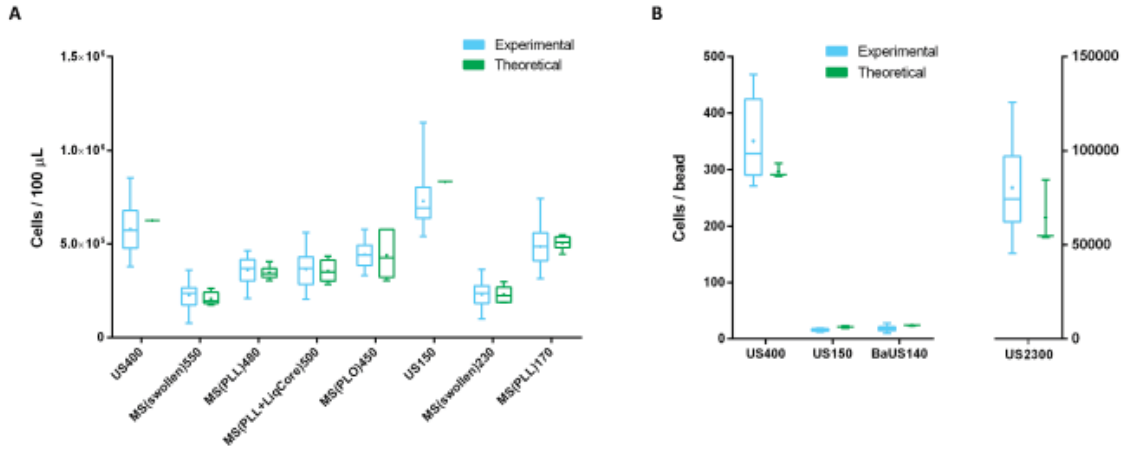

Figure 14. Experimental and theoretical results obtained for cells/V_S (V_S = 100 µL) (A) and cells/sphere (B). Due to the different scales, two Y-axes are displayed on the cells/sphere box plot. Left Y-axis shows the scale for the spheres of diameters smaller or equal to 400 µm and right Y-axis shows the scale for spheres of 2300 µm of diameter. The mean value is plotted with a dot in every case. Mann-Whitney-Wilcoxon test showed no significant differences between the theoretical and the experimental median values in any case.

The obtained data showed that the theoretical results matched the experimental ones, with a positive strong correlation in all cases, proving the ability of the three formulas to predict the real cells/sphere, spheres/V_S and cells/V_S values. The variability of the experimental results is relatively high in some cases but it could be expected as the protocols include many steps that imply different sources of error. First of all, the automated cell counting presents an approximate coefficient of variation (CV) of 2.6% [85]. Regarding the diameters of the tested spheres, the polydispersity affects both the effect that the diameter values have on the formulas (which is powered by three), but also the packing fraction values. Also the different sphere arrangements could lead to variability in the number of particles that could fit in a given volume, even if we stablished a soft agitation between waiting times, that helps achieving a more compact jammed state. Moreover, the process needed to count the encapsulated cells, involves the digestion of the spheres that, depending on the particle type, can be a difficult process.

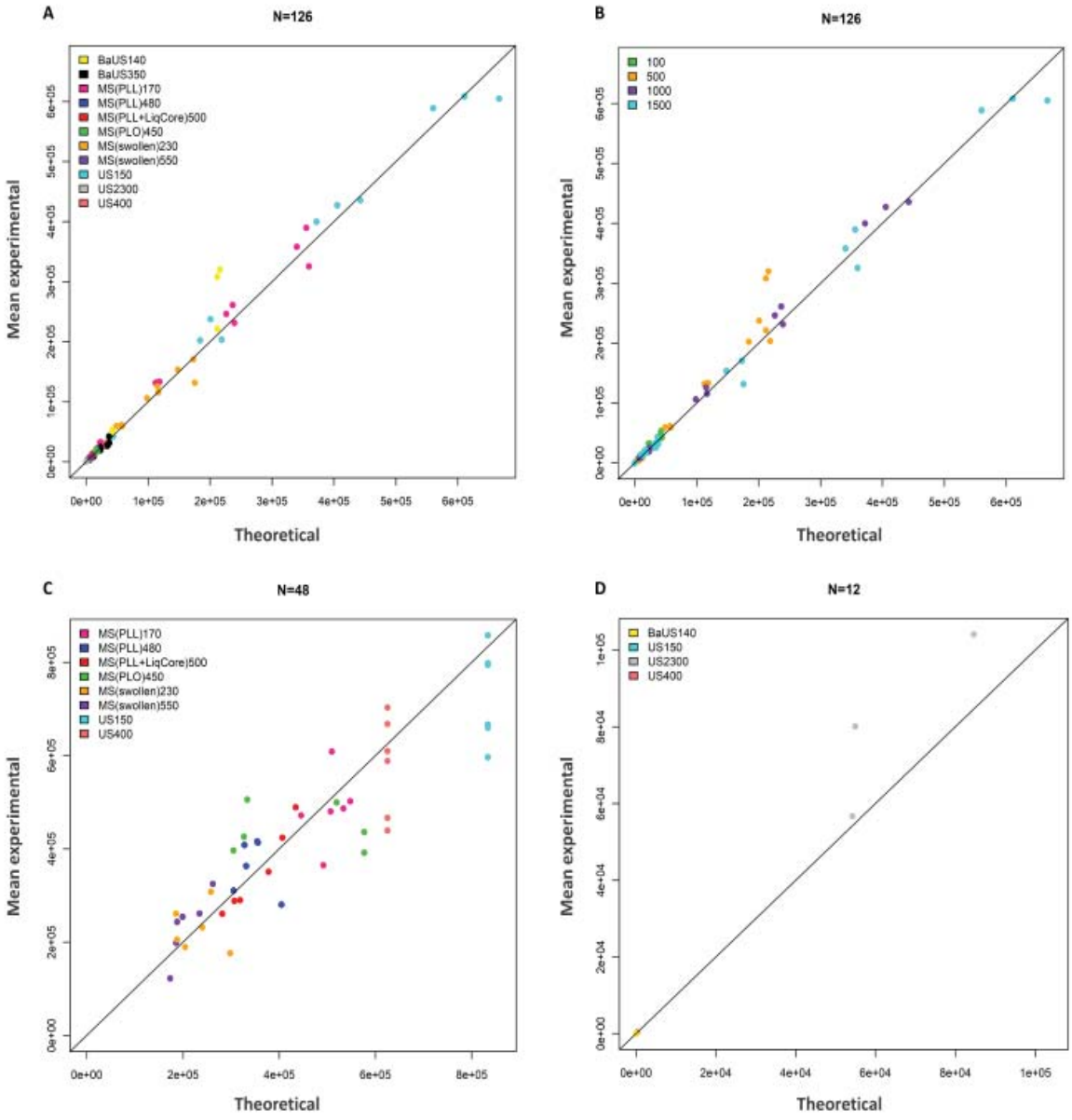

E

	N	cor	p
Spheres/V_S	126	0,992	*<0.001*
Cells/V_S	48	0,899	*<0.001*
Cells/sphere	12	0,992	*<0.001*

Figure 15. Linear correlation analyses between theoretical and experimental data. The results obtained for spheres/V_S were colored based on the different sphere types **(A)** and volumes **(B)**. The results for cells/V_S **(C)** and cells/sphere **(D)** were colored based on the different sphere types. Pearson correlation coefficients were close to 1 in every case and the p values were statistically significant (<0.001) **(E).**

It is important to note that the simulated packing fraction values seemed to adequately describe the real values of the alginate sphere batches even if the physical-mechanical characteristics of the real spheres differ from the simulated ones. Alginate beads and MCs are known to present surface roughness and charges, while none of these parameters were included on the simulations [83,86-89]. Moreover, the polydispersity of the elaborated batches of microparticles ranged from 2% to 8% and only a fixed 5% polydispersion was included on the simulations. These results confirmed our hypothesis that moderate surface roughness or charges, or common polydispersity in sphere sizes do not notably change packing fraction values, which makes it possible to extrapolate the results obtained from the simulations to different hydrogel spherical microparticles.

. It could be expected that spherical particles, surrounded by a fluid were the sphere to fluid density ratio ($\rho s/\rho f$) ratio falls within the tested range of 1-1.5 (probably it would be possible to extrapolate the applicability to higher ratios), would generate comparable packing fractions, if no other parameters are changed and as long as the ratio of container to sphere size is big enough and the number of spheres are sufficient to form a proper packing density. The mathematical model also takes into account possible volume changes caused by shrinking or swelling of the polymer due to particle-elaborating procedures, which is a very common phenomenon when working with hydrogels. The designed equations take into account all these changes just by end-point measurements, making otherwise complex phenomena, easy to quantify.

Caution should be taken when spheres of elevated roughness or electrostatic charges are used, or when the polydispersity of the batches remarkably surpasses the stablished 5%. These approximate values should not be taken into account neither when very high numbers of spheres are used, as the behavior of the packing fraction could vary with the increase of the packing weight. In addition, it is highly recommendable to adjust the diameters for every batch if notable variability is expected, as small changes in this parameter can lead to noticeable differences on the results (diameters are powered by three on the formulas).

Altogether, this is intended to become a general standard guide for accurate dose control in spherical hydrogel drug/cell delivery systems. Since all empirical procedures entail an intrinsic variability, the error accumulated through serial procedures may distort the actual values. On the contrary, we demonstrated that the estimated values obtained by the present mathematical model, which include the simulated packing fraction values, represent reliable central points to set as reference for many measurements in the daily clinical or laboratory routine.

REFERENCES

[1] Orive G, Santos E, Pedraz JL, Hernandez RM. Application of cell encapsulation for controlled delivery of biological therapeutics. Adv Drug Deliv Rev 2014; DOI: 10.1016/j.addr.2013.07.009

[2] Orive G, Santos E, Poncelet D, Hernández RM, Pedraz JL, Wahlberg LU et al. Cell encapsulation: technical and clinical advances. Trends Pharmacol Sci 2015; DOI: 10.1016/j.tips.2015.05.003

[3] Gonzalez-Pujana A, Santos E, Orive G, Pedraz JL, Hernandez RM. Cell microencapsulation technology: Current vision of its therapeutic potential through the administration routes. J Drug Deliv Sci Tec 2017; DOI: 10.1016/j.jddst.2017.03.028

[4] Lee KY and Mooney DJ. Alginate: properties and biomedical applications. Prog Polym Sci 2012; DOI: 10.1016/j.progpolymsci.2011.06.003

[5] Orive G, Hernandez RM, Gascon AR, Igartua M, Pedraz JL. Development and optimisation of alginate-PMCG-alginate microcapsules for cell immobilisation. Int J Pharm 2003; DOI: S0378517303002011

[6] Haque T, Chen H, Ouyang W, Martoni C, Lawuyi B, Urbanska AM et al. In vitro study of alginate-chitosan microcapsules: an alternative to liver cell transplants for the treatment of liver failure. Biotechnol Lett 2005; DOI: 10.1007/s10529-005-0687-3

[7] Ponce S, Orive G, Hernandez R, Gascon AR, Pedraz JL, de Haan BJ et al. Chemistry and the biological response against immunoisolating alginate-polycation capsules of different composition. Biomaterials 2006; DOI: S0142-9612(06)00432-7

[8] Soon-Shiong P, Heintz RE, Merideth N, Yao QX, Yao Z, Zheng T et al. Insulin independence in a type 1 diabetic patient after encapsulated islet transplantation. Lancet 1994; DOI: S0140-6736(94)90067-1

[9] Hasse C, Klock G, Schlosser A, Zimmermann U, Rothmund M. Parathyroid allotransplantation without immunosuppression.Lancet 1997; DOI: S0140-6736(05)62473-7

[10] Lohr M, Bago ZT, Bergmeister H, Ceijna M, Freund M, Gelbmann W et al. Cell therapy using microencapsulated 293 cells transfected with a gene construct expressing CYP2B1,

an ifosfamide converting enzyme, instilled intra-arterially in patients with advanced-stage pancreatic carcinoma: a phase I/II study. J Mol Med (Berl) 1999; DOI: 10.1007/s001090050366

[11] Lohr M, Hoffmeyer A, Kroger J, Freund M, Hain J, Holle A et al. Microencapsulated cell-mediated treatment of inoperable pancreatic carcinoma. Lancet 2001; DOI: S0140673600047498

[12] Salmons B, Lohr M, Gunzburg WH. Treatment of inoperable pancreatic carcinoma using a cell-based local chemotherapy: results of a phase I/II clinical trial. J Gastroenterol 2003; 38 Suppl 15:78-84

[13] Calafiore R, Basta G, Luca G, Lemmi A, Montanucci MP, Calabrese G et al. Microencapsulated pancreatic islet allografts into nonimmunosuppressed patients with type 1 diabetes: first two cases. Diabetes Care 2006; DOI: 29/1/137

[14] Elliott RB, Escobar L, Tan PL, Muzina M, Zwain S, Buchanan C. Live encapsulated porcine islets from a type 1 diabetic patient 9.5 yr after xenotransplantation. Xenotransplantation 2007; DOI: XEN384

[15] Tuch BE, Keogh GW, Williams LJ, Wu W, Foster JL, Vaithilingam V et al. Safety and viability of microencapsulated human islets transplanted into diabetic humans. Diabetes Care 2009; DOI: 10.2337/dc09-0744

[16] Cabane P, Gac P, Amat J, Pineda P, Rossi R, Caviedes R et al. Allotransplant of microencapsulated parathyroid tissue in severe postsurgical hypoparathyroidism: a case report. Transplant Proc 2009; DOI: 10.1016/j.transproceed.2009.06.211

[17] Basta G, Montanucci P, Luca G, Boselli C, Noya G, Barbaro B et al. Long-term metabolic and immunological follow-up of nonimmunosuppressed patients with type 1 diabetes treated with microencapsulated islet allografts: four cases. Diabetes Care 2011; DOI: 10.2337/dc11-0731

[18] Heile A and Brinker T. Clinical translation of stem cell therapy in traumatic brain injury: the potential of encapsulated mesenchymal cell biodelivery of glucagon-like peptide-1. Dialogues Clin Neurosci 2011; 13(3): 279-286

[19] Jacobs-Tulleneers-Thevissen D, Chintinne M, Ling Z, Gillard P, Schoonjans L, Delvaux G et al. Sustained function of alginate-encapsulated human islet cell implants in the peritoneal cavity of mice leading to a pilot study in a type 1 diabetic patient. Diabetologia 2013; DOI: 10.1007/s00125-013-2906-0

[20] Lohr JM, Haas SL, Kroger JC, Friess HM, Hoft R, Goretzki PE et al. Encapsulated cells expressing a chemotherapeutic activating enzyme allow the targeting of subtoxic chemotherapy and are safe and efficacious: data from two clinical trials in pancreatic cancer. Pharmaceutics 2014; DOI: 10.3390/pharmaceutics6030447

[21] Snow B, Mulroy E, Bok A, Simpson M, Smith A, Taylor K et al. A phase IIb, randomised, double-blind, placebo-controlled, dose-ranging investigation of the safety and efficacy of

NTCELL((R)) [immunoprotected (alginate-encapsulated) porcine choroid plexus cells for xenotransplantation] in patients with Parkinson's disease. Parkinsonism Relat Disord 2019; DOI: S1353-8020(18)30500-5

[22] Yucesan E, Basoglu H, Goncu B, Akbas F, Ersoy YE, Aysan E. Microencapsulated parathyroid allotransplantation in the omental tissue. Artif Organs 2019; DOI: 10.1111/aor.13475

[23] Rokstad AM, Lacik I, de Vos P, Strand BL. Advances in biocompatibility and physico-chemical characterization of microspheres for cell encapsulation. Adv Drug Deliv Rev 2014; DOI: 10.1016/j.addr.2013.07.010

[24] He H, Luedke E, Zhang X, Yu B, Schmitt A, McClarren B et al. A naonoporous cell-therapy device with controllable biodegradation for long-term drug release. J Control Release 2013; DOI: 10.1016/j.jconrel.2012.11.020

[25] Weber W and Fussenegger M. Emerging biomedical applications of synthetic biology. Nat Rev Genet 2011; DOI: 10.1038/nrg3094

[26] Gubeli RJ, Burger K, Weber W. Synthetic biology for mammalian cell technology and materials sciences. Biotechnol Adv 2013; DOI: 10.1016/j.biotechadv.2012.01.007

[27] Zanotti L, Sarukhan A, Dander E, Castor M, Cibella J, Soldani C et al. Encapsulated mesenchymal stem cells for in vivo immunomodulation. Leukemia 2013; DOI: 10.1038/leu.2012.202

[28] Mao AS, Özkale B, Shah NJ, Vining KH, Descombes T, Zhang L et al. Programmable microencapsulation for enhanced mesenchymal stem cell persistence and immunomodulation. Proc Natl Acad Sci USA 2019; DOI: 10.1073/pnas.1819415116

[29] Fath-Bayati L and Ai J. Assessment of mesenchymal stem cell effect on foreign body response induced by intraperitoneally implanted alginate spheres. J Biomed Mater Res A 2020; DOI: 10.1002/jbm.a.36795

[30] Takahashi K and Yamanaka S. Induction of pluripotent stem cells from mouse embryonic and adult fibroblast cultures by defined factors. Cell 2006; DOI: S0092-8674(06)00976-7

[31] Horiguchi I, Chowdhury MM, Sakai Y, Tabata Y. Proliferation, morphology, and pluripotency of mouse induced pluripotent stem cells in three different types of alginate beads for mass production. Biotechnol Prog 2014; DOI: 10.1002/btpr.1891

[32] Ankrum JA, Ong JF, Karp JM. Mesenchymal stem cells: immune evasive, not immune privileged. Nat Biotechnol 2014; DOI: 10.1038/nbt.2816

[33] Faiella W and Atoui R. Immunotolerant Properties of Mesenchymal Stem Cells: Updated Review. Stem Cells Int 2016; DOI: 10.1155/2016/1859567

[34] Abdi R, Fiorina P, Adra CN, Atkinson M, Sayegh MH. Immunomodulation by mesenchymal stem cells: a potential therapeutic strategy for type 1 diabetes. Diabetes 2008; DOI: 10.2337/db08-0180

[35] Hoogduijn MJ, Popp F, Verbeek R, Masoodi M, Nicolaou A, Baan C et al. The

immunomodulatory properties of mesenchymal stem cells and their use for immunotherapy. Int Immunopharmacol 2010; DOI: 10.1016/j.intimp.2010.06.019

[36] Ranganath SH, Levy O, Inamdar MS, Karp JM. Harnessing the mesenchymal stem cell secretome for the treatment of cardiovascular disease. Cell Stem Cell 2012; DOI: 10.1016/j.stem.2012.02.005

[37] Shi Y, Su J, Roberts AI, Shou P, Rabson AB, Ren G. How mesenchymal stem cells interact with tissue immune responses. Trends Immunol 2012; DOI: 10.1016/j.it.2011.11.004

[38] Gao F, Chiu SM, Motan DA, Zhang Z, Chen L, Ji HL et al. Mesenchymal stem cells and immunomodulation: current status and future prospects. Cell Death Dis 2016; DOI: 10.1038/cddis.2015.327

[39] Garate A, Ciriza J, Casado JG, Blazquez R, Pedraz JL, Orive G et al. Assessment of the Behavior of Mesenchymal Stem Cells Immobilized in Biomimetic Alginate Microcapsules. Mol Pharm 2015; DOI: 10.1021/acs.molpharmaceut.5b00419

[40] Gurruchaga H, Ciriza J, Saenz del Burgo L, Rodriguez-Madoz JR, Santos E, Prosper F et al. Cryopreservation of microencapsulated murine mesenchymal stem cells genetically engineered to secrete erythropoietin. Int J Pharm 2015; DOI: 10.1016/j.ijpharm.2015.02.047

[41] Lopez-Mendez TB, Santos-Vizcaino E, Blanco FJ, Pedraz JL, Hernandez RM, Orive G. Improved control over MSCs behavior within 3D matrices by using different cell loads in both in vitro and in vivo environments. Int J Pharm 2017; DOI: S0378-5173(17)30869-4

[42] Gonzalez-Pujana A, Rementeria A, Blanco FJ, Igartua M, Pedraz JL, Santos-Vizcaino E et al. The role of osmolarity adjusting agents in the regulation of encapsulated cell behavior to provide a safer and more predictable delivery of therapeutics. Drug Deliv 2017; DOI: 10.1080/10717544.2017.1391894

[43] Liu ZC and Chang TM. Intrasplenic transplantation of bioencapsulated mesenchymal stem cells improves the recovery rates of 90% partial hepatectomized rats. Stem Cells Int 2012; DOI: 10.1155/2012/697094

[44] Meier RP, Mahou R, Morel P, Meyer J, Montanari E, Muller YD et al. Microencapsulated human mesenchymal stem cells decrease liver fibrosis in mice. J Hepatol 2015; DOI: 10.1016/j.jhep.2014.10.030

[45] Diekmann S, Glockner P, Bader A. The influence of different cultivation conditions on the metabolic functionality of encapsulated primary hepatocytes. Int J Artif Organs 2007; DOI: 10.1177/039139880703000303

[46] Harm S, Stroble K, Hartmann J, Falkenhagen D. Alginate-encapsulated human hepatoma C3A cells for use in a bioartificial liver device - the hybrid-MDS. Int J Artif Organs 2009; DOI: 49D3145D-793D-4022-9DF3-56D48E5C874A

[47] Ito T, Itakura S, Todorov I, Rawson J, Asari S, Shintaku J et al. Mesenchymal stem cell and islet co-transplantation promotes graft revascularization and function. Transplantation 2010; DOI: 10.1097/tp.0b013e3181db09c4

[48] Longoni B, Szilagyi E, Quaranta P, Paoli GT, Tripodi S, Urbani S et al. Mesenchymal stem cells prevent acute rejection and prolong graft function in pancreatic islet transplantation. Diabetes Technol Ther 2010; DOI: 10.1089/dia.2009.0154

[49] Kerby A, Jones ES, Jones PM, King AJ. Co-transplantation of islets with mesenchymal stem cells in microcapsules demonstrates graft outcome can be improved in an isolated-graft model of islet transplantation in mice. Cytotherapy 2013; DOI: 10.1016/j.jcyt.2012.10.018

[50] Vaithilingam V, Evans MDM, Lewy DM, Bean PA, Bal S, Tuch BE. Co-encapsulation and co-transplantation of mesenchymal stem cells reduces pericapsular fibrosis and improves encapsulated islet survival and function when allografted. Sci Rep 2017; DOI: 10.1038/s41598-017-10359-1

[51] Wen Q, Zhou C, Luo W, Zhou M, Ma L. Pro-osteogenic effects of fibrin glue in treatment of avascular necrosis of the femoral head in vivo by hepatocyte growth factor-transgenic mesenchymal stem cells. J Transl Med 2014; DOI: 10.1186/1479-5876-12-114

[52] Li YY, Cheng HW, Cheung KMC, Chan D, Chan BP. Mesenchymal stem cell-collagen microspheres for articular cartilage repair: Cell density and differentiation status. Acta Biomater 2014; DOI: 10.1016/j.actbio.2014.01.002

[53] Moshaverinia A, Chen C, Xu X, Akiyama K, Ansari S, Zadeh HH et al. Bone regeneration potential of stem cells derived from periodontal ligament or gingival tissue sources encapsulated in RGD-modified alginate scaffold. Tissue Eng Part A 2014; DOI: 10.1089/ten.TEA.2013.0229

[54] Trouche E, Girod Fullana S, Mias C, Ceccaldi C, Tortosa F, Seguelas MH et al. Evaluation of alginate microspheres for mesenchymal stem cell engraftment on solid organ. Cell Transplant 2010; DOI: 10.3727/096368910X514297

[55] Hu J, Li H, Chi G, Yang Z, Zhao Y, Liu W et al. IL-1RA gene-transfected bone marrow-derived mesenchymal stem cells in APA microcapsules could alleviate rheumatoid arthritis. Int J Clin Exp Med 2015; 8(1): 706–13.

[56] Han Y, Tao R, Han Y, Sun T, Chai J, Xu G et al. Microencapsulated VEGF gene–modified umbilical cord mesenchymal stromal cells promote the vascularization of tissue-engineered dermis: an experimental study. Cytotherapy 2014; DOI: 10.1016/j.jcyt.2013.10.014

[57] Barminko J, Kim JH, Otsuka S, Gray A, Schloss R, Grumet M et al. Encapsulated mesenchymal stromal cells for in vivo transplantation. Biotechnol Bioeng 2011; DOI: 10.1002/bit.23233

[58] Landazuri N, Levit RD, Joseph G, Ortega-Legaspi JM, Flores CA, Weiss D et al. Alginate microencapsulation of human mesenchymal stem cells as a strategy to enhance paracrine-mediated vascular recovery after hindlimb ischaemia. J Tissue Eng Regen Med 2016; DOI: 10.1002/term.1680

[59] Attia N, Santos E, Abdelmouty H, Arafa S, Zohdy N, Hernandez RM et al. Behaviour and ultrastructure of human bone marrow-derived mesenchymal stem cells

immobilised in alginate-poly-l-lysine-alginate microcapsules. J Microencapsul 2014; DOI: 10.3109/02652048.2014.898706

[60] Sanz-Nogues C, Horan J, Thompson K, Howard L, Ryan G, Kassem M et al. Inefficiency in macromolecular transport of SCS-based microcapsules affects viability of primary human mesenchymal stem cells but not of immortalized cells. J Biomed Mater Res A 2015; DOI: 10.1002/jbm.a.35493

[61] McClatchey AI and Yap AS. Contact inhibition (of proliferation) redux. Curr Opin Cell Biol 2012; DOI: 10.1016/j.ceb.2012.06.009

[62] Park SJ, Shin S, Koo OJ, Moon JH, Jang G, Ahn C et al. Functional improvement of porcine neonatal pancreatic cell clusters via conformal encapsulation using an air-driven encapsulator. Exp Mol Med 2012; DOI: 10.3858/emm.2012.44.1.001

[63] Rhind N and Russell P. Signaling Pathways that Regulate Cell Division. Cold Spring Harb Perspect Biol 2012; DOI: 10.1101/cshperspect.a005942

[64] Rodrigues M, Griffith LG, Wells A. Growth factor regulation of proliferation and survival of multipotential stromal cells. Stem Cell Res Ther 2010. DOI: 10.1186/scrt32

[65] Garate A, Murua A, Orive G, Hernandez RM, Pedraz JL. Stem cells in alginate bioscaffolds. Ther Deliv 2012; DOI: 10.4155/tde.12.53

[66] Kastellorizios M, Tipnis N, Burgess DJ. Foreign Body Reaction to Subcutaneous Implants. Adv Exp Med Biol 2015; DOI: 10.1007/978-3-319-18603-0_6

[67] Kyurkchiev D, Bochev I, Ivanova-Todorova E, Mourdjeva M, Oreshkova T, Belemezova K et al. Secretion of immunoregulatory cytokines by mesenchymal stem cells. World J Stem Cells 2014; DOI: 10.4252/wjsc.v6.i5.552

[68] Goren A, Dahan N, Goren E, Baruch L, Machluf M. Encapsulated human mesenchymal stem cells: a unique hypoimmunogenic platform for long-term cellular therapy. FASEB J 2010; DOI: 10.1096/fj.09-131888

[69] Pittman K and Kubes P. Damage-associated molecular patterns control neutrophil recruitment. J Innate Immun 2013; DOI: 10.1159/000347132

[70] Hirsiger S, Simmen HP, Werner CM, Wanner GA, Rittirsch D. Danger signals activating the immune response after trauma. Mediators Inflamm 2012; DOI: 10.1155/2012/315941

[71] Kaczmarek A, Vandenabeele P, Krysko DV. Necroptosis: the release of damage-associated molecular patterns and its physiological relevance. Immunity 2013; DOI: 10.1016/j.immuni.2013.02.003

[72] Tang D, Kang R, Coyne CB, Zeh HJ, Lotze MT. PAMPs and DAMPs: signal 0s that spur autophagy and immunity. Immunol Rev 2012; DOI: 10.1111/j.1600-065X.2012.01146.x

[73] Wilson JL, Najia MA, Saeed R, McDevitt TC. Alginate encapsulation parameters influence the differentiation of microencapsulated embryonic stem cell aggregates. Biotechnol Bioeng 2014; DOI: 10.1002/bit.25121

[74] Mukhopadhyay S and Peixinho J. Packings of deformable spheres. Phys Rev E Stat

Nonlin Soft Matter Phys 2011; DOI: 10.1103/PhysRevE.84.011302

[75] van Hecke M. Jamming of soft particles: geometry, mechanics, scaling and isostaticity. J Phys Condens Matter 2009; DOI: 10.1088/0953-8984/22/3/033101

[76] Visscher WM and Bolsterli M. Random packing of equal and unequal spheres in two and three dimensions. Nature 1972; DOI: 10.1038/239504a0

[77] Jodrey WS and Tory EM. Computer simulation of close random packing of equal spheres. Phys Rev A 1985; DOI: 10.1103/PhysRevA.32.2347

[78] Tobochnik J and Chapin PM. Monte Carlo simulation of hard spheres near random closest packing using spherical boundary conditions. J Chem Phys 1988; DOI: 10.1063/1.454542

[79] An X and Li C. Experiments on densifying packing of equal spheres by two-dimensional vibration. Particuology 2013; DOI: 10.1016/j.partic.2012.06.019

[80] Lachhab T and Weill C. Compression of a soft sphere packing. Eur Phys J B 1999; DOI: 10.1007/s100510050742

[81] Suzuki M, Shinmura T, Iimura K, Hirota M. Study of the wall effect on particle packing structure using X-ray micro computed tomography. ADV Powder Technol 2008; DOI: 10.1163/156855208X293817

[82] Sohn HY and Moreland C. The effect of particle size distribution on packing density. Can J Chem Eng 1968; DOI: 10.1002/cjce.5450460305

[83] Lekka M, Sainz-Serp D, Kulik AJ, Wandrey C. Hydrogel microspheres: influence of chemical composition on surface morphology, local elastic properties, and bulk mechanical characteristics. Langmuir 2004; DOI: 10.1021/la048389h

[84] Morch YA, Donati I, Strand BL, Skjak-Braek G. Effect of Ca2+, Ba2+, and Sr2+ on alginate microbeads. Biomacromolecules 2006; DOI: 10.1021/bm060010d

[85] https://www.bio-rad.com/webroot/web/pdf/lsr/literature/Bulletin_6003.pdf; 2020 [Accessed 2 September 2020]

[86] Abbah SA, Lu WW, Peng SL, Aladin DMK, Li ZY, Tam WK et al. Extracellular matrix stability of primary mammalian chondrocytes and intervertebral disc cells cultured in alginate-based microbead hydrogels. Cell Transplant 2008; DOI: 10.3727/096368908787236648

[87] de Vos P, Spasojevic M, de Haan BJ, Faas MM. The association between in vivo physicochemical changes and inflammatory responses against alginate based microcapsules. Biomaterials 2012; DOI: 10.1016/j.biomaterials.2012.04.039

[88] Virumbrales-Muñoz M, Santos-Vizcaino E, Paz L, Gallardo-Moreno A, Orive G, Hernandez RM et al. Force spectroscopy-based simultaneous topographical and mechanical characterization to study polymer-to-polymer interactions in coated alginate microspheres. Sci Rep 2019; DOI: 10.1038/s41598-019-56547-z

[89] Hajifathaliha F, Mahboubi A, Nematollahi L, Mohit E, Bolourchian N. Comparison of different cationic polymers efficacy in fabrication of alginate multilayer microcapsules. Asian J Pharm Sci 2020; DOI: 10.1016/j.ajps.2018.11.007

CONCLUSIONS

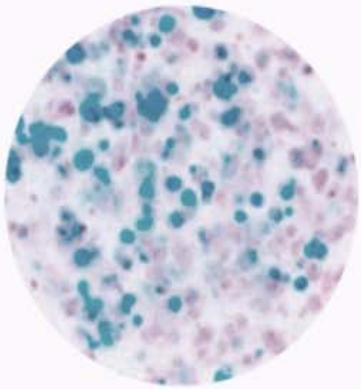

CONCLUSIONS

According with the results obtained in the previously described experiments, the main conclusions of this work include:

1. In the first part of this doctoral thesis, the influence of different genetically modified D1 mesenchymal stromal cell (D1-MSC) loads was analyzed, in alginate based cell microencapsulation systems, both *in vitro* and *in vivo*. The results obtained *in vitro* suggested that higher cell loads could result in more controlled cell behavior and a constant release of the therapeutic factor. Conversely, the enriched environment found *in vivo*, produced a rapid increase of the cell load in all groups, but especially in those with higher cell densities, leading to the appearance of intracapsular necrosis and implant failure.

2. Disparate levels of cell proliferation were pointed as the main difference between the *in vitro* and *in vivo* behaviors, for all groups tested. The specific combination of this highly proliferative cell line with a relatively permissive microcapsule structure led to an excessive cell division that prevented the correct observation of other phenomena. Thus, more studies, in which the proliferation rates are controlled, are needed to elucidate the pending questions.

3. In the second part of this work, a complete and practical mathematical model was defined, which allows accurate control of the administered dose of cells/drug in a broad range of hydrogel-based particulate systems. The model can be applied in any case were the described end-point parameters, ϕ_0, ϕ_1, d_0, d_1 and V_p/V_s, can be measured, to easily calculate cells or drug/sphere, cells or drug/V_s and spheres/V_s.

4. The designed mathematical model was experimentally validated with the complex example of cell microencapsulation systems for sustained drug delivery. The model was able to accurately predict the experimentally obtained values for cells/sphere, cells/V_s and spheres/V_s, for the elaborated particle batches (following the most common microcapsule elaboration protocols).

5. The simulated packing fraction values for hydrogel microspheres, necessary for the implementation of the model but difficult to be measured experimentally, can be confidently extrapolated to very diverse situations as long as a few assumptions are met, which makes them useful for a wide range of biomedical applications.